Pharmacometric approaches for linking pharmacokinetic and pharmacodynamic models of sunitinib and pazopanib with clinical outcome

Dissertation

zur Erlangung des Doktorgrades (Dr. rer. nat)

der Mathematisch-Naturwissenschaftlichen Fakultät

der Rheinischen Friedrich-Wilhelms-Universität Bonn

vorgelegt von

ACHIM FRITSCH

aus

Düsseldorf

Bonn 2018

Angefertigt mit Genehmigung der Mathematisch-Naturwissenschaftlichen Fakultät
der Rheinischen Friedrich-Wilhelms-Universität Bonn

Erstgutachter: Prof. Dr. Ulrich Jaehde

Zweitgutachter: Prof. Dr. Georg Hempel

Tag der Promotion: 12. Juli 2018

Erscheinungsjahr: 2018

Danksagung

An erster Stelle möchte ich meinem Doktorvater Herrn Prof. Ulrich Jaehde danken, der mir dieses interessante und wichtige Projekt anvertraut hat und durch seine fachliche und persönliche Unterstützung, die zahlreichen wissenschaftlichen Diskussionen und Bestärkungen bei schwierigen Entscheidungen, maßgeblich zum erfolgreichen Abschluss dieser Arbeit beigetragen hat.

Weiterhin danke ich Herrn Prof. Georg Hempel für die Übernahme des Koreferats, sowie Herrn Prof. Gerd Bendas und Herrn Dr. Stefan Hauser für die Bereitschaft Teil der Prüfungskommission zu sein.

Ein besonderer Dank gilt dem gesamten EuroTARGET Konsortium für die tolle wissenschaftliche Kooperation, auch über Ländergrenzen hinaus. Insbesondere hervorheben möchte ich an dieser Stelle Herrn Prof. Henk-Jan Guchelaar, Frau Dr. Meta Diekstra und Herrn Dr. Dirk Jan Moes, die im Rahmen des gemeinsamen Arbeitspaketes einen wertvollen Beitrag zu dieser Arbeit geleistet haben. Ebenso danke ich allen Ärzten und Krankenschwestern und –pflegern in den Prüfzentren für ihr Engagement und die nette und kollegiale Zusammenarbeit.

Für die Unterstützung in allen regulatorischen und organisatorischen Fragen danke ich den Kollegen und Kolleginnen der CESAR in Wien, die als Sponsor der zugrundeliegenden Studie fungierte. Mein besonderer Dank gilt hier vor allem Herrn Dr. Max Roessler und Frau Dr. Berta Moritz, die jederzeit hilfsbereit und kompetent für Fragen und Diskussionen zur Verfügung standen

Herrn Prof. Fritz Sörgel und Frau Dr. Martina Kinzig sowie dem gesamten Team des IBMP danke ich für die Bestimmung der benötigten Plasmakonzentrationen von Sunitinib und Pazopanib via LC-MS/MS.

Für seine Unterstützung im Rahmen der Biomarkeranalytik, möchte ich Herrn Malte Hellwig danken, der mit seiner Erfahrung im Gebiet der Immunoassays eine große Hilfe im Labor war.

Gerne möchte ich auch Frau Prof. Dr. Kloft danken, die mir durch die Aufnahme in das PharMetrX Programm nicht nur einen hilfreichen Einstieg in das Gebiet der Pharmakometrie ermöglicht, sondern auch einen fachlichen und freundschaftlichen Austausch mit Kolleginnen und Kollegen dieser wissenschaftlichen Disziplin über die Promotion hinaus geschaffen hat.

Herrn Dr. Maximilian Kullmann, Herrn Dr. Hauke Rühs, Herrn Jan Schlender und Herrn Julian Beyer danke ich für die Bereitschaft das Korrekturlesen dieser Arbeit zu übernehmen.

Den Kollegen im Arbeitskreis Klinische Pharmazie danke ich für die tolle gemeinsame Zeit, den Rückhalt und die Unterstützung auch in schwierigen Zeiten. Insbesondere danke ich dabei meinen Bürokollegen Dr. Maximilian Kullmann, Dr. André Wilmer, Frau Patricia Kleiner, Frau Kerstin Bitter, Frau Verena Kurth sowie Frau Imke Ortland.

Ein großer Dank und mein größter Respekt gebührt allen Patienten, die trotz ihrer schweren Erkrankung bereit waren an diesem Projekt teilzunehmen, um einen Beitrag für die Verbesserung der Therapie des Nierenzellkarzinoms leisten zu können.

Abschließend möchte ich gerne meiner Familie, meinen Freunden und meiner Freundin Christine danken, die mich zu jederzeit und uneingeschränkt unterstützt haben und immer in mich vertraut haben.

Für meine Familie

“*I'm a scientist and I know what constitutes proof. But the reason I call myself by my childhood name is to remind myself that a scientist must also be absolutely like a child. If he sees a thing, he must say that he sees it, whether it was what he thought he was going to see or not. See first, think later, then test. But always see first. Otherwise you will only see what you were expecting. Most scientists forget that.*”

- Douglas Adams, *So long, and thanks for all the fish*

ABBREVIATIONS

5-FU	Fluorouracil
AC	Active concentration
AMP	Amplitude
AUC	Area under the curve
BMI	Body mass index
BSA	Body surface area
BSL	Baseline
BQL	Below quantification limit
ccRCC	Clear cell renal cell carcinoma
CDD	Case deletion diagnostics
CI	Confidence interval
cKIT	Receptor tyrosine kinase Kit
C_{max}	Maximum plasma concentrations
CSF	Colony stimulating factor
CTCAE	Common terminology criteria for adverse events
CV	Coefficient of variation
CWRES	Conditonal weighted residuals
DCE-MRI	Dynamic contrast-enhanced magnetic resonance imaging
DCE-USI	Dynamic-contrast-enhanced ultrasound imaging
dOFV	Change in objective function value
DNA	Deoxyribonucleic acid
DV	Dependent variable
EBE	Empirical bayes estimates
ECM	Extracellular matric
eCRF	Electronic case report form
EFF	Effect
ELISA	Enzyme linked immunosorbent assay
EMA	European Medicines Agency
E_{max}	Maximum level of effect
EPC	Endothelial progenitor cells
EuroTARGET	European collaborative project on Targeted therapy in Renal cell cancer: GEnetic and Tumor-related biomarkers for response and toxicity

EuT-PKPD Study	EuroTARGET Pharmacokinetics/Pharmacodynamics Study
FDA	US Food and Drug Administration
FLT-3	Fms-like tyrosine kinase 3
FO	First order
FOCE	First order conditional estimation
FOLFIRI	Folinic acid, fluorouracil, irinotecan
GIST	Gastrointestinal stroma tumors
GOF	Goodness-of-fit
HER2	Human epidermal growth factor receptor 2
HIF	Hypoxia-inducible factor
IFN-α	Interferon alpha
IIV	Interindividual variability
INH	Fractional inhibition
IOV	Interoccasion variability
IPRED	Individual predictions
IWRES	Individual weighted residuals
LC-MS	Liquid chromatography, mass spectrometer
MMP	Matrix metalloprotease
mRCC	Metastatic renal cell carcinoma
MSKCC	Memorial Sloan Kettering Cancer Center
mTOR	Mechanistic target of rapamycin
mTORC1	Mechanistic target of rapamycin complex 1
MTT	Mean transit time
NN	Number of transit compartments
NCA	Noncompartmental analysis
NCI	National cancer institute
NLME	Nonlinear mixed effects
NONMEM	Nonlinear mixed effects modeling
NRP	Neuropilin
OBJ	Objective Function
OFV	Objective function value
OS	Overall survival
P	Proportion (ratio of components)
PBPK	Physiology-based pharmacokinetics

pcVPC	Prediction-corrected visual predictive check
PD	Pharmacodynamics
PDGFR	Platelet derived growth factor receptor
PFS	Progression-free survival
PGI2	Prostaglandine I2
Pgp	P-Glykoprotein
PI	Prediction Interval
PK	Pharmacokinetics
pNET	Pancreatic neuroendocrine tumor
PRED	Population predictions
PS	Phase shift
PsN	Pearl speaks NONMEM
QC	Quality control
QQ	Quantile-Quantile
RCC	Renal cell carcinoma
REB	Rebound
RECIST	Response evaluation criteria in solid tumors
RET	rearranged during transfection
RNA	Ribonucleic acid
RPE	Relative prediction error
RSME	Root-squared mean error
SD	Standard deviation
SE	Standard error
SmPC	Summary of product characteristics
SNP	Single nucleotide polymorphism
SOP	Standard operating procedure
sVEGFR	Soluble vascular endothelial growth factor receptor
TAD	Time after dose
TDM	Therapeutic drug monitoring
TKI	Tyrosine kinase inhibitor
TTE	Time-to-event
TTP	Time-to-progression
VEGF	Vascular endothelial growth factor
VEGFR	Vascular endothelial growth factor receptor

VHL	Von-Hippel Lindau
VPC	Visual predictive check
WHO	World Health Organization
WP	Work package
WRES	Weighted residuals

TABLE OF CONTENTS

1 INTRODUCTION

1.1 Targeted therapies in cancer treatment

1.1.1 General considerations

The treatment of cancer is one of the fastest approaching medical fields and subject to constant change. In 2015 alone, 20 new drugs were approved by the US Food and Drug Administration (FDA) for various cancer types, mostly addressing new therapeutic targets [**1**]. However, conventional cytotoxic drugs were, and still are in some indications, the backbone of cancer therapy. After a major breakthrough in the mid of the 20th century, where it could be shown that the combination of several cytotoxic drugs can be highly beneficial for the patient, chemotherapeutic regimens as we know them today were developed and further enhanced over the course of time [**2**]. While efficient in some patients, the outcome of chemotherapy can be highly variable. Due to their lack of specificity for tumor cells, cytotoxic drugs are usually associated with often severe adverse events (AE) [**3**]. A better understanding of carcinogenesis and tumor pathophysiology led to the development of several new classes of drugs which aimed to improve the major shortcomings of conventional chemotherapies. Despite their often highly different modes of action these new drugs are gathered under the term *targeted therapy*.

Targeted therapy comprises all treatment approaches which aim to specifically intervene in defined processes related to carcinogenesis. Due to their higher specificity, those therapies should, in contrast to the conventional cytotoxic drugs, ideally increase efficacy and lower the risk of developing typical AE such as nausea, alopecia and myelosuppression [**4**]. Targeted therapies can be subdivided based on their mechanism or chemical and/or biological structure. The National Cancer Institute of the United States (NCI) defines the following categories:

- Hormone therapies
- Signal transduction inhibitors
- Gene expression modulators
- Apoptosis inducers
- Angiogenesis inhibitors

- Immunotherapies
- Monoclonal antibodies that deliver toxic molecules

The first drug labeled as targeted cancer therapy was the monoclonal antibody rituximab which selectively binds the CD20 antigen on the cell surface. Rituximab was approved in 1997 for patients with B-cell non-Hodgkin lymphoma no longer responding to any other treatment options [**5**].

In 2015, targeted therapies accounted for almost 50% of all cancer therapy costs worldwide [**6**]. An analysis in Germany, France, Italy, Spain and UK showed that between 500,000 and 600,000 patients were treated with targeted therapies of any kind at time of data acquisition (2014). This accounts for 32% of all cancer drugs used in the respective countries [**7**]. As shown in Figure 1.1, Germany is the leading country concerning the use of targeted therapies with a share of more than one third of all cancer treatments. Currently, over 80 substances associated with targeted therapy are approved by the FDA and European Medicine Agency (EMA), with more potential candidates currently in clinical trials [**8**].

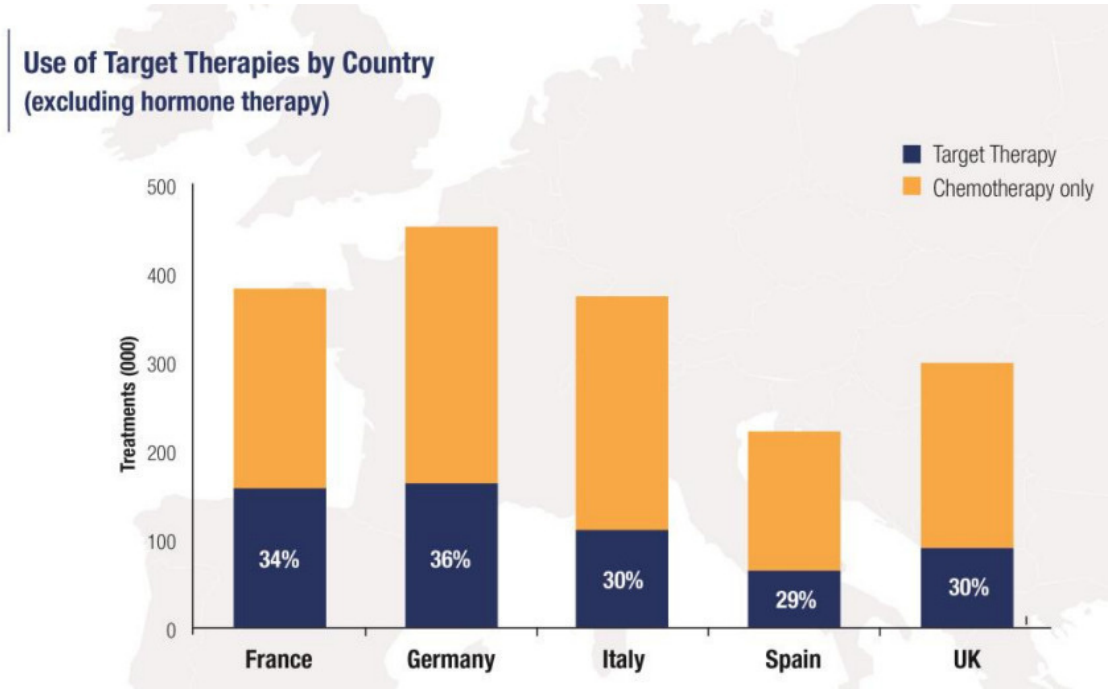

Fig. 1.1: Results of the OncoView study by Cegedim Strategic Data [**7**].

1.1.2 Angiogenesis inhibition

One of the most promising mechanisms identified for potential drug targets was tumor angiogenesis. The therapeutic value of angiogenesis in cancer therapy was first mentioned by Judah Folkman in 1971 [**9**]. Angiogenesis is necessary for several physiological processes, such as wound healing or during pregnancy, but is also involved in disease development, e.g. ischemia, rheumatoid arthritis and cancer [**10**]. More precisely, angiogenesis is the process of sprouting new vessels from existing ones. Angiogenesis has to be differentiated from vasculogenesis, which describes the development of entirely new vessels from angioblasts or other progenitor cells, as it happens during embryogenesis (Figure 1.2) and intussusception. The latter is the term for vessels which are divided by endoluminal migration of endothelial cells resulting in two or more new vessels [**11**].

Similar mechanisms are triggered by a tumor once it reaches a critical size, usually about ≥ 2 mm. Up to this point, neoplasms are able to cover all nutritional needs by passive diffusion [**11**]. Thus, the main triggers for tumor induced angiogenesis are hypoxia and nutrient deficiency. By release of pro-angiogenic factors, such as vascular endothelial growth factor (VEGF), the tumor shifts the balance towards increased angiogenesis. This process is often referred to as the “angiogenic switch” [**10**,**11**]. In context of tumor-induced angiogenesis the term “vascular mimicry” was established: Tumor cells are able to differentiate into endothelial-like cells and can be part of existing vessels or form entirely new ones (Figure 1.2). However, tumor induced angiogenesis results in comparatively chaotic structures which often provide only irregular supply. In the worst case this can lead to necrosis in tumor areas with critical nutrient shortage over a certain period of time [**10**,**11**].

Angiogenesis is a multifactorial process with a high number of signaling pathways involved, of which some, like the mTOR or VEGF pathways, proved to be therapeutic targets. Naturally, targeting only isolated pathways or proteins, increases the risk for development of resistance to the respective therapies. Currently two main modes of resistance are discussed [**12**,**13**]: The concept of *adaptive* or *evasive resistance* describes the first mechanism, which is a direct reaction to the anti-angiogenic treatment as alternative signaling pathways are activated and more pro-angiogenic cells are recruited from the bone marrow.

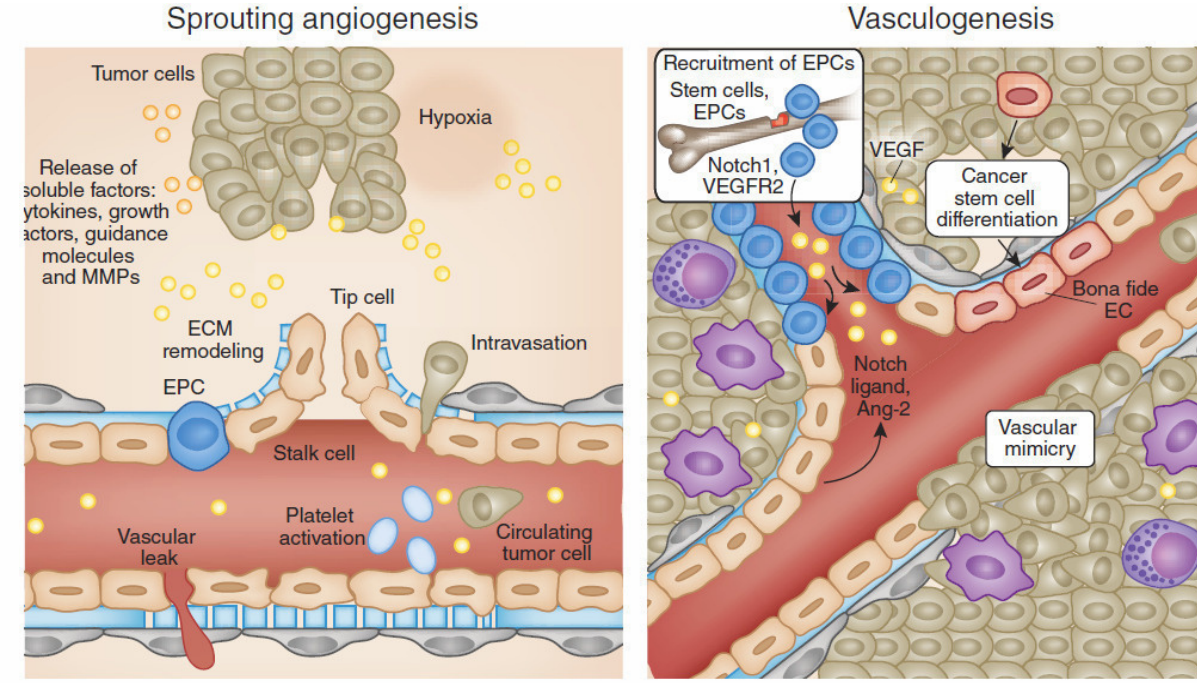

Fig. 1.2: Different mechanism of sprouting angiogenesis and vasculogenesis [**10**]. EC = Endothelial cells, ECM = Extracellular matrix, EPC = Endothelial progenitor cells, MMP = Matrix metalloprotease, VEGF = Vascular endothelial growth factor, sVEGFR-2 = Soluble vascular endothelial growth factor receptor

Furthermore, an increased tight pericyte count is observed, which can serve as protection for tumor blood vessels. A more aggressive migration of tumor cells in non-tumor tissue can also be a result of inhibition of angiogenesis. The second mode of resistance describes the already existing *indifference* or *non-responsiveness* of a tumor to antiangiogenic drugs even before starting the treatment. Thus, the optimal combination and sequence of anti-angiogenic treatments are still under discussion and the basis of several studies [**14**,**15**].

The VEGF pathway

The VEGF pathway is critically important to (tumor-) angiogenesis and a target of various drugs, including VEGF antibodies and tyrosine-kinase inhibitors (TKI). Most research has concentrated on this pathway. The most crucial receptors and their respective ligands are shown in Figure 1.3.

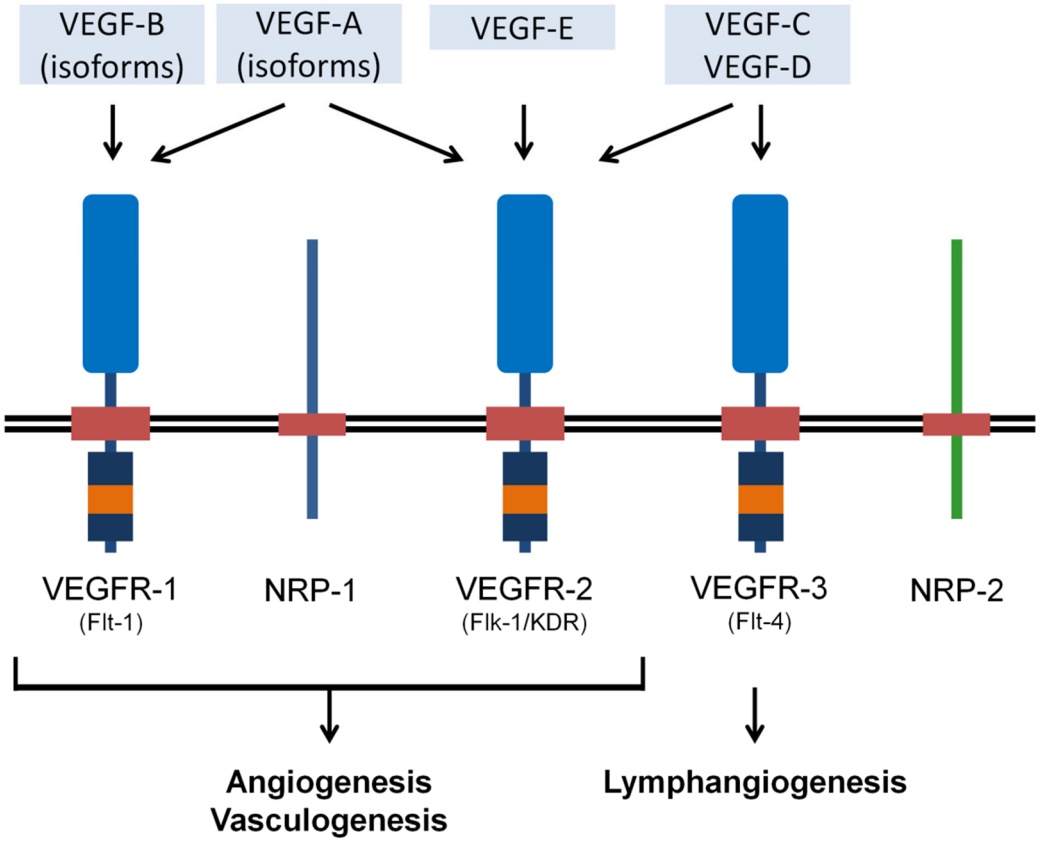

Fig. 1.3: VEGF receptor signaling pathway (modified from [**17**] and [**18**]). VEGF(R) = Vascular endothelial growth factor (receptor), NRP = Neuropilin

Signaling is mediated via different VEGF homologs which can be further subdivided in several isoforms. Depending on receptor specificity and affinity these growth factors trigger different effects. VEGF-A, which is often referred to as VEGF, is one of the most important ligands. In animal studies it could be shown that VEGF-A deficient mice are not capable of surviving due to its crucial role in angio- and vasculogenesis [**16**]. Angio- and vasculogenesis are mainly regulated via vascular endothelial growth factor receptor (VEGFR) -1 and -2 which are expressed ubiquitously on endothelial cells, with VEGFR-2 being the most common one. VEGFR-3 is primarily expressed in lymphatic endothelial cells. Hence, it serves as a mediator in lymphangiogenesis. In addition to the receptor tyrosine kinases VEGFR-1 to 3, neuropilin (NRP) -1 and -2 have been identified as co-receptors. These are highly specific for one isoform of VEGF ($VEGF_{165}$) and can increase the affinity of VEGF to its other receptors [**11**,**17**].

Effects mediated by VEGF through binding the respective receptors include increased vessel permeability, activation of endothelial cells, increased endothelial proliferation and endothelial invasion and migration [**19**]. Furthermore, it was shown that VEGF regulates blood pressure via promotion of NO-synthase expression and NO activity mainly via VEGFR-2 [**20**,**21**].

A key factor for VEGF expression is hypoxia. Hypoxia triggers the dimerization of hypoxia inducible factor-1 α and β (HIF-1) which results in an increased transcription of VEGF. HIF-1 originates from the so called "Von Hippel-Lindau" (VHL) tumor suppressor gene. VHL has a crucial role in renal cell carcinoma as patients with mutations in the VHL gene are likely to develop this malignancy (Section 1.2 and Figure 1.4). Other important regulators include various oncogenes such as p53 or transcription factors [**17**].

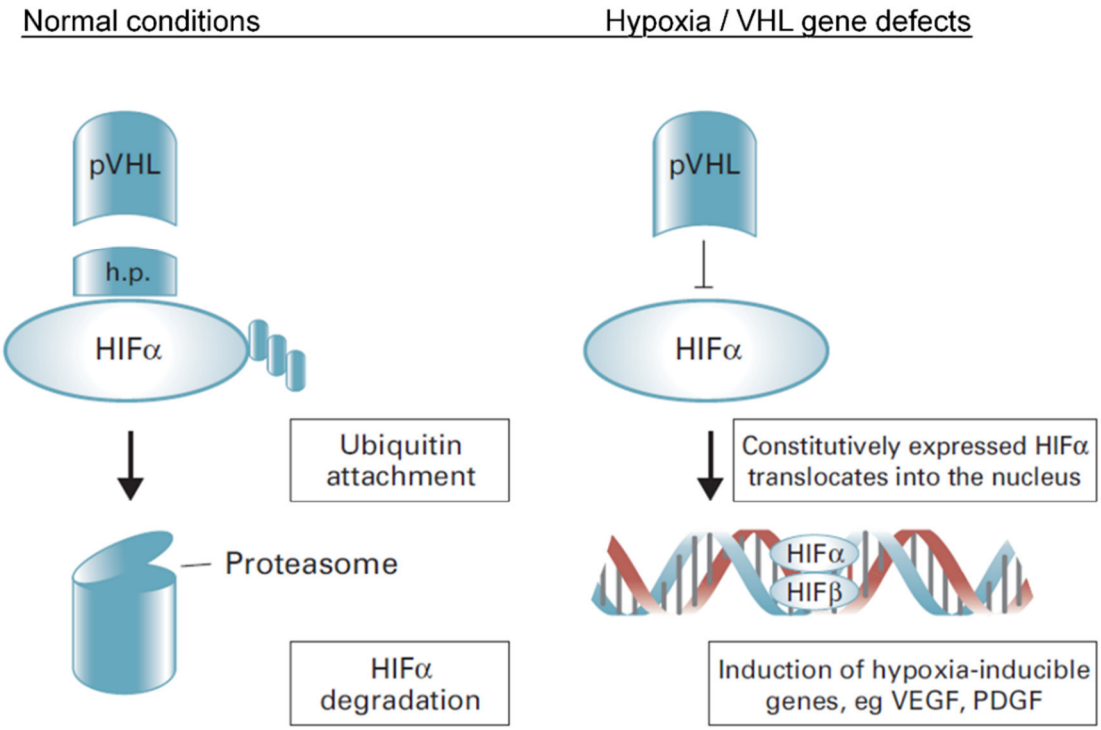

Fig. 1.4: Effects of the VHL gene product on angiogenesis under normal conditions and in case of hypoxia (modified from [**18**]).
HIF = Hypoxia-inducible factor, VHL = Von Hippel-Lindau, PDGF = Platelet-derived growth factor, VEGF = Vascular endothelial growth factor

Soluble VEGF receptors

Soluble forms of all three VEGF receptors have been identified, however their exact physiological function is not yet fully understood [**22**–**24**]. In general, these soluble receptors are able to bind VEGF and its variants to a comparable degree or with an even higher affinity as the membrane-bound forms. This led to the assumption that sVEGF receptors fulfill regulative tasks in angio- and lymphangiogenesis. Among all three soluble receptors sVEGFR-1 is the best investigated. It could be shown that it has crucial physiological roles in e.g. embryogenesis and corneal avascularity and is also involved in numerous pathological processes, such as the development of preeclampsia during pregnancy [**25**,**26**]. Interestingly, one of the main functions of the soluble isoform of VEGFR-2 seems to be the regulation of lymphangiogenesis as a splice variant is binding VEGF-C with a high affinity [**27**]. sVEGFR-2 has been investigated in various tumor entities regarding its role in cancer development and during angiogenesis. In this context, it was also observed that sVEGFR-2 plasma concentrations are downregulated as reaction to antiangiogenic therapies [**24**,**28**]. The important role of sVEGFR-3 in corneal alymphaticity suggests regulatory functions in lymphangiogenesis [**29**]. Similar to sVEGFR-2, sVEGFR-3 plasma concentrations decrease under antiangiogenic treatment and are therefore heavily investigated as potential biomarkers for therapies targeting the VEGF pathway [**30**–**32**].

Drugs targeting tumor angiogenesis

In 2004, bevacizumab (Avastin®, Roche), the first drug in the class of angiogenesis inhibitors, was authorized by the FDA for treatment of colorectal cancer patients. Bevacizumab targets VEGF-A which is an important mediator in the VEGF pathway (as described above). However, bevacizumab is usually applied in addition to conventional cytotoxic drugs, depending on the indication [**33**]. A distinct feature of bevacizumab is an increased efficacy in glioblastoma patients when applied as single agent, which led to the approval for this indication in 2009 by the FDA [**34**]. In the years thereafter several drugs with different targets in the VEGF pathway were approved. One of the more important subclasses of antiangiogenic treatments are the multi-tyrosine kinase inhibitors (TKI). While imatinib (Glivec®) is considered as the first TKI, the first drug specifically targeting VEGFR-1 and 2 was sorafenib (Nexavar®) in 2006 [**35**,**36**]. Sorafenib was shortly followed by several other VEGF-specific TKI including

sunitinib and pazopanib, which are described in more detail later (Sections 1.1.3 and 1.1.4).

Another important class of angiogenesis inhibitors include the “mammalian target of rapamycin” (mTOR) -inhibitors everolimus (Afinitor®) and temsirolimus (Torisel®) [**37**]. The mTOR is a serine/threonine kinase with a crucial regulative role for cell growth, proliferation and also angiogenesis [**38**]. By inhibition of the mTOR complex 1 (mTORC1) (Figure 1.7) the transcription and translation of several proteins important for cell proliferation is hindered. Of particular importance is the decreased translation of HIF-1α resulting in lower VEGF plasma levels and consequently to an impaired angiogenesis [**38**,**39**].

Adverse events associated with antiangiogenic treatment

Whereas antiangiogenic agents in general have moderate toxicity compared to most conventional cytotoxic drugs, angiogenesis inhibition can still result in therapy-limiting adverse events.

Hypertension is one of the most often reported adverse events under antiangiogenic treatment [**40**–**43**]. Mechanistically, increased blood pressure is a result of reduced vasodilatation as VEGF triggers the release of NO and prostaglandin I2 (PGI2) under normal conditions. Additionally an effect on baroreceptors is discussed since it could be shown in animal experiments that an infusion with VEGF reduces the relevant signaling pathways resulting in a decreased blood pressure. However, the mechanism of this effect is still unknown. A long-term consequence of angiogenesis inhibition is the density reduction of smaller vessels and capillaries (“rarefaction”) which can also lead to hypertension due to increased vascular resistance [**44**]. In a more recent study in patients treated with sunitinib, increased levels of the highly potent vasoconstrictor endothelin-1 were observed, which may contribute to the increase of blood pressure [**45**].

Hematologic toxicity such as anemia, leukopenia or thrombocytopenia is commonly observed in sunitinib patients and, with a lower frequency, also in pazopanib and sorafenib treated patients [**36**,**46**,**47**]. The exact mechanism of these adverse events is not known. However, as VEGF receptors are commonly expressed on hematopoietic progenitor cells inhibition of these might prevent the maturation process [**44**,**48**].

Kumar *et al.* investigated the different kinase selectivity of sunitinib, pazopanib and sorafenib with the result that the latter ones show a lower activity against the KIT (stem cell factor)-receptor (cKIT) and Fms-like tyrosine kinase 3 (FLT-3). As both receptors are factors in the genesis of hematopoietic cells, this might serve as an explanation for the frequency disparity [**48**].

Hypothyroidism was reported by various studies as a common adverse event under sunitinib treatment independent of tumor entity [**49**,**50**]. In a review from 2011 by Wolter *et al.* three prospective clinical trials in renal cell carcinoma (RCC) patients treated with pazopanib were evaluated with respect to reported hypothyroidism. Here, the incidence was comparably low with only 4% (26 of 578 patients) [**51**]. Similarly, other TKI, such as sorafenib, show also lower rates of thyroid dysfunction compared to sunitinib [**52**,**53**]. In a meta-analysis from 2014 12 studies with patients treated with sunitinib, axitinib or cediranib were investigated. However, no statistically significant difference between sunitinib and cediranib regarding hypothyroidism incidence was found. A comparison between axitinib and sunitinib was not possible due to low patient numbers in the axitinib group [**54**]. As a result, the mechanism of TKI-induced thyroid dysfunction was mainly investigated for sunitinib. Though, the mode of action of this adverse event is not yet fully understood, direct toxic effects of sunitinib leading to shrinkage of thyroid tissue are amongst the most popular theories [**55**].

1.1.3 Sunitinib

Sunitinib was first authorized by the FDA and EMA in 2006 under the label Sutent® [**46**]. Initially, marketing authorization was granted for gastro-intestinal stroma tumors (GIST) as well as renal cell carcinomas. In a phase III study with 312 imatinib-resistant GIST patients it was shown that median time-to-progression (TTP) was significantly increased in patients treated with sunitinib (4 weeks on and 2 weeks off treatment) compared to placebo (26.6 weeks vs 6.4 weeks) [**56**]. Similar results were shown in the authorization study including 750 treatment-naïve patients with metastasized renal cell carcinoma (mRCC) receiving 50 mg sunitinib daily in a 4/2 schedule, with 4 weeks continuous dosing and two weeks off treatment. Median progression-free survival (PFS) was significantly increased compared to the standard treatment with interferon (IFN)-α (11.1 months vs 4.1 months) [**57**]. Since 2010 sunitinib is also approved for patients with non-resectable or metastasized pancreatic neuroendocrine tumors

(pNET) [**46**]. While in general more tolerated than conventional cytotoxic drugs sunitinib still may cause severe adverse events. As mentioned in Section 1.1.2 most common adverse events (1 in 10 patients) include, amongst others, hypertension, hypothyroidism, fatigue and myelosuppression [**46**].

Pharmacologically, sunitinib is an inhibitor of several receptor-tyrosine kinases which are associated with angiogenesis and the growth of metastases. Sunitinib inhibits platelet-derived growth factor (PDGF) receptor α and β, VEGF receptor 1-3, cKIT, FLT-3 receptor, colony stimulating factor 1 (CSF 1) receptor as well as the "rearranged during transfection" (RET) receptor [**46**,**58**].

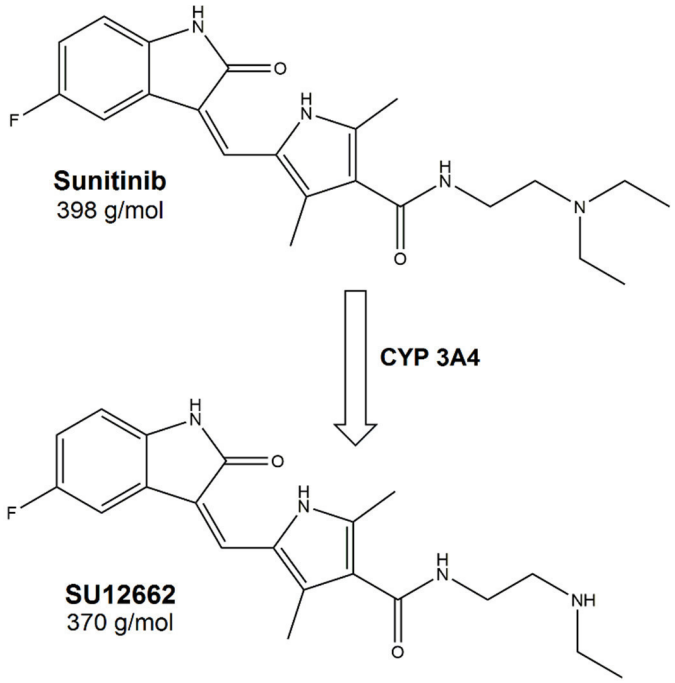

Fig. 1.5: Chemical structure of sunitinib and its active metabolite SU12662 with molecular weights. Sunitinib is a pyrrole class tyrosine kinase inhibitors. SU12662 is formed by oxidative elimination of one ethyl group.

As shown in Figure 1.5, sunitinib is primarily metabolized by cytochrome P450 3A4 which leads to the active metabolite N-desethyl-sunitinib (SU12662). The metabolite shows similar pharmacodynamic and pharmacokinetic effects and is responsible for 23 to 27% of total drug exposure. The volume of distribution is about 2230 L, the elimination half-life approximately 40 to 60 h for sunitinib and 80 to 110 h for the active metabolite. Plasma protein binding is reported with 95% for sunitinib and 90% for

SU12662, respectively. With 50 to 72% feces is the main route of excretion for sunitinib, while up to 20% can be found in urine [**46**,**59**].

As mentioned above, sunitinib is usually administered once daily in cycles of 6 weeks with 4 weeks on and 2 weeks off treatment. Depending on the indication the dose varies between 25 and 50 mg daily [**46**]. Although other regimens such as a 2/1 or continuous treatments were tested in smaller studies, there is still no evidence of a superiority compared to the standard schedule. However, Kalra *et al.* pointed out that no valuable studies which directly compared different schedules except a comparison between the classical 4/2 scheme and continuously dosing are available. Here, only a small benefit with respect to toxicity could be observed [**60**].

1.1.4 Pazopanib

Marketing authorization for pazopanib was granted in the United States in 2009 followed by a European-wide approval by the EMA in 2010. Besides first-line therapy for advanced RCC pazopanib is also indicated in soft tissue sarcomas [**47**]. In the authorization study for mRCC with 435 patients it could be shown, that pazopanib improved progression-free survival compared to placebo significantly (median PFS: 9.2 vs 4.2 months) when applied in a dose of 800 mg continuously. Furthermore, a subgroup analysis revealed, that also patients pretreated with cytokines can benefit compared to placebo (median PFS: 7.4 vs 4.2 months) [**61**]. For pretreated metastatic soft-tissue sarcoma, 372 patients randomized to a pazopanib and a placebo group were compared in a phase III trial. Median PFS was significantly higher under daily administration of 800 mg pazopanib compared to placebo (median PFS: 4.6 vs 1.6 months) [**62**]. Most common adverse events under pazopanib treatment include hypertension, myelosuppression and fatigue [**47**].

The pharmacological properties of pazopanib are comparable with sunitinib: as an oral multi-tyrosine kinase inhibitor pazopanib targets VEGF receptor -1, -2 and -3, PDGFR-α and -β as well as c-KIT.

Pazopanib is primarily metabolized by CYP3A4 and partly by CYP1A2 and CYP2C8. There are 4 metabolites which only contribute for 6% of the overall exposure. In-vivo binding to human plasma proteins is higher than 99% which results in a low volume of

distribution. Excretion is primarily via feces with renal elimination accounting for only < 4%. The elimination half-life is stated with 30.9 h [**47**,**59**].

Oral absorption of pazopanib is most likely limited by solubility as doses above 800 mg do not lead to a proportional increase in steady-state concentrations [**63**]. However, it was shown that crushing the tablet before administration can increase rate and extent of absorption [**64**]. Furthermore, pazopanib bioavailability is dependent on food intake: compared to fasted state fed condition increases the area under the plasma concentration-time curve (AUC) and the maximum observed plasma concentration (C_{max}) by almost two-fold. A difference between high or low-fat meals was not observed [**65**].

In contrast to sunitinib the normal dosing schedule does not include a treatment-free interval and it is applied continuously in doses ranging between 400 mg and 800 mg on a daily basis [**47**]. The chemical structure of pazopanib is shown in Figure 1.6.

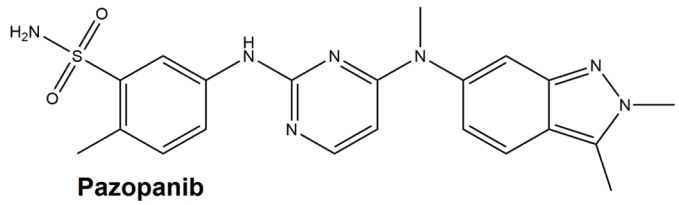

Pazopanib
438 g/mol

Fig. 1.6: Chemical structure of pazopanib with molecular weight.
Pazopanib belongs to the pyrimidine class tyrosine kinase inhibitors.

1.2 Metastasized renal cell carcinoma

1.2.1 Definition and classification

Kidney cancer of any type is currently the 12th most common cancer worldwide with 337 860 new cases in 2012 [**66**]. Renal cell carcinomas (RCC) account for over 90% of all renal malignancies [**67**]. However, incidences highly vary between gender and age groups. Of all new cases in 2012 46.8% were registered in patients above 65 years [**66**]. When considering genders separately males are more affected than females at a ratio of almost 2:1 (63.3% vs 36.7%). Furthermore, differences between nations and ethnicities can be observed, as most cases occur in well-developed countries, mainly North America and Europe. This is in accordance with life-style related risk factors,

which include, amongst others, obesity, smoking and hypertension [**67**–**69**]. Beside these extrinsic aspects, several hereditary and genetic risk factors have been identified [**69**].

The World Health Organization (WHO) classification of RCCs differentiates between numerous histological subtypes [**70**]: most common are clear-cell, papillary and chromophobe entities. Clear cell carcinomas (ccRCC) account for the majority of all RCCs (70 – 80%). Usually ccRCC arise sporadic, though genetic dispositions such as the VHL disease can trigger the development of carcinomas (Figure 1.4). As a consequence the incidence of certain tumor types is increased in these patients. Seemingly VHL plays also an important role in non-hereditary malignancies as 18-82% of all sporadic ccRCC show somatic mutations in the VHL gene [**71**].

Beside pathological differences, the defined RCC subtype provides value as prognostic marker. Patients diagnosed with ccRCC seem to have a significantly worse prognosis compared to the other two subtypes [**18**,**67**,**71**].

1.2.2 Treatment options

Localized renal cell carcinomas are best treated with surgical interventions. The newest guideline suggests that nephron-sparing surgeries provide the same benefit for the patients as radical nephrectomies. However, in mRCC cytoreductive surgeries are no longer curative and have, in most cases, only palliative use [**67**,**68**].

Conventional chemotherapies show only moderate to no effect in mRCC patients. The only agent of this category which is still mentioned in the guidelines is fluorouracil in combination with interleukin-2. Until the first antiangiogenic treatments emerged, immunotherapy using interferon-α or interleukin-2 was the gold standard. Nowadays these agents are rarely used, as the risk-benefit balance and response rates are worse than those of modern targeted therapy. The decision which agent to use as initial treatment was usually based on the so called Memorial Sloan Kettering Cancer Center (MSKCC) score, which includes the Karnofsky performance score, hemoglobin, calcium (corrected), time of diagnosis until first-line therapy and LDH [**67**,**68**]. As this score was developed when patients were treated mainly with immunotherapy, a validated score was needed for the newer targeted agents. This is available with the Heng Score [**72**]. A comparison of both scores is shown in Table 1.1.

Tab. 1.1: Comparison between MSKCC and Heng Score [**73**]

MSKCC Score	Heng Score
– Karnofsky-Score < 80%	– Karnofsky-Score < 80%
– Hemoglobin < reference value	– Hemoglobin < reference value
– Calcium[1] > 10 mg/dL	– Calcium* > 10 mg/dL
– Time from diagnosis to therapy < 12 month	– Time from diagnosis to therapy < 12 month
– LDH > 1.5 fold increase compared to reference value	– Neutrophilic granulocytes > reference value
	– Thrombocytes > reference value

[1]Corrected for serum albumin

Each risk factor accounts for one point, if the criteria is fulfilled. Dependent on the number of points the patient can be assigned to a risk group: favorable (0 points), intermediate (1-2 points) or poor (3-6 points). This stratification is then used for therapy choice.

Second- and third-line therapies are then chosen based on the previous treatment option. For instance, patients who received a TKI as first-line therapy are usually treated with nivolumab or cabozantinib. Second choice are the TKIs axitinib and sorafenib as well as the mTOR inhibitor everolimus. On the other hand a first-line therapy with immunological agents qualifies for a second-line with the TKIs axitinib, sorafenib or pazopanib. An overview of the respective targets of all relevant targeted agents is given in Figure 1.7.

Pazopanib versus Sunitinib

Both agents are indicated for first-line therapy of mRCC and their efficacy seems to be largely equivalent. In a phase IV study with 1110 clear cell mRCC patients it was shown that PFS was comparable between both drugs when administered in their standard regimen and that pazopanib is non-inferior to sunitinib (Hazard ratio (HR): 1.05; Confidence interval (CI) 90%: 0.9 – 1.22). With respect to adverse events pazopanib proved to be superior to sunitinib with lower incidences of fatigue (63% vs 55%), hand-foot syndrome (50% vs 29%) and thrombocytopenia (78% vs 41%) [**74**]. The so called PISCES study investigated patient-reported outcomes in a double-blind, cross-over

approach using health-related quality of life as endpoint. Patients were either treated with pazopanib or sunitinib for 10 weeks followed by a two weeks wash-out period and the switched consecutive treatment for another 10 weeks. In the final intention-to-treat analysis 114 of 169 initially recruited mRCC patients were considered. Here, 70% preferred pazopanib over sunitinib. Patients' preference was mainly influenced by a higher overall quality of life and decreased incidence of adverse events in the pazopanib group [**75**].

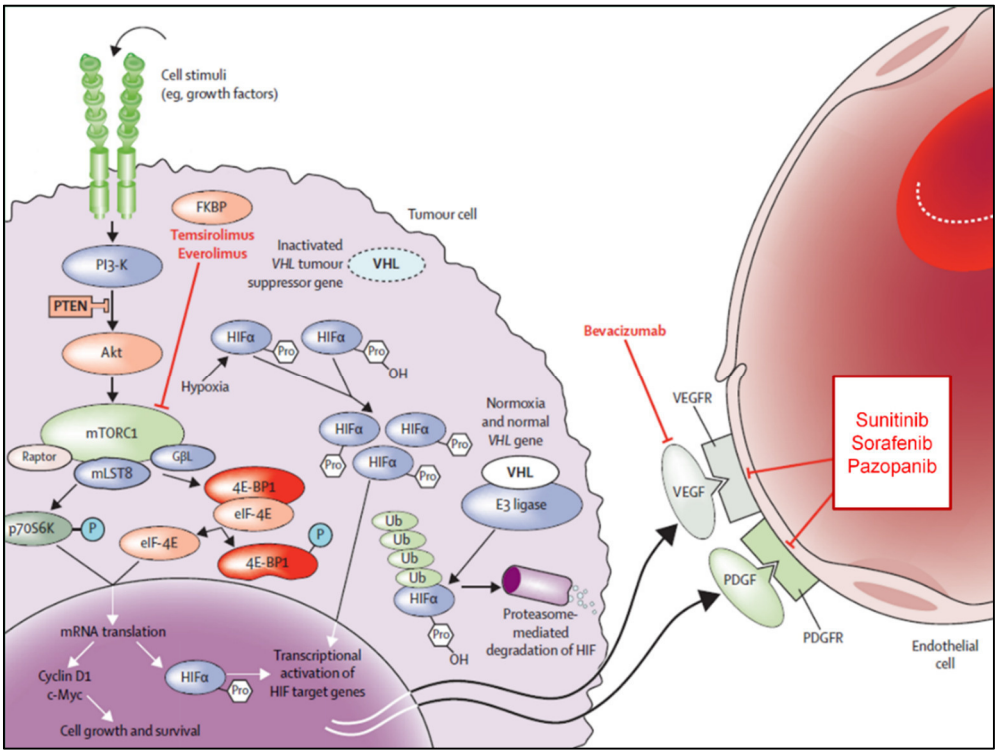

Fig. 1.7: Relevant therapeutic pathways and targets in renal cell carcinoma (modified from [**18**]).
HIF = Hypoxia inducible factor, VHL = Von Hippel-Lindau, PDGF(R) = Platelet derived growth factor (receptor), VEGF(R) = Vascular endothelial growth factor (receptor)

1.3 Biomarkers

1.3.1 Definitions and general considerations

According to the NCI a biomarker is defined as "*a biological molecule found in blood, other body fluids, or tissues that is a sign of a normal or abnormal process, or condition or disease. A biomarker may be used to see how well the body responds to a treatment*

for a disease or condition." [**4**]. The "Biomarkers Definitions Working Group" provides a slightly broader definition and includes all objectively quantifiable characteristics which can be used as "*an indicator of normal biological processes, pathogenic processes, or pharmacological responses to a therapeutic intervention*" [**76**].

Medical biomarkers can be further categorized depending on the type of application. A *diagnostic* biomarker is used for a more detailed diagnosis and discrimination of subtypes of a specific disease e.g. a tumor types. *Prognostic* biomarkers provide information on the outcome of a disease independent of treatment, while a *predictive* marker is usually used to estimate the therapy outcome for a patient [**76**]. Under certain circumstances biomarkers can serve as surrogate for clinical endpoints. Per definition all surrogate endpoints are biomarkers, but not all biomarkers are surrogate endpoints. A surrogate endpoint is therefore a biomarker allowing to draw conclusions on a clinical endpoint e.g. survival [**4**,**76**]. Surrogate endpoints are of great value for clinical drug development as they often allow faster approval and reduced time and cost expenses. Between 2008 and 2012, 56 cancer drugs were approved by the FDA with 36 (67%) using a surrogate endpoint in the authorization studies [**77**].

1.3.2 Biomarkers for cancer treatments

While targeted drugs are a major improvement over the previously used cytotoxic therapies, the decision which agent or dose might provide the most benefit for the individual patient is still mostly based on empirical knowledge. Up to now there are only few valuable objective methods to differentiate non-responders from responders for certain targeted therapies. Hence, considerable effort has been put in the search for predictive biomarkers. Of particular interest is the genetic profile of the patient and the tumor.

Pharmacogenetics and pharmacogenomics are often interchangeably used as there is no universally accepted definition; however, the term pharmacogenetics is mostly applied to describe the differences in drug effects among individual patients with respect to the presence of different gene variants in form of single nucleotide polymorphisms (SNPs). In contrast, the focus of pharmacogenomics is the so called *compound variability*. Particularly, this means the investigation of drug effects on gene expression and their usage for drug discovery [**78**]. Currently, there are only few

examples for pharmacogenetically-guided therapy decisions in cancer treatment, the most prominent one being the monoclonal antibody trastuzumab (Herceptin®, Roche). Trastuzumab is directed against the human epidermal growth factor receptor 2 (HER2) and highly effective in breast cancer patients with a HER2 overexpression in combination with chemotherapy. Hence, determination of the HER2 genotype prior to therapy start is obligatory [**79**,**80**]. At present, the FDA lists 204 drugs with pharmacogenetics biomarkers in drug labeling with 71 only in the field of oncology. However, most recommendations are not required and only optional which potentially hinders the implementation in clinical practice [**81**].

Beside genetic biomarkers, pharmacokinetic disposition (Section 1.4.3) or pharmacodynamic response to a drug are investigated for their predictive potential for efficacy or toxicity. In case of TKI there is already a wide spectrum of possible biomarkers. Most of them can be considered as TKI class effects which were or currently are investigated in various tumor types for their predictive performance. For instance, the plasma concentrations of sVEGFR-2 and -3, circulating endothelial cells and the increase of blood pressure which would all fulfill the criteria as easy-to-measure surrogates for efficacy or toxicity [**28**,**82**,**83**]. However, despite some promising results there is still no biomarker of this kind recommended for any angiogenesis inhibitor [**67**,**68**,**81**].

1.4 Pharmacometrics

1.4.1 General considerations

Pharmacometrics is an interdisciplinary field combining aspects of pharmacology with statistics and computer sciences. General aim of this discipline is to quantify the pharmacological response of a drug and to use the resulting mathematical models for further exploration and extrapolation [**84**]. Originally, pharmacometrics developed from the field of pharmacokinetics (PK) which can now be seen as the “fundament” of pharmacometric research. Pharmacokinetics itself deals with all processes involved in the fate of a drug once it is administered. These are often referred as LADME which is the abbreviation for **L**iberation, **A**bsorption, **D**istribution, **M**etabolism and **E**xcretion. In lay terms, this is explained as “*what the body does to the drug*” whereas pharmacodynamics (PD) describes “*what the drug does to the body*”. Pharmacokinetic

research usually consists of the analysis of plasma concentration-time data of a drug. Here, two basic methods can be used. In case of dense sampling, thus many informative data points, a non-compartmental analysis (NCA) is a feasible approach. In essence, a NCA is a statistical evaluation of the data without any prior assumptions. This allows the calculation of important pharmacokinetic parameters such as AUC, C_{max} and the drugs half-life [**85**]. However, if not enough data points are available this method becomes unreliable. Alternatively, a model-based analysis can be conducted. By choosing a mathematical model to describe the underlying data it is possible to generate reliable estimates of key pharmacokinetic parameters [**84**–**86**]. Similar principles apply for pharmacodynamic data analysis. Whereas a model-independent approach is also possible, model-based evaluations are far more common with often classical linear or E_{max} models as basis for dose-response relationships [**85**].

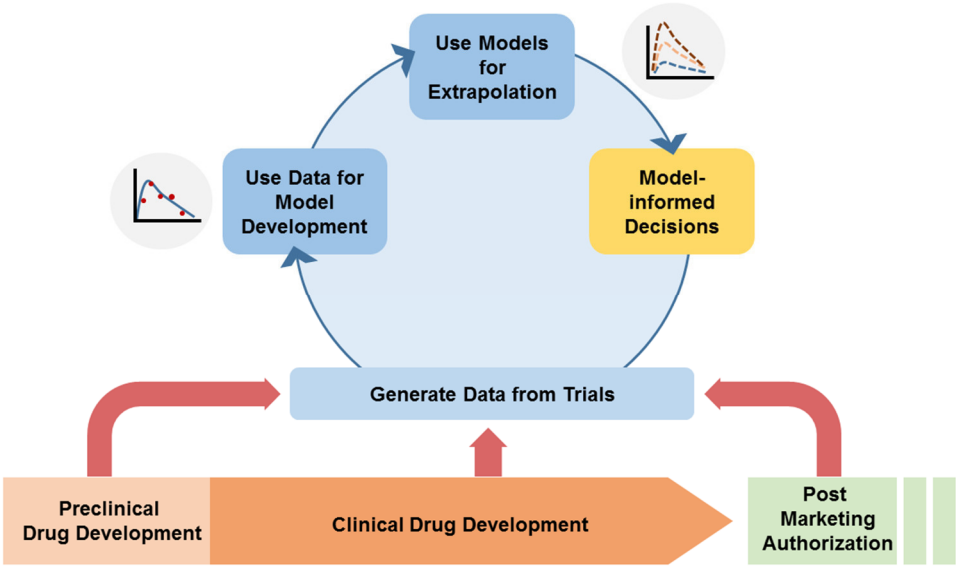

Fig. 1.8: General implementation of pharmacometric approaches in drug development.

However, these methods are limited to single or small cohorts of patients as each individual has to be evaluated separately. To overcome this limitation, population PK/PD is a common approach to analyze large patient groups and quantify inter-individual differences (Section 1.4.2). Another field that evolved from basic pharmacokinetics is the so called physiologically-based pharmacokinetics (PBPK). In contrast to population pharmacokinetics, where an appropriate model is chosen based

on the underlying data, PBPK models feature important physiological processes and include the physicochemical properties of the drug. Therefore PBPK is referred to as a “bottom-up” approach, while population PK/PD is a “top-down” analysis [**87**]. The general concept of pharmacometric analyses in drug development is presented in Figure 1.8.

1.4.2 Principles of population pharmacokinetics and –dynamics

The term population pharmacokinetics was originally established by Lewis Sheiner and Stuart Beal who are considered as pioneers in this field. The software package NONMEM® which they originally developed (**Non**-linear **M**ixed **E**ffects **m**odeling) is still the gold standard for population analysis pharmaceutical industry and academia [**88**]. A detailed methodological description can be found in Section 3.8.1.

Classical methods to cope with population pharmacokinetic data comprise the *naïve pooling* as well as the *two-stage* approach. Naïve pooling is the simplest method of, but also the least preferable, since the individual data from all patients is pooled and analyzed in one step. The result is a mean response without taking variability among patients into account. This method can be useful when the overall variability is small, for example in preclinical data from standardized animals [**84**]. The two-stage approach uses the individual estimates from each patient to calculate population parameters. In the first stage a pharmacokinetic model of choice is fitted to each individual’s data. From these data a population mean as well as a variance can be calculated for each parameter [**84**].

With non-linear mixed effects (NLME) models it is possible to analyze all patients in one step and to obtain mean population estimates of the PK/PD parameters of interest as well as the variability. This allows the evaluation of large data sets with sparse sampling without relying on separate individual estimations for each patient [**86**,**89**]. Population PK/PD models are not only useful for descriptive analyses, but may also allow extrapolation based on the underlying data to investigate e.g. dosing regimens which were not part of the original study. By linking PK/PD models with models for clinical outcome it is further possible to simulate whole clinical trials and use the results as guidance for study planning. This so called “model-informed drug development” can be applied to every phase of clinical (or pre-clinical) drug development and is gaining

importance in pharmaceutical industry [**90**,**91**]. Moreover, population PK/PD models can serve as basis for dose individualization and help identifying clinically relevant influential factors on PK and PD.

1.4.3 PK/PD dose individualization in oncology

The NCI defines *personalized medicine* as "*a form of medicine that uses information about a person's genes, proteins, and environment to prevent, diagnose, and treat disease. In cancer, personalized medicine uses specific information about a person's tumor to help diagnose, plan treatment, find out how well treatment is working, or make a prognosis*" [**4**]. Hence, dose individualization can be considered as a part of personalized treatment, as the best drug from a therapeutic perspective needs to be adapted to the inter-individual differences in pharmacokinetic and pharmacodynamic response of a patient.

For dose individualization it is therefore possible to target a pharmacokinetic parameter correlating with pharmacodynamics or, if feasible, by using a pharmacodynamic parameter.

Therapeutic drug monitoring

The term *therapeutic drug monitoring* (TDM) refers to a specific method of pharmacokinetic dose individualization. Here, the dose is adapted based on a pharmacokinetic target quantifying drug exposure in the patient, e.g. the plasma concentration or the area under the concentration-time curve (AUC) of a specific drug. More precisely, TDM is a pharmacokinetic dose adaption with feedback mechanism, as the target parameter is controlled in defined intervals over the course of the therapy. This allows a precise correction of the dose if needed. To keep the additional burden for the patients to a minimum only very few samples are collected for dose calculation [**92**]. This is possible due to the use of the so called Bayes method of conditional probability, which is implemented in almost all modern TDM software programs and is described in more detail in Section 3.8.4 [**93**]. Particularly, this means an existing pharmacokinetic model with known mean response and known variability is used to estimate individual parameters under the condition of a given pharmacokinetic target like the plasma concentration of the respective drug and other influential factors. The

individual parameters can then be used to simulate concentration-profiles and to optimize dose strength and interval.

As this method is quite costly and time-consuming, it is not viable for all drugs. Major requirements include a known quantitative relationship between pharmacokinetics and -dynamics, a narrow therapeutic index and a high inter- and intraindividual variability [**94**].

Applications in oncology

While the criteria for PK/PD dosing, more precisely TDM, are fulfilled by a lot of anticancer drugs, it is not a commonly used approach in oncology [**95**,**96**]. Although it has already been proved to have a weak correlation in most cases, body surface area (BSA) is still one of the most used parameters for dose adjustment of cytotoxic drugs. However, only 30% of inter-individual variability can be explained by BSA [**3**]. Prominent examples of anticancer drugs where pharmacokinetic methods for dose adaptations are used include carboplatin and fluorouracil (5-FU). For carboplatin an empirical formula can be used for dose calculation which relies on the estimated creatinine clearance and a defined target AUC [**97**]. However, the platinum plasma concentration or AUC is usually not measured to control for an adequate dosing so that the feedback control of a TDM is missing. 5-FU is applied via continuous infusion. Because of the short elimination half-life of 10 to 20 minutes, the AUC can be calculated with a simple formula, often referred to as “rectangle” – equation due to the shape of the concentration-time curve of 5-FU. Based on predefined algorithms a percentage dose increase or decrease can be chosen with respect to the calculated AUC value [**98**]. Despite some promising results, a TDM for 5-FU is usually not performed in clinical practice.

Modern targeted therapies are usually applied in fixed dose regimens with adaptions mostly based on the occurrence of certain adverse events. However, TKIs show large inter-individual variation in PK/PD parameters [**59**,**96**]. In addition, oral administration introduces several complications such as additional drug-drug or drug-food interactions, e.g. observed for pazopanib and sorafenib with increased drug exposure when taken after a meal. Oral therapies are also potentially prone to poor adherence, which is known from other medical fields, and can also be observed in targeted cancer

therapies [**96**,**99**]. Recent reviews summarized potential reasons for non-adherence in oral cancer therapies: among others the incidence of adverse events as well as duration of therapy were mentioned as crucial [**100**,**101**]. Both factors may be reduced with optimized and individualized treatments.

1.5 Outcome analysis

1.5.1 Survival analysis

Main purpose of every cancer treatment is to maximize the survival of the patient while maintaining a certain degree of quality of life. In general, survival analysis in oncology differentiates between two types of clinical endpoint: overall survival (OS) and progression-free survival (PFS). OS comprises the period from treatment start until the patient's death regardless of the cause. In contrast, PFS includes the time until disease progression [**4**]. PFS is often used as main endpoint, especially in pivotal phase III studies, as it allows shorter observation times and is usually a good predictor for OS [99]. Furthermore, with the emergence of sequential therapies in almost all fields of oncology, the value a drug cannot be assessed by the OS when second and third-line therapies may vary among patients [**102**].

One classical and common non-parametric method is the Kaplan-Meier analysis, which was already developed in 1958 by two biostatisticians Edward Kaplan and Paul Meier. The Kaplan-Meier analysis solves a problem which is frequent in survival data: patients dropping out of the study or undefined reasons before the endpoint or the end of the study is achieved, so called *right-censored data* [**103**]. The patients affected are not removed from the analysis but included in the calculation of the results. Another important method was introduced by David Cox in 1972. While two or more groups can be compared with the Kaplan-Meier method using the log-rank test, it is not possible to test continuous or time-dependent influence factors. This was enabled by the Cox regression model allowing the calculation of the probability per time unit that an event occurs in a patient using the so-called hazard function [**103**]. Model-based time-to-event (TTE) analysis can be considered as the evolution of the Cox regression model. By linking PK/PD models with an outcome model it is possible to quantify the effects of a therapeutic intervention and to estimate their variability [**104**]. Ideally, such a model can be used to simulate clinical set-ups of interest or do discriminate between

responders or non-responders (see Section 3.11. for a more detailed description of the methodology).

1.5.2 Toxicity analysis

Management of toxic effects caused by anticancer treatments has always been one key intervention to the success of a therapy. In the worst case, adverse events can lead to therapy failure and, depending on severity, cause permanent damage or death. However, the strength of an adverse event is not easily determined, especially when no objective parameter, e.g. laboratory values, can be measured or the patients themselves have to rate it based on scales or questionnaires. In most cases this automatically leads to a bias either introduced by the physician or the patient. In oncology, toxicity is evaluated by the so called Common Terminology Criteria for Adverse Events (CTCAE) [**105**]. This scale orders toxicity into five categories ranging from grade 1 (mild) to grade 5 (death). A more detailed description of all grades is presented in Table 1.2.

Tab 1.2: Toxicity grades according to CTCAE v 4.03 [**105**]

Grade	Description
1	Mild; asymptomatic or mild symptoms
2	Moderate; minimal, local or noninvasive intervention indicated
3	Severe or medically significant but not immediately life-threatening
4	Life threatening consequences
5	Death related to adverse events

While grading allows a better comparability across patients it is also associated with a loss of information. This is of particular importance, when the grade of an adverse event is included in the dose adaption algorithm as it has been tested for 5-FU [**98**]. Similar to model-based survival analysis, models for adverse events can help to quantify the relationship between drug exposition and toxic response, and to identify influential factors across populations. Although this is possible by analogous TTE approaches, where an event is defined as the occurrence of an adverse event, semi-mechanistic models are more common. A good example is the model for

chemotherapy-induced myelosuppression allowing a prediction of the extent of myelosuppression independent of the drug used [**106**]. As the authors stated this model could be used for either drug development or to determine the effect of different dosage strategies (Figure 1.9).

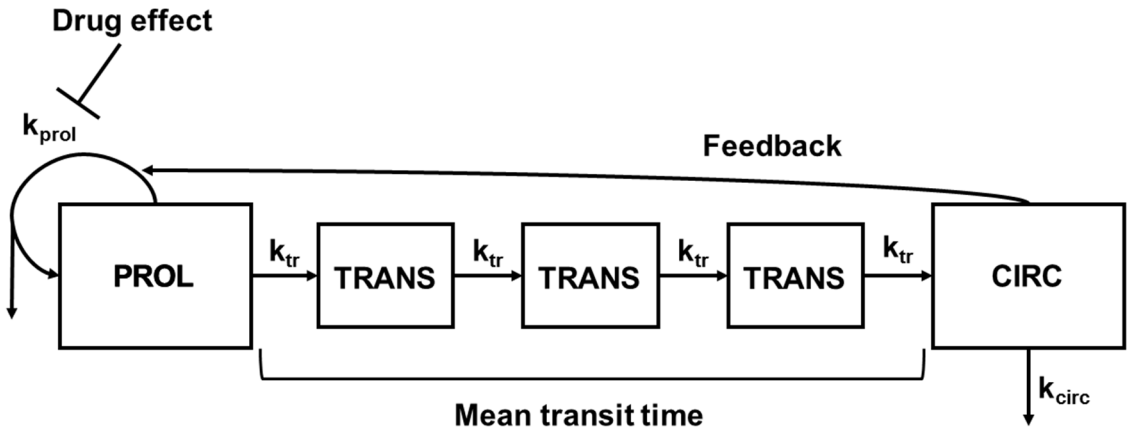

Fig. 1.9.: Semi-mechanistic model for chemotherapy-induced myelosuppression by Friberg *et al.* (modified from [**106**]). Compartments represent the different states of neutrophils: Drug effect and a feedback effect regulate cell proliferation.
PROL = proliferating cells, CIRC = circulating cells, TRANS = intermediate progenitor cells, k_{tr}, k_{prol}, k_{circ} = rate constants between different states.

While this approach is highly informative, it is not applicable for all types of toxicity as either the required data is not available or, as stated above, no objectively quantifiable parameter exists. Hence, alternative methods are being approached. The most promising is the use of Markov models which is already established in other fields of science. Markov models can make use of categorical data by estimating the probability of developing an adverse event of a certain CTCAE grade based on the current state (see Section 3.11.4. for a more detailed description of the methodology). One of the first pharmacometric applications of Markov models was performed by Karlsson *et al.,* who modeled the probability of different sleep states during temazepam therapy [**107**]. In a more recent investigation Markov models have been successfully integrated in a modeling framework for lung cancer patients treated with erlotinib [**108**].

2 AIMS AND OBJECTIVES

Pharmacometric approaches have the potential to individualize and guide anticancer therapies. However, the multi-tyrosine kinase inhibitors (TKI) pazopanib and suntinib, which are common first-line therapies in patients with metastasized renal cell carcinoma (mRCC), are still applied in fixed-dose regimens. Thus, the inter-individual variability of drug exposure may be responsible for differences in response or toxicity. The development of more rational dosing strategies based on pharmacokinetic and pharmacodynamic (PK/PD) models is therefore a promising strategy to optimize mRCC treatment.

Aim of this work was to develop pharmacometric models for sunitinib and pazopanib and to integrate them into a greater modeling framework for mRCC patients (Figure 2.1). Pharmacokinetics of both TKIs were linked to a pharmacodynamic response such as plasma concentration of sVEGFR-2, sVEGFR-3 or blood pressure. In a final step the established models were linked to models for clinical outcome, in particular progression-free survival and toxicity, to explore the potential relationships.

Data for sunitinib-treated mCRC patients as well as healthy volunteers was already available from a previous study. Therefore, a first step was to generate similar data for mRCC patients. This was done within the EuroTARGET project, which aimed to identify predictive biomarkers in mRCC using a diverse range of state-of-the-art methods.

In case of sunitinib, a pharmacokinetic model for the parent drug and its active metabolite SU12662, which was based on data from healthy volunteers by Lindauer *et al.* [**109**], served as basis for model development. This model was compared to another published semi-mechanistic model by Yu *et al.* [**110**]. For pazopanib, no internally developed model was available; hence a literature research was conducted to identify suitable pharmacokinetic models. The pharmacodynamic models for sVEGFR-2, sVEGFR-3 and blood pressure developed for healthy volunteers by Lindauer *et al.* were adapted to cancer patients and linked to the respective pharmacokinetic models.

The developed models for both substances were then used to estimate individual pharmacokinetic and pharmacodynamic parameters. Based on these findings outcome models were established to explore the relationship between pharmacokinetics, biomarker response and the endpoints progression-free survival and toxicity. In

particular, a time-to-event (TTE) model was developed to describe the patients' progression-free survival during first line-therapy with sunitinib or pazopanib, whereas toxicity was integrated into the modeling framework with a Markovian approach and, in case of blood pressure, with a semi-mechanistic model.

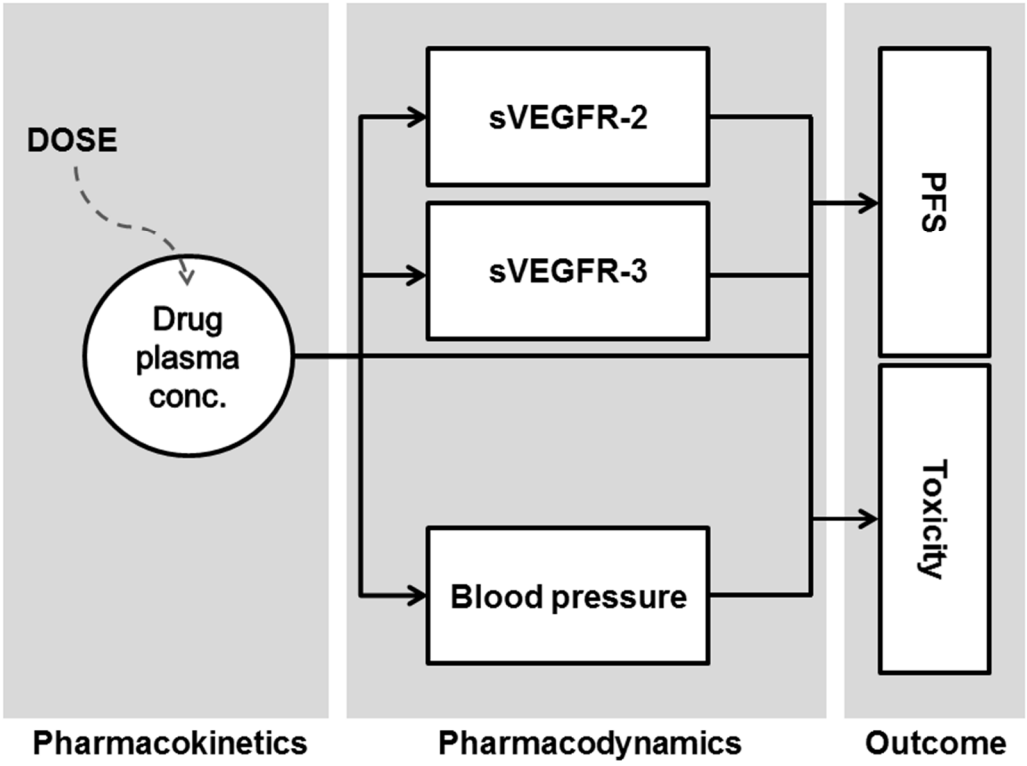

Fig. 2.1: Scheme of a PK/PD modeling framework for sunitinib and pazopanib. Conc. = Concentration, PFS = Progression-free survival; sVEGFR = soluble vascular endothelial growth factor receptor

3 MATERIAL AND METHODS

3.1 Materials

Relevant material used for the underlying analytical methods as well as the technical equipment and software packages used for modeling and simulation activities is summarized in Tables 3.1. to 3.4.

3.1.1 Chemical substances and reagents

Tab. 3.1: ELISA Kits and related reagents

Name	Company
Human VEGF R2/KDR Quantikine® ELISA Kit Catalog Number : SVR200 *Contains:* – VEGF R2 Microplate – VEGF R2 Conjugate – VEGF R2 Standard – Assay Diluent RD1W – Cell Lysis Buffer 2 – Calibrator Diluent RD6-31 – Wash Buffer Concentrate – Color Reagent A (Hydrogen peroxide) – Color Reagent B (Tetramethylbenzidine) – Stop solution (N sulfuric acid) – Plate sealers	R&D Systems, Minneapolis, USA
Human sVEGF R3/Flt-4 DuoSet® ELISA Catalog Number: DY349 *Contains:* – Capture Antibody – Detection Antibody – Standard sVEGF R3 (Flt-4) – Streptavidin-HRP	R&D Systems, Minneapolis, USA

Tab. 3.1 continuation	
DuoSet® Ancillary Reagent Kit 2 Catalog Number: DY008 Contains: – ELISA Plate-Coating Buffer – Reagent Diluent Concentrate 2 – Stop Solution – Color Reagent A (Hydrogen peroxide) – Color Reagent B (Tetramethylbenzidine) – Wash Buffer Concentrate – Clear Microplates – ELISA Plate Sealers	R&D Systems, Minneapolis, USA
CrossDown® Buffer	Appli Chem, Darmstadt
Fetal Calf Serum (FCD)	Sigma-Aldrich, St. Louis, USA
PURELAB® Plus Water	ELGA Berkefeld GmbH
Sodium Chloride (NaCl)	-
Potassium Chloride (KCl)	-
Biphasic Hydrated Sodium Phosphate (Na_2HPO_4)	-
Potassium Dihydrogen Phosphate (KH_2PO_4)	-

3.1.2 Solutions and Buffer

Tab. 3.2: Overview on solutions and buffers used and their composition

Constituent	
Phosphate buffered saline (PBS buffer)	
137 mM NaCl	8.0 g
2.7 mM KCl	0.2 g
8.1 mM Na2HPO4	1.15 g
1.5 mM KH2PO4	0.204 g
PURELAB® Plus Water	Ad 1000 mL
pH 7.2 – 7.4	
sterile-filtered with a 0.2 µm filter	

Tab. 3.2 continuation	
Reagent Diluent (1:10)	
Reagent Diluent Concentrate 2	1 P
PURELAB® Plus Water	9 P
Substrate Solution (1:1)	
Color Reagent A	1 P
Color Reagent B	1 P
Wash Buffer Dilution (1:25)	
Wash Buffer Concentrate	20 mL
PURELAB® Plus Water	Ad 500 mL
Capture Antibody Dilution	-
Detection Antibody Solution	-
Streptavidin-HRP	-

3.1.3 Consumables

Tab. 3.3: Consumables for one-time usage

Name	Company
Sarstedt K-Monovetten®	Sarstedt AG & Co, Nümbrecht
Micro tubes 1.5 mL (lightprotected)	Sarstedt AG & Co, Nümbrecht
Pipettes and glass vessels	-
Pipette tips	Greiner Labortechnik, Frickenhausen

3.1.4 Technical Equipment

Tab. 3.4: Technical equipment used for drug and biomarker analysis

Name	Company
Single-channel pipette E4 XLS (10 – 100 µL, 100 – 1000 µL)	Mettler Toledo GmbH, Gießen
Multi-channel pipette (12 channels) Transferpette® (10 – 100 µL, 30 – 300 µL)	Brand GmbH & Co KG, Wertheim

Tab. 3.4 continuation	
accu-jet® pro pipette controller	Brand GmbH & Co KG, Wertheim
Vortex-Mixer ZXE3	Velp Scientifica srl, Usmate (MP), Italien
Edmund Bühler® TH 15l Incubator	Edmund Bühler GmbH Lab Tec, Hechingen
Unimax® 1010 shaker	Heidolph Instruments GmbH & Co KG, Schwabach
Multiscan® EX Multiwellreader *Quartz-Wolfram halogen lamp (450 nm, 570 nm)*	Thermo Electron Corporation, Vantaa, Finland

3.1.5 Software

Tab. 3.5: Software used for modeling and associated tasks

Name	Company/Authors
NONMEM® 7.3	Icon Development Solutions, Ellicott City, MD, USA
Pearl-speaks-NONMEM® (PsN) v4.4.8 and beyond	Mats Karlsson, Andrew Hooker, Rikard Nordgren, Kajsa Harling (2013-2015)
Pirana® v2.9.1 and beyond	Pirana Software & Consulting BV 2014
R v3.2.3 and beyond	R Foundation for Statistical Computing, Vienna, Austria
Including the packages:	
Xpose	Niclas Jonsson, Mats Karlsson (2014)
Lattice	Deepayan Sarkar (2016)
drc	Christia Ritz, Jens C. Streibig (2016)
reshape2	Hadley Wickham (2016)
survival	Terry M. Therneau (2016)
coin	Torsten Hothorn (2008)
ggplot2	Hadley Wickham (2009)
clinfun	Venkatraman E. Seshan (2016)
Microsoft Excel® 2007	Microsoft Corporation, Redmond, USA

NONMEM® [**88**] was used for the pharmacokinetic and pharmacodynamic data analysis. Pearl-speaks-NONMEM® (PsN) served as an additional toolbox for computationally intensive statistical methods including bootstraps, visual predictive checks (VPC) and case deletion diagnostics (CDD) for model qualification as well as stepwise covariate analysis [**111**]. Pirana® is a user interface developed for NONMEM® and was used to simplify model and data management [**112**].

Graphical analysis was primarily conducted using the statistical programming language R including various supplementary packages [**113**]. *Xpose* is a package specifically developed to process output from NONMEM and to generate plots for non-linear mixed effects models, e.g. Goodness-of-fit (GOF) plots and VPCs [**114**]. *Lattice* and *ggplot2* are packages for advanced graphics in R [**115**,**116**]. For dataset generation and management, the R package *reshape2* as well as Microsoft Excel® were used dependent on the specific task [**117**,**118**]. The package *drc* was used for generating standard curves for the biomarker analytics and calculating the respective results [**119**] Survival analyses were conducted using the *survival* package together with the *coin* and *clinfun* packages for the permutation tests [**120**–**122**].

3.1.6 Hardware

All modeling tasks were performed on an Intel i7® 4970 processor with 4 physical and 4 theoretical threads (*Hyperthreading*) on a Windows 64-Bit platform.

3.2 The EuroTARGET project

3.2.1 Objectives

EuroTARGET denotes for "*European collaborative project on Targeted therapy in Renal cell cancer: Genetic and Tumor-related biomarkers for response and toxicity*". The general aim was to identify and characterize host- and tumor-related predictive biomarkers for response to targeted therapy in patients with metastasized renal cell carcinoma (mRCC). For this purpose several state-of-the-art approaches were combined to generate as much information as possible on host- and tumor-specific factors which could potentially be predictive for therapy outcome.

Hence, the main aim can be further divided into several objectives, where each work package contributed results with different approaches and methodology. A complete description of the work packages can be found in Section 3.2.2, Figure 3.1 and Table 3.6.

The following list comprises all project objectives ordered according to the study protocol without assigning them to specific work packages or project partners:

- *Create a standardized European clinical databank and bio-repository (germline DNA of all patients and serum and frozen tumor tissue of a subgroup) of a large series of patients with mRCC treated with different targeted agents.*
- *Identify genetic markers for treatment response and toxicity by performing high-resolution germline whole-genome profiling in patients treated with sunitinib or sorafenib*
- *Identify exon and microRNA expression markers for treatment response and toxicity by gene expression profiling of tumors from patients with and without good response*
- *Identify kinase activity profiles related to TKI response*
- *Identify promoter hypermethylations markers in TKI response*
- *Identify resulting protein profiles corresponding to genomic, epigenetic and expression alterations related to TKI response*
- *Replicate all identified markers in independent patient series*
- *Study the functional relevance of replicated markers/networks in vitro by knock-out and knock-in transfection experiments*
- *Identify differentially expressed proteins before and after knock-down/ upregulation of genes of interest*
- *Identify plasma drug and metabolite levels as phenotype of results*
- *Explore the possibility of individualizing dosage regimens by integrating biomarker concentration – time profiles into PK/PD models for sunitinib (and pazopanib)*

- *Conduct integrated bioinformatical analyses of the results obtained by all different approaches in order to maximize the probability to find new markers and to understand the interrelatedness between them*
- *Construct new risk stratification criteria to be used for personalized mRCC patient management*
- *Disseminate the new knowledge to medical oncologists, urologists and the scientific community*

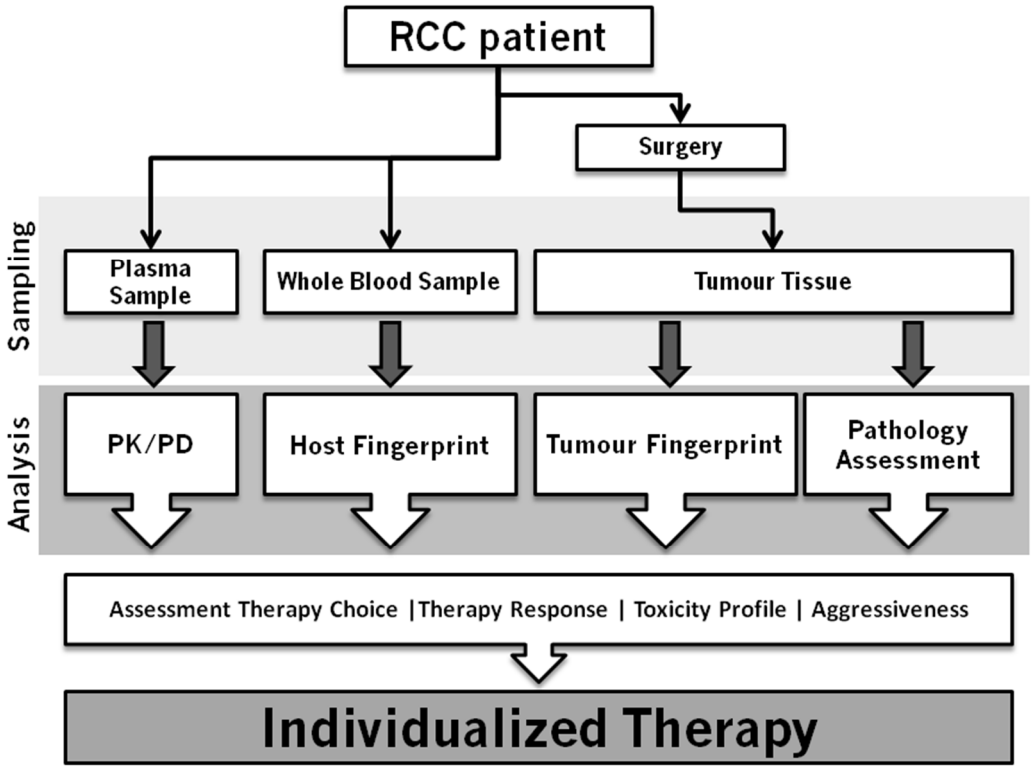

Fig. 3.1: General concept of the EuroTARGET project.

3.2.2 Project design and duration

The EuroTARGET project was designed as a European-wide non-interventional prospective cohort study with an overall duration of 5 years [**123**].

Based on their expertise, project partners were assigned to 12 different work packages with one partner taking supervision on all tasks of the respective package. An overview on all work packages, their main subjects and the responsible project partner can be found in Table 3.6. Focus of the underlying work were the results of work packages 2 and 7 in a subcohort of the EuroTARGET study population which was additionally

monitored over a defined period during the first-line therapy with sunitinib or pazopanib (Section 3.3). Therefore, methods used in other work packages are not explained here in detail as it would be beyond the scope of this thesis.

Design and methods of work packages 2 and 7 are addressed in the following paragraphs beginning with 3.3.

Tab. 3.6: Overview of EuroTARGET work packages

WP	Description	Lead participant
1	Retrospective and prospective collection of clinical data, genomic DNA and tumor tissue	University of Cambridge
2	Genetic profiling of mRCC patients	Leiden University Medical Center
3	Transcription profiling of tumor material from mRCC patients	Radboud University Medical Center, Nijmegen
4	Kinase activity profiling of mRCC	PamGene, s-Hertogenbosch
5	DNA methylation biomarkers of mRCC	Bellvitge Biomedical Research Institute, Barcelona
6	Functional studies	University Hospital Homburg/Saar
7	PK/PD studies (EuT-PK/PD substudy)	University of Bonn
8	Data management	deCODE Genetics, Reykjavik
9	Integrated data analysis	Netherlands Cancer Institute, Amsterdam
10	Dissemination and Training	Central European Society for Anticancer Drug Research, Vienna
11	Ethics	Institut national de santé et de la recherché médicale, Paris
12	Project Management	Radboud University medical Center, Nijmegen

WP = Work package

3.2.3 Patients

Patients were applicable for the EuroTARGET project if they were 18 and above years old, newly diagnosed with metastatic renal cell carcinoma and did not receive a treatment for their metastatic disease. Furthermore, patients had to be able to understand the patient information and to give informed consent. Recruitment was conducted in Germany, Austria, Switzerland, The Netherlands, United Kingdom, Iceland and Romania. Although the study was planned as prospective study, retrospective inclusion of patients was also possible under the requirement that at least one blood sample was available for germline analysis.

It was planned to include a total of 1100 patients. There was no intention to test a formal hypothesis. Hence, a sample size calculation was not conducted.

3.2.4 Medication

All possible targeted first-line therapies according to the recent guidelines for metastasized renal cell carcinoma were allowed. Since this study had a purely observational purpose, no dose or treatment recommendations were given.

3.2.5 Sampling procedure

Each patient was asked to donate 8-10 mL whole blood either collected in Lithium-Heparin or EDTA tubes for germline analysis. Blood samples were then stored at -20°C or, preferably, -80°C until analysis.

Tumor tissue was collected from each patient, if available. Fresh frozen tumor material stored at -80°C was preferable; however, paraffin blocks were also a valid option. All tumor samples were reviewed by a designated reference pathologist and then sent to the respective project partners for further analyses.

3.2.6 Endpoints

Progression-free survival (PFS) was chosen as primary endpoint with progression ideally defined with respect to the *Response Evaluation Criteria In Solid Tumors* (RECIST) [**124**]. Usually, the RECIST assessment is not part of the clinical routine;

hence, progression documented based on the treating physicians' expert opinion was also viable when no RECIST information was available.

Treatment toxicity was determined as secondary endpoint. Documentation was handled using the *Common Terminology Criteria for Adverse events* (CTCAE,v 4.03) [**105**]. Only adverse events with grade 3 or higher had to be captured in the electronic case report form (eCRF). However, low-grade toxicity could be documented indirectly, when it was the reason for a dose reduction of the drug.

3.3 The EuroTARGET-PK/PD (EuT-PKPD) sub-study

3.3.1 Objectives

The EuT-PKPD study was designed as a sub-study of the EuroTARGET project and comprised the work packages 2 and 7. Main objective was to develop pharmacokinetic and pharmacodynamic models by linking sunitinib and pazopanib plasma concentrations with biomarker response, here, sVEGFR-2/3 plasma concentrations and blood pressure. The final PK/PD models were then used to analyze correlations between individual pharmacokinetic disposition, pharmacodynamic response and clinical outcome, in particular progression-free survival and therapy-related toxicity.

In addition, several genotypes were preselected from the literature which have shown potential predictive performance or influence on pharmacokinetic, especially sunitinib, and pharmacodynamic parameters as well as outcome (Appendix **A**).

3.3.2 Study design

The study was conducted as a multi-centric, prospective, open-label, non-randomized single-arm phase IV trial. Unlike the main EuroTARGET project, it was not possible to keep this work package completely observational due to the legal requirements regarding the use of blood samples for pharmacokinetic analyses in Germany. Therefore, this work package was handled as a clinical phase IV study embedded in the overarching EuroTARGET project. As a consequence, all inclusion criteria for the observational EuroTARGET project also applied to sub-study patients in addition to the stricter criteria necessary for a phase IV study. To avoid recruitment errors "Participation in the EuroTARGET project" was added as an additional requirement for

inclusion in the phase IV sub-study. This ensured that only one study population was generated and that patients additionally participating in the sub-study were documented in the same eCRF as all other patients in the EuroTARGET project. However, additional paper CRFs were needed to document sampling times for pharmacokinetic samples, blood pressure measurements and adverse events below grade 3.

In total, 9 centers actively recruited patients for this sub-study. Seven were located in Germany and two in The Netherlands.

Study duration was limited to 18 weeks of treatment which corresponds to 3 regular sunitinib cycles. In this time frame all sub-study procedures had to be conducted. However, patients who completed the phase IV study remained in the non-interventional part of the EuroTARGET project and were observed for a minimum of 6 additional months or until disease progression. Official censoring date for all patients was the 1th of July 2015.

3.3.3 Patients

Patients were eligible for this study with an age equal or above 18 years, diagnosed metastasized renal cell carcinoma and a planned first-line therapy with either sunitinib or pazopanib. Furthermore, the participation in the EuroTARGET project was a requirement for the inclusion (Section 3.3.2). Each patient who met the inclusion criteria was asked to sign two informed consent forms, one for the EuroTARGET project and another one for the EuT-PK/PD sub-study. Both were consistent with the newest version of the declaration of Helsinki [**125**].

In total, 44 patients were included, with 27 patients receiving sunitinib and 17 pazopanib. One sunitinib patient was excluded from all analyses due to the lack of plasma samples beyond a baseline measurement. Additionally, three patients (two sunitinib patients and one pazopanib patient) were excluded from the outcome analyses, since the TKI treatment during the study period was not first- but second-line. However, the pharmacokinetic data from these patients was still used for PK/PD model development.

Patients' demographics (median and range) per study center and independent of the study drug are listed in Table 3.7.

Tab. 3.7: Patients demographics stratified by study center and total (median and range)

ID[1]	Age [years]	Gender [m/f]	Weight [kg]	Height [cm]	BMI [kg/m^2]	Drug [S/P]
1	54 (51 - 74)	4/0	84.5 (83.0 - 87.5)	184 (155 – 186)	25.2 (24.9 – 34.5)	4/0
2	69.5 (57 – 75)	5/1	80.0 (75.5 – 83.5)	179 (162 – 181)	25.7 (23.0 – 30.5)	6/0
4	64 (47 – 77)	4/2	75.5 (64.5 – 98.0)	172 (160 – 183)	26.9 (22.3 – 29.3)	0/6
7	67.5 (55 – 77)	2/2	96.0 NA	159 (158 – 172)	32.4 NA	2/2
8	67 (65 – 74)	3/1	81.5 (71.0 – 98.0)	178 (165 – 186)	26.7 (24.0 – 28-3)	3/1
9	62 (43 – 80)	6/1	85.5 (71.0 – 106.0)	180.5 (175 – 185)	26.3 (23.2 – 31.7)	5/2
10	65 (60 – 70)	2/0	70.5 (65 – 76)	174.5 (167 – 182)	23.1 (22.9 – 23.3)	2/0
14	75 (67 – 87)	1/2	71.0 (64.0 – 72.0)	168 NA	25.5 NA	0/3
15	70.5 (48 – 82)	6/2	77.0 (76.0 – 91.0)	170 (170 – 185)	26.3 (22.5 – 31.5)	5/3
T	65 (43 - 87)	33/11	80.0 (64.0 – 106.0)	175 (155 – 186)	26 (22 – 35)	27/17

[1]Number assigned to each center according to the study protocol. Note that not all EuroTARGET centers participated in the sub-study

m = Male, = Female; S = Sunitinib, P = Pazopanib; NA = Not applicable, T = Total

BMI = Body mass index

3.3.4 Medication

Patients were treated in accordance to the newest guidelines for the treatment of mRCC, the respective summary of product characteristics (SmPC) of sunitinib or pazopanib and the treating physician's discretion [**46**,**47**]. No dosing recommendations

were made in the study protocol and the decision which drug to use was entirely up to the treating physician.

Sunitinib was usually applied in cycles of 6 weeks with a daily dose of 50 mg in patients with mRCC. One therapy cycle included 4 weeks on treatment and a therapy intermission of two weeks. Besides, alternative schemes like 37.5 mg daily in a 2 weeks on/1 week off cycle were also applicable dependent on the treating physician's discretion or other considerations [**46**]. Standard treatment with pazopanib consisted of 400 to 800 mg daily without interruptions [**47**].

3.3.5 Sampling procedure

During the study period up to 12 plasma samples were collected from each patient. All samples had to be taken during routine check-ups. As these were timed differently in the between study centers, there was no fixed sampling schedule. Except for a mandatory baseline measurement before treatment start, each center was free to develop a schedule according to their specific clinical routine. An example of a possible sampling scheme for sunitinib is shown in Figure 3.2.

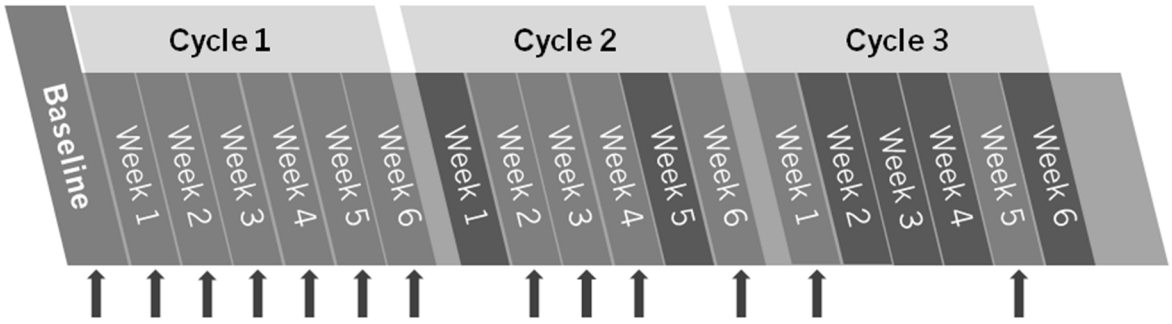

Fig. 3.2: Example of a sampling schedule for a sunitinib patient receiving a standard 4 on/2 weeks off sunitinib cycle. Arrows indicate sampling time-points.

Since pazopanib is not applied in treatment cycles, a scheme dividing the plasma samples within the first 18 weeks of treatment was applicable.

Once taken, samples were further processed in the respective study center. All samples were centrifuged at 1000 g and 4°C for 15 minutes within 30 minutes after

collection. Plasma was then split into 6 aliquots per sample and stored in light-protected micro tubes at -80°C until analysis.

3.3.6 Endpoints

Endpoints were chosen in accordance with the main EuroTARGET study (Section 3.2.6). Outcome was analyzed as progression-free survival, which was defined as the time from treatment start to documented disease progression.

Progression was defined as follows:

- *Progressive disease specified by RECIST* [**124**]
- *Therapy stop/change due to progression*
- *New lesion occurred during first-line therapy (date of diagnosis as progression)*
- *Death due to the malignancy*

Events were counted as censored data, when the treatment was stopped or changed due to a documented toxicity or without any reason, the patient was lost to follow up, or no progression occurred until the official censoring date.

3.4 The C-II-005 study

In order to improve the precision of parameter estimates the final EuroTARGET cohort of patients receiving sunitinib was pooled with patients from the C-II-005 study for model development. Demographics of this cohort can be found in Table 3.8.

The C-II-005 study was performed to investigate the beneficial effect of sunitinib as add-on to a FOLFIRI therapy schedule including folinate, fluorouracil, and irinotecan, in patients with metastasized colorectal cancer (mCRC) and liver metastases. Primary endpoint was the reduction of tumor vessel permeability and blood flow determined by dynamic-contrast-enhanced magnetic resonance imaging as well as dynamic-contrast-enhanced ultrasound imaging (DCE-MRI and DCE-USI). Time-to-progression (TTP) was defined as a secondary endpoint. Twenty eight patients were included into the clinical trial receiving a daily dose of 37.5 mg sunitinib on a 4 weeks on/2 weeks off treatment schedule in addition to (FOLFIRI) as first-line therapy. Seven patients were excluded from the analysis because of missing drug administration (n = 5),

missing data (n = 1), or uncertainty in the documentation of sunitinib intake (n = 1). In case of toxicity, sunitinib therapy was interrupted or continued after dose reduction to 25 mg per day until the symptoms disappeared. Sunitinib was administered around breakfast between 7 and 10 am and FOLFIRI was infused biweekly always after sunitinib intake [**126**,**127**].

A detailed PK/PD analysis of the C-II-005 study was conducted by Kanefendt [**126**]. Data from this study was used to improve the PK/PD modeling process and to and to increase the chance of correctly identifying genetic covariates for model parameters which are independent of tumor entity.

Tab.3.8: Demographics for the cohort of mCRC patients (median and range) [**126**]

Parameter	Unit	Median	Range
Age	years	61	33 – 85
Sex	m/f	12/9	-
Weight	kg	73	57 – 106
Height	cm	172	149 – 184
BMI	kg/m^2	26.0	13.3 – 39.3

3.5 Drug and biomarker analysis

Plasma concentrations of sunitinib, SU12662 and pazopanib were analyzed at the Institute for Biomedical and Pharmaceutical Research (IBMP) in Heroldsberg by Christoph Stelzer and Dr. Martina Kinzig under supervision of Prof. Dr. Fritz Sörgel. All substances were analyzed by LC-MS/MS using a Tripel-Quadrupol Mass spectrometer for detection (Applied Biosystems/MDS Sciex API 5000^{TM} LC-MS/MS, Framingham, USA).

3.5.1 Sunitinib and N-Desethylsunitinib (SU12662)

Sunitinib and SU12662 plasma concentrations were analyzed using a method validated according to the recent guidelines of the European Medicines Agency (EMA) and the FDA [**128**,**129**]. Samples were strictly protected from light during the measurement procedure. D5-sunitinib served as internal standard for quantification. Lower limit of quantification was determined with 0.06 ng/mL for both, parent drug and

metabolite. Absolute recovery was reported with 86.0% for sunitinib and 84.8% for SU12662. Likewise analytical recovery was equally high for both substances, with 99.8–109.1% for sunitinib and 99.9–106.2% for SU12662. Linearity was guaranteed over a concentration range of 0.06 – 100 ng/mL with $r^2 > 0.999$. Additionally, both analytes proved to have a high between-day precision (1.6–6.1% sunitinib, 1.1–5.3% SU12662) [**130**].

3.5.2 Pazopanib

The method used for determination of pazopanib concentrations in plasma were based on a LC/MS method published by Sparidans *et al.* [**131**].

Analogously to sunitinib, pazopanib plasma concentrations were analyzed using a method validated according to recent guidelines of the European Medicines Agency (EMA) and the FDA [**128**,**129**]. Samples were strictly protected from light during the measurement procedure. [13C,2H3]-Pazopanib served as internal standard for quantification. Lower limit of quantification was determined with 0.109 µg/mL. Absolute recovery was reported with 92%. Likewise analytical recovery was equally high with 94.8 to 101.8%. Linearity was guaranteed over a concentration range of 0.109 – 107 µg/mL with $r^2 > 0.999$. Additionally, pazopanib proved to have a high between-day precision (2.2 – 10.4%).

3.5.3 sVEGFR-2

For quantification of sVEGFR-2 in plasma a commercially available immune assays by R&D Systems were used [**132**]. Reproducibility was guaranteed by abiding to internally developed standard operating procedures (SOP) (Appendix **B.IV**). Each run was documented with the respective form (Appendix **C**). Relevant information regarding the assay precision, linearity and sensitivity can be found in Table 3.9.

Quality control (QC) samples in three different concentrations were generated from a different batch of the standard solution. All samples as well as the standards were measured in duplicate while quality control samples analyzed only once.

The VEGFR-2 concentrations were calculated with a four parametric logistic curve fit using the *drc* package in R. Baseline values were defined as concentrations measured

before the first drug intake. The mean of the measured biomarker response at each time-point was used for generating concentration-time profiles stratified by the study drug. In order to detect possible confounders, individual concentration-time profiles were plotted and investigated.

Tab. 3.9: Validation criteria for the determination of sVEGFR-2 in plasma [**127**]

Parameter	
Lower limit of quantification[1]	4.6 pg/mL
Between-day precision (CV %)[1]	5.7 - 7.0%
Within-day precision (CV %)[1]	2.9 - 4.2%

[1]Determined by R&D Systems

3.5.4 sVEGFR-3

sVEGFR-3 concentrations were determined with a previously developed and validated method by Kanefendt *et al.* using an Elisa DuoSet® [**133**,**134**]. Reproducibility was guaranteed by abiding to internally developed SOPs (Appendix **B.IV**). Each run was documented with the respective form (Appendix **C**). Quality control samples in three different concentrations were generated from a different batch of the standard solution. All samples as well as the standard were measured in duplicate whereas quality control samples were quantified only once. The validation criteria can be found in Table 3.10.

The concentrations were calculated with a four parametric logistic curve fit using the *drc* package in R®. The mean of the measured biomarker response at each time-point was used for generating concentration-time profiles stratified by the study drug. Baseline values were defined as concentrations measured before the first drug intake. In order to detect possible confounders, individual concentration-time profiles were plotted and investigated.

Tab. 3.10: Validation criteria for the determination of sVEGFR-3 in plasma (modified from [**126**,**134**])

Parameter	
Lower limit of quantification[1]	513.9 pg/mL
Between-day precision (CV %)	18.3%
Within-day precision (CV %)	4.9%

[1]Not determined. Based on calibration curve

3.6 Statistical analysis

Statistical analysis of the soluble biomarkers sVEGFR-2 and sVEGFR-3 as well as blood pressure was performed using R. As two drugs were investigated all analyses were performed for both drugs combined and for each treatment subgroup in order to rule out major differences.

3.6.1 Outlier analysis

To identify potential outliers, boxplots of the absolute sVEGFR-2 and -3 concentrations were generated. Since the sampling time-points were not unified across patients, all measurements were stratified by week of treatment with a maximum observation time of 18 weeks. If necessary, sunitinib and pazopanib were administered in different doses; therefore, absolute biomarker concentration values were dose normalized before plotting. This guaranteed that no values were mistakenly identified as outliers. Baseline values (treatment week 0) were excluded from the dose normalization and compared separately [**135**]. Outliers were determined using a model-based approach by calculating the conditional weighted residuals (CWRES, Section 3.8.3.). A value greater or equal 6 or lower or equal -6 was considered as an outlier. If applicable, the respective observation was excluded from the analysis and the influence on parameter estimates was investigated.

3.6.2 Assessment of normality

Parametric statistical tests require the data to be normality distributed. Although physiological parameters are usually non-normally distributed, it is still necessary to verify this assumption in order to avoid errors by using the wrong test statistics [**135**].

In case of violations of the normality assumption, non-parametric methods are highly recommended for testing e.g. correlations.

Normality was tested via graphical examination by generating histograms and quantile-quantile plots stratified by protein and by treatment. In addition, the Shapiro-Wilk test was performed with the same stratification pattern. For this test the following calculation was performed [**135**]:

$$W = \frac{\left[\sum_{i=1}^{n} a_i x_{[i]}\right]^2}{\sum_{i=1}^{n}(x_i - \bar{x})^2} \quad \text{(Eq. 3.1)}$$

With *W* as the statistic of interest, *n* as independent and identically distributed observations from a normal distribution with unspecified mean and variance. a_i represents constants that are functions of *n*. The null hypothesis states that the data is normally distributed, whereas the alternative hypothesis implies that the distribution is not normal. With a significance level of $p < 0.05$ the null hypothesis can be rejected.

3.6.3 Correlation analysis

Since both, sVEGFR-2 as well as sVEGFR-3, are involved in tumor angiogenesis and down-regulated under TKI therapy, the correlation between the plasma concentrations of both proteins was quantified. Correlation was assessed graphically by linear regression and the determination of the correlation coefficient *r*. In addition the Spearman's rank correlation coefficient (r_s) was calculated [**135**]:

$$r_s = \frac{S_{xy}}{\sqrt{S_x^2 S_y^2}} \quad \text{(Eq. 3.2)}$$

S_{xy} denotes for covariance between *x* and *y* and $S_{x/y}$ for the variance of *x* and *y*, respectively.

3.6.4 Comparison of mean biomarker levels across treatment groups

To detect differences in drug response the mean levels of sVEGFR-2 and sVEGFR-3 per treatment week were compared between the respective groups of patients either treated with sunitinib or pazopanib. For this purpose the Mann-Whitney-Wilcoxon test was used, which is applicable for comparing a non-normally distributed continuous variable in two groups [**135**].

3.7 Genetic analysis

The selection of single nucleotide polymorphisms (SNPs) was based on previously reported studies ($p < 0.05$) of SNPs associated with the treatment outcome of sunitinib (or pazopanib) with regard to toxicity and efficacy. Herein, the focus was on SNPs that are likely to have an effect on VEGF or VEGF receptors, blood pressure, and SNP associations from confirmatory studies in large cohorts. Selected SNPs or combination of SNPs were included as covariates if they improved the respective model significantly. A list of the selected SNPs can be found in Appendix **A**.

SNP analysis was performed at the University of Leiden in the group of Prof. Henk-Jan Guchelaar by Dr. Meta Diekstra. Germline DNA was isolated from whole blood samples using the Chemagic® Blood kit (PerkinElmer). Genotyping was performed on the selected SNPs, using Taqman probes (Applied Biosystems, Nieuwerkerk aan den Ijssel, the Netherlands) on the LightCycler480® Real-Time PCR Instrument (Roche Applied Science, Almere, The Netherlands). Quality control procedures included SNP genotyping plots for each assay. To test for inconsistencies, 5% of all samples were measured as duplicates. Samples with a call rate below 80% were excluded from the analysis. All SNPs were tested for the Hardy-Weinberg equilibrium [**136**].

3.8 Pharmacokinetic/pharmacodynamic data analysis

3.8.1 Non-Linear Mixed Effects modeling

Non-Linear Mixed Effects (NLME) modeling is the gold standard in population analysis. As initially stated (Section 1.4.2), this method allows the analysis of datasets with only sparse individual sampling. In addition to typical estimates of the respective PK/PD parameters it is possible to quantify the variability within the population and, if sufficient data is available, to explain this variability by inclusion of covariate effects.

The term NLME is derived from the different effects which are investigated with a population models. *Mixed effects* comprise the so called *fixed effects*, which refer to the population parameters without inclusion of variability, but also includes covariate effects. On the other hand, *random effects* comprise all forms of estimated variability in the model. In this study, the software NONMEM® was used for population PK/PD analysis [**88**]. NONMEM® is written in FORTRAN 90/95, which is still evident in the modified syntax that is used to define models. The software consists of several core

modules with different tasks within the overall package. An overview of the structure of NONMEM® is shown in Figure 3.3.

NM-TRAN is a module which translates the user-supplied data and control files into readable data for NONMEM®. A compiler is necessary for adequate translation of the code into a format which can be executed by the computer. NONMEM® itself does not directly provide models, but relies on user written subroutines for parameter estimations via the command PRED. However, NONMEM® also includes the so-called PREDPP module which is short for *PRED for Population Pharmacokinetics*. This module simplifies the model building process to a certain degree as it already includes subroutines helpful for population analysis as well as subroutines which provide already analytical solutions for simple one, two or three compartment models. In the simplest case, only PK or PD model parameters and a residual error model have to be specified. Though, it is also possible to define more sophisticated models with differential equations in PREDPP using the $DES option [**88**].

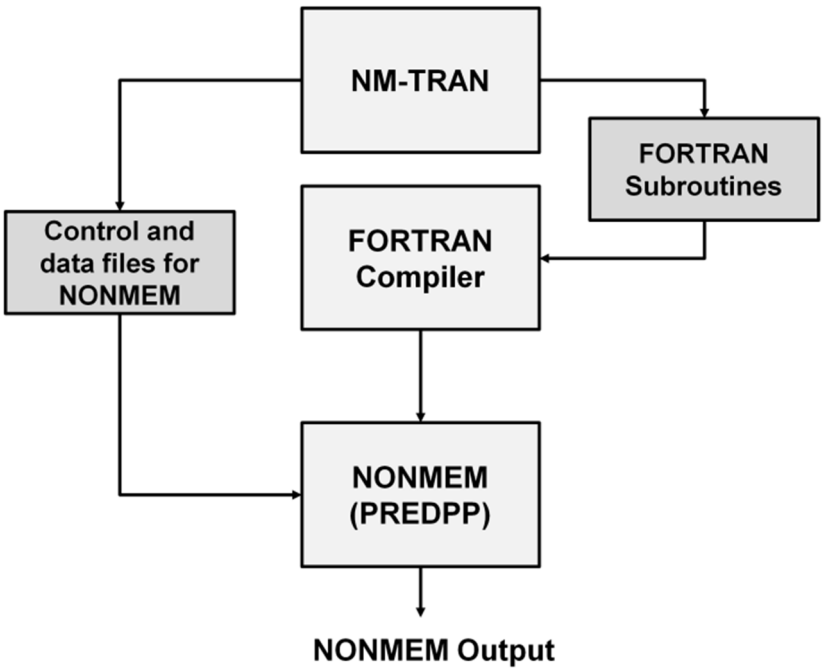

Fig. 3.3: Scheme of the general structure of NONMEM® and important steps (modified from [**88**]).

Fixed effects are referred to as THETA (θ) in the NONMEM® while random effects are further differentiated into inter-individual (IIV) (ETA, η), intra-occasion (IOV) (KAPPA, κ) and residual variability (EPSILON, ε). Variability is assumed to be normally distributed across all random effects with a mean 0 and a variance of ω^2, κ^2 or σ^2, respectively (Section 3.8.2).

Methodologically, NONMEM® uses a maximum likelihood approach with an objective function (OBJ) based on extended least squares to obtain parameter estimates which provide the best fit to the underlying data. In the simplest case a population pharmacokinetic model can be described as follows:

$$Y = f(\theta|x) + \varepsilon \quad \text{(Eq. 3.3)}$$

Where θ denotes for the model parameter vector *x* for the dependent variable, ε for the residual variability. Assuming that the total residual variance of *Y* is a function of the structural model *f(θ;x)* it can be simplified:

$$Var(Y) = \sigma^2[g\big(f(\theta|x)\big)]^2 \quad \text{(Eq. 3.4)}$$

With *g* being the variance function with respect to *f(θ;x)* and σ^2 the variance of the random variable ε.

Based on this, the OBJ can be written as:

$$OBJ = \sum_{i=1}^{n}\left[\frac{[Y_i - f(x_i|\theta)]^2}{Var(Y)} + ln[Var(Y)]\right] \quad \text{(Eq. 3.5)}$$

Where *n* is the number of patients in the investigated population and Y_i, x_i and θ refer to the vectors of dependent and independent variables as well as model parameters.

Even though NONMEM® uses a maximum likelihood approach for parameter estimation, the OBJ is calculated as two times the negative log-likelihood; hence, the OBJ is minimized during parameter estimation [**84**,**86**,**88**]. However, due to the inclusion of random effects, especially inter-individual variability, the calculation of the likelihood is no longer trivial as no analytical solution exists. Therefore, NONMEM® uses an approximation of the true model by linearization. The most basic variant of this approach implemented in NONMEM® is the first-order (FO) method which relies on a first-order Taylor series. Mathematically, a Taylor series is a polynomial function which is used to approximate a function at a point x given the original function and its derivatives at the initial point. The order of a Taylor series is given by the number and degree of derivations that are added up to the original function. By definition, a first-

order Taylor series includes the first derivation of the base function [**86**]. As NONMEM® performs the linearization at η=0 using only population mean values, an additional step, called POSTHOC, is required after the estimation in order to obtain individual parameter estimates. While the FO is approved for simple modeling problems, it could be shown that it is less reliable in more sophisticated models as it may introduce bias. A well-established method is the first-order conditional estimation (FOCE), which is essentially an improved FO algorithm. FOCE uses the same first-order expansion as the FO method with the difference that conditional individual estimates are used instead of setting η equal to 0. Furthermore, FOCE allows to address the potential η,ε-interaction which is relevant when certain residual error models are used that incorporate the residual variance as a function of the model prediction (Section 3.8.2) [**84**,**86**,**88**]. Another common method is the Laplacian approach: similar to FOCE, Laplacian is also a conditional estimation method, however, a second-order Taylor expansion is used in this case. Laplacian has proved to be reliable and particularly useful for time-to-event and other categorical data as it does not need to calculate a likelihood and is directly minimized [**88**,**137**].

3.8.2 Model development

A population model usually consists of three submodels: a *structural* model or *base* model, a *stochastic* model and a *covariate* model [**84**,**86**]. Development of a population model starts with the choice of an appropriate structural model. This comprises the compartmental model with fixed effect parameters to describe the relevant pharmacokinetic processes such as absorption, distribution and elimination. Graphical inspection of the data was performed for an initial assumption on the required number of distribution compartments and the kinetics of the absorption and elimination process. Goodness-of-fit (GOF) plots and changes in the objective function value (OFV) were compared in all tested models. Furthermore, visual predictive checks (VPCs) were generated for candidate models; this process is explained in detail in Section 3.8.3.

Once a proper structural model was selected, random effects were tested on each parameter. As stated above, variability was differentiated in three levels, which require different approaches for a correct implementation into the model: Inter-individual (IIV), inter-occasion (IOV) and residual variability.

Inter-individual variability

Inter-individual variability (IIV), describes differences between individuals in a population of interest. While other models are possible, the standard approach is to model IIV with a log-normal distribution (Equation 3.6) as this constraints the pharmacokinetic parameters to be greater than zero. This is of particular importance for physiological parameters such as clearance and volumes [**84**,**85**,**137**].

$$\theta_i = \theta_\mu \cdot e^{\eta_i} \quad \text{(Eq. 3.6)}$$

θ_i denotes for the individual parameter estimate, θ_μ represents the population mean and η_i the deviation from this mean for patient *i*. The underlying assumption is that η_i has a mean of zero and a variance of ω^2. When assuming that all parameters are uncorrelated, the variance-covariance matrix can be expressed as a diagonal matrix. However, NONMEM® allows the implementation of block matrices to address and estimate correlations between model parameters.

IIV is usually stated as coefficient of variation (CV). This can be calculated using the following equation [**86**]:

$$CV(\%) = \sqrt{e^{\omega^2} - 1} \cdot 100\% \quad \text{(Eq. 3.7)}$$

IIV was tested on all relevant pharmacokinetic and pharmacodynamic parameters during model development. If necessary, correlations between parameters were handled by introduction of off-diagonal elements in the variance-covariance matrices.

Inter-occasion variability

Inter-occasion variability (IOV) describes the variation of pharmacokinetic parameters within one individual. Various reasons for time dependency of a parameter exist and they can be a consequence of intrinsic, e.g. pathophysiological, or extrinsic changes and influence factors. For example, if the clearance of a drug is dependent on renal function a progressive renal impairment will have a significant impact on this parameter.

In oncology it is common to interpret therapy cycles as different occasions, since they span over a long time period with or without treatment intermission. The importance of modeling IOV was pointed out by Karlsson *et al*. in 1993. The implementation of IOV

can prevent the false data acceptance of covariates and reduce bias of parameter estimates [**138**].

IOV, denoted with κ, is modeled on the same level of random effects as IIV:

$$\theta_i = \theta_\mu \cdot e^{(\eta_i + \kappa_j)} \quad \text{(Eq. 3.8)}$$

Hence, the additional parameter κ_j denotes for the deviation from the population mean with respect to occasion *j*. The impact of IOV was tested on relevant parameters, if applicable. An occasion was either defined as treatment cycle of sunitinib, which corresponds to 6 weeks of pazopanib treatment, or as treatment week.

Residual variability

Residual variability comprises all variability which cannot be explained by IIV, IOV or covariate effects. This includes for example assay variability, errors in dosing histories but also model misspecification. To account for this, a proper residual error model has to be chosen.

The most common residual error models include an additive (Equation 3.3), a proportional (Equation 3.9) and a combined error model (Equation 3.10):

$$Y = f(\theta|x) \cdot (1 + \varepsilon) \quad \text{(Eq. 3.9)}$$

$$Y = f(\theta|x) \cdot (1 + \varepsilon_1) + \varepsilon_2 \quad \text{(Eq. 3.10)}$$

The additive model assumes an error of the same absolute magnitude across the range of plasma concentrations. In contrast, the proportional error applies a fixed coefficient of variation which results in smaller absolute errors for low values and vice versa. The combined error model is most useful when there is a wide range of plasma concentration measurements, since the additive error usually applies to smaller concentrations and the proportional error to values of higher magnitude [**86**,**137**]. The usual assumption is that the residual error is equal across all patients. However, this is not always the case, especially when data from different studies is pooled in one dataset as different sampling and analytical approaches may result in varying residual errors across studies. This can be resolved by estimating center or study specific residual errors.

Even though all samples analyzed in this study were processed in the same laboratories, residual errors in all models were tested for systematic differences among patient groups.

Covariate model

Covariates are described by fixed effects to explain parts of the inter-individual variability of a pharmacokinetic parameter. Usually, covariate analysis is performed in a step-wise manner [**86**,**137**]. Preselected covariates, based on clinical relevance and graphical analysis, are implemented into the model in a forward search process. Covariates which led to a significant decrease of the objective function value ($p < 0.05$) are kept for the next step. The final forward model is then re-evaluated by backwards elimination of each covariate with a stricter significance level ($p < 0.01$). If a covariate effect was still significant in this step, it was kept in the model.

However, if the investigated population is too small it is difficult to detect a covariate effect. To take this into account, potential covariates were identified in the literature and then tested manually in addition to the step-wise approach in this study. The advantage is that the quantity of the possible effect is already known, and the underlying study could be used as verification for previous findings. Clinical and biological relevance of newly identified covariates was carefully assessed.

A full list of all covariates tested in the respective models can be found in Appendix **A**.

3.8.3 Model qualification

Model qualification covers methods which allow determining the overall fit of the model, the validity of estimated parameters and if the model is suitable for extrapolation, for example simulation of different dosing regimens which were not part of the original dataset. Due to the lag of validation data set and a small sample size, which did not allow data splitting, only internal qualification methods were used [**84**,**139**].

Likelihood ratio test

The objective function value (OFV) provided by NONMEM® (Section 3.8.1) was used primarily for model comparison of nested models depending on the degrees of freedom, or more exactly, the number of parameters that changed between models. The objective function used by NONMEM® is defined by minus twice the log-likelihood with respect to the model parameters. The difference of this value between two nested models (dOFV) is chi-square distributed. In this case the term “nested” refers to models

which can be converted into each other by addition or removal of one or several parameters. As a result, the statistical significance of a parameter or several parameters can be assessed by comparing the dOFV with the respective statistic from the chi-square distribution [**88**]. For one degree of freedom, which translates to one additional parameter in the model, the OFV has to decrease by at least 3.84 to confirm a significant improvement of the model fit with a p-value less than 0.05. Depending on the chosen significance criteria and the number of parameters included or removed from a model different threshold values were apply.

Goodness-of-fit plots

Goodness-of-fit (GOF) plots can be used to graphically assess the model fit and help to identify model misspecifications. To avoid misinterpretation and ensure easy comparability these plots were standardized depending on the model drug [**84**,**139**].

General GOF plots include *population predictions vs. observations* and *individual predictions vs. observations*. Both types of plots were used to assess the goodness-of-fit with regard to the estimates of population parameters, without taking inter-individual variability into account, and individual parameter estimates. X- and Y-axis were fixed to have the same length with a line of identity dividing the plot exactly by half. Furthermore, a *locally weighted scatterplot smoothing* (LOESS) was added for a better identification of potentially ill-conditioned patterns in the plot [**139**].

Depending on the purpose, different types of residuals are needed and have to be computed beforehand to generate plots for model evaluation. Weighted residuals are calculated by NONMEM® based on the older FO method, whether this method was used for parameter estimation or not. In the worst case this can lead to false decisions during the modeling process. Hence, the individual weighted (IWRES) and the conditional weighted residuals (CWRES) were used in the underlying analyses [**140**].

Individual weighted residuals

Individual weighted residuals (IWRES) were calculated by using the difference between the observed dependent variable (DV) and individual model predictions (IPRED) divided by the square root of the variance σ^2 as weighting factor. The variance is defined by the residual error model (Section 3.8.2)

$$IWRES = \frac{DV - IPRED}{\sqrt{\sigma^2}} \quad \text{(Eq. 3.11)}$$

Conditional weighted residuals

As FOCE with η,ε-interaction (Section 3.8.1) is the estimation method of choice, standard residuals are no longer a reliable diagnostic tool, due to their reliance on the older FO method. However, Hooker *et al.* introduced conditional weighted residuals (CWRES) in 2007 which are now a standard diagnostic criterion [**140**]. Therefore, CWRES were automatically calculated for every run.

$$CWRES = \frac{y_i - f_{FOCE}(\theta, x_i)}{\sqrt{\sigma^2_{FOCE}(y_i)}} \quad \text{(Eq. 3.12)}$$

By using Equation 3.12 the (estimation by using FOCE) empirical Bayes estimates (EBE) are taken into account for residual computation whereas the usual WRES are calculated at η = 0.

One major assumption is that residuals are normally distributed with a mean of 0 and variance σ^2 (Section 3.8.1). Graphically, this can be assessed using quantile-quantile plots as well as histograms of CWRES. The former uses the residual quantiles and plots them against the quantiles of the normal distribution. Whereas information between both types of plots is comparable, quantile-quantile plots are more sensitive to violations of the underlying assumptions and can therefore be used in addition to classical histogram plots.

To identify model misspecifications, especially of the structural and residual model, plots of *CWRES vs. PRED* and *CWRES vs. TIME* and/or *TIME AFTER DOSE (TAD)* were used. Furthermore, plots of |*IWRES*| vs *PRED* and vs. *TIME* were used to evaluate the residual error model regarding the independence of residuals, (individual) predictions and the independent variable, respectively [**139**]. All plots were generated after every model run using the R packages *lattice* and *xpose* (Section 3.1.5).

η- and ε-Shrinkage

Individual estimates of population pharmacokinetic model parameters are highly dependent on the quality of the underlying data. While the strength of NLME modeling is the analysis of sparse data, too sparse data or varying data quality among patients can lead to uninformative parameter estimates. In an extreme case the individual would be identical to the population estimates. A misleadingly lower estimate of the variance would be the result.

This phenomenon is called η-shrinkage and can be calculated with the following equation

$$\eta - Shrinkage = 1 - \frac{SD(\eta EBE)}{\omega} \quad \text{(Eq. 3.13)}$$

Where $SD(\eta EBE)$ denotes for the standard deviation from the population mean and ω is the standard deviation of the population.

Similarly, the lack of sufficient data for the proposed model can lead to a systematic decrease of IWRES (see above) which is also called “overfitting” or ε-shrinkage. Analogous to the η-shrinkage, ε-shrinkage can be calculated as follows:

$$\varepsilon - Shrinkage = 1 - SD(IWRES) \quad \text{(Eq. 3.14)}$$

There is no defined cut-off value for η- or ε-Shrinkage, but a commonly used threshold is that either value should not exceed 30% [**141**]. Shrinkage was calculated for every relevant model parameter, if applicable.

Bootstrap

Nonparametric bootstraps were used to obtain standard errors (SE) and confidence intervals (CI) for model parameters. By randomly sampling from the original data set with replacement, *n* new data sets were generated and used for re-estimation of the model parameters. Each data set consisted of the same number of patients; however, the composition of each set varied as patients could be drawn multiple times or not at all. Based on the number of replicates, the bootstrap results were used to calculate the variance, and hence standard errors, and confidence intervals of the model parameters without knowing the true distribution of the data [**86**].

The bootstrap variance Var_B is calculated using the estimated parameter vector $f(x_i^*)$ and the number of replicates n.

$$Var_B = \frac{\sum_{i=1}^{n}\left[f(x_i^*) - \frac{\sum_{i=1}^{n} f(x_i^*)}{n}\right]^2}{n-1} \quad \text{(Eq. 3.15)}$$

By taking the square root of the variance an estimate of the standard error was calculated. By default CIs were obtained using the percentile method, assuming that the parameter estimates were asymptotically normally distributed around their means. All bootstrap estimates were ranked according to their value, confidence interval boundaries were then calculated by N(α/2) and N(1-α/2), respectively [**86**].

In this study, 1000 replicates per bootstrap were generated, which is in accordance with the common practice and population pharmacokinetic guidelines [**84**]. The 95th and 5th percentile were then used for calculation of the respective CIs. In case of asymmetrical bootstrap distributions the accelerated bias-corrected (BCa) method could be used [**84**,**111**]. Here, two additional parameters are calculated: *b* to correct for asymmetry and *a* to correct for skewness. The equation for calculating bias-corrected confidence intervals is then given by:

$$N \cdot \varphi\left[b \pm \frac{Z_{\alpha/2} + b}{1 - a(Z_{\alpha/2} + b)}\right] \quad \text{(Eq. 3.16)}$$

Where *N* denotes for the bootstrap sample size, *φ* for the standard normal distribution and *Z* for the *Z*-distribution. The process of resampling and re-estimation of datasets and model parameters was automated by using PsN [**111**].

Visual predictive check

Visual predictive checks (VPCs) are a simulation based diagnostic tool for nonlinear mixed effect models. Here, the model of interest is used to simulate data based on the final estimates including variability, hence sampling from the OMEGA and SIGMA matrices corresponding to inter-individual and residual variability [**89**]. The simulated predictions are then graphically compared to the observed data. By binning of the independent variable (usually “Time”) it is assured that all observed data points are grouped within other values of comparable magnitude and in a similar observation time. It is common practice to use bins equal to the number of observations per patient.

However, it is also possible to automatically assign observations into bins in cases where a manual subdivision is not feasible [**142**,**143**].

Prediction-corrected VPCs (pcVPC) are a further advanced version of the original approach proposed by Bergstrand *et al.* [**144**]. This method is of particular importance when data with differences in independent variables, e.g. doses or covariate effects, is analyzed as it corrects for these. This is done by normalization of the observed and simulated dependent variable with respect to the median prediction of each bin:

$$pcY_{ij} = LB_{ij} + (Y_{ij} - LB_{ij}) \cdot \frac{PRED_{bin} - LB_{ij}}{PRED_{ij} - LB_{ij}} \qquad \text{(Eq. 3.17)}$$

Where pcY_{ij} denotes for the prediction-corrected observation of the *ith* individual at the *jth* time-point and *LB* is the lower bound at the respective time-point *j* of individual *i*. $PRED_{bin}$ is the mean population prediction, while $PRED_{ij}$ corresponds to the population prediction of individual *i* at time *j*.

pcVPCs were generated based on 1000 simulated datasets with regard to the original data structure. Bin arrays were constructed based on the weeks on treatment and sampling schedules. Graphical presentation of the VPC results included the simulated and observed mean as well as the 90% prediction interval with the respective 95% confidence bands. Due to the heterogeneity of the sampling schedules across the study centers and due to the fact that, in case of sunitinib, two different patient cohorts were analyzed simultaneously only the first cycle is shown in the plots. For pazopanib the first 6 weeks on treatment were chosen to ensure comparability. VPCs of the full observation time for each drug can be found in Appendix **D**. Furthermore, VPCs for sunitinib PK and PK/PD models were stratified by tumor entity to detect potential differences between both studies. VPCs used for evaluating the survival model show the observed Kaplan-Meier estimates with a 90% prediction interval and were stratified by covariates if necessary. In the same way the results of the toxicity models are presented. Here, the observed fraction of patients, who developed a certain adverse event over time with a 90% prediction interval is shown.

Case deletion diagnostics

Case deletion diagnostics (CDD) were used to identify individuals with influential characteristics within the dataset. In addition, CDD allowed the calculation of bias for every model parameter. In principle CDD resembles the so called *jackknife* approach

where n new datasets are generated by removing one individual at a time. Model parameters are then re-estimated for each set. In this case *n* equates to the number of individuals in the original data set [**86**,**145**]. The *jackknife* estimate of a model parameter $\hat{\theta}$ is defined by

$$\hat{\theta}_{JACK} = \frac{1}{n}\sum_{i=1}^{n}\hat{\theta}_{i(JACK)} \quad \text{(Eq. 3.18)}$$

With $\hat{\theta}_{i(JACK)}$ as the parameter estimate at the *ith* jackknife sample [**146**].

Based on this value it is possible to calculate the jackknife bias, which is the average deviation of the replicated parameter estimates from the original estimate [**84**,**145**]:

$$B_{JACK} = (n-1)\cdot(\hat{\theta}_{JACK} - \hat{\theta}) \quad \text{(Eq. 3.19)}$$

Influential subjects can be accessed graphically by plotting the calculated covariance ratios versus the Cook's distance. Cook's distance is a metric which quantifies the change of parameter estimates when a specific subject is removed from the dataset, whereas an increase of the covariance ratio is an indicator for a change in parameter variability [**86**]. Furthermore, it is possible to assess the relative changes of each model parameter separately to identify subjects with a high influence on the estimate.

Resampling and re-estimation of datasets and model parameters was automated by using PsN [**111**].

3.8.4 Bayes estimation

Bayesian estimation is a common mathematical approach in Therapeutic Drug Monitoring (TDM) to gather information on individual pharmacokinetic parameters based on an a priori probability which comprises the known distribution of the pharmacokinetic parameters in the model and a posteriori probability including the plasma concentration(s) of the respective patient. Basis for this method is the Bayes theorem with describes the conditional probability of an event *A* provided *B* [**92**]:

$$P(A|B) = \frac{P(B|A)\cdot P(A)}{P(B)} \quad \text{(Eq. 3.20)}$$

With *P(B|A)* being the probability of *B* provided *A* and *P(A)* and *P(B)* the probabilities for *A* and *B*, respectively. Applied to pharmacokinetics, the same problem can be stated as the probability of a model parameter vector *A* (e.g. clearance, volume of

distribution) provided plasma concentration *B*. The advantage of this method is that even in situations where only very limited data is available, reliable parameter estimates can be obtained.

For application in NONMEM® all model parameters were fixed to their respective value from the literature (a priori probability) and used for prediction of the individual pharmacokinetic parameters based on the sparse samples available (a posterori probability). The estimated individual plasma concentrations of each patient were used to calculate the relative prediction error (RPE, Equation 3.21) which served as a tool to identify potential outliers in the data set. A RPE of 50% was set as threshold for excluding a value from the analysis.

3.8.5 Handling of missing data

Missing data was handled according to predefined rules. For continuous covariates the population mean was used as imputed value whereas for categorical covariates the most common expression in the respective population was chosen for imputation. In case of missing time of drug intake or missing sampling time two options were available. If at least one dosing or sampling time was documented, this was also used for all cases were this information was missing. Only in the case of a complete lack of data on drug intake the clock time was set to 8.00 a.m. assuming that an administration in the morning was the most likely scenario. In the same way, clock time was set to 12.00 p.m. for all cases with no information on sampling time, assuming that a routine check-up was most likely scheduled during mid-day. However, since these are rather uncertain assumptions, the influence of dosing time was assessed in a sensitivity analysis (Section 3.8.6).

3.8.6 Sensitivity analysis

Fixed model parameters

Due to the nature of sparse data, not all parameters of a highly sophisticated semi-mechanistic model can be or should be estimated. In case of physiological processes, e.g. liver blood flow, it is a common approach to fix related model parameters to values obtained from the literature. However, this demands a high confidence in the reported value as all other model parameters could potentially be influenced by this value,

introducing a bias in the worst case. To test the influence of the fixed model parameters in the underlying study, a sensitivity analysis was performed [**147**]. The parameters of concern were therefore varied between -50 and +50% of the final value used in the analysis. Variation of all non-fixed model parameters was quantified using the relative prediction error (RPE) which is defined as

$$RPE\ (\%) = \frac{\theta_{new} - \theta_{base}}{\theta_{new}} \qquad \text{(Eq. 3.21)}$$

Where θ_{new} denotes for the parameter estimate obtained after varying the concerned fixed model parameter and θ_{base} for the original estimate, respectively.

Time of drug intake

Since the time of drug intake was only documented poorly and the clock-time had to be imputed (Section 3.8.5) in several cases, a sensitivity analysis quantifying the influence of dosing time was performed. Therefore, time of drug intake was randomly varied for each occasion between +3 and -3 hours. This procedure was repeated 50 times. Based on the parameter estimates of each model the RPE was calculated.

3.8.7 Data below the quantification limit

Data below the limit of quantification (BQL) can be informative and have a significant effect on parameter estimates of a PK/PD if not handled correctly. Several methods on how to approach BQL data in modeling can be found in the literature. Two of the most common methods are referred to as M1 and M3 [**148**,**149**].

M1 denotes for the removal of all BQL values from the dataset, thus ignoring this data completely. While this approach is widely used and reliable if the amount of BQL data is low, there is a certain probability of introducing a bias into the parameter estimates. A more sophisticated approach is the M3 method. Here, BQL values are included into the model fitting process and the likelihood that these values are effectively below the quantification limit is estimated [**148**]. Ideally this should avoid misinterpretation of BQL values and reduce bias which can be introduced by omitting these data points [**148**,**149**]. According to recent comparison between all available methods the M3 approach is currently the method of choice for handling BQL data [**150**].

However, as the relative number of BQL data in the underlying study was below 2% the M1 method was decided to be sufficient.

3.9 Pharmacokinetic models

3.9.1 Sunitinib and N-Desethylsunitinib (SU12662)

Two published semi-mechanistic models for sunitinib and its active metabolite SU12662 were considered as basis for describing the study data.

The model proposed by Lindauer *et al*. [**109**], used a transit-compartment approach to describe the delayed absorption of sunitinib and takes into account the fraction of the parent drug which is metabolized to SU12662 pre-systemically, before entering systemic circulation. Distribution of sunitinib is described by a two-compartment model, whereas for SU12662 only one compartment was sufficient. The fraction metabolized to SU12662 (F_M) was fixed to 0.21, however the ratio of pre-systemic (*pre*) to systemic (*sys*) metabolite formation (*RPS*) could be estimated with the given parameterization of the model:

$$F_M = F_{M,pre} + \left(1 - F_{M,pre}\right) \cdot F_{M,sys} \quad \text{(Eq. 3.22)}$$

$$RPS = \frac{F_{M,pre}}{F_{M,sys}} \quad \text{(Eq. 3.23)}$$

Basis for this model was a data set of 12 healthy volunteers (6 male and 6 female) who received 50 mg sunitinib for 3 or 5 consecutive days [**109**]. This model was successfully applied by Kanefendt *et al*. to describe sunitinib and SU12662 pharmacokinetics in 21 patients with colorectal cancer originating from the C-II-005 study (Section 3.4) [**126**].

The second model that was tested was developed by Yu *et al.* [**110**] based on data from 70 cancer patients with doses ranging from 25 to 50 mg daily. Here, pre-systemic metabolization of sunitinib to its active metabolite was described by a hypothetical enzyme compartment. This was assumed to be in equilibrium with the central compartment, connected by the hepatic blood flow (Q_H) which was fixed to 80 L/h scaled by weight relative to a standard weight of 70 kg.

The hypothetical compartment was parameterized as follows, with C_H being the calculated concentration:

$$C_H = \frac{k_a \cdot A_D + Q_H \cdot \frac{A_{c,suntinib}}{V_{c,sunitinib}}}{Q_H + CL_{sunitinib}} \quad \text{(Eq. 3.24)}$$

k_a denotes for the absorption rate constant while A_D and $A_{c,sunitinib}$ represent the amounts in the dosing or central compartment, respectively. $CL_{sunitinib}$ and $V_{c,sunitinib}$ denote for the clearance and volume of distribution of the central compartment of sunitinib, respectively [**110**].

Distribution was, in contrast to the model by Lindauer *et al*. described by a one-compartment model for sunitinib and a two-compartment model for SU12662. For comparison with the reported estimates all relevant parameters were also scaled by patients' weight relative to a standard weight of 70 kg in this study.

3.9.2 Pazopanib

Two population pharmacokinetic models for pazopanib were published so far. Imbs *et al.* used a simple one-compartment model with a dosing lag-time to account for delays in absorption processes [**151**]. The model was based on data from 25 patients who received pazopanib in combination with bevacizumab. Yu *et al.* used a semi-mechanistic approach to cope with the rather complex absorption process of pazopanib (Section 1.1.4) [**152**]. Pharmakokinetics were described using a two-compartment model with two first-order absorption rate constants. One fraction of the dose was absorbed instantaneously whereas the rest followed with a defined lag-time. In addition, the relative dose-related fraction absorbed (rF_{Dose}) was accounted with an E_{max} model:

$$rF_{Dose} = \frac{E_{max} \cdot (Dose - 200)}{ED_{50} + (Dose - 200)} \quad \text{(Eq. 3.25)}$$

Here, E_{max} describes the maximum effect of the dose on the bioavailable fraction. ED_{50} represents the dose level with half of the maximal bioavailable fraction at a dose of 200 mg. Furthermore, Yu *et al.* observed that pazopanib bioavailability decreases over time with significant differences between expected plasma concentrations after a single dose and at steady-state.

To acknowledge this, an exponential time-decrease was applied to bioavailable fraction:

$$rF_{Time} = 1 - E_d + E_d \cdot e^{-\lambda \cdot Time} \quad \text{(Eq. 3.26)}$$

Where E_d denotes for the maximum effect of time.The relative fraction absorbed *rF* was assumed to be 1 if no influencing factors were present. The effects of time and dose on *rF* could be described by the following equation.

$$rF = 1 \cdot rF_{Dose} \cdot rF_{Time} \quad \text{(Eq. 3.27)}$$

Due to sparse sampling and missing information on drug intake and measurement times for pazopanib it was difficult to obtain reliable population parameter estimates with the chosen model. Hence, a Bayesian approach as described in Section 3.8.4 was used to estimate individual pharmacokinetic parameters for each patient.

Whereas both models were tested for applicability on the underlying data set, the semi-mechanistic approach by Yu *et al.* was used for the final analysis due to the superiority of the model regarding already included information on pazopanib pharmacokinetics.

3.10 Pharmacokinetic/pharmacodynamic models

The final pharmacokinetic models for sunitinib, its active metabolite and pazopanib were linked in individual pharmacokinetic/pharmacodynamic (PK/PD) models for each biomarker to quantify the relationship between drug plasma concentrations and biomarker response. Individual pharmacokinetic parameters of each patient were used to calculate plasma concentration-time profiles of the respective drug as influence factor for changes in sVEGFR-2 and sVEGFR-3 plasma concentrations as well as blood pressure over time.

3.10.1 sVEGFR-2

The pharmacodynamic model for sVEGFR-2 was originally developed by Lindauer *et al.* in healthy volunteers and linked with the respective pharmacokinetic model for sunitinib and SU12662 (Section 3.9.1) [**109**]. Applicability for cancer patients was already demonstrated by Kanefendt *et al*. in the analysis of mCRC patients alone [**126**]. In this study, this model was tested for its applicability in both tumor entities in patients treated with sunitinib and pazopanib, respectively.

In the following the links between PK and PD models are separately described for the study drugs sunitinib and pazopanib.

Sunitinib

VEGFR-2 plasma levels during sunitinib therapy were described using an indirect response model:

$$\frac{dsVEGFR2}{dt} = k_{in} \cdot \left[\frac{1}{(1 + \alpha_{sVEGFR2} \cdot INH)}\right] - k_{out} \cdot sVEGFR2 \qquad \text{(Eq. 3.28)}$$

k_{in} is a zero-order production rate, which was assumed to be equal to the product of individual sVEGFR-2 baseline value ($BL_{sVEGFR-2}$) and the first-order elimination rate k_{out}. Mathematically, the baseline can then be calculated by the quotient of k_{in} and k_{out}. α denotes for the intrinsic activity of sunitinib on sVEGFR-2 production. The inhibitory function *INH* comprises a hyperbolic function which describes the fractional tyrosine kinase inhibition of sunitinib and SU12662 based on the total unbound active concentration (AC_U). This approach assumes an identical potency of both molecules, which has been reported by Faivre *et al.* [**153**]. The fixed value of the dissociation constant (K_D) was originally derived from Mendel *et al.* [**58**], whereas protein binding values for both substances were fixed to 0.95 and 0.90 for sunitinib and its active metabolite, respectively [**46**,**59**]:

$$INH = \frac{AC_U}{K_D + AC_U} \qquad \text{(Eq. 3.29)}$$

Pazopanib

As the pharmacodynamics can be regarded comparable between both TKIs, the same base indirect response model was initially used for pazopanib. However, the drug-specific component, *INH*, had to be defined for pazopanib as the original PK/PD model was developed solely for sunitinib. In case of pazopanib, the active concentration is equal to the total concentration with a protein-bound fraction reported between >0.99 and >0.999 [**47**,**59**,**151**]. Several fixed values in this range were tested in the model. However, due to the model structure the actual effect was negligible. The value chosen in the final model was 0.999, which is more in accordance with the overall data from the literature.

Furthermore, different transducer signals were tested for pazopanib. These included, in addition to the inverse linear relationship used in the PK/PD models for sunitinib (Equation 3.28), a linear (with γ fixed to 1), a power (Equation 3.30) and a hyperbolic relationship (Equation 3.31). Fractional tyrosine kinase inhibition (*INH*) was calculated

using the active, unbound concentration of pazopanib and the in vitro dissociation constant (K_D) reported in the SmPC of Votrient® (Equation 3.29) [**47**]. It was also explored if the active concentration of pazopanib is better suited to describe the effect (*EFF*) on sVEGFR-2 plasma concentration in the respective models.

The following equations were tested in addition to Equation 3.28 during model development:

$$EFF = 1 + \alpha \cdot INH/AC_u^{\gamma} \quad \text{(Eq. 3.30)}$$

$$EFF = 1 + \frac{\alpha \cdot INH/AC_u}{(INH_{50} + INH/AC_u)} \quad \text{(Eq. 3.31)}$$

Besides that, an E_{max}-model was also tested for comparison as potential relationship between PK and PD. As increasing sVEGFR-2 levels were observed in some patients while still on treatment according to the documented dosing schemes, the implementation of resistance models was investigated by testing feedback models.

Feedback-mechanism

A potential feedback mechanism induced by pazopanib was tested and integrated based on the neutropenia model by Friberg *et al.* [**106**]. Here, a rebound effect (*REB*) is calculated based on the individual baseline value of sVEGFR-2 relative to the current sVEGFR-2 concentration at time *t*. An additional exponent *γ* was included to account for the steepness of the effect:

$$REB = \left(\frac{Baseline_{sVEGFR2}}{sVEGFR2(t)}\right)^{\gamma} \quad \text{(Eq. 3.32)}$$

3.10.2 sVEGFR-3

The pharmacodynamic model for sVEGFR-3 was originally developed by Kanefendt *et al*. in patients with mCRC treated with sunitinib based on the sVEGFR-2 model reported by Lindauer *et al.* [**109**,**126**]. Here, this model was tested for its applicability in both tumor entities in patients treated with sunitinib and pazopanib, respectively.

In the following the links between PK and PD models are separately described for the study dugs sunitinib and pazopanib.

Sunitinib

As stated above the analogous indirect response model with an inverse linear relationship was already shown to be applicable for sunitinib-treated mCRC patients. Hence, the same approach detailed in Section 3.10.1 was used for model development analyzing data from both cohorts.

Pazopanib

Comparable to sVEGFR-2 no PK/PD relation for pazopanib was known from the literature. Again, the model developed for linking sunitinib pharmacokinetics with sVEGFR-2 plasma concentrations served as basis for model development. Hence, as detailed in section 3.10.1, three different transducer signal models as well as E_{max} and feedback relationships were tested for linking pazopanib pharmacokinetics with sVEGFR-3 response. The dissociation constant (K_D) necessary for calculation of an *INH* (Equation 3.29) value was taken from in the official EPAR/SmPC of Votrient® [**47**]

3.10.3 Blood Pressure

The model for systolic and diastolic blood pressure used in this study was also developed based on data from 12 healthy volunteers by Lindauer *et al.* [**109**]. The impact of sunitinib on patients' blood pressure was described by two separate signals: an immediate and a time-delayed effect. The immediate effect was set equivalent to the fractional inhibition by sunitinib (*INH*, Equation 3.29).

The time-delayed effect was described by using the following equation:

$$\frac{dDINC}{dt} = \frac{1}{\tau} \cdot (INH - DINC) \qquad \text{(Eq. 3.33)}$$

Where τ denotes for the time needed until the effect occurs and *DINC* for the time-delayed effect.

Diastolic and systolic blood pressure ($BP_{sys/dia}$) were then described by the sum of both signals linked by a proportionality factor *R* which quantified the proportional contribution of the slower signal to the overall effect:

$$BP_{sys/dia} = BSL_{sys/dia} \cdot \left[1 + \alpha_{sys/dia} \cdot (INH + R \cdot DINC)\right] \qquad \text{(Eq. 3.34)}$$

Where, $BSL_{sys/dia}$ denotes for the baseline systolic or diastolic blood pressure. Analogous to the other pharmacodynamics models used $\alpha_{sys/dia}$ denotes for the intrinsic activity of sunitinib and its metabolite.

The individual blood pressure baseline ($BSLm_{sys/dia}$) was assumed to be variable over the course of a day. Therefore, a model reflecting the circadian rhythm of blood pressure was implemented. This model was parameterized with two cosine terms whereas *AMP1* and *AMP2* represented the amplitudes and *PS1* and *PS2* the phase shifts:

$$BSL_{sys/dia} = BSLm_{sys/dia} \cdot \left[1 + \begin{pmatrix} AMP1 \cdot \cos\left(\frac{TIME \cdot 2\pi}{24} - PS1\right) \\ + \\ AMP2 \cdot \cos\left(\frac{TIME \cdot 2\pi}{24} - PS2\right) \end{pmatrix}\right] \qquad \text{(Eq. 3.35)}$$

As this model is highly parameterized and only sparse blood pressure measurements were available for each patient, several values of this model had to be fixed to the respective estimates reported by Lindauer *et al.* [**109**].

3.11 Survival analysis

In general, methods for analyzing survival data can be categorized in parametric and non-parametric approaches. Both were applied in this thesis. Non-parametric survival analysis does not rely on a fixed amount of model parameters and makes no assumptions on the underlying distribution. The main advantage of this type of analysis is that it is easy to use and interpret as it provides a fast summary of the data. On the other hand, the implementation of potential predictors is limited [**103**,**154**]. In contrast,

parametric methods assume a defined distribution of the underlying data and allow the implementation of potential influential variables. The most common distributions used in models are shown in Section 3.11.3 (Equation 3.45 – 3.47).

Key feature of all types of survival analyses is that the various types of censored data are taken into consideration [**103**,**155**]:

- *Right-censored*: Data is described as right-censored when patients drop out of a study for undefined reasons before the endpoint or the end of the study is achieved. Right-censoring can be further classified into three subtypes:
    - *Type I*: Censoring of patients at time of study end due to not achieving the expected endpoint (e.g. not developing a progressive disease).
    - *Type II*: Censoring of patients due to premature termination of a study when the expected number of events already occurred.
    - *Randomly censored*: Censoring of patients leaving the study prematurely due to unknown reasons (Lost to follow-up)
- *Interval censored*: Censoring of patients within a certain time interval, as the exact date is not known.
- *Left censored*: Censoring of patients when an event already happened in an undefined time in the past.

Whereas right-censored data, including the various subtypes, is quite common in survival analysis, left-censored data is usually not to be expected.

The mathematical basis for survival analysis is given by the *survivor* and the *hazard function*. The survivor function is defined as [**103**]:

$$S(t) = P(T \geq t) = 1 - F(t) \qquad \text{(Eq. 3.36)}$$

Where *F(t)* is

$$F(t) = \int_0^t f(u)du \qquad \text{(Eq. 3.37)}$$

F(t) is the cumulative distribution function of a random variable *T* which describes the distribution of survival at time *t* and is determined by the integral of its probability density function *f(u)*. Based on this the survival function *S(t)* expresses the probability that an event has not occurred by time *t* with P(T≥t). Applied to progression-free

survival as endpoint *T* describes the time until progression and *S(t)* the probability of not developing a progressive disease after time *t* [**103**,**156**].

The hazard function *h(t)* describes the instantaneous risk of an event at time *t*. Mathematically, *h(t)* is defined by

$$h(t) = \lim_{\Delta t \to 0} \frac{P[(t \leq T < t + \Delta t) | T \geq t]}{\Delta t} \quad \text{(Eq. 3.38)}$$

Where *Δt* is an additional time frame of survival beyond time *t* [**103**,**155**,**156**]. The hazard rate can be calculated from the relationship between the survivor function and probability density function *f(t)*, which is the derivative of *F(t)*:

$$f(t) = S(t) \cdot h(t) \quad \text{(Eq. 3.39)}$$

Progression-free survival under first-line therapy with sunitinib and pazopanib, as described in section 3.3.6, was evaluated as endpoint in all survival analyses. Progression was denoted with 1 and censored data with 0. The non-parametric Kaplan-Meier analysis is described in section 3.11.1. Parametric methods used in this work comprise the Cox regression analysis as well as a model-based time-to-event (TTE) approach using NONMEM® described in section 3.11.2 and 3.11.3., respectively.

3.11.1 Kaplan-Meier analysis

The Kaplan-Meier analysis is one of the most common non-parametric methods used in survival analysis. Probability of survival (or the probability of not suffering from a progression) can be calculated by multiplying the quotient of patients still alive, which results from the difference between the number of patients at risk n_i and the number of patients with an actual event d_i at time t_i, and divided by the patients at risk at time t_i for each observed time-point:

$$\hat{S}(t_i) = \prod_{i=1}^{k} \left(\frac{n_i - d_i}{n_i} \right) \quad \text{(Eq. 3.40)}$$

Where $\hat{S}(t_i)$ denotes for the estimate of the survivor function at time t_i with *k* as vector of observed time-points [**103**,**155**].

For graphical analysis the cumulative probability of survival (or no progression) was plotted against the observation time. Censored data was denoted with a vertical line at the respective point in time. Potential influential factors on progression were tested in

univariate analyses. While covariates with only two characteristic values, like gender or prior nephrectomy, could be used without modification, continuous covariates had to be categorized. Here, categorization was limited to two groups per variable using the median as indicator. Single nucleotide polymorphisms, which were already categorized, were dichotomized. A list of all tested covariates is shown in Appendix **A.**

For assessing potential effects the log-rank test was applied and the p value was calculated. In addition, it was necessary to prove these results with a permutation test, due to the small sample size as otherwise p values could be false significant. Kaplan-Meier analysis was performed using the *survival* package of R whereas the *coin* package was used for permutation tests (Table 3.5) [**120**,**157**].

3.11.2 Cox regression

The Cox regression model is a semi-parametric model for survival data based on the proportional hazard model. The general expression is given by

$$h(t) = h_0(t) \cdot e^{\psi} \qquad \text{(Eq. 3.41)}$$

In this case ψ is the linear combination of covariates X_i and their corresponding hazard β:

$$\psi = \beta_1 \cdot X_{1i} + \beta_2 \cdot X_{2i} \ldots + \beta_n \cdot X_{ni} \qquad \text{(Eq. 3.42)}$$

$h_0(t)$ can be described as the baseline hazard without any influential factor acknowledged. The baseline hazard $h_0(t)$ is an unknown entity as the only requirement is that $h_0(t) > 0$; however by using a maximum likelihood approach the model parameters can be estimated [**103**]. In principle the Cox regression is used to compare groups of patients or the influence of covariates based on the *hazard ratio* (HR) which is in general the quotient of hazard functions of two groups with the main assumption that the hazard is constant over time [**158**]:

$$HR = \frac{h_A(t)}{h_B(t)} \qquad \text{(Eq. 3.43)}$$

For parameter estimation the log-likelihood function of the proportional hazard model is maximized. This function is specified by [**103**]:

$$LogL(\beta) = \sum_{i=1}^{n} D_i \left[\beta X_i - \sum_{s \in R(t_i)} e^{\beta X_n}\right] \qquad \text{(Eq. 3.44)}$$

with D_i being the event indicator which is zero in case of a right censored event and one in case of a documented progression. X_i is a vector of covariates for the *ith*

individual with a progression event and the term on the right hand side sums up all patients at risk at time t_i. The standard method used in the *survival* package in R is the *efron* algorithm which is a modified version of the likelihood approach explained above. However, this method was primarily designed for dealing with tied observations [**159**]. With regard to the low sample size in the underlying cohort every event could be assigned to a specific subject. Hence, the use of *efron* compared to the standard approach did not result in different parameter estimates.

Covariates were tested in a stepwise manner, analogously to the covariate analyses for the PK/PD models. The significance criterion for forward inclusion was set to $p > 0.05$ and for backward exclusion to $p < 0.01$. P values were calculated using the Wald- and the Likelihood ratio test. Appropriateness of included covariates was assessed by calculation of 95% confidence intervals for the estimated β, if possible. Here, the null hypothesis (no effect of the respective covariate) could be rejected, if zero was not included in the interval. Furthermore, the final models were used for simulation of survival curves and compared. A list of all tested covariates is shown in Appendix **A**.

Cox regression was performed using the *survival* package of R [**120**].

3.11.3 Model-based time-to-event analysis

A model-based time-to-event (TTE) approach allows, in contrast to the classical survival analysis methods, the direct connection of a PK/PD model with an outcome model. In principle, this corresponds to the proportional hazard model used in the Cox regression analysis. The hazard β is then estimated similarly to a rate constant in a pharmacokinetic model and shares the same unit of time^{-1}.

Different distributions were tested in this study. The most common distribution used in TTE analysis is the exponential distribution with the assumption of a constant hazard ($\beta = 0$) (Equation 3.45). Due to the relatively short observation times, a constant hazard model is usually the appropriate choice for oncology studies. However, additionally two time-dependent models were investigated for their applicability. The Gompertz model assumes an exponential increase of the baseline hazard over time (Equation 3.46) while the Weibull distribution (Equation 3.47) shows a stronger increase of the hazard in the beginning becoming almost linear at later time-points [**104**].

$$h(t) = \lambda_0 \cdot e^{\beta} \quad \text{(Eq. 3.45)}$$

$$h(t) = \lambda_0 \cdot e^{\beta \cdot t} \quad \text{(Eq. 3.46)}$$

$$h(t) = \lambda_0 \cdot e^{\beta \cdot \ln(t)} \quad \text{(Eq. 3.47)}$$

A graphical presentation of all three functions is shown in Figure 3.4. Covariates tested included the categorical factors which were also investigated in the classical approaches as well as time-dependent covariates. These comprised the plasma concentrations and AUC values of sunitinib, SU12662 and pazopanib as well as the biomarkers sVEGFR-2/3 and blood pressure. For this purpose the developed PK/PD models were linked with the TTE model in a PK/PD/outcome model. Thus, the respective exposure parameters could be calculated for every point in time based on the individual pharmacokinetic or pharmacodynamic parameter estimates. A covariate was kept in the model when its inclusion led to a significant decrease of the objective function value (-3.84 with one degree of freedom, p = 0.05). Model appropriateness was evaluated, similar to the PK/PD models, with visual predictive checks by simulating 1000 replicates using the final model parameters and comparing the results to the observed survival data using PsN (Section 3.1.5) [**111**]. Model-based TTE was conducted using NONMEM® [**88**].

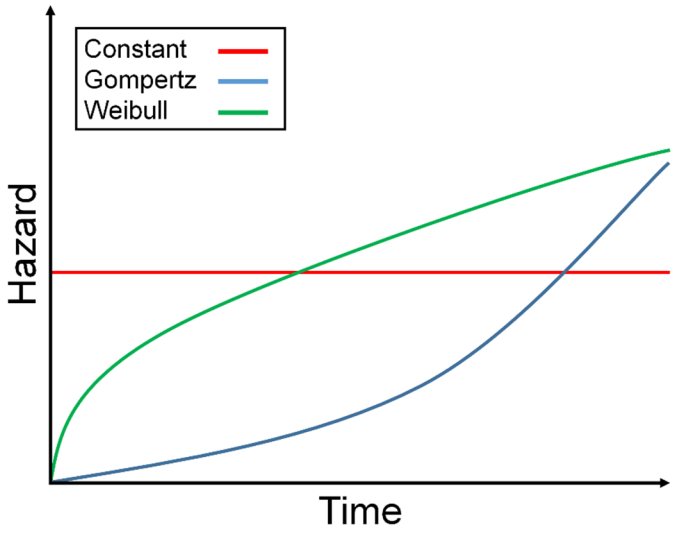

Fig. 3.4: Graphical presentation of the investigated distributions in the model-based time-to-event analysis.

3.12 Markov models for toxicity analysis

With the exception of hypertension, which was quantified as blood pressure in mmHg over the course of the study in all patients, severity of therapy-related toxicity was documented using the latest version of the CTCAE v4.03 [**105**] (Section 1.5.2, Tab. 1.2).

To describe this data appropriately, Markov models were developed to capture the presence of certain adverse events and their respective grade over the course of the study duration. As only limited data was available for the pazopanib cohort, development of these models was solely conducted for sunitinib patients and adverse events with a high incidence. The two most common adverse events observed in renal cell cancer patients treated with sunitinib patients were myelosuppression as well as fatigue. *Myelosuppression* comprised all blood-related adverse events such as anemia, neutropenia, thrombocytopenia and pancytopenia. If two blood-related adverse events occurred simultaneously in one patient, the one with the highest documented CTCAE grade was included in the analysis. In total, 9 of 24 sunitinib patients developed a myelosuppression of any grade during the first-line therapy and 9 a fatigue of any grade.

A general statistical approach for analysis of ordered categorical data is the proportional odds model [**160**]. This method allows the modeling of the probability of a certain event based on multiple influence factors [**154**]. For a binominal case, e.g. no toxicity or a severity grade of 1, the model can be written as

$$logit(p) = \log\left(\frac{p}{1-p}\right) = \alpha \cdot \beta X \qquad \text{(Eq. 3.48)}$$

Here, *logit(p)* is the logarithm of the odd *p* suffering from grade 1 toxicity. *β* describes the strength of influence of variable *X* on *p* and *α* can be interpreted as baseline risk [**160**,**161**]. If multiple factors should be acknowledged in the model this can be expressed by a linear relationship, similar to the equivalent parameter in the proportional hazard model. Main assumption of this approach is that coefficient *β* is identical for every step within the categorized data. In case of drug related toxicity, this means that the increase in risk of sustaining a certain grade quantified by *β* is equal for every grade [**162**].

However, one drawback of this method is that all observations are treated as independent, which can be quite problematic with regard to the reliability of the

estimated probabilities [**160**]. To cope with this issue a first-order continuous-time Markov process was implemented to describe the probabilities of transitions between the different toxicity grades in this study. Contrary to the proportional odds model, the probability of transition between states is dependent solely on the current observation, which is referred to as the *Markov property*. All other states in the past are ignored and have no influence on the transitions [**84**]. The general definition of the *Markov property* is given by [**163**]:

$$P(X_{n+1} = j | X_1 = i_1, \dots, X_{n-1} = i_{n-1}, X_n = i) \quad \text{(Eq. 3.49)}$$

X is a random variable with a discrete number of possible states, in this case the potential CTCAE grades. Assuming that *n* defines the current time then the equation states that the next transition is independent of past events given the actual event.

However, in this thesis a continuous-time Markov model was used, hence the *Markov property* changes as follows:

$$P(X_{t+r} = j | X_r = i) \quad \text{(Eq. 3.50)}$$

Where *t* is defined as time at which state *i* is prevalent and *r* is the time period the state *i* lasts. Analogous to the discrete case (Equation 3.49) the *Markov property* is defined as memoryless as the possible transition in another state *j* or the remaining time in the current state *i* is independent of the time already spent in *i* [**163**].

Analogously to a pharmacokinetic model, a continuous-time Markov process can be modeled using a compartmental approach. Each compartment represents a possible state with the amounts in a compartment as probabilities which sum up to one in total. Transitions between compartments are modeled with rate constants interpreted as probabilities for changing the state based on the current state, e.g. k_{01} for transition between no adverse event and CTCAE grade 1 [**163**,**164**]. Rate constants describing the change to a higher grade can be referred to as “worsening rates”, while “recovery rates” characterize the opposite direction. Mathematically, these processes are described with ordinary differential equations.

The number of possible transitions is dependent on the observed data. Usually, it can be expected that a toxicity increases gradually over time, so that when severity reaches grade 3 the patient has already undergone grade 1 and 2. However, in this study it was more often the case that the first grade documented of any toxicity was grade 2 or higher. With regard to the CTCAE grading, it is possible that toxicity was nearly asymptomatic in the beginning or worsened so fast that no differentiation was possible.

Therefore a model which only allowed transitions from the current to the next higher or lower state served as basis for analysis. A similar approach was already successfully applied to lung cancer patients receiving erlotinib continuously on a daily basis [**108**]. Several reductions of the primary model were tested by assuming that rate constants between states are possibly indistinguishable. For comparison a model which allowed transitions between all compartments, e.g. switching from the highest grade back to the lowest was also considered. The influence of drug exposure (or biomarker response) on the worsening and recovery rate constants for blood-related toxicity of any grade was tested by using

- *total drug concentration over time*
- *active, unbound drug concentration over time*
- *cumulative, active, unbound drug AUC over time*
- *sVEGFR-2/3 plasma concentration over time*
- *sVEGFR-2/3 plasma concentration relative to estimated baseline over time*

In case of missing time frames, e.g. the start of an adverse event was documented, but the time-point of recovery was not specified, the duration was set to the end of drug intake of the respective cycle. Regardless of the on- or off-phase of sunitinib, the minimum duration of an adverse event was assumed to be one week. Model performance was evaluated using visual predictive checks for categorical data. The model was qualified using the methods as described in Section 3.8.3. Parameter estimation was performed using NONMEM® [**88**].

4 RESULTS

4.1 Biomarker and drug analysis

4.1.1 sVEGFR-2

Quality control

Quality control (QC) samples were analyzed during each assay run to confirm the specifications given on precision and accuracy given by the manufacturer. Since plasma samples were not available from another cohort of patients, QC samples were generated from a different batch of the sVEGFR-2 Kit. Except for one measurement, the concentrations of all quality control samples were within the reference range. An overview of the QC results for sVEGFR-2 is shown in Table 4.1.

Tab. 4.1: Mean and relative standard deviation (CV, %) of quality control (QC) samples for the sVEGFR-2 analysis

Reference range	Mean [pg/mL]	CV [%]
216 - 370	315.5	14.8
1171 - 1920	1297.9	10.5
2340 - 3413	2541.0	8.1

Concentration-time profiles (mRCC patients)

Baseline values were available of 39 patients (88.6%), 25 (92.6%) treated with sunitinib and 14 (82.4%) with pazopanib. Missing baseline values were either a result of missing samples or the lack of enough material for analysis.

Mean and median baseline value of the overall population were 9368.4 pg/mL and 9117.5 pg/mL with a range of 5561.7 – 14211.6 pg/mL, respectively. When building subgroups for each drug treatment an arithmetic mean and median of 8982.3 pg/mL and 8890.4 pg/mL (range: 5561.7 – 14211.6 pg/mL) were observed for sunitinib patients. For pazopanib patients these values denoted with 9937.2 and 9743.6 (range: 7676.7 – 12679.1 pg/mL), respectively. Figure 4.1 and Figure 4.2 show the mean concentration of sVEGFR-2 over the course of the study in patients treated with sunitinib and pazopanib, respectively.

As expected, sVEGFR-2 concentrations increased to rise again once the off-phase of the first cycle started after 4 weeks of continuous dosing in sunitinib patients. Pazopanib was given on a daily basis without interruptions; hence the sVEGFR-2 plasma concentrations did not recover and stayed on a comparable level during the whole treatment. Since not all patients were treated over the whole period of 18 weeks the most reliable results for biomarker response could be obtained for the first six weeks.

The lowest mean concentration during the first cycle was reached in the fourth treatment week for sunitinib with an absolute value of 5069.2 pg/mL which denotes with 0.54 relative to baseline. After the same period of time the mean sVEGFR-2 plasma concentration under pazopanib treatment denoted with 6179.2 pg/mL. Whereas the absolute response was slightly lower after 4 weeks of treatment the relative response to pazopanib was comparable with 0.56.

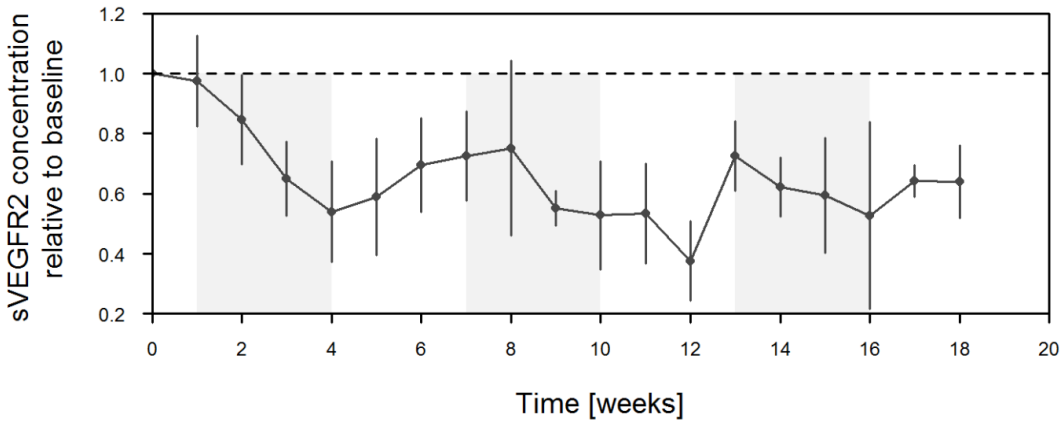

Fig. 4.1: Mean relative sVEGFR-2 concentration over time for the first 18 weeks after treatment start with sunitinib (not dose normalized). The dashed line indicates the mean sVEGFR-2 baseline value of sunitinib patients. Light-grey boxes indicate the time on treatment.

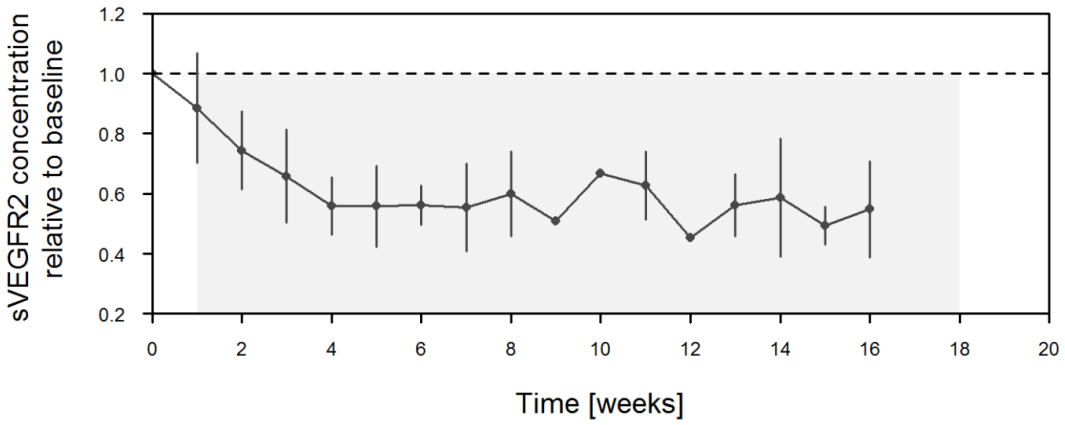

Fig. 4.2: Mean relative sVEGFR-2 concentration over time for the 18 weeks after treatment start pazopanib (not dose normalized). The dashed line indicates the mean sVEGFR-2 baseline value of pazopanib patients. The light-grey box indicate the time on treatment.

Assessment of normality

Normality of the sVEGFR-2 plasma concentrations was assessed graphically with QQ-Plots (Figure 4.3) and using the Shapiro-Wilk test.

For sunitinib and pazopanib patients combined, the test indicated non-normally distributed data with a highly significant p value of 0.00004. This was confirmed when building subgroups per treatment resulting in a p value of 0.0008 for sunitinib and 0.004 for pazopanib.

The combined data was then log-transformed and tested again. However, this had no effect on the overall results with a p-value of 0.001 still indicating non-normally distributed data. As a consequence of these findings, solely non-parametric methods were used for further analyses (Correlation analysis, 4.1.3).

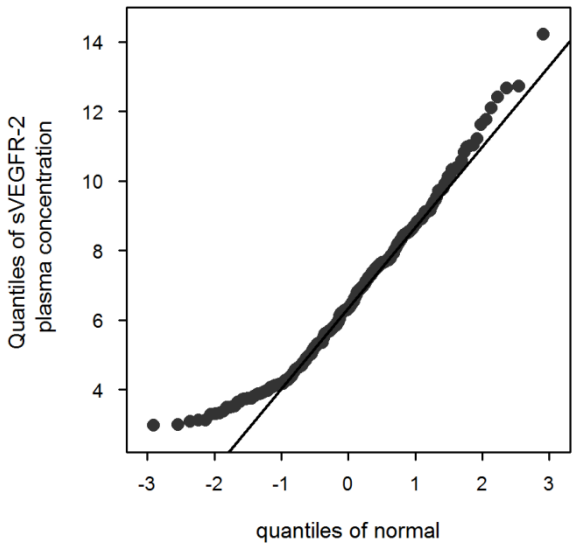

Fig. 4.3: Quantile-Quantile plot of absolute sVEGFR-2 concentrations versus the quantiles of normal.

Comparison of mean response between sunitinib and pazopanib

The Mann-Whitney-U test was used to compare the mean responses during the first 4 treatment weeks, which corresponds to one on-phase of a sunitinib cycle. sVEGFR-2 response was stronger with sunitinib, independent of dosage. Relative to the mean baseline value of each treatment group, sVEGFR-2 plasma levels are decreased by 43.9% in sunitinib and 37.8% in pazopanib patients in week 4. A comparison of mean sVEGFR-2 response to the respective treatment is shown in Table 4.2.

Comparison mRCC and mCRC patients (Sunitinib)

For mCRC patients, a median baseline value of 9362 pg/mL (range: 7869 – 9941 pg/mL) was observed, which is slightly higher compared to mRCC patients with a median of 8890.4 pg/mL (range: 5561.7 – 14211.6 pg/mL). However, the difference was not significantly different. Similar to the mRCC cohort the maximum reduction of sVEGFR-2 plasma concentration was achieved after 4 weeks of treatment.

Tab. 4.2: Comparison of mean sVEGFR-2 response between sunitinib and pazopanib for the first 4 weeks of treatment independent of dose (mRCC patients)

Treatment week	Mean sVEGFR-2 concentration [pg/mL]	Mean sVEGFR-2 concentration [pg/mL]	p value
	Sunitinib	Pazopanib	
1	8003.6	9116.0	0.26
2	7282.4	7876.2	0.31
3	6197.8	7033.5	0.34
4	5069.2	6179.1	0.24

4.1.2 sVEGFR-3

Quality control

Quality control samples were analyzed during each assay run to confirm precision and accuracy given by the manufacturer. Since plasma samples were not available from another cohort of patient, QC samples were generated from a different batch of the sVEGFR-3 Kit. Mean values and relative standard deviations are shown in Table 4.3.

Tab. 4.3: Mean and relative standard deviation (CV, %) of quality controls for sVEGFR-3

Reference concentration [pg/mL]	Mean [pg/mL]	CV [%]
10000.0	9997.2	3.1
6000.0	5937.5	4.8
2045.5	2142.7	7.2

Concentration-time profiles (mRCC patients)

Baseline values were available from 39 patients (88.6%), 24 (88.9%) treated with sunitinib and 15 (88.2%) with pazopanib. Missing baseline values were either a result of missing samples or the lack of enough material for analysis.

Mean and median baseline values of the overall population were 65365.6 pg/mL and 63132.7 pg/mL with a range of 35854.5 – 103886 pg/mL, respectively. When analyzing subgroups for each drug treatment a mean and median of 65433.8 and 64442.1 (range: 35754.5 – 103886) pg/mL can be observed for sunitinib. For pazopanib patients, these values were comparable with 65256.4 and 60247.3 (range: 37159.0 – 95998.2) pg/mL. Figure 4.4 and Figure 4.5 show the mean concentration of sVEGFR-3 over the course of the study in patients treated with sunitinib and pazopanib, respectively.

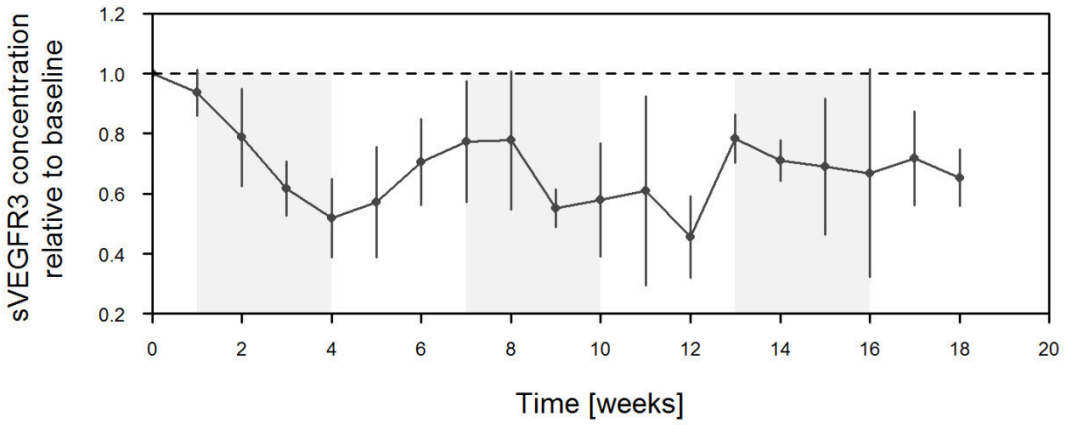

Fig. 4.4: Mean relative sVEGFR-3 concentration over time for the first 18 weeks after treatment start with sunitinib (not dose normalized). The dashed line indicates the mean sVEGFR-3 baseline value of sunitinib patients. Light-grey boxes indicate the time on treatment.

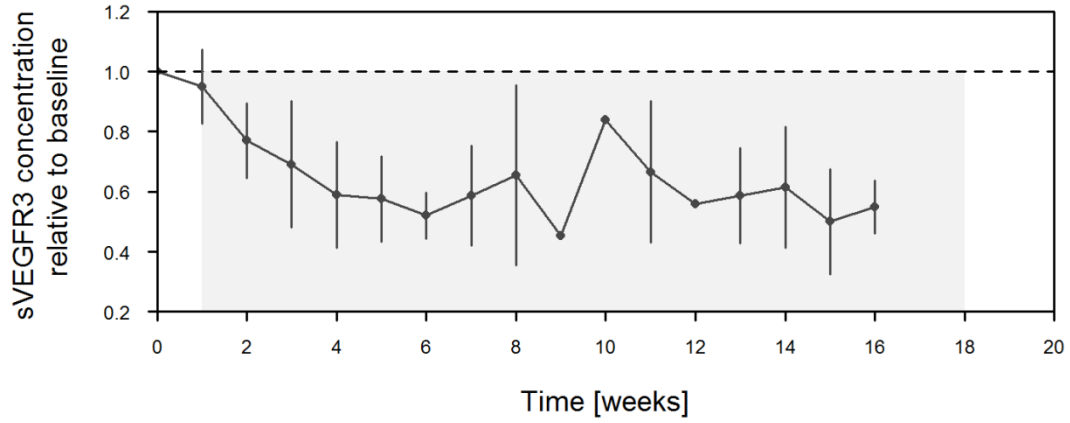

Fig. 4.5: Mean relative sVEGFR-3 concentration over time for the first 18 weeks after treatment start pazopanib (not dose normalized). The dashed line indicates the mean sVEGFR-3 baseline value of pazopanib patients. Light-grey boxes indicate the time on treatment.

Assessment of normality

Analogously to the sVEGFR-2 analysis, normality of the sVEGFR-3 plasma concentrations was assessed graphically with QQ-Plots (Figure 4.6) and using the Shapiro-Wilk test.

For sunitinib and pazopanib patients combined, the test indicated non-normally distributed data with a highly significant p value < 0.0001. This was confirmed when analyzing subgroups per treatment resulting in a p value < 0.0001 for sunitinib and < 0.01 for pazopanib.

The combined data was then log-transformed and tested again. However, this had no effect on the overall results with a p value < 0.0002 still indicating non-normally distributed data. As a consequence of these findings further analyses used solely non-parametric methods (Correlation analysis, Section 4.1.3)

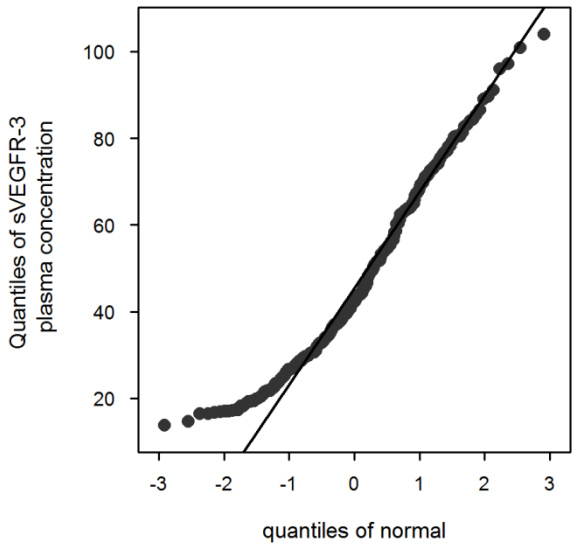

Fig. 4.6: Quantile-Quantile plot of absolute sVEGFR-3 concentrations versus the quantiles of normal.

Comparison of mean response between sunitinib and pazopanib

Whereas the absolute concentrations differed at least at week 4 quite substantially, the difference was not statistically significant (Table 4.4). When comparing the mean sVEGFR-3 decrease relative to baseline this becomes more evident. At treatment week 4 pazopanib led to a 41% lower sVEGFR-3 plasma concentration compared to baseline, whereas the effect of sunitinib was slightly stronger with 48%.

Comparison mRCC and mCRC patients (only sunitinib)

For mCRC patients a median baseline value of 17501 (range: 14617 – 30632) pg/mL was observed, which was significantly lower compared to mRCC patients with a median of 63133 (range of 35854.5 – 103886) pg/mL. Similarly to the mRCC cohort the maximum reduction of sVEGFR-3 plasma concentration was achieved after 4 weeks of treatment.

Tab. 4.4: Comparison of mean sVEGFR-3 response between sunitinib and pazopanib for the first 4 weeks of treatment

Treatment week	Mean sVEGFR-3 concentration [pg/mL]	Mean sVEGFR-3 concentration [pg/mL]	p value
	Sunitinib	Pazopanib	
1	65511.6	62826.9	0.45
2	54453.4	54405.0	0.78
3	39239.16	45604.0	0.43
4	31730.01	41679.6	0.38

4.1.3 Correlation analysis of sVEGFR-2 and sVEGFR-3 plasma concentrations

Correlation between sVEGFR-2 and sVEGFR-3 response to sunitinib and pazopanib was assessed by graphical inspection (Figure 4.7) and calculation of the Spearman's correlation coefficient (Table 4.5). The use of Spearman's correlation coefficient was necessary due to the non-normal nature of the underlying data. Correlation coefficients for the combined cohort as well as separated by drugs were in a similar range, indicating that both proteins were comparable in their informative value.

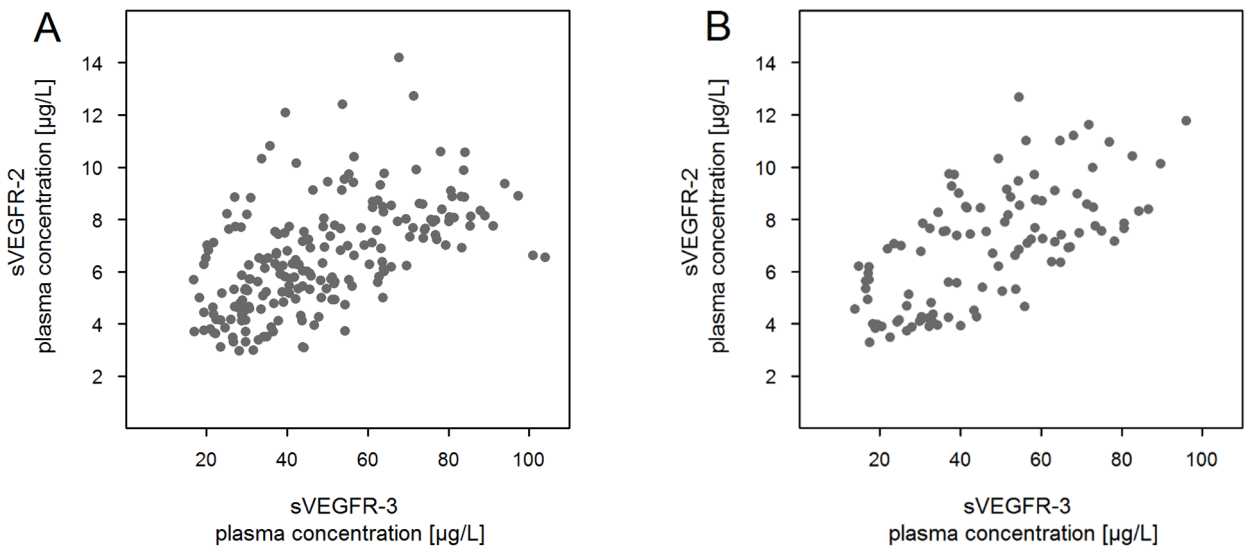

Fig. 4.7: Scatterplots of sVEGFR-2 and sVEGFR-3 plasma concentrations. (A = under sunitinib treatment, B = under pazopanib treatment)

Tab. 4.5: Correlation analysis sVEGFR-2 and sVEGFR-3

Treatment	Spearman's correlation coefficient
Sunitinib/Pazopanib	0.616
Sunitinib only	0.593
Pazopanib only	0.658

4.1.4 Blood pressure

Blood pressure measurements were conducted based on the same schedule for determined for plasma sampling. At least one measured value was available for 42 of 44 patients, including 26 sunitinib and 16 pazopanib patients. Diagnosed hypertension was documented for 31 patients (21 sunitinib, 10 pazopanib) while at least 28 patients (18 sunitinib, 10 pazopanib) did already receive an antihypertensive treatment before or right after starting the targeted therapy.

In total, 300 measurements were available for analysis. The mean response during therapy separated for sunitinib and pazopanib is shown in Figure 4.8.

Baseline measurements were available for 41 of 44 patients (93.2%) with 25 accounting for sunitinib (92.6%) and 16 for pazopanib (94.1%). Mean and median systolic blood pressure at treatment start was 138.2 mmHg and 136.0 mmHg with a range between 99.0 and 179.0 mmHg. After dividing the cohort in subgroups per study drug a mean and median of 140.0 mmHg and 137.0 mmHg (range: 99.0 – 179.0 mmHg) was observed for sunitinib patients and 135.4 mmHg and 133.0 mmHg (range: 106.0 – 168.0 mmHg) for pazopanib, respectively.

Diastolic blood pressure baseline values ranged between 66.0 and 105.0 mmHg for all patients with a mean of 82.0 mmHg and a median of 83.0 mmHg. With regard to the different treatment groups a mean and median of 83.6 mmHg and 86.0 mmHg (range: 66.0 – 105.0 mmHg) resulted for sunitinib and 79.4 mmHg and 78.0 mmHg (range: 66.0 – 102.0 mmHg) for pazopanib, respectively.

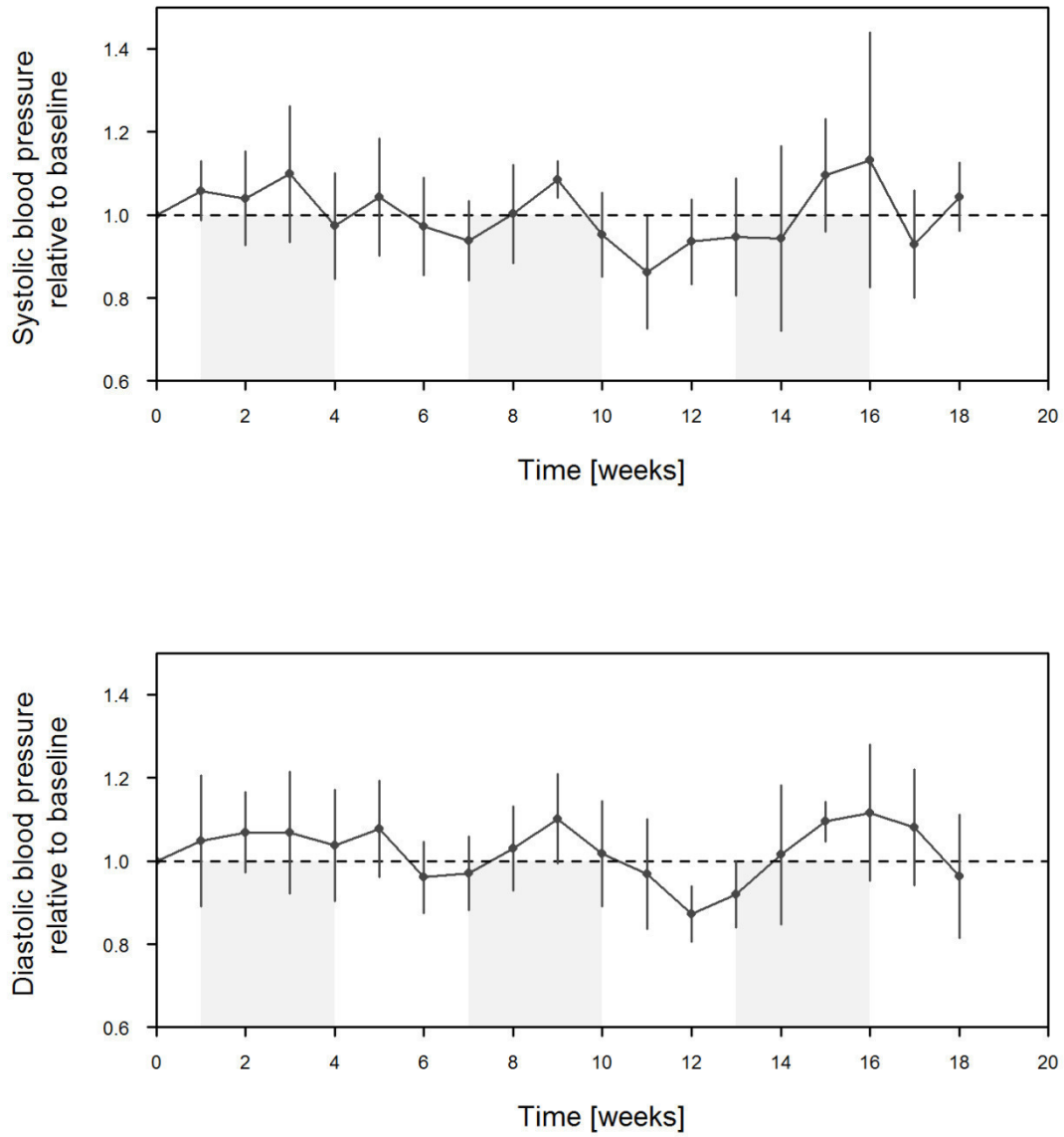

Fig. 4.8.A: Mean relative systolic (upper panel) and diastolic (lower panel) blood pressure over time for the first 18 weeks after treatment start with sunitinib. The dashed line indicates the mean blood pressure baseline value of sunitinib patients. Light-grey boxes indicate the time on treatment.

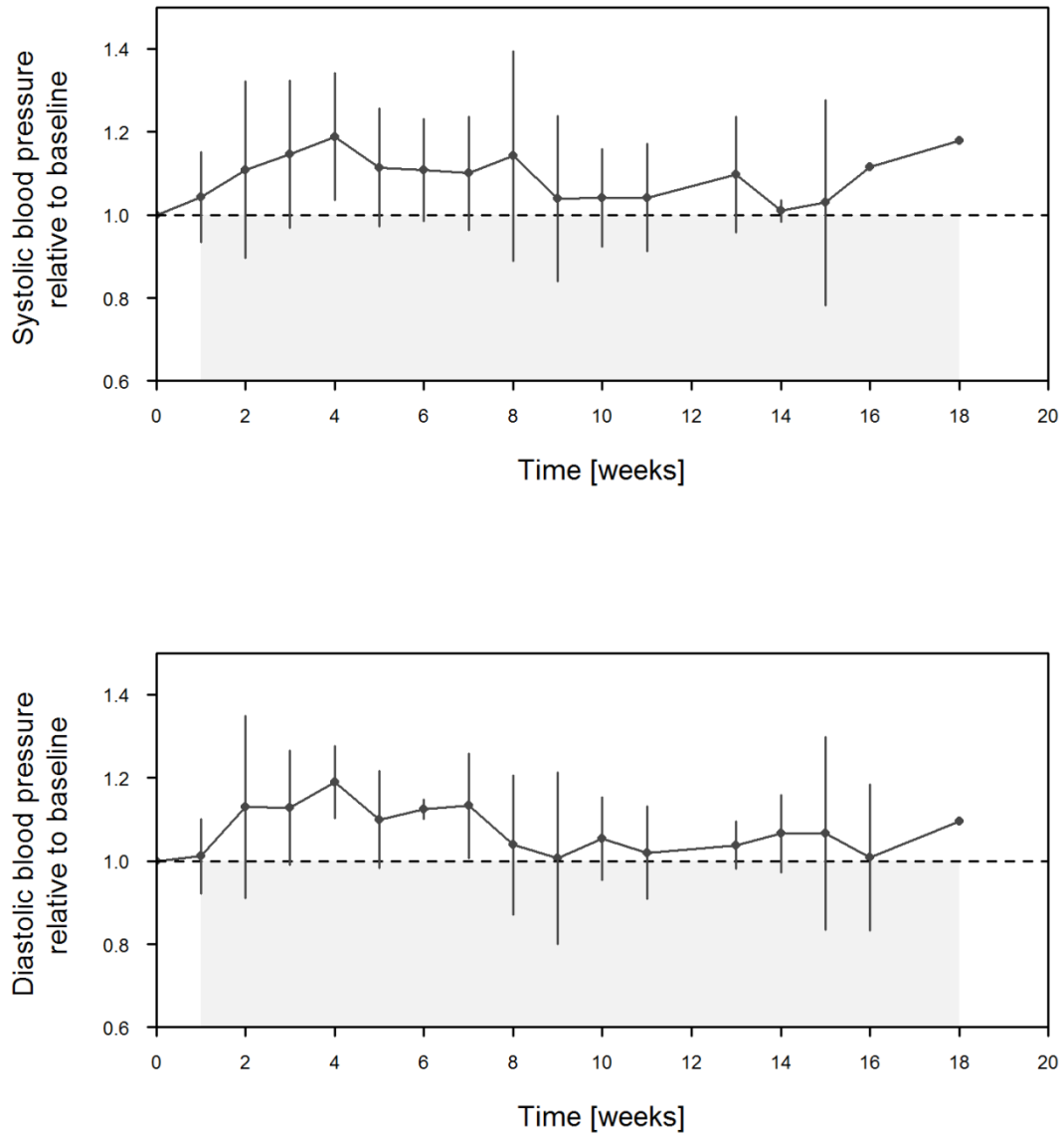

Fig. 4.8.B: Mean relative systolic (upper panel) and diastolic blood (lower panel) pressure over time for the first 18 weeks after treatment start with pazopanib. The dashed line indicates the mean blood pressure baseline value of pazopanib patients. Light-grey boxes indicate the time on treatment.

Comparison of mean response between sunitinib and pazopanib

Mean response of systolic and diastolic blood pressure show the expected fluctuation under sunitinib therapy with increasing values during on-phases and a decrease even below the initial baseline value in off-phases. Since pazopanib is administered on a daily basis without interruptions a stable increase of systolic and diastolic blood pressure was observed with a maximum after 4 weeks of treatment.The Mann-Whitney-U test was used to compare the mean responses during the first 4 treatment weeks, which corresponds to one on-phase of a sunitinib cycle. Mean values per week and per drug and their corresponding p values are shown in Table 4.6 A for systolic and in Table 4.6 B for diastolic blood pressure. There was no statistically significant difference between the mean blood pressure response in sunitinib and pazopanib after the first 4 treatment weeks.

Tab. 4.6 A: Comparison of mean systolic blood pressure response between sunitinib and pazopanib for the first 4 weeks of treatment

Treatment week	Mean systolic blood pressure [mmHg]	Mean systolic blood pressure [mmHg]	p value
	Sunitinib	Pazopanib	
1	134.9	138.2	0.48
2	140.8	147.5	0.47
3	157.5	150.6	0.59
4	138.2	155.0	0.06

Tab. 4.6 B: Comparison of mean diastolic blood pressure response between sunitinib and pazopanib for the first 4 weeks of treatment

Treatment week	Mean diastolic blood pressure [mmHg]	Mean diastolic blood pressure [mmHg]	p value
	Sunitinib	Pazopanib	
1	83.4	86.5	0.51
2	85.1	88.2	0.36
3	91.6	87.4	0.44
4	84.4	90.3	0.25

4.1.5 Sunitinib and N-Desethylsunitinib (SU12662)

374 samples from 26 mRCC patients were available for analysis (excluding baseline measurements for biomarker analysis before treatment start). 8 samples (2.1%) were below the limit of quantification for sunitinib or SU12662, respectively. Referring to the M1 method (Section 3.8.7), these values were excluded from the dataset. For details on the measurements in the included mCRC patients please refer to Kanefendt *et al*. [**126**].

Link between pharmacokinetics and pharmacodynamic response

The relationship between sunitinib pharmacokinetics and biomarker response in mRCC patients was assessed by graphical inspection of the mean response of the respective biomarker and the *INH* calculated from the mean measured active concentration of sunitinib and SU12662 (Equation 3.29). This PK/PD relationship was previously proposed by Lindauer *et al.* in healthy volunteers [**109**].

As the Figures 4.9 A-D indicate, the effects of active, unbound sunitinib and SU12662 concentration were time-delayed and full response was reached later in the treatment cycle. During the off-phase of two weeks the concentrations of sVEGFR-2 and sVEGFR-3 as well as blood pressure recovered.

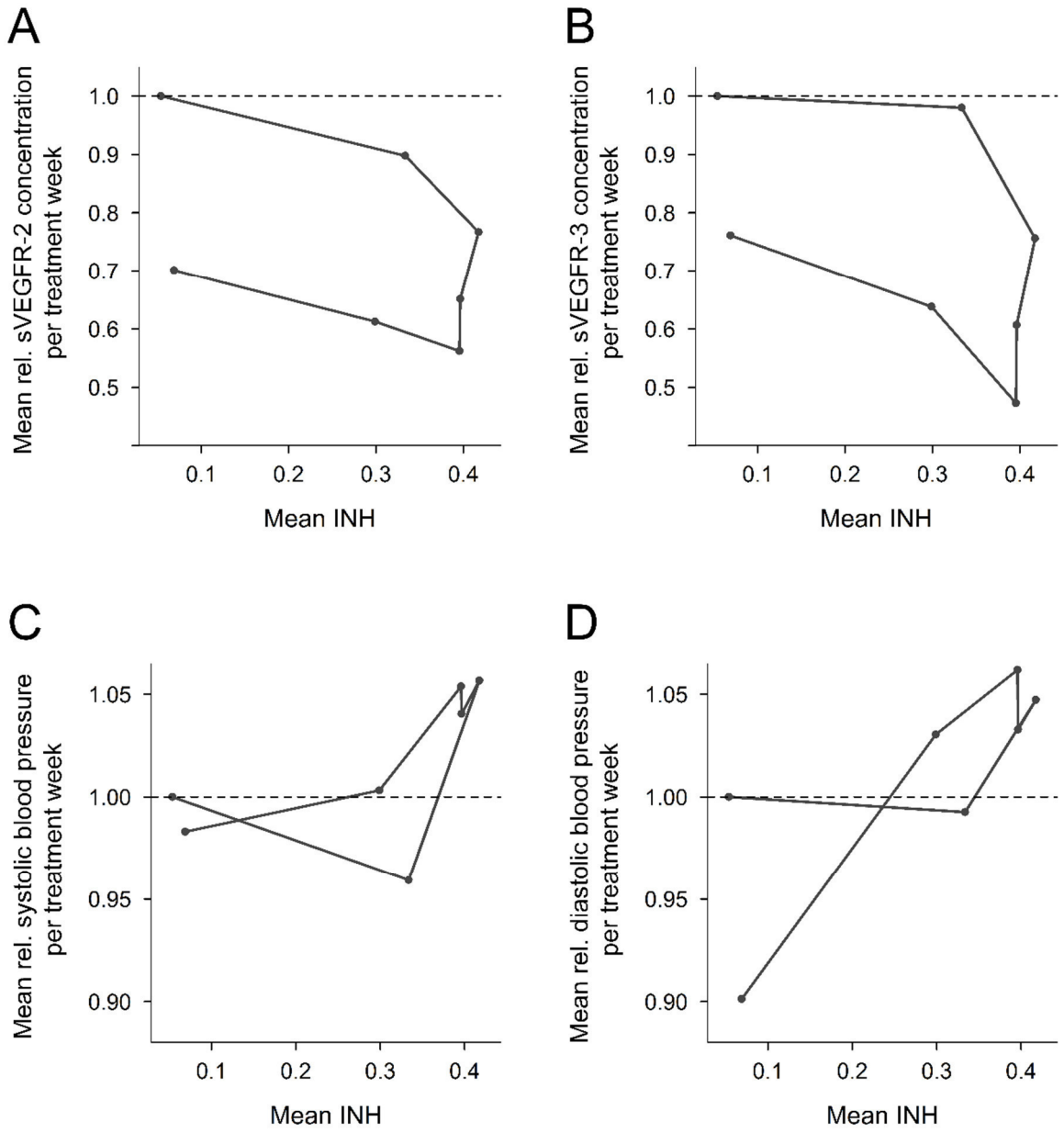

Fig. 4.9: Mean relative sVEGFR-2 concentration (**A**), mean relative sVEGFR-3 concentration (**B**), mean relative systolic blood pressure (**C**) and mean relative diastolic blood pressure (**D**) vs. inhibitory function (*INH*) for the first 6 weeks of sunitinib treatment.

.

4.1.6 Pazopanib

98 samples from 17 mRCC patients were available for analysis (excluding baseline measurements for biomarker analysis before treatment start). 3 samples (3.1%) were below the limit of quantification for pazopanib (0.1086 µg/mL). Referring to the M1 method, these values were excluded from the dataset (Section 3.8.7).

Link between pharmacokinetics and pharmacodynamic response

The relationship between pazopanib pharmacokinetics and the pharmacodynamic response was assessed by graphical inspection. Here, the plasma concentration of pazopanib and the calculated *INH* for pazopanib were plotted against the respective pharmacodynamic parameter. As the final PK/PD models used the total plasma concentration of pazopanib to describe the pharmacodynamic effects on blood pressure, sVEGFR-2 and sVEGFR-3, (see Section 4.3) only this relationship is presented in Figure 4.10 A-D.

Similarly to sunitinib, a time delay between the plasma concentrations of pazopanib and the maximum decrease or increase of the respective pharmacodynamic effect was observed. The usual therapy scheme does not include an off-phase without drug administration comparable to sunitinib, but is given continuously instead. Therefore, a hysteresis curve could not observed in the underlying data.

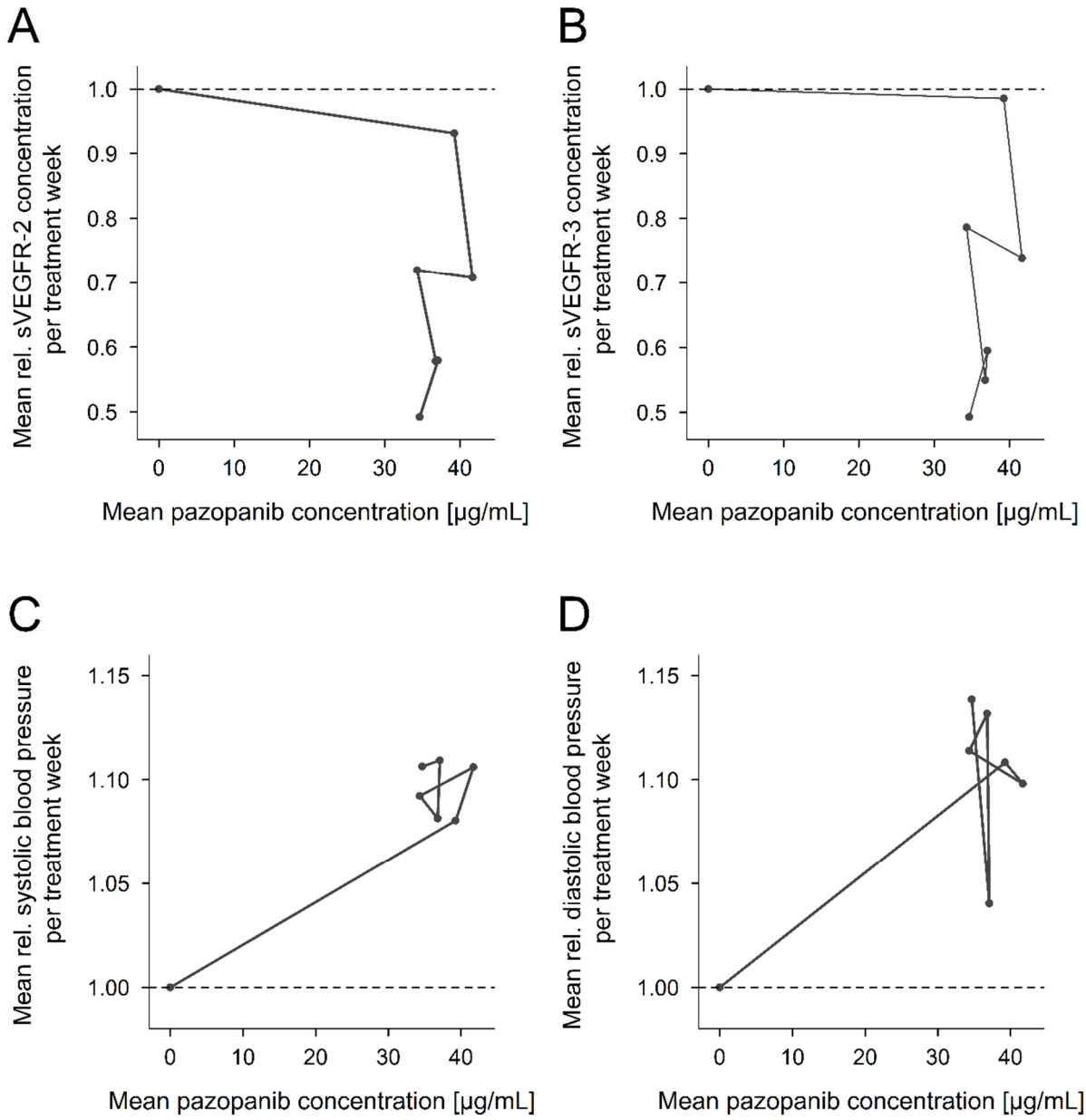

Fig. 4.10: Mean relative sVEGFR-2 concentration (**A**), mean relative sVEGFR-3 concentration (**B**), mean relative systolic blood pressure (**C**) and mean relative diastolic blood pressure (**D**) vs. the mean pazopanib plasma concentration for the first 6 weeks of pazopanib treatment.

4.2 Pharmacokinetic Models

4.2.1 Sunitinib and N-Desethylsunitinib (SU12662)

Model development based on Lindauer et al. [**109**]

Absorption was described via a transit compartment model. The respective parameters could not be estimated with enough precision with the underlying data and were therefore fixed to the values reported by Lindauer *et al.* [**109**]. The estimated population parameters of the remaining model parameters of the base model were different to what was previously reported in other analyses [**109**,**126**].

To account for missing dosing information in some cases, a parameter to estimate the variability on time of drug intake was considered. Introduction of this parameter led to an OFV decrease by 776.8 ($p < 0.0001$) and highly improved the overall model fit. However, the estimation of an inter-individual variability (IIV) on this parameter did not improve the model fit further. This was especially obvious when comparing the individual concentration vs time plots before and after the inclusion, which did not show any improvement. The same was observed when fixing the IIV to an arbitrary high value. Similar to the previous analysis of the mCRC patient data alone by Kanefendt *et al*. [**126**], the introduction of an additional peripheral compartment for SU12662 led to a significant improvement of the model (-30.2, $p < 0.0001$). However, the population parameter for the peripheral volume of the parent drug could not be estimated with enough precision and was therefore fixed to the reference value reported by Lindauer *et al*. [**109**] Separate proportional residual errors were best describing the remaining residual variability of the model.

IIV estimated on clearance, central volume of sunitinib ($V1_{Sunitinib}$), central volume of SU12662 ($V1_{SU12662}$) and the fraction metabolized to SU12662 (F_M) improved the model further. The removal of those parameters from the model led to significant worsening of the objective function value ($CL_{Sunitinib}$: +55.1 $p < 0.0001$, $V1_{Sunitinib}$: +20.3 $p < 0.0001$, $V1_{SU12662}$: +25.3 $p < 0.0001$, F_M: +106.7 $p < 0.0001$). Estimation of a covariance between the IIV of $CL_{Sunitinib}$ and the IIV of $V1_{Sunitinib}$ decreased the objective function value (OFV) by 20.9 and was therefore kept in the model.

η- and ε-Shrinkage was below 20% for all estimated parameters, hence a model misspecification regarding the statistical model could be excluded.

Inter-occasion variability (IOV), based on therapy cycles of sunitinib, was tested on IIV of $CL_{Sunitinib}$ and $V1_{Sunitinib}$, but did not lead to a statistically significant model improvement, indicating that the pharmacokinetics to not vary over time.

Based on analysis of the CWRES, six observations were removed from the dataset, exceeding values over or under 4.5 and -4.5, respectively. Even though not all of these values did exceed the threshold of ± 6 for outliers defined in Section 3.6.1, their influence on the model parameters was investigated. The percentage change of the model parameters after exclusion is shown in Table 4.7.

Tab. 4.7.: Percentage changes of population parameters after exclusion of potential outliers

Parameter	Unit	Percentage change after outlier exclusion
$CL_{Sunitinib}$	[L/h]	-1.18
$V1_{Sunitinib}$	[L]	-1.75
$V2_{Sunitinib}$	[L]	*Parameter fixed*
Q_P	[L/h]	+2.74
$CL_{SU12662}$	[L/h]	-0.50
$V1_{SU12662}$	[L]	+2.43
$V2_{SU12662}$	[L]	-6.41
Q_M	[L/h]	-19.78
Lag-time	[h]	+4.47
$\eta CL_{Sunitinib}$		+0.64
$\eta V1_{Sunitinib}$		-0.53
$\eta V1_{SU12662}$		-41.10
ηF_M		+1.54

Final parameter estimates of this model can be found in Table 4.8 B.

Model development based on Yu et al. [**110**]

Similarly to the reference model, liver blood flow (Q_H) was fixed to 80 L/h and the fraction metabolized to SU12662 to 0.21. A second compartment for sunitinib improved the model fit significantly (dOFV -128.5, $p < 0.0001$). However, the volume for the respective compartment could not be estimated with sufficient precision and was therefore fixed to a value previously reported by Houk *et al.* (Table 4.8 A) [**165**]. Fixing this parameter increased the OFV by 11.6. However, compared to the base model, the effect was still highly significant (dOFV 118.9, $p < 0.0001$). Similar to the reference model, clearance and volume parameters were scaled to a reference body weight of 70 kg to allow a better comparison with the literature values. In case of missing weight data the value was set to the respective population mean, stratified by gender. A proportional error model described the residual variability for both molecules best.

IIV was estimated for sunitinib clearance, central volume of sunitinib and SU12662 as well as the fraction metabolized to SU12662. Removal of these parameters from the model led to significant worsening of the model fit (CL +90.6 $p < 0.0001$, $V1_{Sunitinib}$ +42.0, $p < 0.0001$; V1 (SU12662) +18.5, $p < 0.0001$; F_M: +134.7, $p < 0.0001$). While the removal of the IIV on the absorption rate constant k_a increased the OFV by 27.3, the η-shrinkage on this parameter was reported with > 40% and was therefore considered as non-reliable estimate of the variability. η- and ε-Shrinkage was below 20% for all other estimated parameters, hence a model-misspecification regarding the statistical model could be excluded.

IOV, based on therapy cycles of sunitinib, was tested on the IIV of CL and IIV of $V1_{Sunitinib}$, but did not lead to a statistically significant model improvement, indicating that the pharmacokinetics did not vary over the course of the therapy.

Model selection

The PK model based on the one published by Yu *et al.* was considered superior and was therefore used for further analysis. This decision was based on the comparison of goodness-of-fit plots, visual predictive checks, and the reliability of the parameter estimates (Figure 4.11 and Appendix **D.I**). An overview on the final parameter estimates including bootstrap residuals and 90% confidence intervals for both models can be found in Table 4.8 A-B.

While the VPCs for both models indicate an adequate description of the data over the course of the therapy, the GOF plots showed that the model based on Lindauer *et al.* was not able to adequately describe maximum plasma concentrations of sunitinib and its metabolite, which is illustrated by a sharper cut-off of the population predictions. In addition, when plotting the individual and population predictions of both models against each other, it becomes more evident, that some higher plasma concentrations are not adequately described when using the model by Lindauer *et al*. (Appendix **D.I**).

In addition the individual predictions, population predictions and CWRES of both models were plotted against each other to identify deviations between predictions. For this purpose identical data sets, thus without the exclusion of the observations mentioned above for the transit compartment based model, were used. These plots indicated that the use of the model based on healthy volunteers led to a mistakenly identification of potential outliers. The respective observations could be described by the other model and were therefore not removed during the modeling process.

Furthermore, the need for a correction parameter to account for missing or unreliable information on dosing time, introduced additional uncertainty when the model based on Lindauer *et al.* was used. This approach was particularly problematic, as it was not possible to estimate variability on the correction factor without destabilizing the model. Hence, one fixed-effect parameter was applied to all patients which leads to a high uncertainty.

A schematic overview of the final structural model can be found in Figure 4.12.

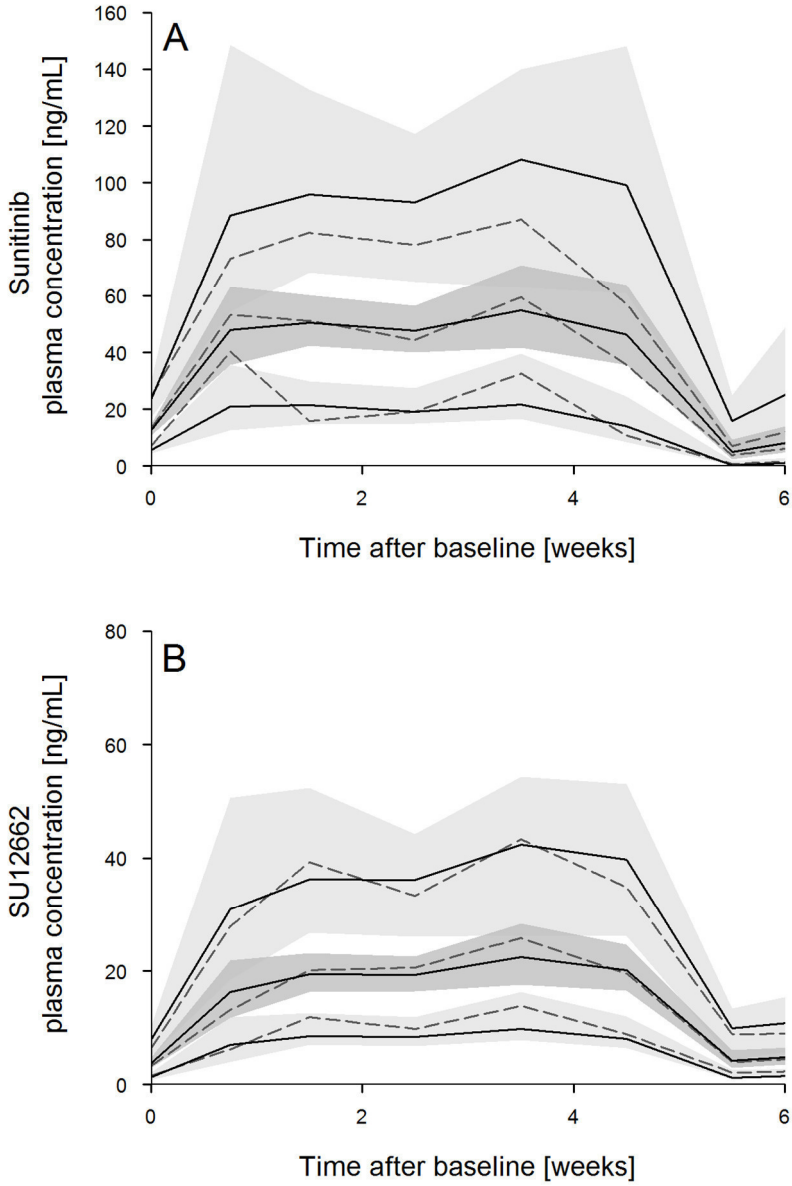

Fig 4.11: Visual predictive check of sunitinib (**A**) and SU12662 (**B**) concentrations for the first 6 weeks of treatment. The black solid lines indicate the mean model prediction and the 90% prediction interval. Dotted lines show the measured mean and interval, respectively. Dark and light grey areas represent the respective confidence bands.

Tab 4.8 A: Final parameter estimates for sunitinib and SU12662 based on the model by Yu *et al.* [**110**]

Parameter	Unit	Estimate (RSE, %)	Mean (Bootstrap)	90% CI
Sunitinib				
k_a	[1/h]	0.133 (34.6)	0.149	0.097 – 0.251
$CL_{Sunitinib}$	[L/h]	33.9 (6.0)	33.9	30.8 – 37.5
$V1_{Sunitinib}$	[L]	1820.0 (6.6)	1812.1	1607.8 – 1812.2
$V2_{Sunitinib}$	[L]	588*	-	-
Q_P	[L/h]	0.371 (18.9)	0.373	0.263 – 0.494
Q_H	[L/h]	80*	-	-
σ_P		-0.367 (14.1)	-0.361	-0.450 – (-0.283)
SU12262				
$CL_{SU12262}$	[L/h]	16.5 (5.4)	16.5	15.0 – 17.9
$V1_{SU12262}$	[L]	730 (14.1)	713.6	545.9 – 872.9
$V2_{SU12262}$	[L]	592 (13.2)	604.9	481.0 – 737.4
Q_M	[L/h]	2.75 (24.6)	2.90	1.96 – 4.27
F_M	-	0.21 *	-	-
σ_M	-	-0.281 (10.8)	-0.276	-0.326 – (-0.229)
IIV				
$\eta CL_{Sunitinib}$	%	30.3 (29.0)	29.0	22.2 – 35.2
$\rho(CL_{Sunitinib}, V1_{Sunitinib})$	.	-0.061 (48.3)	-0.069	-0.127 – (-0.019)
$\rho(CL_{Sunitinib}, F_M)$	%	-0.0425 (40.8)	-0.0392	-0.0671 – (-0.0130)
$\eta V1_{Sunitinib}$	%	25.3 (30.3)	23.0	18.0 – 29.7
$\rho(V1_{Sunitinib}, V1_{SU12662})$	-	0.0481 (51.8)	0.0534	0.0091 - 0.0996
$\eta V1_{SU12262}$	%	42.9 (54.8)	46.5	30.3 – 65.9
ηF_M	%	34.6 (20.5)	33.5	27.5 – 38.7

*Parameter fixed

Tab 4.8 B: Final parameter estimates for sunitinib and SU12662 based on the model by Lindauer *et al.* [**109**]

Parameter	Unit	Estimate (RSE, %)	Mean (Bootstrap)	90% CI
Sunitinib				
k_a	[1/h]	0.54*	-	
$CL_{Sunitinib}$	[L/h]	41.8 (6)	41.0	36.9 – 45.5
$V1_{Sunitinib}$	[L]	3350 (7)	3330	2952 - 3772
$V2_{Sunitinib}$	[L]	221*	-	-
Q_P	[L/h]	0.674 (29)	0.677	0.368 – 1.037
NN	-	1.46*		-
RFP	-	1.91*		-
MTT	[h]	1.48*		-
Lag-time	[h]	-3.97	-3.87	-4.83 - -2.79
σ_P mRCC	-	-0.328 (20)	-0.318	-0.430 - (-0.221)
σ_P mCRC	-	-0.365 (15)	-0.355	-0.446 – (-0.249)
SU12262				
$CL_{SU12262}$	[L/h]	19.8 (5)	19.62	17.84 – 21.66
$V1_{SU12262}$	[L]	2110 (8)	2080	1793 - 2376
$V2_{SU12262}$	[L]	540 (13)	575	445 – 731
Q_M	[L/h]	1.46 (26)	1.56	0.98 – 2.43
F_M	-	0.21*	-	
σ_M mRCC	-	0.322 (11)	0.320	0.260 – 0.382
σ_M mCRC		0.273 (9)	0.268	0.224 – 0.308
IIV				
$\eta CL_{Sunitinib}$	%	41.4 (15)	38.3	28.7 – 47.6
$\rho(CL_{Sunitinib}, V1_{Sunitinib})$	-	0.153	0.144	0.074 – 0.225
$\eta V1_{Sunitinib}$	%	45.3 (16)	43.2	27.2 – 47.5
$\eta V1_{SU12262}$	%	32.2 (20)	32.3	21.1 – 44.7
ηF_M	%	46.8 (11)	43.7	35.8 – 51.6

RFP = ratio of presystemic to systemic metabolite formation; MTT = mean transit time; NN = Number of transit compartments**;** *Parameter fixed

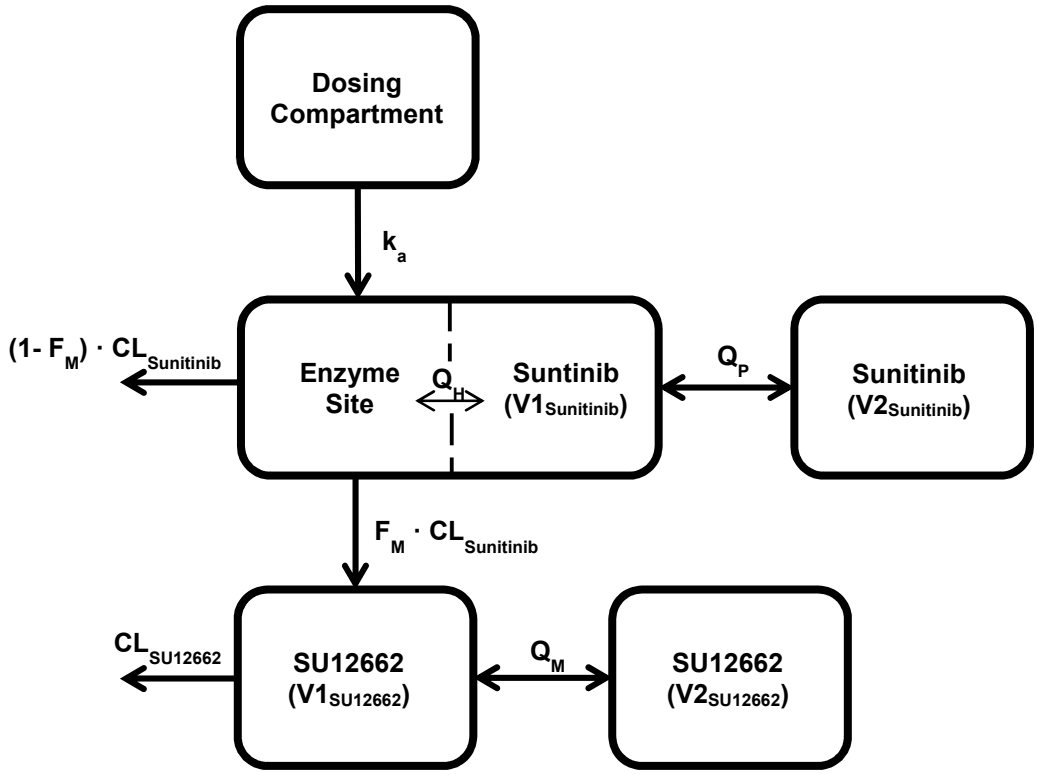

Fig. 4.12: Schematic overview of the structure of the pharmacokinetic model for sunitinib and its active metabolite (modified from Yu *et al.* [**110**]).

Covariate Analysis

The systematic covariate search did not reveal any significant effects on one of the model parameters. Of particular interest was the effect of the ABCB1 SNP on clearance, which was previously reported by Diekstra *et al.* [**166**]. However, this effect could not be reproduced with the underlying data. An overview on all covariates tested can be found in Appendix **A**.

Influence of fixed parameters in the final model

Variation of the fixed parameters of Q_H, $V2_{Sunitinib}$ and F_M resulted in differences between the estimated population means of the final model and the respective modified models. When fixing the value for Q_H between -50 and +50% the highest effect could be observed for the central volumes of sunitinib and SU12662 with a RPE varying between -23.6 - 11.5% and -19.5 – 42.5%, respectively. However, mean RPE was below 12% for all parameters and the estimated means were all within the 90 % confidence interval of the final model.

The variation of $V2_{Sunitinib}$ only affected the estimate of the intercompartmental clearance (Q_P) between the central and the peripheral compartment of with a RPE varying between -10.8 and 13.5%. Again, mean RPE was fairly low for all parameters with a maximum of 0.43% for Q_P. Estimated means were all within the 90% confidence interval of the final model.

Varying the fraction metabolized to SU12662 led to expected results. Due to the close relationship to all parameters related to the active metabolite, in detail the metabolite clearance, the central and peripheral volume and the intercompartmental clearance, changing the metabolized fraction resulted in comparable variations in these parameters.

Influence of dosing time in the final model

Due to the inconsistent documentation of dosing time in the mRCC dataset and the fixed dosing time-point for the mCRC patients, the influence of the time of drug intake was investigated in a sensitivity analysis. Absorption rate constant (k_a), in particular, was affected by dosing time with a RPE of -36.9%. However, mean (0.084 h^{-1}) and median (0.065 h^{-1}) were still within the 90% confidence interval of the final parameter estimate. Furthermore, the peripheral volume of distribution and the intercompartmental clearance related to SU12622 showed a rather large variation with a RPE of -21.7 and 26.5%, respectively. Again, mean and median of both parameters were still within the 90% confidence interval of the final parameter estimates of the reference model.

Similarly affected was the residual error estimated for sunitinib, which was increased by 25.2% on average. Inter-individual variability on the central compartment of SU12662 varied also by a rather large margin with an estimated RPE of 29.8%. Yet, all 50 simulated data resulted in comparable parameter estimates with the main influence on the absorption process, which was expected due to variability and quality in data available for drug intake. Since all parameters estimates were always within the bootstrap confidence interval of the main model, the influence of dosing time was considered negligible. Fixing the time of drug intake using a consequent rule, as described in 3.8.5, resulted in reliable parameter estimates, given the fact that the quality of documentation was variable in the underlying study. Results of the sensitivity analysis are shown in Table 4.9.

Tab. 4.9: Results of the sensitivity analysis with respect to dosing time

Parameter	Unit	Estimate	CI (90%)	Mean	Median	RPE, %
k_a	1/h	0.133	0.010 – 0.250	0.084	0.065	-36.9
$V1_{Sunitinib}$	L	1820	1607.8 – 1812.2	1778.6	1780	-2.3
$CL_{Sunitinib}$	L/h	33.9	30.8 – 37.5	35.3	35.4	4.2
$CL_{SU12662}$	L/h	16.5	15.0 – 17.9	16.97	16.9	2.8
$V1_{SU12662}$	L	730	545.9 – 872.9	571.36	571	-21.7
Q_M	L/h	2.75	1.96 – 4.27	3.48	3.4	26.5
$V2_{SU12662}$	L	592	481.0 – 737.4	615.33	633.5	3.9
Q_P	L/h	0.371	0.263 – 0.494	0.353	0.3555	-4.9
σ_P	-	-0.367	-0.45 - -0.283	-0.459	-0.457	25.2
σ_M	-	-0.281	-0.326 - -0.229	-0.297	-0.295	5.5
$\eta V1_{Sunitinib}$	%	25.3	24.5 - 30.0	29.50	29	16.6
$\eta V1_{SU12262}$	%	42.9	42.42 - 66.3	55.68	47.9	29.8
$\eta CL_{Sunitinib}$	%	30.3	29 - 35.9	28.34	29.2	-6.5
ηF_M	%	34.6	33.5 - 39.0	34.52	35.2	-0.2

4.2.2 Pazopanib

Since only limited pharmacokinetic data on patients treated with pazopanib was available. A Bayesian approach was chosen to obtain individual pharmacokinetic parameters for each individual patient. Basis for this analysis was the model published by Yu *et al.* [**152**]**.** No structural changes were made to this model and all population parameters and their respective variability were fixed to the reported values, with the exception of IOV, as this parameter was very specific to the published analysis (Table 4.10). A schematic overview of the final model used can be found in Figure 4.13.

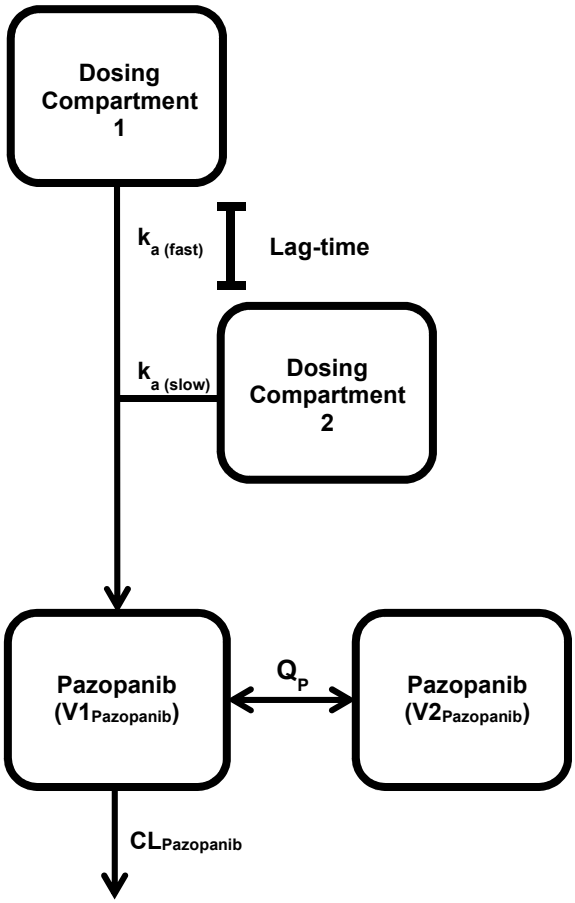

Fig. 4.13: Schematic overview of the structure of the pharmacokinetic model for pazopanib (modified from Yu *et al.* [**152**]).

In this model IIV was only considered for pazopanib clearance ($CL_{Pazopanib}$) the fast absorption rate constant ($k_{a(fast)}$), peripheral volume of distribution ($V2_{Pazopanib}$) and bioavailable fraction (F). Hence, only these parameters varied across the patients in this study. Descriptive statistics for each model parameter are shown in Table 4.11.

Tab 4.10: Parameter estimates for pazopanib pharmacokinetics reported by Yu *et al*. [**152**]

Parameter	Unit	Estimate	RSE (%)	IIV (%)	IOV (%)
$k_{a(fast)}$	h^{-1}	0.40	31	140	-
$k_{a(slow)}$	h^{-1}	0.12	28	-	-
F_{fast}	%	36.1	34	-	-
F_{slow}	%	63.9	34	-	-
Lag-time	h	0.98	6	-	-
$CL_{Pazopanib}$	L/h	0.27	23	30.9	-
$V1_{Pazopanib}$	L	2.43	34	-	-
Q_P	L/h	0.99	29	-	-
$V2_{Pazopanib}$	L	25.1	27	98.2	-
Rel. F at dose 200 mg	-	1*	-	35.6	75.5
Max effect of dose level on F	-	1*	-	-	-
Half max dose level	mg	480	23	-	-
Decrease of F over time	%	50.1	27	-	-
Decay constant	day^{-1}	0.15	43	-	-

Tab. 4.11: Descriptive statistics of individual parameter estimates for pazopanib based on the model by Yu *et al.* [**152**]

Statistic	$CL_{Pazopanib}$ [L/h]	$V_{Pazopanib}$ [L]	$k_{a(fast)}$ [h^{-1}]	Rel. F at dose 200 mg
Mean	0.24	29.61	0.81	0.36
Median	0.23	23.50	0.52	0.34
Range	0.18 – 0.35	3.73 – 95.32	0.08 – 4.25	0.24 – 0.57
SD	0.05	23.74	0.99	0.10
Relative SD (%)	19.15	80.18	121.66	27.08

SD = Standard deviation

4.3 PK/PD models

4.3.1 sVEGFR-2

Sunitinib

The model originally developed for healthy volunteers and for sVEGFR-2 could successfully be adapted to patients with mRCC and mCRC. The concentration-time profile of the soluble receptor was best described using an inverse-linear link between PK and PD (Section 3.10.1). An E_{max} model was tested for comparison but did not result in a statistically significant improvement of the model fit.

Tab. 4.12: Final parameter estimates of the sunitinib PK/PD model for sVEGFR-2

Parameter	Unit	Estimate (RSE, %)	Mean (Bootstrap)	Median (Bootstrap)	90% CI (Bootstrap)
Structural model					
Baseline	pg/mL	9030 (2.9)	9038	9030	8602 – 9477
α	-	2.31 (8.8)	2.31	2.31	1.98 – 2.64
k_{out}	1/h	0.0043 (7.6)	0.0043	0.0043	0.0038 – 0.0049
K_D	µg/mL	4*	-	-	-
Statistical model					
σ	-	0.124 (6.8)	0.122	0.122	0.108 – 0-136
η (Baseline)	%	19.9 (21.4)	19.4	19.2	16.0 – 22.8
Covariate model					
Tumor type on α	-	-0.328 (24.6)	-0.322	-0.329	-0.440 – -0-186
FLT-1 on α	-	-0.565 (25.4)	-0.557	-0.562	-0.787 – -0-319
ABCR2 on α	-	-0.311 (37.9)	-0.307	-0.306	-0.497 – -0-117

FLT-1 = VEGFR-3 rs6877011; ABCR2 = ABCB1 rs2032582

In contrast to the reference model by Lindauer *et al.*, the residual error was best described by a proportional error model. A combined additive and proportional error model did not result in a significant improvement of the model fit (dOFV = -2.64). Neither did the subdivision of the residual error by tumor type (mRCC vs mCRC). Using solely an additive residual error even worsened the overall model performance (dOFV

= +11.59). While the inclusion of IOV per cycle on the estimated baseline and α did result in a significant decrease of the OFV (-11.59 and -15.85, respectively), the estimated parameter was not reliable due to a high RSE and a shrinkage above 40% in both cases. Furthermore, the estimated IOV on sVEGFR-2 baseline was relatively low with 9% and therefore most likely not relevant.

Including an IIV on sVEGFR-2 baseline, intrinsic activity α and degradation constant k_{out} lead to a highly significant decrease of the OFV by -261.4 ($p < 0.0001$). However, after stepwise elimination of each IIV from the full statistical model only η (α) and η (Baseline) were kept. The removal of η (k_{out}) showed no significant worsening of the model fit (dOFV = +3.52) and was therefore not included in the final model. However, after the full covariate model was established, the IIV on α approached zero and was removed without any effect on the model fit and the OFV, respectively.

Final parameter estimates and the respective bootstrap mean, median and 90% confidence interval can be found in Table 4.12. For comparison the estimates for each parameter from the original analysis in healthy volunteers is also shown.

Covariate analysis

Systematic covariate search revealed three statistically significant covariates which were kept in the final model:

- *Higher intrinsic activity of sunitinib/SU12662 for patients with mRCC*
  Compared to mRCC patients, mCRC patients showed a 32.8% lower intrinsic activity of sunitinib on sVEGFR-2 levels (2.31 vs 1.55). Exclusion of this covariate in the final backward elimination step increased the OFV by 8.78 ($p = 0.003$)
- *Decreased intrinsic activity of sunitinib/SU12662 for patients with VEGFR-3 rs6877011 (1=CG/GG;0=CC):*
  Patients with a CG/GG allele showed a 56.5% decreased intrinsic activity α compared to the wildtype (2.31 vs 1.00 in case of mRCC patients and 1.55 vs 0.65 for mCRC patients). Exclusion of this covariate in the final backward elimination step increased the OFV by 12.35 ($p = 0.0004$).

- *Decreased intrinsic activity of sunitinib/SU12662 for patients with ABCB1 rs2032582 (1=GT/TT; 0=GG)*
  Patients with a GT/TT allele had a 31.1% decreased intrinsic activity of sunitinib (2.31 vs 1.59 in case of mRCC patients and 1.55 vs 1.07 for mCRC patients) on sVEGFR-2 levels compared to wildtype GG carriers. Exclusion of this covariate in the final backward elimination step increased the OFV by 6.7 (p = 0.01).

In the full covariate model shrinkage on α increased above the threshold value of 30 % (Section 3.8.3). Removing this parameter from the model increased the OFV by 2.42.

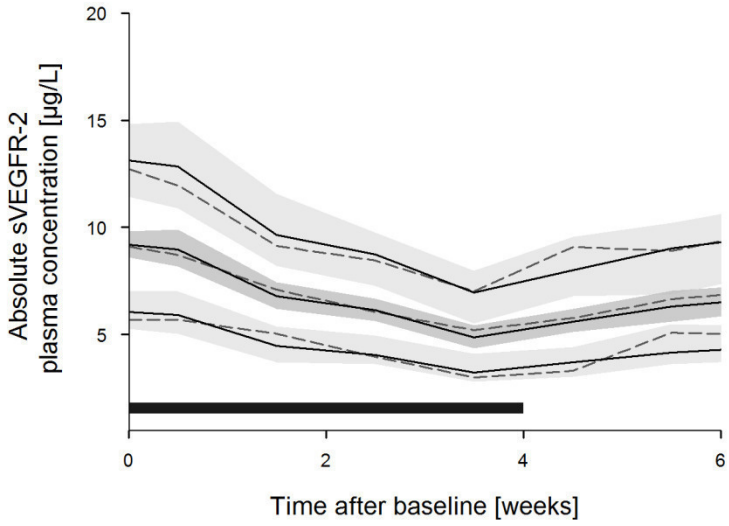

Fig 4.14: Visual predictive check of sVEGFR-2 for the first 6 weeks of sunitinib treatment. The black solid lines indicate the mean model prediction and the 90% prediction interval. Dotted lines show the measured mean and interval, respectively. Dark and light grey areas represent the respective confidence bands. The dark-grey rectangle represents the time on treatment.

The pcVPC indicates that the model is able to sufficiently describe the underlying data. No model misspecification or systematic errors could be identified in the GOF plots. However the population predictions (PRED) vs. dependent variable (DV) plot shows a cut-off at high concentrations, indicating that these cannot be described well by the population model. This is most likely explained by the individual sVEGFR-2 baseline

values, since the PRED do not include inter-individual variations, applying the same baseline value for all patients. (Appendix **D.II**). The covariate effects are listed in Table 4.12, where FLT-1 denotes for *VEGFR-3 rs6877011* and ABCR2 for *ABCB1 rs2032582.*

Pazopanib

sVEGFR-2 plasma concentrations during pazopanib treatment were also best described with an inverse-linear relationship of the active pazopanib concentration and the turnover rate constant k_{in}. The E_{max} and the power function provided comparable results regarding the overall fit. However, the turnover model using an inverse linear relationship was preferred as a similar relationship between sunitinib pharmacokinetics and sVEGFR-2 was already successfully established (see above). Using the fractional tyrosine kinase inhibition *INH* (Equation 3.29) instead of the active concentration worsened the model fit significantly (dOFV = +5.2). Furthermore, goodness-of-fit plots indicated that low plasma concentrations of sVEGFR-2 could not be predicted sufficiently enough using *INH*. Active concentration of pazopanib assumed a protein binding of 99.9% [**45**]. Parameter estimates, except for the magnitude of α, were not influenced by this value.

Applying an IIV on sVEGFR-2 baseline, α and k_{out} decreased the OFV significantly by 96.52. Systematically removing each parameter again from the model worsened the model fit in all cases. OFV increased by 23.9 when fixing IIV on sVEGFR-2 baseline concentration to 0 and by 30.5 and 18.2 for IIV on α and k_{out} respectively.

Although the exclusion of IIV on k_{out} worsened the model fit significantly, this parameter introduced a high bias of the model parameters. A case deletion diagnostic (CDD) analysis revealed a bias of 281.7% for η (α), 75.5% for α and 82.5% for η (Baseline). Removing the parameter from the model reduced the bias (η (α): 9.8%, α: 22.1%, η (Baseline): 41.2%) and stabilized the model. Estimation of correlations between model parameters had no significant impact on the model performance.

Table 4.13 shows an overview of the final parameter estimates including bootstrap confidence intervals. The respective pcVPC is shown in Figure 4.15.

Tab. 4.13: Final parameter estimates of the pazopanib PK/PD model for sVEGFR-2

Parameter	Unit	Estimate (RSE, %)	Mean (Bootstrap)	Median (Bootstrap)	90% CI (Bootstrap)
Structural model					
Baseline	pg/mL	9820 (3.4)	9825	9825	9271 – 10390
α	-	22.1 (21.4)	22.5	21.5	15.7 – 30.9
k_{out}	1/h	0.0038 (27.9)	0.0040	0.0040	0.0022 – 0.0059
Statistical model					
Residual Error	pg/mL	846 (21.6)	794	818	593 – 981
η (Baseline)	%	12.7 (38.0)	12.4	12.2	8.0 – 15.9
η (α)	%	46 (48.2)	46.0	44.9	26.7 – 62.8

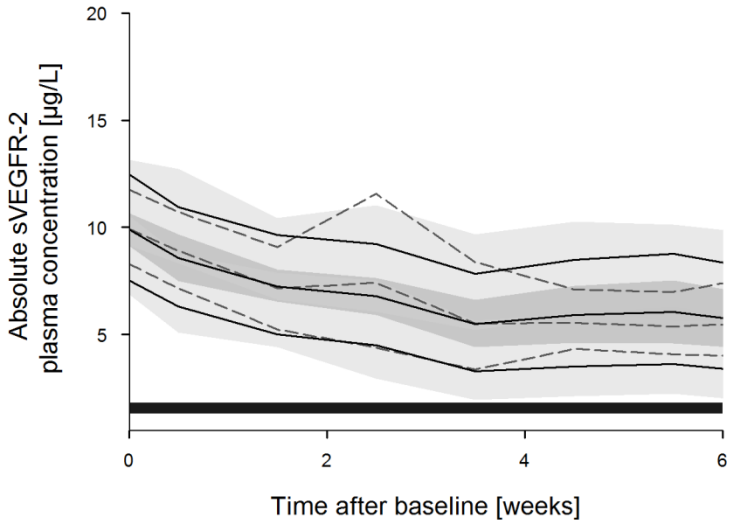

Fig. 4.15: Visual predictive check of sVEGFR-2 for the first 6 weeks of pazopanib treatment. The black solid lines indicate the mean model prediction and the 90% prediction interval. Dotted lines show the measured mean and interval, respectively. Dark and light grey areas represent the respective confidence bands. The dark-grey rectangle represents the time on treatment.

4.3.2 sVEGFR-3

Sunitinib

The model originally developed for healthy volunteers and for sVEGFR-2 could successfully be adapted to patients with mRCC and mCRC. Again, the concentration time profile of the soluble receptor was best describe using an inverse-linear link between PK and PD. Introduction of IIV on all model parameters except K_D, which was fixed to a literature value, led to a highly significant decrease of the OFV (dOFV: -743.56). Yet, the estimated variability on k_{out} showed a shrinkage higher than the threshold value of 30% and was therefore removed. This did not lead to a significant worsening of the model (dOFV: 0.79). Inter-occasion variability was tested on both, the intrinsic activity α and the baseline values, but did not result in a significant model improvement (dOFV:-1.96 and -3.31, respectively). Estimation of a covariance between α and the sVEGFR-3 baseline value further improved the model, decreasing the OFV significantly by -8.03.

Covariate analysis

In the covariate analysis one influential factor was identified. The inclusion of “tumor entity” on the estimated baseline value of sVEGFR-3 highly improved the model fit, shown by an increase of 53.68 in the OFV after removal of this parameter. The population mean for mRCC patients was estimated to be 63500 pg/mL, whereas for mCRC patients a lower value of 22733 pg/mL was predicted.

Goodness-of-fit plots of the final model can be found in Appendix **D.III**. Whereas the IPRED vs DV plot, where inter-individual variability is taken into account, suggests a good model performance, the PRED vs DV graphics reveal that the maximum concentrations of sVEGFR-3 cannot be adequately be described using the population model, showing a cut-off at a certain concentration. The same was observed for sVEGFR-2 and can also be explained by the estimated baseline concentration at time zero, which is a set to an identical value for all patients. However, the pcVPC shown in Figure 4.16 indicates that the model is able to describe the data sufficiently well.

An overview on the final model parameters and their respective 90% bootstrap confidence interval and standard error is shown in Table 4.14.

Tab. 4.14: Final parameter estimates of the sunitinib PK/PD model for sVEGFR-3

Parameter	Unit	Estimate (RSE, %)	Mean (Bootstrap)	Median (Bootstrap)	90% CI (Bootstrap)
Structural model					
Baseline	pg/mL	63500 (5.9)	63750	63853	57305 – 69800
α	-	1.74 (9.8)	1.76	1.75	1.49 – 2.05
k_{out}	1/h	0.0053 (7.2)	0.0054	0.0054	0.0047 – 0.0060
K_D	µg/mL	4*	-	-	-
Statistical model					
Residual Error	-	0.15 (6.9)	0.15	0.15	0.13 – 0.17
η (Baseline)	%	42.6 (24.4)	40.1	39.8	31.8 – 48.1
η (α)	%	54.3 (43.5)	51.3	50.3	30.9 -68.8
ρ (Baseline, α)	-	0.123 (39.6)	0.123	0.122	0.045 – 0.209
Covariate model					
Tumor type on baseline	-	-0.642 (6.5)	-0.640		-0.703 – (-0.569)

*Parameter fixed

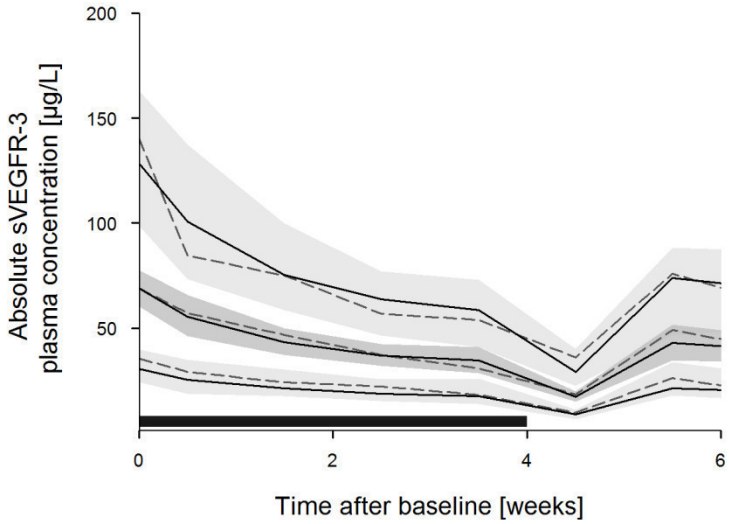

Fig 4.16: Visual predictive check of sVEGFR-2 for the first 6 weeks of sunitinib treatment. The black solid lines indicate the mean model prediction and the 90% prediction interval. Dotted lines show the measured mean and interval, respectively. Dark and light grey areas represent the respective confidence bands. The dark-grey rectangle represents the time on treatment.

Pazopanib

Several models showed potential to be best describing PK/PD relationship between pazopanib and sVEGFR-3.

Using the fractional inhibition (*INH*, Equation 3.29) as influence factor in an inverse-linear model resulted in poor estimation of low observed concentration. When using only the active concentration the model fit highly improved (dOFV: – 20.98). Using a direct linear approach decreased the OFV further. However, when adding IIV on all relevant parameters both models performed equally well. VPCs indicated that the inverse-linear relationship was favorable in this case. Due to the parameterization of the model, the choice of the fraction of protein binding had no significant influence on parameter estimates except for the magnitude of α. A pcVPC of the final model is shown in Figure 4.17.

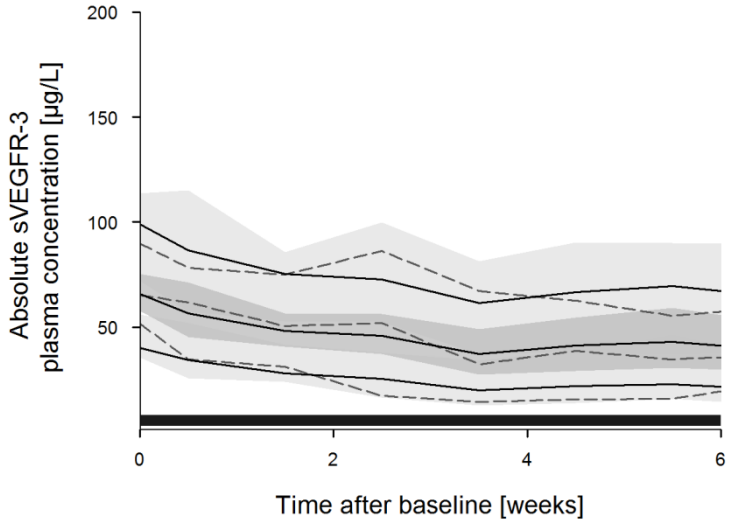

Fig 4.17: Visual predictive check of sVEGFR-3 for the first 6 weeks of pazopanib treatment. The black solid lines indicate the mean model prediction and the 90% prediction interval. Dotted lines show the measured mean and interval, respectively. Dark and light grey areas represent the respective confidence bands. The dark-grey rectangle represents the time on treatment.

Introduction of IIV on model parameters improved the fit significantly (dOFV: -106.2). However, comparable to the model for sVEGFR-2 in pazopanib patients, IIV on k_{out} resulted in a high bias for almost all parameters (α: 80.4%, k_{out}: 568.0%, η (α): 175.4%). Removal of η (k_{out}) resolved this issue sufficiently (α: 27.5%, kout: 7.1%, η (α): 121.7%) with a moderate increase of the OFV only.

Table 4.15 shows an overview of the final parameter estimates including bootstrap confidence intervals.

Tab 4.15: Final parameter estimates of the pazopanib PK/PD model for sVEGFR-3

Parameter	Unit	Estimate (RSE, %)	Mean (Bootstrap)	Median (Bootstrap)	90% CI (Bootstrap)
Structural model					
Baseline	pg/mL	64300 (5.2)	64300	64178	58672 - 70047
α	-	17.5 (16.5)	18.3	18.0	13.9 – 23.5
k_{out}	1/h	0.0047 (23)	0.0048	0.0047	0.0032 – 0.0069
Statistical model					
Residual error	%	14.2 (13.0)	13.6	13.8	11.0 – 16.0
η (Baseline)	%	23.6 (39.4)	23.1	22.7	15.0 – 30.2
η (α)	%	61.9 (49.0)	56.1	56.0	24.1 – 75.0

4.3.3 Blood pressure

Sunitinib

Similar to the PD models for sVEGFR-2 and -3, the blood pressure model used was originally developed using data from healthy volunteers. In this study it could be successfully adapted to patients with mRCC. In the base model all parameters describing the circadian variation of systolic and diastolic blood pressure were fixed to their respective reference values from healthy volunteers. Estimation of these parameters was not possible due to the sparse sampling and documentation gaps (e.g. missing day-time). Residual error was best described using separate proportional models for systolic and diastolic blood pressure.

Introduction of an IIV on the estimated baseline values for systolic and diastolic blood pressure, as well as for the respective intrinsic activities (α) improved the model fit significantly shown by a combined OFV decrease of -214.18. By removing the IIV from baseline systolic and diastolic blood pressure the OFV increased by 30.3 and 42.8 ($p < 0.0001$), respectively. A statistically significant worsening of the model fit was also observed when removing the estimated IIV from both intrinsic activity parameters. The OFV increased by 8.2 ($p < 0.01$) and 6.0 ($p < 0.025$). However, both parameters showed a high shrinkage value (> 30%). Estimation of a covariance between systolic and diastolic IIV decreased the OFV by -14.86. Though, the estimated correlation was nearly 100%. Therefore, the statistical model was restructured with both fixed-effect parameters for intrinsic activity sharing one η parameter connected via a proportionality factor [**86**]. Here, an additional parameter is estimated, which accounted for the correlation between the variability on both intrinsic activities α. Whereas the OFV did not change significantly, shrinkage on both parameters decreased below the threshold value, leading to more reliable estimates. Removing the IIV on both activity parameters from the model showed a significant worsening of the model fit (dOFV = 27.2). Final parameter estimates including RSE, bootstrap mean and median values as well as the 90% confidence interval are shown in Table 4.16

Covariate analysis

Since blood pressure data was only available for 25 mRCC patients, only selected covariates were tested manually using the same criteria for significance ($p < 0.05$ for forward inclusion and $p < 0.01$ for backward elimination). Covariates tested included diagnosed hypertension at time of treatment start and the intake of antihypertensive medication during the targeted therapy. Here, especially the fixed parameters for circadian variation were of interest. A significant effect was found for the covariate “antihypertensive medication” (BPTRT) on the second amplitude parameter (AMP_2), which was decreased by 202% (90% CI: 80-315). This resulted in a more even course of systolic and diastolic blood pressure throughout the day.

The visual predictive checks for systolic and diastolic blood pressure are shown in Figure 4.18. Whereas the time course of blood pressure could be well described during the first 6 weeks of sunitinib treatment, predictions were less reliable at later time-points, as the VPC of the full time period indicates (Appendix **D.X**). This can also be

observed in the GOF plots shown (Appendix **D.IV**). The PRED vs DV plot clearly indicates that the model cannot cope with unexpectedly high blood pressure values.

Furthermore, residuals were evenly distributed and did not show any model misspecification.

Tab 4.16: Final parameter estimates of the sunitinib PK/PD model for systolic and diastolic blood pressure

Parameter	Unit	Estimate (RSE, %)	Mean (Bootstrap)	Median (Bootstrap)	90% CI (Bootstrap)
Structural model					
BSL_{syst}	mmHg	138.0 (2.2)	137.8	137.8	132.7 – 142.6
$BSL_{diast.}$	mmHg	82.8 (1.9)	82.8	82.8	80.2 – 85.43
α_{syst}	-	0.064 (30.9)	0.064	0.063	0.034 – 0.098
α_{diast}		0.048 (38.5)	0.048	0.047	0.020 -0.080
τ	h	121*	-	-	-
PS_1	-	0*	-	-	-
PS_2	-	1.4*	-	-	-
AMP_1	-	0.025*	-	-	-
AMP_2	-	-0.016*	-	-	-
σ_{syst}	-	0.094 (10.2)	0.093	0.093	0.077 – 0.110
σ_{diast}	-	0.079 (6.3)	0.079	0.079	0.07 – 0.087
Prop. factor	-	1.21 (27)	1.25	1.23	0.85 – 1.69
Statistical model					
η (BSL_{syst})	%	9.3 (46.7)	9.1	8.9	5.2 – 12.2
η (BSL_{diast})	%	7.4 (28.7)	7.2	7.2	5.1 – 8.8
η (α_{syst})	%	105.8 (105.1)	89.0	82.7	42.6 – 123.2
η (α_{diast})	%	105.8 (105.1)	89.0	82.7	42.6 – 123.2
Covariate model					
BPTRT on AMP_2	-	-2.02 (36.3)	-1.99	-1.99	-3.15 - -0.80

BSL = Baseline; PS = Phase shift; AMP = Amplitude; BPTRT = Treated hypertension; Prop. factor = Proportionality factor ; *Parameter fixed

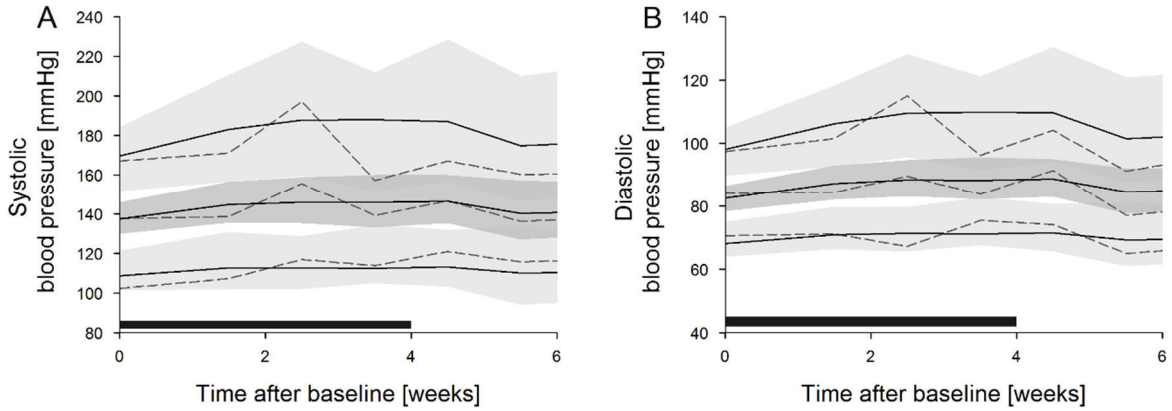

Fig 4.17: Visual predictive check for systolic (**A**) and diastolic (**B**) blood pressure during the first six weeks on sunitinib treatment. Black solid lines indicate the mean model prediction and the 90% prediction interval. Dotted lines show the measured mean and interval, respectively. Dark and light grey areas represent the respective confidence bands. The dark-grey rectangle represents the time on treatment.

Simulations

Based on these findings simulations were performed to illustrate the effect of antihypertensive treatment during sunitinib therapy. Figure 4.19 shows the simulated systolic and diastolic blood pressure after one intake of 50 mg sunitinib with and without antihypertensive medication. Here, the course of blood pressure is flatter, with delayed extreme values due to the co-medication. It has to be noted that here only the direct effect of sunitinib on blood pressure is shown, and the delayed one is missing due to the simulated intake of only one dose.

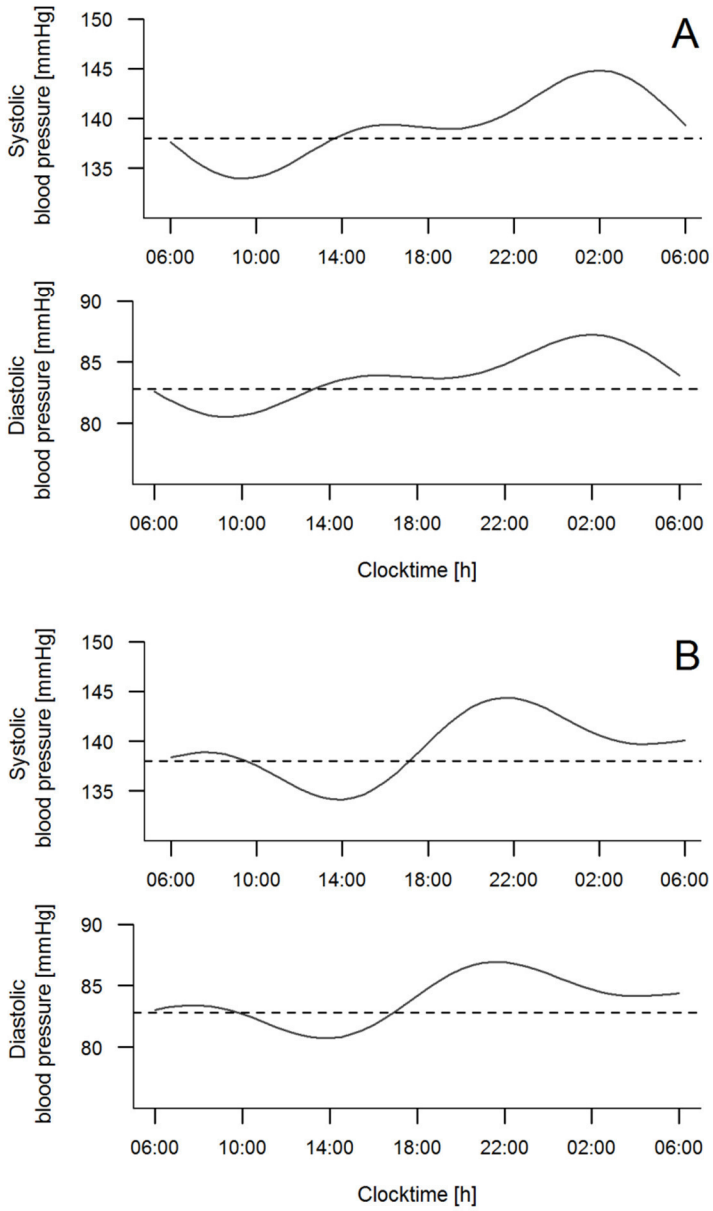

Fig. 4.18: Simulated systolic/diastolic blood pressure for one day after a single dose of 50 mg sunitinib with (**A**) and without (**B**) antihypertensive treatment.

Pazopanib

Based on the PK/PD model developed for sunitinib, several potential relationships for linking pazopanib pharmacokinetics with systolic and diastolic blood pressure were tested. Parameters describing the circadian rhythm of blood pressure could not be estimated and were fixed to the values reported by Lindauer *et al*. [**109**] Best results were obtained using active, unbound pazopanib concentration as predictor. Intrinsic activity α was quantitatively comparable for systolic and diastolic blood pressure;

hence, estimation of one αfor both physiological parameters did not result in a statistically significant worsening of the model fit (dOFV = +0.16).

Significant improvements were achieved by estimating IIV on both baseline parameters (dOFV = -96.6), while the estimates for IIV on α approached zero signaling a non-significant effect. Final parameter estimates including RSE, bootstrap mean and median values as well as the 90% confidence interval are shown in Table 4.17

Tab 4.17: Final parameter estimates of the pazopanib PK/PD model for blood pressure

Parameter	Unit	Estimate (RSE, %)	Mean (Bootstrap)	Median (Bootstrap)	90% CI (Bootstrap)
Structural model					
BSL_{syst}	mmHg	130.0	130.6	130.7	122.2 – 138.2
BSL_{diast}	mmHg	80.2	80.5	80.3	76.6 – 84.8
$\alpha_{syst/diast}$	-	0.91	0.87	0.87	0.39 – 1.32
τ	h	121*	-	-	-
PS_1	-	0*	-	-	-
PS_2	-	1.4*	-	-	-
AMP_1	-	0.025*	-	-	-
AMP_2	-	-0.016*	-	-	-
$\sigma_{sys/dia}$	-	0.091	0.093	0.094	0.079 – 0.107
Statistical model					
η (BSL_{syst})	%	6.8	6.3	6.3	3.6 – 8.2
η (BSL_{diast})	%	7.8	7.6	7.6	2.4 – 11.0
Covariate model					
BPDIAG on BSL_{syst}	-	0.091	0.091	0.094	0.019 – 0.172

BSL = Baseline; PS = Phase shift; AMP = Amplitude; BPDIAG = Diagnosed hypertension; *Parameter fixed

Covariate analysis

Due to the small samples size only the influence of diagnosed hypertension as well as active antihypertensive therapy was tested as potential covariate effects.

Here, patients diagnosed with hypertension had a 9.1% increased mean systolic blood pressure baseline throughout the day. Inclusion of this effect into the model decreased the OFV significantly by 4.2 ($p < 0.05$). Furthermore, diagnosed blood pressure had an effect on amplitude 1 (AMP_1, dOFV = -5.5, $p < 0.05$). However, inclusion of both effects simultaneously showed no significant improvement over the univariate approach. Furthermore, the effect on AMP_1 was clinically not plausible. Therefore the final model featured only the increased systolic baseline blood pressure in patients with diagnosed hypertension. The effect of antihypertensive treatment on AMP_2 found in the sunitinib cohort could not be observed here.

A pcVPC of the final model is shown in Fig 4.20. The blood pressure values during the first six weeks can be predicted reasonably well, while later time-points showed wider prediction intervals due to the sparse data (Appendix **D.XII**).

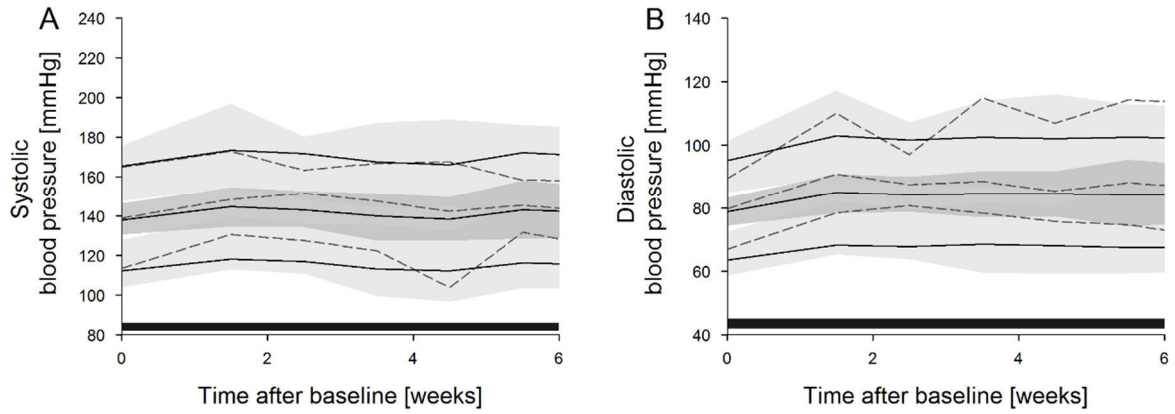

Fig. 4.20: Visual predictive check for systolic (**A**) and diastolic (**B**) blood pressure during the first six weeks on pazopanib treatment. Black solid lines indicate the mean model prediction and the 90% prediction interval. Dotted lines show the measured mean and interval, respectively. Dark and light grey areas represent the respective confidence bands. The dark-grey rectangle represents the time on treatment.

4.4 Survival analysis

4.4.1 Kaplan-Meier analysis and Cox regression

Details on the registered events and which patients were included in the analysis can be found in Appendix **E**.

Kaplan-Meier analysis (*Sunitinib)*

Median PFS for sunitinib patients was calculated with 6.9 months (CI 95%: 4.1 – 12.7 months, n = 24). For the Kaplan-Meier analysis all continuous covariates were dichotomized to allow comparison between two groups, respectively. Patients were subdivided by the population median of the sVEGFR-2 and sVEGFR-3 baseline value. For sVEGFR-2 this resulted in 11 patients with a higher baseline level than the median of 8814.68 pg/mL and 13 patients below this threshold. Median baseline of sVEGFR-3 for patients investigated was calculated with 63132.66 pg/mL (10 patients above and 14 patients below). Dichotomized baseline levels of both circulating proteins showed a significant favorable effect for patients with a sVEGFR-2 or sVEGFR-3 baseline below the population median on PFS (sVEGFR-2, p = 0.005; sVEGFR-3, p = 0.02). Total AUC and total steady-state concentration above the population median showed a weak but favorable effect for patients with values below the population median (p = 0.048).

However, permutation tests with n = 100000 confirmed only the effects found for sVEGFR-2 and 3 baseline values above the population median (p = 0.008 and 0.03).

Median survival for patients with sVEGFR-2 baseline levels above the population median were estimated with 4.73 months vs 12.65 months. A similar result could be observed for sVEGFR-3 with a median survival of 4.11 months vs. 9.07 months. The Kaplan-Meier plot for patients treated with sunitinib is shown in Figure 4.21.

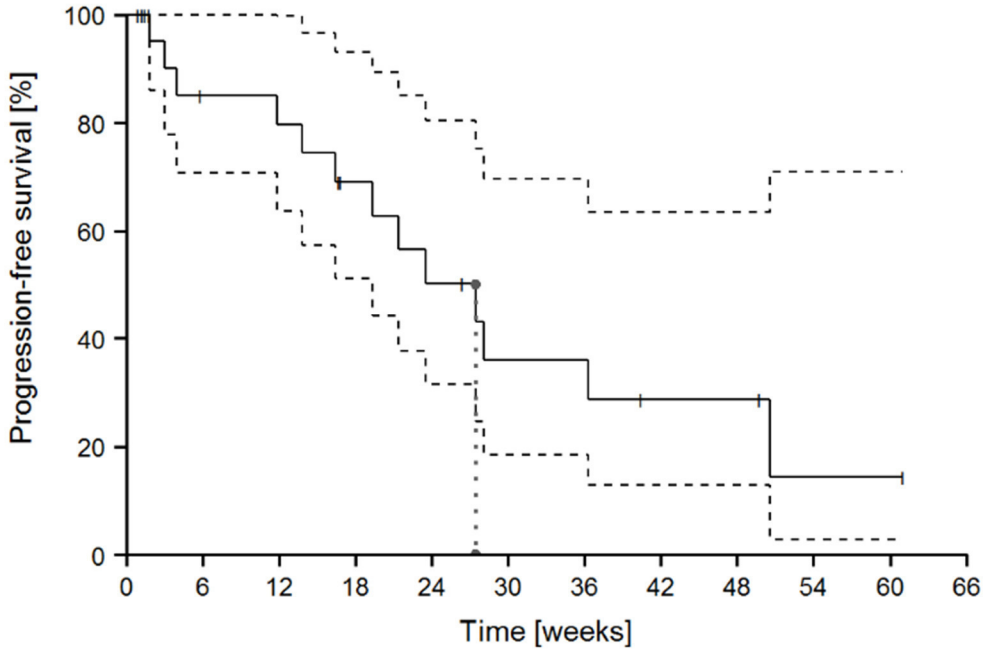

Fig. 4.21: Kaplan-Meier plot for patients treated with sunitinib including 95% confidence interval. The dotted vertical line indicates the median survival.

Cox regression (Sunitinib)

The results from the Kaplan-Meier analysis could be confirmed in a Cox regression analysis. In the univariate analysis the hazard ratio (HR) for a sVEGFR-2 baseline above the population median was estimated with 5.60 (p = 0.006, CI 90%: 1.82-17.24). For sVEGFR-3 the HR amounted for 3.74 (p = 0.031, CI 90%: 1.36-10.27). Furthermore the absolute sVEGFR-2 baseline value in µg/L also showed a significant effect in this analysis with a hazard ratio of 1.00028 (p = 0.044, CI 90 %:1.00006-1.00049). However, the only significant covariates after multivariate analysis were the dichotomized baseline values of both soluble proteins (Table 4.18).

Predicted survival curves using either sVEGFR-2 or sVEGFR-3 baseline as predictor are comparable and no difference between both covariates can be observed (Figure 4.22)

Tab. 4.18: Results of the multivariate Cox regression for sunitinib

Covariate	Hazard ratio	p value
All significant covariates included		
sVEGFR-2 baseline above pop. median	4.64	0.061
sVEGFR-3 baseline above pop. median	6.27	0.018
Absolute sVEGFR-2 baseline	1.0003	0.990
Age	0.926	0.061
Reduced covariate model		
sVEGFR-2 baseline above pop. median	4.68	0.017
sVEGFR-3 baseline above pop. median	6.28	0.014
Age	0.93	0.053
Final covariate model		
sVEGFR-2 baseline above pop. median	7.50	0.006
sVEGFR-3 baseline above pop. median	5.36	0.015

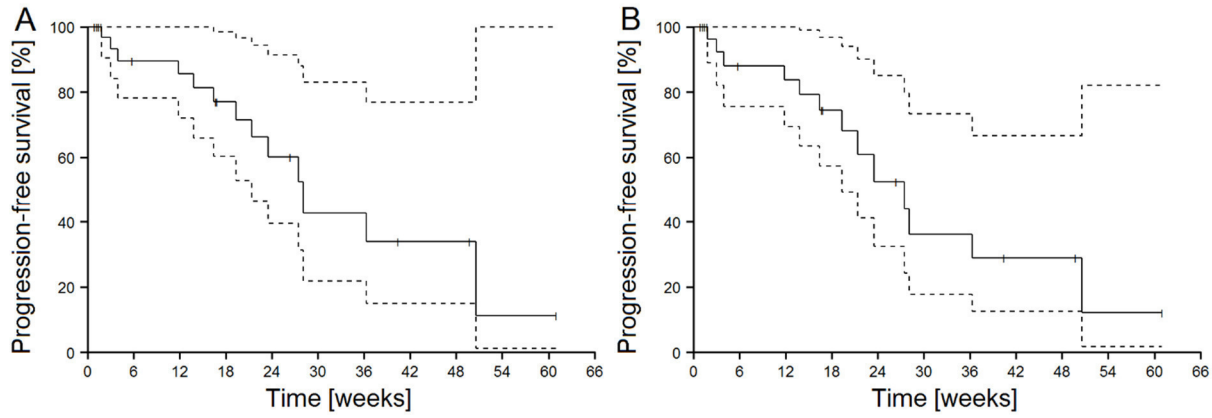

Fig. 4.22: Predicted survival curves by the Cox regression model using (**A**) the sVEGFR-2 baseline (dichotomized) and (**B**) the sVEGFR-3 baseline (dichotomized).

Kaplan-Meier analysis (*Pazopanib)*

Median survival for pazopanib patients was calculated with 12.1 months (80% CI: 5.3 – 12.5 month). Similar to patients treated with sunitinib the dichotomized covariates based on the sVEGFR-2 and sVEGFR-3 baseline values were evaluated. Threshold values for sVEGFR-2 and sVEGFR-3 in this cohort were set to 9938.4 pg/mL and 62412.3 pg/mL, respectively. Patients with a high sVEGFR-2 baseline value had a median survival of 2.3 months compared to 12.4 months in the other group. However, the effect was not statistically significant (p = 0.051). The other tested covariates (radiotherapy, nephrectomy/metastasectomy, sVEGFR-3 baseline) did not have a statistically significant effect on PFS in pazopanib patients. The Kaplan-Meier plot for patients treated with pazopanib is shown in Figure 4.23.

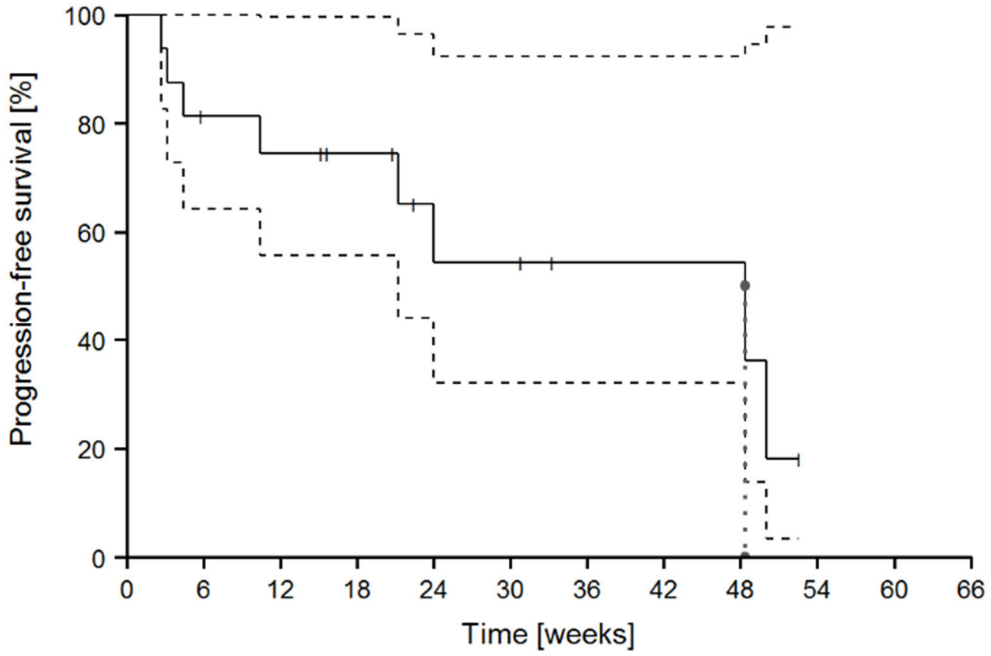

Fig. 4.23: Kaplan-Meier plot for patients treated with pazopanib including 95% confidence interval. The dotted vertical line indicates the median survival.

Cox regression (Pazopanib)

Cox regression analysis in the pazopanib cohort did not reveal any significant predictors for PFS. However, the strongest effect was observed for baseline sVEGFR-2 (dichotomized) with a HR of 5.1 (p = 0.06), which is comparable in effect strength to sunitinib for the same covariate. In contrast, the effect strength of the dichotomized sVEGFR-3 baseline levels was comparatively low in this cohort with a HR of 1.19 (p = 0.85). Absolute sVEGFR-2 and sVEGFR-3 baseline concentrations as continuous covariates were even less informative (HR: 1.0003, p = 0.92 and 1.000007, p = 0.81).

As stated above, other covariates tested were not significant either. A full list of all covariates tested can be found in Appendix **A**.

Kaplan-Meier analysis (*Sunitinib and pazopanib combined)*

A Kaplan-Meier analysis was also performed for all patients (n = 40) regardless of treatment group. Median survival in both groups combined was 6.9 months (CI 95%: 5.3 – 12.5). The respective Kaplan-Meier plot is shown in Figure 4.24.A. However, both treatments did not differ statistically significant from each other (p = 0.73) (Figure 24 B). A sVEGFR-2 baseline value above the median of the investigated population of 9049 pg/mL (n = 40) was again associated with a longer PFS (p = 0.003). Here, 17 patients were above and 23 below this threshold. Median survival was calculated with 5.4 vs. 12.5 months. The same effect was observed for sVEGFR-3: dividing the population in two groups below and above the median of 63133 pg/mL showed a favorable prognosis for patients with lower baseline concentrations (p = 0.041). The other tested covariates did not reveal any additional effects.

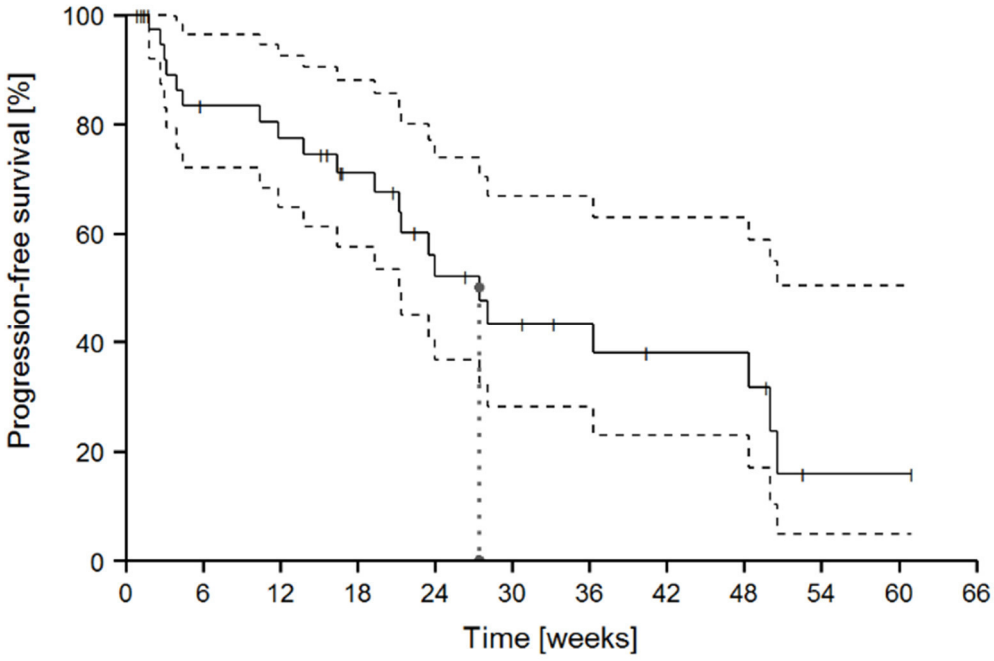

Fig. 4.23.A: Kaplan-Meier plot of both treatment groups (no stratification) including 95% confidence interval. The dotted vertical line indicates the median survival.

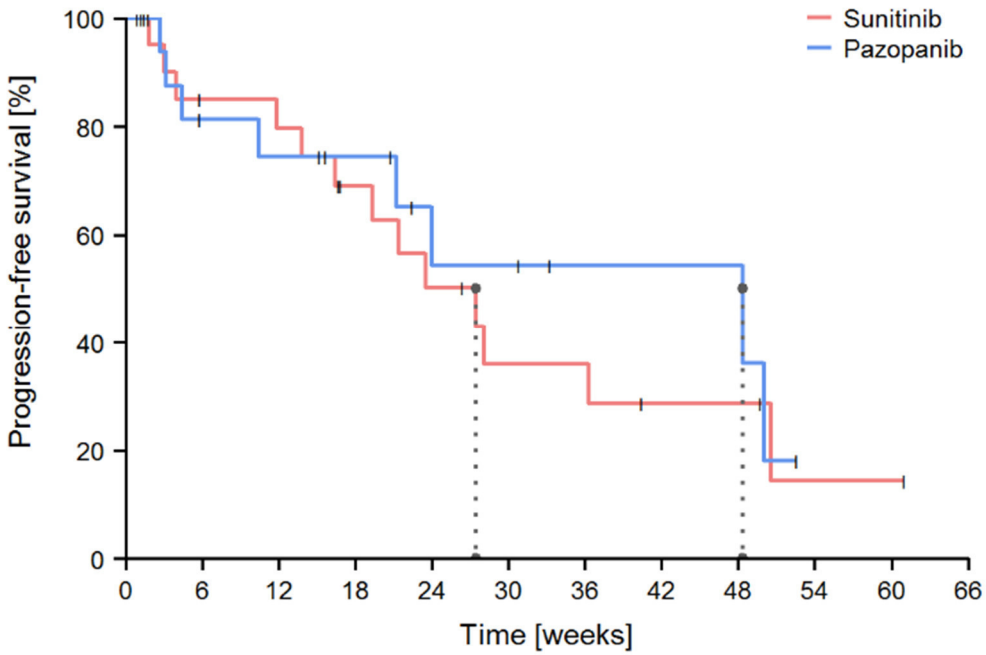

Fig. 4.23.B: Kaplan-Meier plot including all patients (stratified by treatment). The dotted vertical lines indicate the median survival for each subgroup.

Cox regression (*Sunitinib and pazopanib combined)*

Comparable to the Cox regression analysis performed for sunitinib patients exclusively, sVEGFR-2 baseline values as well as the dichotomized covariate showed statistically significant effects with hazard ratios estimated with 1.00028 (p = 0.026, 95% CI: 1.00008 – 1.00048) and 3.86 (p = 0.006, 95% CI: 1.66 – 8.97), respectively. In addition, a sVEGFR-3 baseline value above the population median also had a borderline significant effect on PFS, though weaker compared to the same parameter for sVEGFR-2 (HR: 2.69, p = 0.050, 95% CI: 1.19 – 6.12). In both cases patients with high baseline value of the respective protein had a lower survival independent of treatment (see also Kaplan-Meier analysis). Furthermore, age showed a weak effect on survival (HR: 0.95, p = 0.036, 95% CI: 0.91 – 0.99). A significant difference between suntinib and pazopanib was not detectable (HR: 0.81, p = 0.64).

Results of the multivariate analysis including all significant covariates from the univariate approach are shown in table 4.19. Here, the effect of absolute sVEGFR-2 baseline concentration as well as the dichotomized covariate were no longer significant. However, as both covariates comprise nearly identical information, absolute sVEGFR-2 baseline was removed for further testing. As a result, all three covariates were significant with the dichotomized sVEGFR-2 and sVEGFR-3 baseline concentrations featuring comparable hazard ratios (HR: 3.5 vs 3.13).

Tab. 4.19: Results of the multivariate Cox regression (sunitinib and pazopanib)

Covariate	Hazard ratio	p value
All significant covariates included		
sVEGFR-2 baseline above pop. median	5.63	0.070
sVEGFR-3 baseline above pop. median	3.84	0.032
Absolute sVEGFR-2 baseline	1.00	0.74
Age	0.97	0.39
Final covariate model		
sVEGFR-2 baseline above pop. median	3.50	0.016
sVEGFR-3 baseline above pop. median	3.13	0.037
Age	0.95	0.045

4.4.2 Model-based time-to-event analysis

Sunitinib

The PFS could be described by a parametric time-to-event (TTE) model assuming exponentially distributed data with a baseline hazard function λ_0 of 0.0252 week^{-1} (90% CI: 0.0168 - 0.0336). The inclusion of the measured sVEGFR-2 baseline value led to a decrease of the OFV by 4.14 ($p < 0.05$) with β defined as the natural logarithm of the HR.

The estimated baseline value of sVEGFR-2 showed a slightly increased effect strength with an estimated β of 0.341 vs. 0.260 for the measured value (dOFV: -4.67). The dichotomized covariate, dividing patients into two groups with baseline values above and below the population median of 8814.68 pg/mL, had the strongest effect with a decrease of the OFV by -6.40 ($p < 0.025$). β was estimated with 1.45 (90% CI: 0.71 – 2.68), which corresponds to a hazard ratio of 4.26. For comparison, when dichotomizing the patients regarding the estimated baseline values the effect was no longer significant (β: 0.786, dOFV: -1.93), indicating that the resulting groups differ, when using model predicted baseline concentrations. sVEGFR-2 plasma concentration over time, relative or absolute to the individual baseline, showed no significant effect (β: 0.923, dOFV = -0.3; β: 0.237, dOFV = -3.7).

None of the other covariates including genotypes, sunitinib pharmacokinetics, sVEGFR-3 and blood pressure showed a statistically significant effect on PFS. The effect of sVEGFR-3 baseline above the population median identified in the Kaplan-Meier and Cox regression analysis could not be confirmed in the model based approach. Inclusion of this parameter did result in a dOFV of -2.42 with an estimated β of 0.867. While the central tendency of the effect was comparable it was statistical not significant. Hence, the best prediction was achieved by using the dichotomized baseline value of sVEGFR-2:

$$\lambda(t)=\lambda_0 \cdot e^{\beta \cdot \text{sVEGFR-2 baseline (dichotomized)}} \qquad \text{(Eq. 4.1)}$$

Parameter estimates of the final model including bootstrap mean, median and confidence intervals can be found in Table 4.20.

Tab 4.20: Final parameter estimates of the time-to-event model for sunitinib patients

Parameter	Unit	Estimate	Mean (Bootstrap)	Median (Bootstrap)	90% CI (Bootstrap)
λ_0	$week^{-1}$	0.0118 (46.3)	0.0121	0.0117	0.0038 – 0.0220
β	-	1.45 (43.3)	1.57	1.49	0.71 – 2.68

The observed Kaplan-Meier curve describing the progression-free survival function of the mRCC patients was within the 90% prediction interval of 1000 simulations and could sufficiently be described by the time-to-event model (Figure 4.25). However, stratification naturally shows wider prediction intervals for the respective subgroups, due to the small sample size in each cohort. However, the description of the underlying data is still acceptable, though difficult for later time-points as a result of censored data (Figure 4.26).

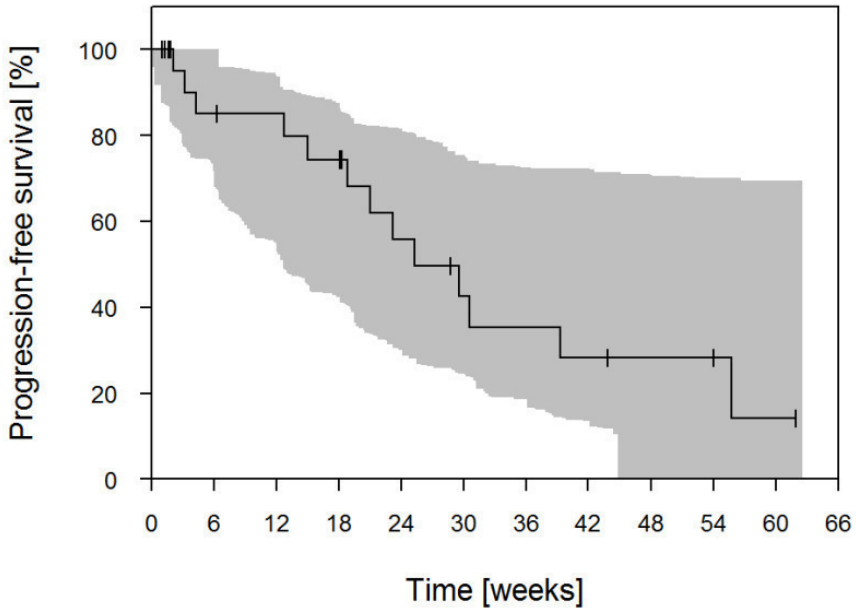

Fig. 4.25: Visual predictive check of the final time-to-event model for sunitinib (no stratification).

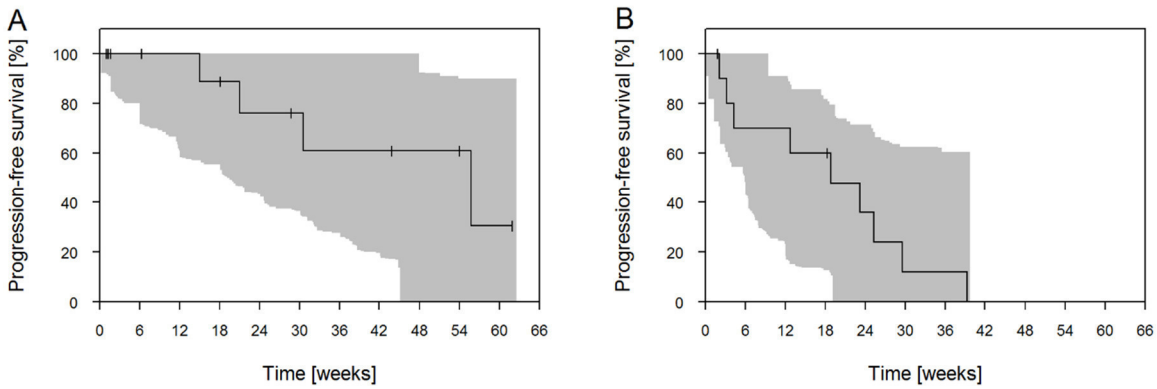

Fig. 4.26: Visual predictive check of the final time-to-event model for sunitinib stratified by covariate with (**A**) sVEGFR-2 baseline below the population median and (**B**) sVEGFR-2 baseline above the population median.

Pazopanib

A separate model-based TTE analysis for pazopanib alone was not performed due to the limited data. However, results after combined analysis, pooling data from both treatment groups, are described in the following section.

Pazopanib and Sunitinib

As for sunitinib alone, PFS was best described by a parametric TTE model with a baseline hazard function λ_0 of 0.0232 week^{-1} (90% CI: 0.0160 – 0.0324 week^{-1}). Estimation of two different baseline hazard parameters for both study drugs had no significant effect, confirming the result of the Kaplan-Meier analysis, that survival was comparable in both treatment arms (dOFV = -0.18, not significant).

In a univariate analysis, sVEGFR-2 baseline concentrations showed significant effects comparable to the analysis in sunitinib patients alone. Inclusion of absolute sVEGFR-2 baseline concentration in µg/L led to a significant decrease of the OFV with an estimated β of 0.247 (dOFV = -4.6) and 0.315 (dOFV = -5.3), if the measured or estimated baseline values were used, respectively. Dividing patients in subgroups below and above the population baseline median also showed a statistically significant effect and comparable results between measured and estimated baseline values with a beta of 0.938 (dOFV = -4.4) and 1.01 (dOFV = -5.0), respectively. In contrast to sunitinib alone, absolute sVEGFR-2 concentration over time had the strongest effect

overall with a dOFV of -8.4.β was estimated with 0.296 L/µg (0.237 L/µg for sunitinib patients alone).

Relative increase in systolic and diastolic blood pressure could also be confirmed as significant covariate in the univariate analysis. Effect strength was comparable in both cases with a β of 12.7 $mmHg^{-1}$ for systolic and diastolic blood pressure, respectively. Introduction of both parameters decreased the OFV significantly each by 6.7 and 6.8, respectively. However, the simultaneous inclusion of systolic and diastolic blood pressure had no further effect, indicating that both parameters have the same predictive value. Both time-dependent covariates, sVEGFR-2 and systolic blood pressure over time were tested in a multivariate approach. When sVEGFR-2 over time and relative systolic blood pressure over time were included simultaneously the OFV decreased by -10.67 (DF = 2, $p < 0.005$). However, removing blood pressure as predictor from the model had no significant effect (dOFV = + 2.27). In contrast, removal of sVEGFR-2 over time showed a borderline significant OFV increase (dOFV= 4.01). Therefore, for the final model only sVEGFR-2(t) was kept:

$$\lambda(t)=\lambda_0 \cdot e^{\beta \cdot sVEGFR\text{-}2\,(t)} \qquad \text{(Eq. 4.2)}$$

An estimated β of 0.292 L/µg corresponds to a hazard ratio of 1.33. For example, a baseline sVEGFR-2 concentration of 10 µg/L is associated to a hazard of 0.069 $week^{-1}$. A decrease by 1 µg/L during treatment therefore reduces the hazard by 25.8% (0.0512 $week^{-1}$). Visual predictive checks indicate that the model can describe the underlying survival data sufficiently well (Figure 4.26). An overview of the estimated parameter values is given in Table 4.21.

Tab 4.21: Final parameter estimates of the time-to-event model for sunitinib and pazopanib patients with absolute sVEGFR-2 concentration over time included as predictor

Parameter	Unit	Estimate	Mean (Bootstrap)	Median (Bootstrap)	90% CI (Bootstrap)
λ_0	$week^{-1}$	0.0037 (78.8)	0.0044	0.0036	0.001 – 0.010
β	L/µg	0.292 (30.9)	0.298	0.296	0.153 – 0.458

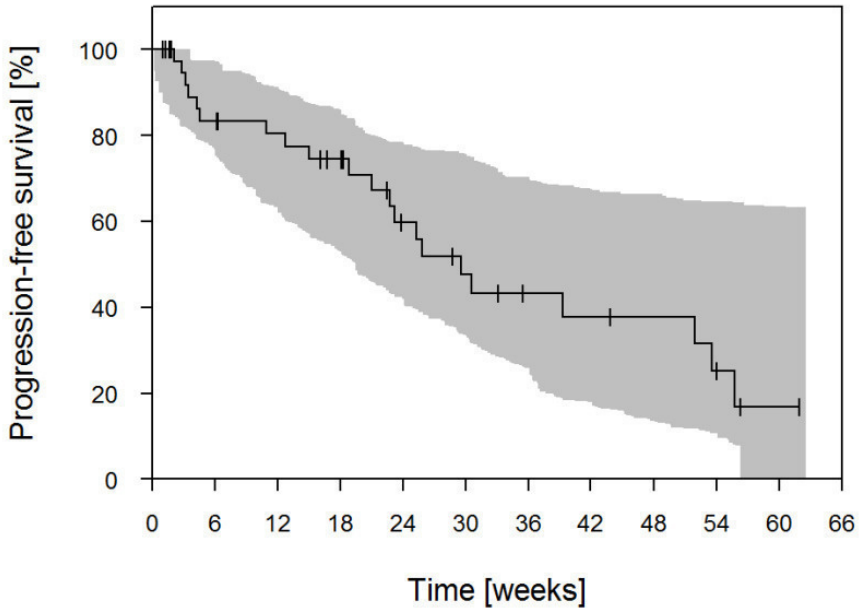

Fig. 4.27: Visual predictive check of the final time-to-event model including sVEGFR-2 over time as predictor stratified for both sunitinib and pazopanib patients.

4.4.3 Simulation of treatment effects

Figure 4.28 shows a simulation using the population estimates for a 4/2 schedule of 50 mg sunitinib daily (A) and 800 mg pazopanib on a continuously basis (B), respectively. As expected the hazard decreases proportionally to the sVEGFR-2 plasma concentration. For comparison, sVEGFR-2 baseline value was set to 10000 pg/mL in both simulations.

In addition, two simulations were performed showing the most common sunitinib regimens in comparison over the course of 18 weeks. Usually, as shown above, sunitinib is administered in 4/2 cycles. However, 2/1 cycles are also common practice in clinical settings. While the total dose is identical in the same time frame, fluctuations of sVEGFR-2 plasma concentrations and therefore in hazard, are lower with a 2/1 regimen (Figure 4.29).

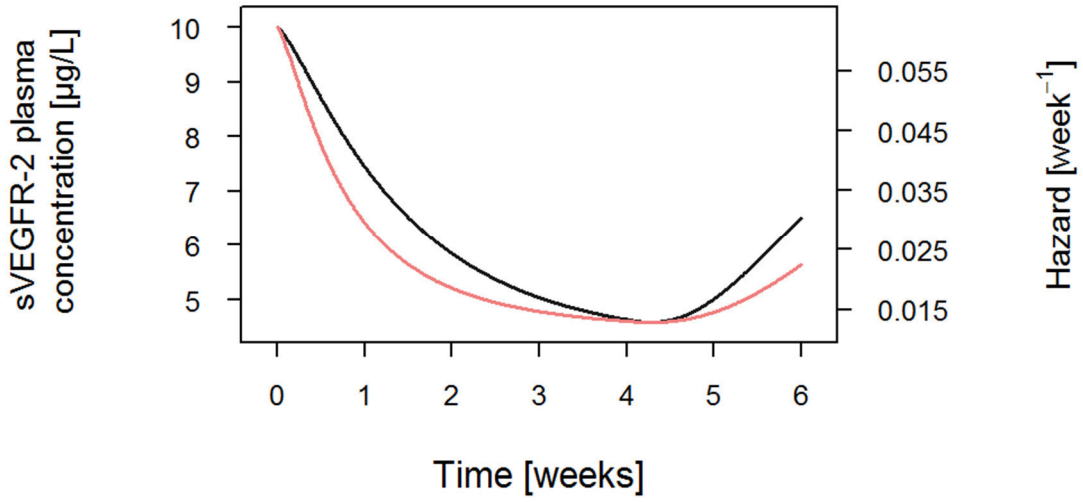

Fig. 4.28 A: Simulated treatment effect during one cycle of sunitinib with 50 mg daily intake (4/2). The black line represents the sVEGFR-2 plasma concentration during treatment and the red one the hazard during treatment.

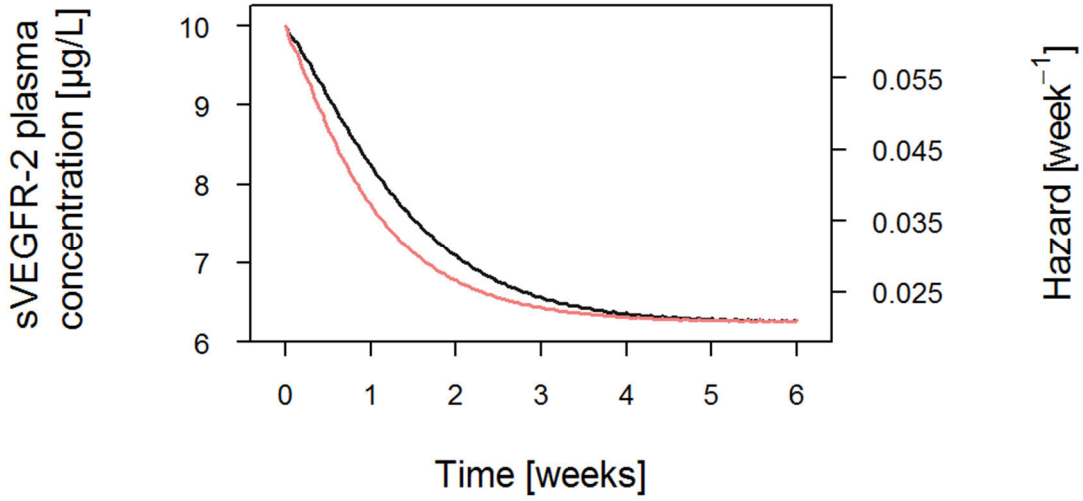

Fig. 4.28 B: Simulated treatment effect during 6 weeks of continuously administered pazopanib with a daily dose of 800 mg. The black line represents the sVEGFR-2 plasma concentration during treatment and the red one the hazard during treatment.

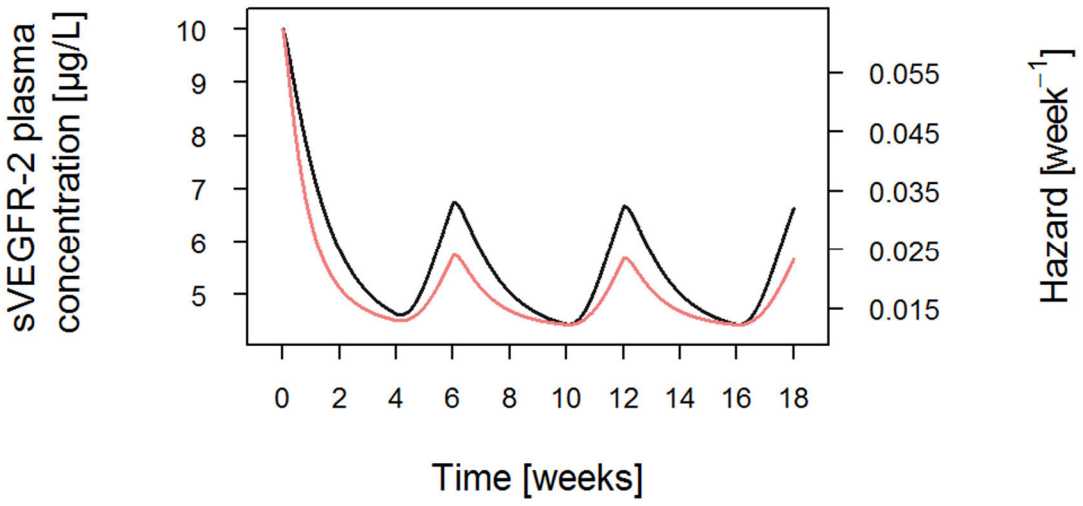

Fig. 4.29 A: Simulated treatment effect during three cycles of sunitinib with 50 mg daily intake (4/2). The black line represents the sVEGFR-2 plasma concentration during treatment and the red one the hazard during treatment.

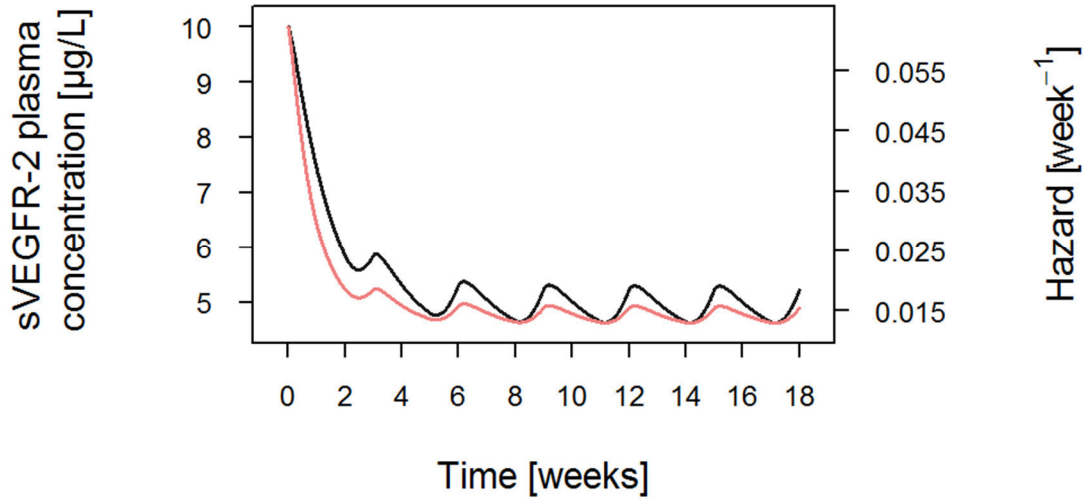

Fig. 4.29 B: Simulated treatment effect during six cycles of sunitinib with 50 mg daily intake (2/1). The black line represents the sVEGFR-2 plasma concentration during treatment and the red one the hazard during treatment.

4.5 Markov models for toxicity analysis

Myelosuppression

Occurrence of myelosuppression of any grade could be described using the "catenary"- model approach proposed by Keizer *et al.* and adapted by Suleiman *et al.* [**108**,**167**]. A model estimating all possible transitions between states was also tested; however, this approach was not feasible for the data of this study, as it relied on too many assumptions regarding non-observed transitions. For a full parameterization rate constants for non-observed transitions had to be fixed to plausible values. E.g. if only transitions between grade 1 and grade 3 were observed, a rate constant for a change from grade 1 to 2 or 2 to 3 could not be estimated and was therefore set equal to the constant for a grade 1 to 3 switch.

The inclusion of a time dependency on worsening rate constants improved the model fit significantly (dOFV = -20.8, $p < 0.0001$). In this case overall probability of developing a myelosuppression of any grade decreased exponentially over the course of the first-line therapy.

Sunitinib treatment had a small effect on worsening rates when adding the cumulative AUC of active, unbound sunitinib and SU12662 (AUC_u) as linear covariate (dOFV = 4.08, $p < 0.05$). Active, unbound sunitinib and SU12662 concentration showed also an effect on recovery rates, when added as exponential covariate (dOFV = 4.59, $p < 0.05$). Here, higher drug concentrations led to a decrease and therefore a lower probability of a transition to a lower grade of the adverse event. However, when both effects were included simultaneously, the model was no longer stable and no reliable parameter estimates could be obtained. Therefore, visual predictive checks were used for decision making. Here, the model which solely relied on the effect of AC_u on recovery rate constants as predictor was superior compared to the model which also included AUC_u on the worsening rates. In addition, the bootstrap analysis revealed that the estimate for the AUC_u effect was unreliable as the 90% CI included zero. Hence, only the effect of AC_u on the recovery rate k_B was kept in the model.

In the final model, the worsening rates k_{01}, k_{12} and k_{23} were parameterized as follows:

$$k_{01/12/23} = TVk_{01/12/23} \cdot e^{(-k_t \cdot t)} \quad \text{(Eq. 4.3)}$$

$$k_B = TVk_B \cdot e^{EFF \cdot AC_u} \quad \text{(Eq. 4.4)}$$

These rate constants describe the probability over time to switch between the respective states of the adverse event. k_B denotes for the recovery rate constant, which describes the probability of decreasing the current grade. k_t quantifies the effect of time on worsening constants k_{01}, k_{12} and k_{23} and *EFF* the estimated drug effect on recovery rate constants scaled by the AC_u. In both cases *TV* denotes for "typical value" and represents the base value of the rate constant without any effect included.

As the incidence of myelosuppression was relatively low and not all patients developed this kind of toxicity of any grade a case deletion diagnostic or jackknife was used to identify highly influential individuals in the dataset. Worsening rate constant k_{23}, in particular, was highly biased as a result of the low adverse event incidence (*jackknife* estimate: 452%). Removal of one specific patient from the data set increased the estimated parameter value by 100.3%. As a consequence the bootstrap analysis for obtaining standard errors and confidence intervals for each parameter was stratified, to ensure that all bootstrap runs included patients with and without an occurrence of this adverse event. This was necessary to avoid biased bootstrap results with respect to the low number of subjects in this study.

Final parameter estimates are shown in Table 4.22. Categorical VPCs indicate that the final model can describe the underlying data sufficiently well (Figure 4.30)

Tab. 4.22: Final parameter estimates of the Markov myelosuppression model for patients treated with sunitinib

Parameter	Unit	Estimate (RSE, %)	Mean (Bootstrap)	Median (Bootstrap)	90% CI (Bootstrap)
k_{01}	day^{-1}	0.0149 (45)	0.0165	0.0157	0.0061 – 0.0299
k_{12}	day^{-1}	0.101 (47)	0.224	0.103	0.044 – 0.408
k_{23}	day^{-1}	0.438 (84)	0.778	0.453	0.129 – 2.79
k_B	day^{-1}	0.058 (44)	0.061	0.059	0.032 – 0.096
k_t	day^{-1}	-0.0207 (28)	-0.0228	-0.0210	-0.0397 – 0.0120
EFF	-	-0.337 (53)	-0.305	-0.329	-0.473 – (-0.088)

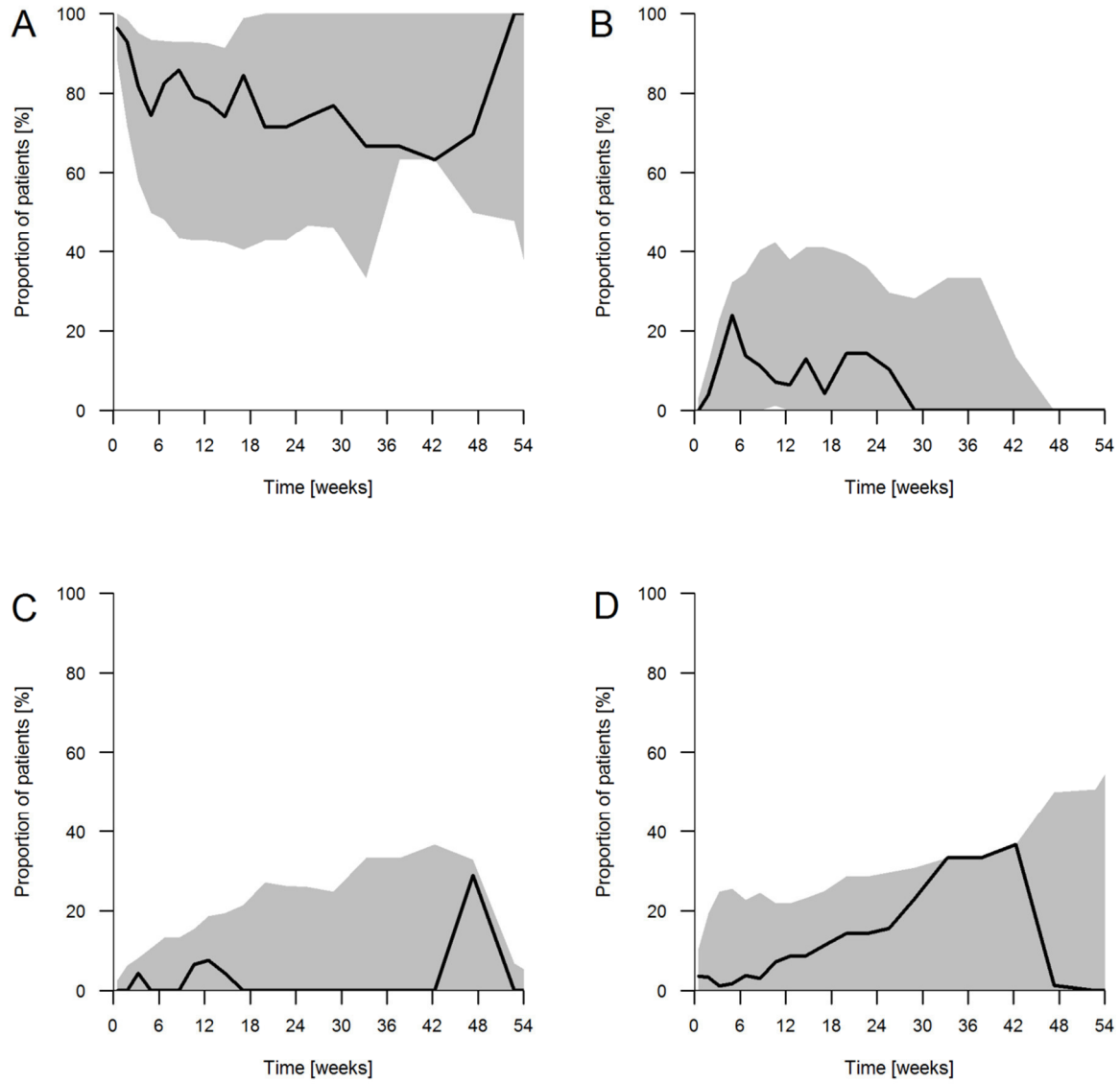

Fig. 4.29: Visual predictive checks for the development of myelosuppression under sunitinib treatment with (**A**) probability of no toxicity, (**B**) CTCAE Grade 1, (**C**) CTCAE Grade 2, and (**D**) CTCAE Grade 3/4.

A simulation for one cycle of 50 mg sunitinib daily intake in 4/2 regime is shown in Figure 4.31. The effect of sunitinib on recovery rates can especially be seen in the off phase, where toxicity of CTCAE grade 2 shows a slight increase due to the transition from higher toxicity grades.

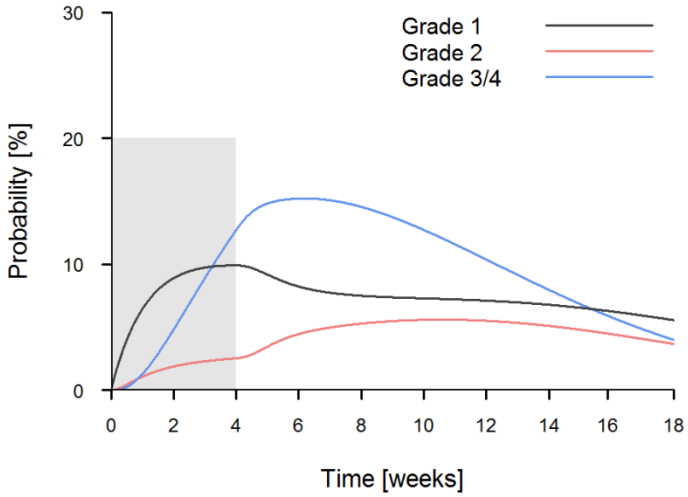

Fig. 4.31: Simulation of a standard sunitinib regimen with 50 mg daily drug intake. Lines represent the probability over time to develop a myelosuppression of the respective grade. The grey rectangle shows the time on treatment.

Fatigue

Analogously to myelosuppression under sunitinib treatment, the development of fatigue of any grade could be described using the "catenary" – model proposed by Suleiman *et al.* [**108**] and Keizer *et al.* [**167**]. A model allowing transitions between all CTCAE grades was rejected for the reasons stated above.

Recovery and worsening rates were parameterized as follows in the final model:

$$k_{01/12/23} = TVk_{01/12/23} \cdot e^{(-k_t \cdot t)} \quad \text{(Eq. 4.5)}$$

$$k_B = TVk_B \quad \text{(Eq. 4.6)}$$

Where *TV* denotes for the "typical value" without any effect included. Initially k_{12} and k_{23} were estimated separately; however, both parameters were highly correlated and could not be estimated with sufficient precision. Hence, those parameter values were set equal. The overall model performance did not worsen significantly by removing one parameter (dOFV = 1.42). Adding a time-dependent constant k_t describing the exponential decay of the worsening rates decreased the OFV significantly by -9.04 ($p < 0.01$). The same function was tested on the recovery rates, but did not improve the model fit significantly. Recovery rates were set equal (k_B) for all transitions. A separate estimation did not result in a significant improvement.

Of the tested covariates none showed a clinically relevant effect. While inclusion of the sVEGFR-3 concentration over the course of the therapy decreased the OFV significantly by -6.8, the effect was contradictory, since a stronger decrease of sVEGFR-3 led to a decreased probability of suffering from fatigue. This, in reverse, would suggest that a higher sunitinib exposition decreases the chance of developing a fatigue. Hence, this effect was not included in the final model and considered as an artifact due to the low patient number and the low incidence of fatigue.

Final parameter estimates including mean, median and 90% bootstrap confidence intervals can be found in Table 4.23.

Categorical visual predictive checks indicate that the model is able to describe the occurrence of fatigue in this mRCC cohort reasonably well, regardless of the low incidence rate during the study period (Figure 4.32)

Tab 4.23: Final parameter estimates of the Markov fatigue model for patients treated with sunitinib

Parameter	Unit	Estimate (RSE, %)	Mean (Bootstrap)	Median (Bootstrap)	90% CI (Bootstrap)
k_{01}	day^{-1}	0.0094 (41.2)	0.0099	0.0091	0.0046 – 0.0173
k_{12}/k_{23}	day^{-1}	0.0935 (81.7)	0.1112	0.0909	0.0239 – 0.2599
k_B	day^{-1}	0.0704 (29.3)	0.0712	0.0695	0.0415 – 0.1078
k_t	day^{-1}	-0.0134 (58.6)	-0.0145	-0.0132	-0.0256 – (-0.007)

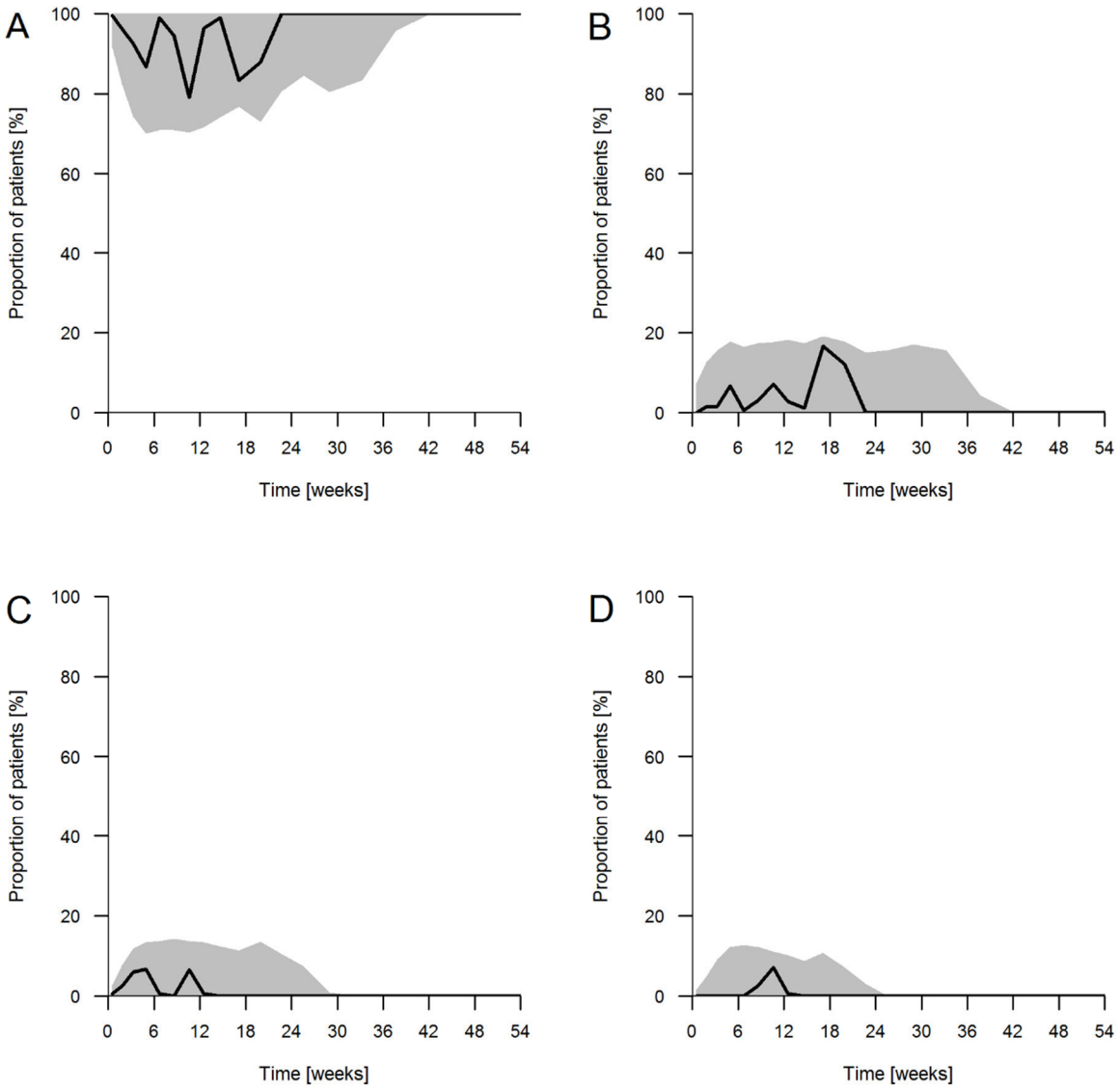

Fig. 4.32: Visual predictive checks for the development of fatigue under sunitinib treatment with (**A**) probability of no toxicity, (**B**) CTCAE Grade 1, (**C**) CTCAE Grade 2, and (**D**) CTCAE Grade 3/4.

5 DISCUSSION

5.1 PK/PD and Biomarker Analysis

5.1.1 Pharmacokinetics

Sunitinib

The developed pharmacokinetic/pharmacodynamic (PK/PD) models adequately describe plasma concentration-time profiles of sunitinib and its active metabolite SU12662 in both tumor entities. Covariate analysis on the PK parameters did not reveal any significant findings. Differences between both studies were not observed, indicating that sunitinib pharmacokinetics are independent of the tumor type. The estimated pharmacokinetic parameters are in the same range compared to other published population PK analyses [**32**,**165**]. Whereas both published semi-mechanistic models were able to describe the data, the rigid transit-compartment model developed by Lindauer *et al.* failed to provide accurate estimates without adding a fixed effects parameter to account for uncertainties in sampling and dosing times. This problem was absent when the model originally developed by Yu *et al*. was used. Nonetheless, the poor documentation is a clear limitation of this study, even though the sensitivity analysis proved that parameter estimates are reliable.

The significant increase of sunitinib clearance in patients with *ABCB1* rs2032582 TT (-18%, p = 0.02) found in previous studies could not be confirmed [**166**]. Presumably, this may be caused by the relatively small and heterogeneous cohort in this study.

Pazopanib

Individual PPK parameters for the investigated study population treated with pazopanib could be estimated using a Bayesian approach with a population PK model published by Yu *et al.* [**110**].

By using this method, the applicability of the model on new datasets could be verified. However, the Bayesian approach limited the pharmacokinetic analysis, as no population parameters were estimated for this study cohort. Therefore, a covariate analysis was not possible and the estimated individual parameters relied on the fixed parameters and their variability based on the original model. With respect to the physiological basis of the model, this approach was still considered to be reliable

enough to use the resulting individual parameters for further analysis. In particular for establishing a link to sVEGFR-2 and sVEGFR-3 plasma concentrations and blood pressure.

As initially stated, absorption of pazopanib is rather complex with respect to extrinsic factors. Notably, the simultaneous intake of food can alter the drug exposure significantly [**64**]. A factor which is difficult to control in a routine clinical setting. Although patients are usually advised to avoid drug intake right after a meal, this cannot be completely ruled out. As the model does not take food effect into account and patient's habits' were not documented, a potential bias may be introduced. One conceivable solution would be to use a mixture model to distinguish between patients who took their medication after a meal or in a fasting state. This would allow the estimation of different absorption parameters per subgroup, with the advantage that grouping is completely data-driven. However, due to the limited data and, in consequence, the use of a Bayesian approach, this method was not applicable in this study. Furthermore, a mixture model is usually used to distinguish between subpopulations with time-independent differences. Theoretically, a food effect could occur in multiple occasions over the course of a therapy, which would make it almost impossible to account for in a mixture model. Another solution could be the estimation of an inter-occasion variability on the respective absorption parameters. This would add a time -dependent random effect, to describe the variability of the drug absorption within a patient from occasion to occasion. However, the same constraints described for the mixture model approach also apply here.

5.1.2 Pharmacodynamic response

sVEGFR-2 and sVEGFR-3

Decreasing plasma concentrations of sVEGFR-2 under sunitinib treatment have been reported and considered as potential biomarker for several cancer types [**28**,**30**,**126**,**168**,**169**]. As expected, a slow decrease over the course of 4 weeks on treatment followed by a subsequent increase in the off-phase could also be observed in this study. However, independent of dose or tumor entity plasma levels did not completely recover after the off-phase. Interestingly, intrinsic activity of sunitinib

showed a significant difference in both tumor entities, with a stronger decrease in sVEGFR-2 plasma concentrations observed for mRCC patients.

This might be an indicator for a tumor specific resistance mechanism or in general for a lower efficacy of sunitinib in mCRC patients. In a double-blind, randomized phase III trial where sunitinib was compared to placebo in addition to the standard regimen consisting of fluorouracil, folinate and irinotecan (FOLFIRI) no benefit in favor for sunitinib could be shown. Quite contrary, median PFS was even lower compared to placebo (7.8 vs 9.2 months), which can probably be explained by a higher rate of severe adverse events [**170**]. Similarly, a phase II study with FOLFIRI plus sunitinib as first-line therapy in Japanese mCRC patients was prematurely discontinued as no additional activity of the combined therapy could be observed [**171**]. In fact, this could well be an isolated problem for sunitinib as other antiangiogenic drugs showed efficacy when combined with standard treatment, such as bevacizumab and the TKI regorafenib [**172**,**173**]. However, it must be noted that regorafenib, even though it was approved by FDA and EMA, is no longer available in Germany as no additional benefit could be shown according to the *Gemeinsamer Bundesausschuss* (G-BA) [**174**].

The presence of the variant G-allele in SNP rs6877011 in VEGFR-3 was associated with a 56.5% decrease in intrinsic activity on sVEGFR-2 response compared to the wild-type in the sunitinib cohort. In a previous study this SNP was shown to be associated with a decrease in PFS in mRCC patients (12 vs 4 months) [**175**]. Interestingly, this SNP effect of G-allele carriers of rs6877011 in VEGFR-3 was not found for intrinsic activity of sunitinib on sVEGFR-3, but on VEGFR-2. This may be explained by a similar binding domain in VEGFR-1, 2 and 3 [**176**]. A SNP in any of the genes encoding these VEGF receptors could result in a conformation change and prevent or stimulate binding of the drug ligand to VEGF-receptors, and change the ability of sunitinib to decrease the concentration of sVEGFR-2 and sVEGFR-3. This assumes that a lower intrinsic activity of sunitinib on sVEGFR-3 also affects sVEGFR-2 plasma concentrations. While this could be explained with a higher impact of a confirmation change on the binding affinity of sVEGFR-2 compared to sVEGFR-3 these results have to be interpreted with caution. With respect to the small patient cohort, it is still possible that the found relationship is an artifact; hence, it needs to be confirmed in a larger study, ideally with a higher number of patients with the respective SNP.

A similar effect as the 31.1% decrease in intrinsic activity of sunitinib in patients with ABCB1 rs2032582 GT/TT compared to wildtype was not reported in the literature so far. However, as stated above the same SNP was previously found to be associated with an increased sunitinib clearance as well as an increased time-to-dose reduction [**166**,**177**]. ABCB1 encodes for the transport protein p-glycoprotein (Pgp), which was shown to be a principal cause for drug resistance in anticancer treatments [**178**]. Furthermore, a high expression was observed in healthy kidney and colon tissue as well as in various tumor tissues including colorectal cancer [**179**]. Interestingly, van der Veldt *et al.* observed an increased PFS in patients with a TCG copy in the ABCB1 haplotype (HR 0.52, p = 0.033) [**180**]. However, similar to the other found influential genetic covariates the results need to be validated in a larger cohort.

The same base model for sVEGFR-2 could also be successfully linked to pazopanib pharmacokinetics. Here, the equation for pharmacodynamic effect on sVEGFR-2 plasma concentrations (*INH*) (Equation 3.29) was replaced with the active pazopanib plasma concentration as it provided a better fit. Using *INH* as a predictor, resulted in poor estimation of lower sVEGFR-2 plasma concentrations. One explanation might be the high protein binding of pazopanib which was assumed with 99.9 %, though reports vary between > 99% and up to > 99.9% [**47**,**59**,**151**,**181**]. In fact, no combination of binding constant and protein bound fraction tested provided a better fit than plasma concentration alone. A possible reason for this could be the high variability of the plasma albumin concentration due to various intrinsic and extrinsic factors in cancer patients, which is the main binding partner for pazopanib [**182**,**183**]. Routine determination of this parameter over the course therapy could help to implement a dynamic plasma protein binding into the model to capture this process more naturally than with a fixed constant leading to improved outcomes. Even though the theoretical protein bound fraction of 99.9% was used to calculate the active pazopanib concentration in the final model, this parameter only affected the scale of the estimate of the intrinsic activity *α*. Essentially, the implantation of protein binding did no longer influence the estimation of the intrinsic activity α, which resulted in a significantly better fit.

Analogously to sVEGFR-2, decreasing concentrations of sVEGFR-3 were reported under antiangiogenic treatment with TKI like sunitinib or pazopanib [**24**,**28**,**126**,**168**,**169**]. The indirect response model originally developed for sVEGFR-2 was applicable for sVEGFR-3 in both tumor entities and also for both study drugs.

Similarly to the model for sVEGFR-2, the *INH* equation was adapted accordingly for pazopanib (see above).

Observed mean baseline values of sVEGFR-3 were in the same magnitude previously reported by Motzer *et al.* ranging between 22300 and 129200 pg/mL for mRCC patients. However, they were significantly higher compared to mCRC patients [**184**]. This finding might indicate a higher expression of this protein in patients with renal cell cancer. Unfortunately, data regarding the baseline values of sVEGFR-3 concentration in plasma in mCRC patients is sparse, as the first- and second-line treatment usually does not involve multi-tyrosine kinase inhibitors [**185**].

Interestingly, some patients showed slightly increasing sVEGFR-2 and sVEGFR-3 plasma concentrations under pazopanib treatment over the course of the study, which lead to the assumption that the effect strength of pazopanib may decrease over time. Yet, the implementation of any kind of mechanistic approach to describe this behavior, e.g. models to account for development of tolerance via feedback response, did not result in a model improvement. This may be attributed to the low patient number and the fact that only some patients showed this phenomenon. Furthermore, pazopanib bioavailability was shown to decrease at steady-state over the course of the therapy, which was taken into account by the PK model. If the reduced response was linked to steady-state concentrations, it should be observable in all patients. However, dose reductions and the possibility of lower adherence in later treatment phases hinder the correct interpretation of the results and make further investigations in a larger cohort mandatory.

Blood pressure

Whereas the model is able to describe the mean increase in systolic and diastolic blood pressure sufficiently well independent of the study drug, the applicability of the model developed based on healthy volunteers is debatable. The main problem is the high parameterization of the model. In consequence, parameters for circadian variation had to be fixed to the values estimated for healthy volunteers as they could not be reliably estimated with the underlying sparse data and missing information on measurement times in a few cases. This is particularly problematic when considering that

hypertension is a risk factor for mRCC and the circadian rhythm is eventually different compared to healthy individuals.

Although measurements in this study were handled with standardized rules and devices, they were still prone to extrinsic distortions of any kind. As all measurements were conducted by physicians or study nurses in the respective centers, spikes of systolic or diastolic blood pressure can also be the result of the so called “white-coat-effect” [**186**]. However, this procedure was necessary to guarantee reliable and comparable measurements across all study centers. Self-measurements by the patients could be a viable alternative, but require additional measures to ensure comparable results, such as journals for documentation, proper instructions by health professionals and a certified device [**187**,**188**]. Another result of this approach was the sparse data especially at later time-points. As a result, the model is able to give reasonable predictions for the first cycle, but becomes unreliable in later cycles. Interestingly, even though parameters for circadian rhythm of blood pressure could not be estimated directly, the effect of blood pressure treatment of any kind could be identified as covariate. As the simulations showed (Figure 4.18), this results in a smoother course of blood pressure over the day. Due to the lack of data, this covariate was dichotomized and the strength of the individual therapy could not be acknowledged, which would most likely improve the model fit even further.

Nevertheless, provided that a large dataset is available, diagnosed hypertension and antihypertensive treatment could potentially be implemented as covariates in the model. For more reliable estimates of the respective parameters a more dense documentation of blood pressure measurements (e.g. a journal given to the patient, see above) would be necessary. Even though this would improve the dataset significantly, the execution can be challenging as this approach could potentially introduce other limitations, e.g. missing values, false documentation or ignoring the SOPs for correct measurements by the patient.

5.2 Pharmacometric approaches for modeling outcome

5.2.1 Model-based time-to-event analysis

Based on the research of the last few years, after the emergence of antiangiogenic therapy, there is strong evidence of a potential relationship between sVEGFR-2 and/or sVEGFR-3 plasma concentration, hypertension and clinical outcome [**24**,**28**,**30**,**32**,**189**,**190**]. These findings could be further confirmed by the results of this study. While the effect of sVEGFR-2 decrease over time was not significant in the model-based time-to-event analysis (HR: 1.26, P = 0.06), patients with a substantially higher baseline value of sVEGFR-2 showed a significantly worse PFS. The estimated HR for patients with a sVEGFR-3 baseline above the population median was 2.38 while not statistically significant (P = 0.2). An effect of similar magnitude (HR: 2.4, 95% CI: 1.13 – 5.11) was reported by Harmon *et al.* for the same covariate [**189**]. Interestingly, both effects were significant in the univariate Cox regression analysis for sunitinib with a HR of 5.60 (CI 90%: 1.82 – 17.24) for sVEGFR-2 baseline above the median and 3.74 (CI 90%: 1.36 – 10.27) for sVEGFR-3, but deviated when both were included simultaneously into the model. Even though our analysis suggests that the effect strength differs based on which biomarker is chosen, the direction is the same for both. This can be interpreted as a sign of high correlation between both soluble receptors; however, the wide confidence interval limits the validity of the results. Yet, these effects could be confirmed in the pooled Cox regression analysis of both treatment groups.

PK/PD models for sunitinib and pazopanib in mRCC patients could be successfully linked to the TTE model. The novelty here was the possibility to test the predictive performance of the investigated biomarkers sVEGFR-2, sVEGFR-3 and blood pressure independent of the study drug. In particular, the modeling framework allows the outcome analysis of two drugs with different pharmacokinetics but comparable pharmacodynamic response in parallel. Previous analyses with similar approaches were mostly limited to one drug, while here the class effects of the TKIs pazopanib and sunitinib could be used for a pooled analysis of all patients. As both drugs show comparable benefits with respect to survival, this kind of analysis can help to further differentiate between non-responders and responders. Interestingly, the absolute decrease in sVEGFR-2 in plasma over time was found to be predictive for PFS in mRCC while the relative decrease had no comparable effect. In a similar approach in

GIST patients the sVEGFR-3 concentration was found to be predictive over time [**32**]. The results of our study suggest that sVEGFR-2 and -3 concentrations are highly correlated which is probably the reason that some studies attribute effects to one protein and vice versa.

Furthermore, absolute systolic blood pressure over time showed a similar effect when included into the model. Probably, sVEGFR-2 and blood pressure describe the same effect, which can be explained by the assumption that increase in blood pressure is most likely related to VEGFR-2 inhibition [**191**]. This is also confirmed by the fact that no additional effects could be observed when both parameters were tested in the model. With respect to the results for the blood pressure model and its limitation in this study population, inclusion of sVEGFR-2 concentration over time as predictor in the final model is the more reliable approach. However, as blood pressure can be measured non-invasive and is in general more accessible, it could be possible to use this approach as well, once a more reliable model for cancer patients, especially with treated or untreated hypertension, is developed.

5.2.2 Markov models for toxicity analysis

Linking pharmacokinetic or pharmacodynamic response with toxicity using continuous-time Markov models is a quite novel approach, and could successfully be applied to the toxicity data from this study. However, overall the incidence of toxicity of any kind was rather low in both treatment arms. As expected, fewer patients in the pazopanib group were affected compared to sunitinib [**74**,**75**]. Since Markov models require a high amount of observed transitions, only the two most common adverse events in this population, myelosuppression and fatigue, could be analyzed [**192**].

The chosen *catenary* - model assumes that a patient undergoes all grades of the respective toxicity until a maximum is reached and vice versa [**108**,**167**]. Hence, rate constants have to be estimated for each transition to describe the model completely. Whereas this approach is plausible from a biological perspective it also requires a dense documentation of adverse events. Otherwise, estimates of rate constants will be rather high, which corresponds to a fast transition, to describe switches which skip grades, e.g. grade 1 to 3. This and the low overall incidence of adverse events are the main limiting factors in this work. In several cases, adverse events were only

documented with grade 3 or higher and once an improvement was observed the documentation stopped. It is possible that these adverse events were not considered clinically significant until they reached a higher grade or were just asymptomatic. Another factor that rendered the situation more complicated was that end-dates of adverse events were missing in some cases. This was particularly an issue in patients who suffered from fatigue during sunitinib treatment. It is quite possible that patients mentioned this toxicity once to a physician or study nurse but it was not followed-up due to being asymptomatic or just not communicated by the patient. Compared to myelosuppression the grading of fatigue is more complicated as it relies on the physicians' discretion or a wide variety of questionnaires for quantification [**193**]. However, the assumption that a fatigue persists at least until the end of a sunitinib cycle allowed the analysis of this data, but also requires a careful interpretation of the results.

Nonetheless, the visual predictive checks indicated that the models could adequately describe the underlying data despite the sparse documentation. The quantitative relationship between myelosuppression and the active sunitinib plasma concentration (AC_u) is an interesting finding as a higher exposure of sunitinib not necessarily increases the probability of a higher CTCAE grade but increases the chance to maintain the current grade for a longer period of time. In fact, the model suggests that sunitinib prolongs the time period in a certain grade. Interestingly, in a similar approach by Hansson *et al*. the relative decrease of sVEGFR-3 was predictive for a higher incidence of myelosuppression in patients with GIST treated with sunitinib [**32**]. While this could not be observed in our study the higher exposure to sunitinib seems likely to be related to the occurrence of myelosuppression independent of the tumor entity.

5.3 Clinical relevance and potential applications

PK/PD models can be a first and important step to develop individualized dosing strategies. A hypothesis generated in a smaller scale study might help to plan studies with a higher sample size and a design to quantify differences in two treatment arms. But even though our study was small in comparison, it was still possible to successfully apply models developed based on other populations and in other indications, and to construct the basis for a larger modeling framework for TKI.

As initially stated, dosing strategies for TKI, especially sunitinib and pazopanib, still mainly follow a “one-fits-all” strategy with a rigid regimen and fixed doses [**67**,**68**]. Although it could be shown that high exposition to sunitinib may be related to increased efficacy, it is also associated with a higher risk of toxicity [**194**]. Similar findings are also documented for pazopanib [**195]**. A trend that could also be verified in our study. In particular, the increase in blood pressure is a class effect which could be described for both dugs in the underlying population. In addition, the risk of maintaining longer periods of myelosuppression of any grade were directly linked to sunitinib pharmacokinetics in the respective Markov model.

However, the implementation of a model-based dosing approach into clinical practice highly depends on the quality of the model and the underlying data, especially when considering a TDM approach for dose individualization. Ideally residual and inter-individual variability is explained by informative covariates which can guide the dosing procedure.

In an *in silico* analysis using Monte Carlo simulations it could be shown that a PK guided dosing approach could increase the time-to-progression by 15-31% in GIST patients treated with sunitinib. Here, a through plasma concentration of < 50 ng/mL was used as target for dose adjustment [**196**]. Noda *et al.* showed in a small cohort that RCC patients with a median total concentration of ≥ 100 ng/mL are associated with a higher incidence of grade 3 toxicity [**197**]. The quantitative relationship between sunitinib exposure and the occurrence of certain types of toxicity may therefore be valuable for future adverse event management strategies.

Pazopanib shows a high inter-individual variability under standard treatment conditions with respect to the $AUC_{0\text{-}24}$. In a feasibility study with 13 patients no benefit for pharmacokinetically guided dosing compared to a fixed dosage regime could be identified. The authors of this study stated that this is possibly due to the lack of knowledge on what causes the variability in pazopanib patients [**198**]. However, a through value in steady state above a limit of 20 µg/mL seems to be associated with a higher efficacy in renal cell carcinoma patients [**195**,**199**]

Besides the already mentioned factors, adherence can be another crucial cause for variability in PK and PD parameters. Indeed, both TKI are a good example on how oral anticancer treatments in an ambulant setting shift the responsibility for therapy success from the treating physician and other health care professionals to the patient. Since

the variability of pazopanib can partly be explained by food effects and variable absorption due to solubility issues at higher doses, adherence to the therapy becomes an even more important aspect [**63**–**65**]. Independent of the drug used, it is necessary to have better parameters to assess therapy success and to distinguish non-responders from non-adherent patients. In a study by Byfield *et al.* it was shown that adherence and persistence is comparable between sunitinib and pazopanib, though almost 40% of patients in each group had a surprisingly low persistence of below 80% [**200**]. An analysis by Margolis *et al.* indicates an even worse scenario: In a retrospective investigation of 2395 mRCC patients more than 50% of the patients were non-adherent based on a mean possession ratio below 80%. Here, sunitinib showed the worst results across all investigated treatments [**201**]. A high inter-individual and residual variability in PK and PD parameters was also observed in our study for both drugs. Even though the identification of several covariates helped to reduce the unknown variability there is still uncertainty left. Partly documentation errors can be accounted for this, but as evidence suggests also unrecognized non-adherence may play a role in addition to unidentified covariates.

Determination of sVEGFR-2 and -3 concentrations in plasma is comparatively easy and cost-effective due to commercially available ELISA kits [**132**,**133**]. In a clinical setting this can be crucial as not every hospital has the technical equipment for a fast analysis of sunitinib or pazopanib. In addition, sunitinib requires light-protected sample handling. Otherwise the analytical results might not be reliable due to degradation [**130**,**202**]. Furthermore, for a viable monitoring approach it is necessary to define target parameters and also ranges for these parameters. Even though sVEGFR-2 and sVEGFR-3 were investigated as potential biomarkers for various cancer types in several studies, none provided guidance for clinical practice [**24**,**28**,**32**,**189**,**203**,**204**]. Although our results suggest that a high baseline value of sVEGFR-2 is associated with a lower PFS, the chosen median as threshold value is based on a relatively small cohort. Another aspect which needs to be considered beforehand is, if sVEGFR-2 baseline values serve as a prognostic or predictive biomarker [**205**]. Here, it is necessary to validate the findings of this study in larger patient groups treated with various first-line therapies for mRCC. The lack of target parameters is even more problematic when considering sVEGFR-2 plasma concentration over time as predictive factor. The developed modeling framework can be highly valuable in this case to guide dosing in a prospective clinical trial.

It was not possible to relate higher sVEGFR levels to tumor load of the individual patients, as this information was not available in the majority of subjects. Currently, there is sparse evidence of a direct quantitative relationship between tumor burden and sVEGFR-2 plasma concentrations in mRCC patients. In a preclinical analysis of various tumor models the relationship between sVEGFR-2 and tumor size was found to be inverse-linear over time in mice. Here, the plasma concentration of sVEGFR-2 decreased with disease progression. The authors concluded that this might be related to the mediation by VEGF which was overexpressed in the investigated tumor models [**206**]. Comparable *in vivo* results in cancer patients are not available. However, it is well known that various tumor types express the membrane-bound variants of VEGFR-1 -2 and -3 as well as other angiogenic factors to a higher extent [**10**,**11**]. Hansen *et al.* reported a significantly higher VEGFR-2 tissue concentration in colorectal carcinoma tumor tissue compared to normal colorectal tissue (127 pg/mL vs 78 pg/mL, $p < 10^{-6}$) [**207**]. By comparing carcinoid neuroendocrine tumors (NET) with pancreatic NET (pNET) Zurita *et al.* showed that sVEGFR-2 expression is significantly higher in the latter tumor type, but did not correlate with tumor burden [**203**]. In an investigation by Bierer *et al.* two RCC subtypes, pRCC and ccRCC (Section 1.2), were compared regarding their expression profile. Interestingly, both subgroups differed in expression of VEGF-C, D and VEGFR-3 even though for the latter the difference was not statistically significant (ccRCC: 44%, pRCC: 61%, $p = 0.11$) [**208**]. We observed a difference in sVEGFR-3 baseline values between mCRC and mRCC patients. This emphasizes the assumption that tumor mass maybe less important than tumor entity or even tumor subtype. Nonetheless, measurement of sVEGFR baseline values could provide a reliable and easy approach for additional risk assessment in mRCC patients in addition to the already established MSKCC- or Heng-Scores (Section 1.2.2)

Since it is common knowledge that patients treated with TKI are likely to develop hypertension, blood pressure was investigated as potential biomarker for therapy response with heterogeneous results across studies [**83**,**191**,**209**–**211**]. In a retrospective analysis by Rini *et al*. it was shown that mRCC patients under sunitinib treatment had an improved PFS when they developed hypertension during therapy (HR: 0.603, $p < 0.001$). These results could not be confirmed in a recent analysis of the COMPARZ study, which aimed to compare PFS in sunitinib and pazopanib patients [**74**,**208**]: here, hypertension was assessed after 4 and 12 weeks of treatment. Whereas a trend towards a positive effect of high blood pressure could be observed

after 4 weeks in both groups (HR: 0.79 for sunitinib and 0.75 for pazopanib), this was not confirmed after week 12.

In theory, blood pressure would be an ideal biomarker as it can be easily measured, even by the patients themselves, without reliance on invasive methods. However, this accessibility comes with several major shortcomings. To be a usable biomarker, measurements have to be reliable and reproducible, which can be difficult as patients and clinicians use different devices and do not necessarily stick to standard procedures. Even under perfect (study) conditions it is almost impossible to collect unbiased blood pressure data, as already discussed in Section 5.1.2.

Another crucial factor is the prevalence of hypertension. Peak incidence of mRCC ranges between 60 and 70 years [**69**]. According to the epidemiologic bulletin of the Robert-Koch Institute (RKI) prevalence of hypertension is up to 33% in the age group of 18 to 79, and 75% between 70 and 80 years in Germany. In total, 70% of these patients are treated with antihypertensive drugs [**212**]. This is an obstacle for the applicability of blood pressure as biomarker, as increases are potentially already suppressed due to antihypertensive treatment in many patients.

Therefore, further investigations in a larger cohort of patients are certainly needed. With a denser sampling it should then be possible to extend the model with relevant information on diagnosis and antihypertensive treatment. But even then it will be quite challenging to define parameters which quantify the effect of a co-medication with respect to the amount of different antihypertensive drugs and regimens. In addition the problems regarding reliability of measurements remain, and need to be carefully addressed. Developing a standard operational procedure including relevant steps and a list of certified devices to guarantee a minimum of consistency across oncological centers could be a possible solution.

The feasibility of more sophisticated dosing approaches could also be hindered by the available dosage strengths of sunitinib and pazopanib [**46**,**47**]. With a minimum dose of 12.5 mg for sunitinib and 400 mg for pazopanib it is quite difficult to target specific ranges of PK or PD parameters. Once a validated approach for individualized dosing is accessible a higher flexibility regarding possible doses is essential.

6 CONCLUSIONS AND OUTLOOK

Personalized medicine is considered as a key factor to optimize treatments, especially in anticancer drug therapy. In order to achieve individualized therapies, a crucial factor is the identification and validation of potential predictors for relevant clinical endpoints. Here, pharmacometric approaches are of excellent value as they allow to quantify the relationships between influential factors and model parameters. In addition, an informed model can be used to extrapolate knowledge to other clinically relevant questions or serve as basis for therapeutic drug monitoring.

In this thesis the basis for a PK/PD modeling framework for mRCC patients was developed for two common first-line therapies. Whereas the relationship between sunitinib pharmacokinetics and the proteins sVEGFR-2 and sVEGFR-3 in plasma was already quantified in healthy volunteers and applied to mCRC patients by Kanefendt *et al.*, here, it could be shown that different tumor entities can show different response to the same treatment [**109**,**126**]. This is particularly evident in the different intrinsic activity of sunitinib in mRCC and mCRC patients with regard to sVEGFR-2 plasma concentrations. Covariates identified in the PD models are biologically plausible, though due to the small cohort especially the genetic influential factors need to be validated in a larger study. Although blood pressure has the potential to be a viable biomarker, this study revealed some limitations in the applicability of the developed model. The highly parameterized model relied on estimates from healthy volunteers due to the sparse sampling approach used here. For a more precise prediction of blood pressure over time several key factors such as physiological changes due to hypertension and active antihypertensive treatment need to be implemented and quantified. In addition, the value of a semi-mechanistic model could be compared to the Markovian approach used for fatigue and myelosuppression. As the CTCAE grading is associated with a potential loss of information, it would be highly intriguing to see if more sophisticated semi-mechanistic models for these adverse events would be more reliable and more precise with regard to outcome prediction.

The published PK model for pazopanib by Yu *et al.* could successfully be used for a Bayesian estimation of the individual PK parameters in our study [**110**]. Furthermore, it allowed to establish the link between the measured biomarkers and pazopanib PK, which represents a novel approach. Even though the models adequately describe the PK/PD relationship of pazopanib, there is still unexplained variability which could not

be addressed in this thesis due to the low patient number and sparse data. Hence, the application of the models in a larger patient cohort and also other indications would be highly informative and may allow the identification of covariates.

As the model-based time-to-event analysis showed, sVEGFR-2 seems to be a potential predictor for PFS in patients with mRCC. This was more evident in the analysis of survival data of both drugs combined, where not only the baseline value was predictive for outcome but also the absolute decrease sVEGFR-2 concentration over time. With commercially available kits for quantification, sVEGFR-2 has a great potential to be a valuable and cost-effective biomarker for dose individualization. Therefore, the next logical step should be to evaluate the effect in a prospective study with a dosing approach based on sVEGFR-2 plasma concentrations compared to standard fixed dose treatment. However, even though the quantitative association could be established, sVEGFR-2 threshold values for dose increase or reduction need to be defined for an adequate clinical application.

Continuous-time Markov models are an excellent method to link PK/PD models with categorical outcome data. The approach used in this study allowed estimating the quantitative relationship between sunitinib exposure and the development of toxicity of a certain grade. However, due to the data limitations the application in this study has to be interpreted as a feasibility analysis. Similar to the other outcome models, the interpretation of the results is limited by the low patient number which corresponds to an overall very low incidence of adverse events. Despite that, the implementation into a modeling framework was successful and provided a first hint on the quantitative relationship between sunitinib exposure and myelosuppression. Of particular interest would be the application to other TKI, especially pazopanib, as this was not possible with our data.

As shown in other studies, modeling frameworks can be highly informative and provide an interesting basis for further analyses. Possible applications can be simulation studies to show the effect of different sunitinib or pazopanib dosing regimens on PFS and toxicity or whole clinical trial simulations. Furthermore, the framework could be extended with other models. Conceivable would be a tumor growth model similar to the one developed by Hansson *et al.* in patients with GIST [**32**]. Tumor growth has the advantage of being a progression parameter on a continuous time scale, which can be informative also in respect to resistance mechanisms [**213**]. In addition, the

interconnection of the existing models could be further extended. For example, the link between Markov models for adverse events and a time-to-event model could provide highly valuable information on the effect of a proper toxicity management on overall survival.

In conclusion, the developed modeling framework gives an insight into the quantitative relationship between the pharmacokinetics, the pharmacodynamic response and the clinical outcome of sunitinib and pazopanib. As it can be easily extended, it also provides a solid basis for further investigations. Additionally, this framework can serve as a template for pharmacometric analyses of other antiangiogenic drugs used in oncology.

7 SUMMARY

This thesis provides the basis for an extensive modeling framework for patients with metastatic renal cell carcinoma (mRCC) treated with two common first-line therapies, sunitinib and pazopanib. As part of the European-wide EuroTARGET project, which aimed at identifying predictive biomarkers in mRCC patients, a pharmacokinetic phase IV study was conducted in Germany and the Netherlands.

Based on a center-specific schedule up to 12 blood samples per patient were collected in conjunction with blood pressure measurements. Plasma concentrations of the respective study drug and the soluble VEGF receptors 2 and 3 were quantified for each time-point using previously established analytical methods. The generated data was pooled with the results from a previous study in mCRC patients treated with sunitinib (C-II-005) for a combined pharmacokinetic/pharmacodynamic analysis.

Published pharmacokinetic and pharmacodynamics (PK/PD) models were used as basis for this work. For both sunitinib and pazopanib, reliable individual pharmacokinetic parameters could be obtained and successfully linked to pharmacodynamic models for the potential biomarkers. An inverse-linear relationship provided the overall best fit for sVEGFR-2, sVEGFR-3 and blood pressure. Covariate analysis of the PK/PD models revealed two single nucleotide polymorphisms (SNPs) with influence on the intrinsic activity of sunitinib on sVEGFR-2 plasma concentrations (VEGFR-3 rs6877011 and ABCB1 rs2032582).

Furthermore, a significant difference in response to sunitinib with respect to sVEGFR-2 between both investigated tumor entities was estimated, indicating a higher activity of sunitinib in mRCC patients. sVEGFR-3 baseline concentrations were significantly higher in mRCC compared to mCRC patients. The final PK/PD models were then used to establish a link to clinical outcome parameters including progression-free survival (PFS) and the two most commonly observed adverse events in the mRCC population. In a model-based time-to-event (TTE) analysis, a high sVEGFR-2 baseline plasma concentration was associated with a worse prognosis for sunitinib patients. In a combined analysis of sunitinib and pazopanib the absolute sVEGFR-2 plasma concentration over time was a potentially predictive factor. Hence, this model allows the prediction of PFS based on the measured sVEGFR-2 plasma concentration.

Myelosuppression and fatigue as treatment-associated adverse events were analyzed separately using first-order continuous Markov models. Here, active sunitinib plasma concentration proved to be influential as a higher exposition did result in prolonged time frames of myelosuppression. However, a similar effect was not observed for fatigue.

The modeling framework presented in this thesis provides a better understanding of the relationship between the exposure, pharmacological response, and clinical outcome of antiangiogenic drugs and is therefore an important step towards finding optimal dosing schedules and identifying potential predictive biomarkers for both drugs. However, it also emphasizes, that it is might be difficult to find general biomarkers for antiangiogenic therapies, which can be applied across different tumor entities.

8 REFERENCES

[1] Center Watch. Drugs approved by FDA in 2015. Accessed: 02/2017. Available at: https://www.centerwatch.com/drug-information/fda-approved drugs/year/2015

[2] ASCO. Cancer progress timeline. Accessed: 02/2017. Available at: http://www.cancerprogress.net/timeline/majormilestones-against-cancer

[3] Rudek M, Chau C, Figg W, HL M. Handbooks of anticancer pharmacokinetics and pharmacodynamics. 2. Edition. New York. Springer; 2014.

[4] National Cancer Institute, NCI. Dictionary of cancer terms. Accessed: 01/2017. Available at: https://www.cancer.gov/

[5] ASCO. Cancer progress timeline: Targeted therapies. Accessed: 01/2017. Available at: http://www.cancerprogress.net/

[6] IMS Health. Development in cancer treatments, market dynamics, patient access and value: Global oncology trend report 2015. Accessed: 01/2017. Available at: http://www.imshealth.com/

[7] Cegedim Strategic Data. Press release: Cancer treatments in the top 5 european countries. Accessed: 01/2017. Available at: http://hugin.info/141732/R/1892907/670743.pdf

[8] FDA. Approved Cancer Drugs. Accessed: 01/2017. Available at: http://www.fda.gov/

[9] Folkman J. Tumor angiogenesis: Therapeutic implications. N Engl J Med. 1971;285:1182–6.

[10] Weis SM, Cheresh DA. Tumor angiogenesis: molecular pathways and therapeutic targets. Nat Med. 2011;17:1359–70.

[11] Mross K. Angiogeneseinhibition in der Onkologie. Bremen: UNI-MED Verlag AG; 2007.

[12] Bergers G, Hanahan D. Modes of resistance to anti-angiogenic therapy. Nat Rev Cancer. 2008;8:592–603.

[13] Azam F, Mehta S, Harris AL. Mechanisms of resistance to antiangiogenesis therapy. Eur J Cancer. 2010;46:1323–32.

[14] Rini BI, Atkins MB. Resistance to targeted therapy in renal-cell carcinoma. Lancet Oncol. 2009;10:992–1000.

[15] Khattak M, Larkin J. Sequential therapy with targeted agents in metastatic renal cell carcinoma: beyond second-line and overcoming drug resistance. World J Urol. 2014;32:19–29.

[16] Ferrara N, Carver-Moore K, Chen H, Dowd M, Lu L, O'Shea KS, *et al*. Heterozygous embryonic lethality induced by targeted inactivation of the VEGF gene. Nature. 1996;380:439–42.

[17] Hicklin DJ, Ellis LM. Role of the vascular endothelial growth factor pathway in tumor growth and angiogenesis. J Clin Oncol. 2005;23:1011–27.

[18] Rini BI, Campbell SC, Escudier B. Renal cell carcinoma. Lancet. 2009;373:1119–32.

[19] Shibuya M. Vascular endothelial growth factor and its receptor system: Physiological functions in angiogenesis and pathological roles in various diseases. J Biochem. 2013;153:13–9.

[20] Facemire CS, Nixon AB, Griffiths R, Hurwitz H, Coffman TM. Vascular endothelial growth factor receptor 2 controls blood pressure by regulating nitric oxide synthase expression. Hypertension. 2009;54:652–8.

[21] Li B, Ogasawara AK, Yang R, Wei W, He GW, Zioncheck TF, *et al*. KDR (VEGF receptor 2) is the major mediator for the hypotensive effect of VEGF. Hypertension. 2002;39:1095–100.

[22] Kendall RL, Wang G, Thomas KA. Identification of a natural soluble form of the vascular endothelial growth factor receptor, FLT-1, and its heterodimerization with KDR. Biochem Biophys Res Commun. 1996;226:324–8.

[23] Ebos JM, Bocci G, Man S, Thorpe PE, Hicklin DJ, Zhou D, *et al*. A naturally occurring soluble form of vascular endothelial growth factor receptor 2 detected in mouse and human plasma. Mol Cancer Res. 2004;2:315–26.

[24] Deprimo SE, Bello CL, Smeraglia J, Baum CM, Spinella D, Rini BI, *et al*. Circulating protein biomarkers of pharmacodynamic activity of sunitinib in patients with metastatic renal cell carcinoma: modulation of VEGF and VEGF-related proteins. J Transl Med. 2007;5:32.

[25] Ambati B, Nozaki M, Singh N, Takeda A. Corneal avascularity is due to soluble VEGF receptor-1. Nature. 2006;443:993–7.

[26] Koga K, Osuga Y, Yoshino O, Hirota Y, Ruimeng X, Hirata T, *et al*. Elevated serum soluble vascular endothelial growth factor receptor 1 (sVEGFR-1) levels in women with preeclampsia. J Clin Endocrinol Metab. 2003;88:2348–51.

[27] Pavlakovic H, Becker J, Albuquerque R, Wilting J, Ambati J. Soluble VEGFR-2: An antilymphangiogenic variant of VEGF receptors. Ann N Y Acad Sci. 2010;1207:e7-15

[28] Norden-Zfoni A, Desai J, Manola J, Beaudry P, Force J, Maki R, *et al*. Blood-Based Biomarkers of SU11248 Activity and Clinical Outcome in Patients with Metastatic Imatinib-Resistant Gastrointestinal Stromal Tumor. Clin Cancer Res. 2007;13:2643–50.

[29] Singh N, Tiem M, Watkins R, Cho YK, Wang Y, Olsen T, *et al*. Soluble vascular endothelial growth factor receptor 3 is essential for corneal alymphaticity. Blood. 2013;121:4242–9.

[30] Yoshiji H, Noguchi R, Ikenaka Y, Kaji K, Shirai Y, Aihara Y, *et al*. Soluble VEGF receptor-2 may be a predictive marker of anti-angiogenic therapy with clinically available safe agents. Oncol Lett. 2011;2:69–73.

[31] Jürgensmeier JM, Schmoll H-J, Robertson JD, Brooks L, Taboada M, Morgan SR, *et al*. Prognostic and predictive value of VEGF, sVEGFR-2 and CEA in mCRC studies comparing cediranib, bevacizumab and chemotherapy. Br J Cancer. 2013;108:1316–23.

[32] Hansson EK, Ma G, Amantea M, French J, Milligan P, Friberg LE, *et al*. PKPD Modeling of predictors for adverse effects and overall survival in sunitinib-treated patients with GIST. CPT Pharmacometrics Syst Pharmacol. 2013;2:e85.

[33] Summary of Product Characteristics: Avastin. Accessed: 01/2017. Available at: http://www.ema.europa.eu/

[34] National Cancer Institute, NCI. FDA Approval for bevacizumab. Accessed: 01/2017. Available at: https://www.cancer.gov/

[35] Summary of Product Characteristics: Glivec. Accessed: 01/2017. Available at: http://www.ema.europa.eu/

[36] Summary of Product Characteristics: Nexavar. Accessed: 01/2017. Available at: http://www.ema.europa.eu/

[37] Summary of Product Characteristics: Torisel. Accessed: 01/2017. Available at: http://www.ema.europa.eu/

[38] Polunovsky VA, Houghton PJ. mTOR pathway and mTOR inhibitors in cancer therapy. New York: Springer; 2010.

[39] Karar J, Maity A. PI3K/AKT/mTOR pathway in angiogenesis. Front Mol Neurosci. 2011;4:1-8.

[40] Zhu X, Wu S, Dahut WL, Parikh CR. Rishs of proteinuria and hypertension with bevacizumab, an antibody against vascular endothelial growth factor: systematic review and meta-analysis. Am J Kidney Dis. 2007;49:186–93.

[41] Funakoshi T, Latif A, Galsky MD. Risk of hypertension in cancer patients treated with sorafenib: an updated systematic review and meta-analysis. J Hum Hypertens. 2013;27:601–11.

[42] Zhu X, Stergiopoulos K, Wu S . Risk of hypertension and renal dysfunction with an angiogenesis inhibitor sunitinib: systematic review and meta-analysis. Acta Oncol (Madr). 2009;48:9–17.

[43] Qi W-X, Lin F, Sun Y-J, Tang L-N, He A-N, Yao Y, *et al*. Incidence and risk of hypertension with pazopanib in patients with cancer: a meta-analysis. Cancer Chemother Pharmacol. 2013;71(2):431–9.

[44] Verheul HMW, Pinedo HM. Possible molecular mechanisms involved in the toxicity of angiogenesis inhibition. Nat Rev Cancer. 2007;7:475–85.

[45] Kappers MHW, Van Esch JHM, Sluiter W, Sleijfer S, Danser AHJ, Van Den Meiracker AH. Hypertension induced by the tyrosine kinase inhibitor sunitinib is associated with increased circulating endothelin-1 levels. Hypertension. 2010;56:675–81.

[46] Summary of Product Characteristics: Sutent. Accessed: 01/2017. Available at: http://www.ema.europa.eu/

[47] Summary of Product Characteristics: Votrient. Accessed: 01/2017. Available at: http://www.ema.europa.eu/

[48] Kumar R, Crouthamel M-C, Rominger DH, Gontarek RR, Tummino PJ, Levin R a, *et al*. Myelosuppression and kinase selectivity of multikinase angiogenesis inhibitors. Br J Cancer. 2009;101:1717–23.

[49] Rini BI, Tamaskar I, Shaheen P, Salas R, Garcia J, Wood L, *et al*. Hypothyroidism in patients with metastatic renal cell carcinoma treated with sunitinib. J Natl Cancer Inst. 2007;99:81–3.

[50] Desai J, Yassa L, Marqusee E, George S, Frates MC, Chen MH, Morgan JA, Dychter SS, Larsen PR, Demetri GD AE. Hypothyroidism after sunitinib treatment for patients with gastrointestinal stromal tumors. Ann Intern Med. 2006;145:660–4.

[51] Wolter P, McCann L, Sternberg CN, Hutson TE, Mehmud F, Pandite LN, *et al*. Incidence of thyroid dysfunction in renal cell carcinoma (RCC) patients treated with pazopanib in prospective clinical trials. J Clin Oncol. 2011;29:4633.

[52] Rini BI, Escudier B, Tomczak P, Kaprin A, Szczylik C, Hutson TE, *et al*. Comparative eff ectiveness of axitinib versus sorafenib in advanced renal cell carcinoma (AXIS): a randomised phase 3 trial. Lancet. 1931;378:1931–9.

[53] Tamaskar I, Bukowski R, Elson P, Ioachimescu AG, Wood L, Dreicer R, *et al*. Thyroid function test abnormalities in patients with metastatic renal cell carcinoma treated with sorafenib. Ann Oncol. 2008;19:265–8.

[54] Abdel-Rahman O, Fouad M. Risk of thyroid dysfunction in patients with solid tumors treated with VEGF receptor tyrosine kinase inhibitors: A critical literature review and meta analysis. Expert Rev Anticancer Ther. 2014;14:1063–73.

[55] Brown RL. Tyrosine kinase inhibitor-induced hypothyroidism: Incidence, etiology, and management. Target Oncol. 2011;6:217–26.

[56] Demetri GD, van Oosterom AT, Garrett CR, Blackstein ME, Shah MH, Verweij J, *et al*. Efficacy and safety of sunitinib in patients with advanced gastrointestinal stromal tumor after failure of imatinib: a randomised controlled trial. Lancet. 2006;368:1329–38.

[57] Motzer RJ, Hutson TE, Tomczak P, Michaelson MD, Bukowski RM, Rixe O, *et al*. Sunitinib versus interferon alfa in metastatic renal-cell carcinoma. N Engl J Med. 2007;356:115–24.

[58] Mendel DB, Laird AD, Xin X, Louie SG, Christensen JG, Li G, *et al*. In vivo antitumor activity of SU11248 , a novel tyrosine kinase inhibitor targeting vascular endothelial growth factor and platelet-derived growth factor receptors : determination of a pharmacokinetic / pharmacodynamic relationship. Clin Cancer Res. 2003;9:327–37.

[59] Di Gion P, Kanefendt F, Lindauer A, Scheffler M, Doroshyenko O, Fuhr U, *et al*. Clinical pharmacokinetics of tyrosine kinase inhibitors. Clin Pharmacokinet. 2011;50:551–603.

[60] Kalra S, Rini BI, Jonasch E. Alternate sunitinib schedules in patients with metastatic renal cell carcinoma. Ann Oncol. 2015;26:1300–4.

[61] Sternberg CN, Davis ID, Mardiak J, Szczylik C, Lee E, Wagstaff J, *et al*. Pazopanib in locally advanced or metastatic renal cell carcinoma: results of a randomized phase III trial. J Clin Oncol. 2010;28:1061–8.

[62] van der Graaf WT a, Blay J-Y, Chawla SP, Kim D-W, Bui-Nguyen B, Casali PG, *et al*. Pazopanib for metastatic soft-tissue sarcoma (PALETTE): a randomised, double-blind, placebo-controlled phase 3 trial. Lancet. 2012;379:1879–86.

[63] Hurwitz HI, Dowlati A, Saini S, Savage S, Suttle B, Gibson DM, *et al*. Phase I trial of pazopanib in patients with advanced cancer. Clin Cancer Res. 2009;15:4220–7.

[64] Heath EI, Chiorean EG, Sweeney CJ, Hodge JP, Lager JJ, Forman K, *et al*. A phase I study of the pharmacokinetic and safety profiles of oral pazopanib with a high-fat or low-fat meal in patients with advanced solid tumors. Clin Pharmacol Ther. 2010;88:818–23.

[65] Heath EI, Forman K, Malburg L, Gainer S, Suttle B, Adams L, *et al*. A phase I pharmacokinetic and safety evaluation of oral pazopanib dosing administered as crushed tablet or oral suspension in patients with advanced solid tumors. Invest New Drugs. 2012;30:1566–74.

[66] WHO. International Agency for Research on Cancer. Globocan 2012: Estimated Cancer Incidence, Mortality and Prevalence Worldwide 2012. Accessed: 01/2017. Available at: http://globocan.iarc.fr/Pages/fact_sheets_population.aspx

[67] European Association of Urology. Guidelines on renal cell carcinoma 2016. Accessed: 01/2017. Available at: http://uroweb.org/

[68] Escudier B, Porta C, Schmidinger M, Rioux-Leclercq N, Bex A, Khoo V, *et al*. Renal cell carcinoma: ESMO Clinical Practice Guidelines for diagnosis, treatment and follow-up. Ann Oncol. 2016;27:v58-v68

[69] Chow WH, Dong LM. Devesa SS. Epidemiology and risk factors for kidney cancer. Nat Rev Urol. 2010;7:245–57.

[70] Moch H, Cubilla AL, Humphrey PA, Reuter VE, Ulbright TM. The 2016 WHO classification of tumors of the urinary system and male genital organs—Part A: renal, penile, and testicular tumors. Eur Urol. 2016;70:93–105.

[71] Zhou M, He H. Pathology of Renal Cell Carcinoma. In: Campbel S, Rini B, editors. Renal Cell Carcinoma: Clinical Management (23-41). New York. Springer; 2013.

[72] Heng DYC, Xie W, Regan MM, Warren M a, Golshayan AR, Sahi C, *et al*. Prognostic factors for overall survival in patients with metastatic renal cell carcinoma treated with vascular endothelial growth factor-targeted agents: results from a large, multicenter study. J Clin Oncol. 2009;27:5794–9.

[73] Rothschild S, Stenner F. Fortgeschrittenes Nierenzellkarzinom - aktuelle Behandlung. Medicalforum. 2012;58:6–10.

[74] Motzer RJ, Hutson TE, Cella D, Reeves J, Hawkins R, Guo J, *et al*. Pazopanib versus sunitinib in metastatic renal-cell carcinoma. N Engl J Med. 2013;369:722–31.

[75] Escudier B, Porta C, Bono P, Powles T, Eisen T, Sternberg CN, *et al*. Randomized, controlled, double-blind, cross-over trial assessing treatment preference for pazopanib versus sunitinib in patients with metastatic renal cell carcinoma: PISCES study. J Clin Oncol. 2014;32:1412–8.

[76] Biomarkers Defintions Working Group. Biomarkers and surrogate endpoints: Preferred definitions and conceptual framework. Clin Pharmacol Ther. 2001;69:89–95.

[77] Kim C, Prasad V. Cancer drugs approved on the basis of a surrogate end point and subsequent overall survival. JAMA Intern Med. 2015;175:1992-4.

[78] Lindpaintner K. Pharmacogenetics and the future of medical practice. Br J Clin Pharmacol. 2002;54:221–30.

[79] Summary of Product Characteristics: Herceptin. Accessed: 01/2017. Available at: http://www.ema.europa.eu/

[80] Slamon DJ, Leyland-Jones B, Shak S, Fuchs H, Paton V, Bajamonde A, *et al*. Use of chemotherapy plus a monoclonal antibody against HER2 for metastatic breast cancer that overexpresses HER2. N Engl J Med. 2001;344:783–92.

[81] FDA. Pharmacogenomic biomarkers in drug labelling. Accessed: 01/2017. Available at: http://www.fda.gov/Drugs/ScienceResearch/ResearchAreas/Pharmacogenetics/ucm083378.htm

[82] Gruenwald V, Beutel G, Schuch-Jantsch S, Reuter C, Ivanyi P, Ganser A, *et al*. Circulating endothelial cells are an early predictor in renal cell carcinoma for tumor response to sunitinib. BMC Cancer. 2010;10:695.

[83] Rini BI, Cohen DP, Lu DR, Chen I, Hariharan S, Gore ME, *et al*. Hypertension as a biomarker of efficacy in patients with metastatic renal cell carcinoma treated with sunitinib. J Natl Cancer Inst. 2011;103:763–73.

[84] Ette EI, Williams PJ. Pharmacometrics : the science of quantitative pharmacology. Hoboken, New Jersey: John Wiley & Sons; 2007.

[85] Derendorf H, Gramatté T, Schäfer HG, Staab A. Pharmakokinetik kompakt. Stuttgart: Deutscher Apothekerverlag; 2010.

[86] Peter L. Bonate. Pharmacokinetic-Pharmacodynamic Modeling and Simulation. New York: Springer; 2011.

[87] Peters SA. Physiologically-Based Pharmacokinetic (PBPK) Modeling and Simulations. Hoboken, New Jersey: John Wiley & Sons; 2012.

[88] Beal SL, Sheiner LB, Boeckmann AJ. NONMEM User Guide – Part I to VII (1989 – 2011). Ellicott City, MD: Icon Development Solutions; 2011.

[89] Owen JS, Fiedler-Kelly J. Introduction to Population Pharmacokinetic / Pharmacodynamic Analysis with Nonlinear Mixed Effects Models. Introduction to Population Pharmacokinetic / Pharmacodynamic Analysis with Nonlinear Mixed Effects Models. Hoboken, New Jersey: John Wiley & Sons; 2014.

[90] Sheiner LB. Learning versus confirming in clinical drug development. Clin Pharmacol Ther. 1997;61:275–91.

[91] Sheiner LB, Steimer J-L. Pharmacokinetic/pharmacodynamic modeling in drug development. Annu Rev Pharmacol Toxicol. 2000;40:67–95.

[92] Burton M, Shaw L, Schentag J, Evans W. Applied pharmacokinetics and pharmacodynamics. Baltimore, Maryland: Lippincott Williams & Wilkins; 2006.

[93] Fuchs A, Csajka C, Thoma Y, Buclin T, Widmer N. Benchmarking therapeutic drug monitoring software: a review of available computer tools. Clin Pharmacokinet. 2013;52:9–22.

[94] Kloft C, Jaehde U. Dosisindividualisierung. In: Jaehde U, Radziwill R, Kloft C. Klinische Pharmazie: Grundlagen und Anwendungen. Stuttgart: Wissenschaftliche Verlagsgesellschaft; 2010.

[95] Paci A, Veal G, Bardin C, Levêque D, Widmer N, Beijnen J, *et al*. Review of therapeutic drug monitoring of anticancer drugs part 1 - Cytotoxics. Eur J Cancer. 2014;50:2010–9.

[96] Widmer N, Bardin C, Chatelut E, Paci A, Beijnen J, Levêque D, *et al*. Review of therapeutic drug monitoring of anticancer drugs part 2 - Targeted therapies. Eur J Cancer. 2014;50:2020–36.

[97] Calvert AH, Newell DR, Gumbrell LA, O'Reilly S, Burnell M, Boxall FE, *et al*. Carboplatin dosage: prospective evaluation of a simple formula based on renal function. J Clin Oncol. 1989;7:1748–56.

[98] Saif MW, Choma A, Salamone SJ, Chu E. Pharmacokinetically guided dose adjustment of 5-fluorouracil: a rational approach to improving therapeutic outcomes. J Natl Cancer Inst. 2009;101:1543–52.

[99] Timmers L, Boons CLM, Moes-Ten J, Smit F, van Peter M, Aerts G, *et al.* Adherence, exposure and patients' experiences with the use of erlotinib in non-small cell lung cancer. J Cancer Res Clin Oncol. 2015;141(8):1481.

[100] Liewer S, Huddleston AN. Oral targeted therapies: managing drug interactions, enhancing adherence and optimizing medication safety in lymphoma patients. Expert Rev Anticancer Ther. 2015;15:453–64.

[101] Huang W, Chen C, Lin S. Medication adherence to oral anticancer drugs: systematic review. Expert Rev Anticancer Ther. 2016;16:423-32.

[102] FDA. Guidance for Industry: Clinical trial endpoints for the approval of cancer drugs and biologics. Accessed: 01/2017. Available at: http://www.fda.gov/

[103] Collet D. Modelling survival data in medical research. Boca Raton, Florida: Chapman & Hall/CRC; 2003.

[104] Holford N. A time to event tutorial for pharmacometricians. CPT Pharmacometrics Syst Pharmacol. 2013;2:e43.

[105] National Cancer Institute, NCI. Common Terminology Criteria for Adverse Events v4.03. 2010 Accessed: 01/2017. Available at: https://evs.nci.nih.gov/

[106] Friberg LE, Henningsson A, Maas H, Nguyen L, Karlsson MO. Model of chemotherapy-induced myelosuppression with parameter consistency across drugs. J Clin Oncol. 2002;15;20:4713–21.

[107] Karlsson MO, Schoemaker RC, Kemp B, Cohen AF, van Gerven JM, Tuk B, *et al*. A pharmacodynamic markov mixed-effects model for the effect of temazepam on sleep. Clin Pharmacol Ther. 2000;68:175–88.

[108] Suleiman AA, Frechen S, Scheffler M, Zander T, Nogova L, Kocher M, *et al*. A modeling and simulation framework for adverse events in erlotinib-treated non-small-cell lung cancer patients. AAPS J. 2015;17:1483–91.

[109] Lindauer A, Di Gion P, Kanefendt F, Tomalik-Scharte D, Kinzig M, Rodamer M, *et al*. Pharmacokinetic/pharmacodynamic modeling of biomarker response to sunitinib in healthy volunteers. Clin Pharmacol Ther. 2010;87:601–8.

[110] Yu H, Steeghs N, Kloth JSL, de Wit D, van Hasselt JGC, van Erp NP, *et al*. Integrated semi-physiological pharmacokinetic model for both sunitinib and its active metabolite SU12662. Br J Clin Pharmacol. 2015;79:809–19.

[111] Lindbom L, Ribbing J, Jonsson EN. Perl-speaks-NONMEM (PsN)--a Perl module for NONMEM related programming. Comput Methods Programs Biomed. 2004;75:85–94.

[112] Keizer RJ, van Benten M, Beijnen JH, Schellens JHM, Huitema ADR. Piraña and PCluster: a modeling environment and cluster infrastructure for NONMEM. Comput Methods Programs Biomed. 2011;101:72–9.

[113] R Development Core Team. R: A language and environment for statistical computing. Vienna: R Foundation for Statistical Computing; 2016.

[114] Jonsson EN, Karlsson MO. Xpose - an S-PLUS based population pharmacokinetic/pharmacodynamic model building aid for NONMEM. Comput Methods Programs Biomed. 1999 ;58:51–64.

[115] Sarkar D. Lattice. New York: Springer; 2008.

[116] Wickham H. ggplot2: Elegant graphics for data analysis. New York: Springer; 2009.

[117] Wickham H. Reshaping Data with the reshape Package. J Stat Softw. 2007;21:1-20

[118] Microsoft Corporation. Microsoft Excel 2007. Redmond, USA.

[119] Ritz C, Baty F, Streibig JC, Gerhard D. Dose-response analysis using R. PLoS One. 2015;10:1-13

[120] Therneau TM, Grambsch PM. Modeling survival data: Extending the cox model. New York: Springer; 2000.

[121] Venkatraman S. clinfun: Clinical trial design and data analysis functions. 2016. Available at: https://cran.r-project.org/package=clinfun

[122] Hothorn T, Hornik K, van de Wiel M, Zeileis A. Implementing a class of permutation tests: The coin package. J Stat Softw. 2008;28:1–23.

[123] van der Zanden LFM, Vermeulen SH, Oskarsdottir A, Maurits JSF, Diekstra MHM, Ambert V, *et al*. Description of the EuroTARGET cohort: A european collaborative project on targeted therapy in renal cell cancer-genetic- and tumor-related biomarkers for response and toxicity. Urol Oncol. 2017;35:e9-16

[124] Eisenhauer EA, Therasse P, Bogaerts J, Schwartz LH, Sargent D, Ford R, *et al*. New response evaluation criteria in solid tumors: revised RECIST guideline (version 1.1). Eur J Cancer. 2009 Jan;45:228–47.

[125] World Medical Association. World Medical Association Declaration of Helsinki. 2008. Accessed: 01/2017. Available at: http://www.wma.net/

[126] Kanefendt F. Analytik und Eignung von Biomarkern zur Vorhersage der Wirksamkeit von Sunitinib mit Hilfe von pharmakokinetischen/pharmakodynamischen Modellen. München: Dr. Hut Verlag; 2013.

[127] Mross K, Scheulen M, Strumberg D, Kuhlmann J, Kanefendt F, Sörgel F, *et al*. FOLFIRI and sunitinib as first-line treatment in metastatic colorectal cancer patients with liver metastases-a CESAR phase II study including pharmacokinetic, biomarker, and imaging data. Int J Clin Pharmacol Ther. 2014;52:642–52.

[128] FDA. Guidance for industry: Analytical procedures and methods validation for drugs and biologics. 2015 Accessed: 01/2017. Available at: http://www.fda.gov/

[129] EMA. Guideline on bioanalytical method validation. 2011. Accessed: 01/2017. Available at: http://www.ema.europa.eu/

[130] Rodamer M, Elsinghorst PW, Kinzig M, Gütschow M, Sörgel F. Development and validation of a liquid chromatography/tandem mass spectrometry procedure for the quantification of sunitinib (SU11248) and its active metabolite, N-desethyl sunitinib (SU12662), in human plasma: application to an explorative study. J Chromatogr B Analyt Technol Biomed Life Sci. 2011;879:695–706.

[131] Sparidans RW, Ahmed TTA, Muilwijk EW, Welzen MEB, Schellens JHM, Beijnen JH. Liquid chromatography-tandem mass spectrometric assay for therapeutic drug monitoring of the tyrosine kinase inhibitor pazopanib in human plasma. J Chromatogr B Analyt Technol Biomed Life Sci. 2012;905:137–40.

[132] Human VEGF R2/KDR Quantikine® ELISA Kit. Catalog Number: SVR200. Minneapolis, USA: R&D Systems.

[133] Human sVEGF R3/Flt-4 DuoSet® ELISA. Catalog Number: DY349. Minneapolis, USA: R&D Systems.

[134] Kanefendt F, Lindauer A, Mross K, Fuhr U, Jaehde U. Determination of soluble vascular endothelial growth factor receptor 3 (sVEGFR-3) in plasma as pharmacodynamic biomarker. J Pharm Biomed Anal. 2012;70:485–91.

[135] Looney SW, Hagan JL. Statistical methods for assessing biomarkers and analyzing biomarker data (109-47). In: Rao C, Miller J, Rao D. Handbook of Statistics. Amsterdam: Elsevier B.V.; 2007.

[136] Diekstra MHM. Pharmacogenetics of sunitinib in metastatic renal cell carcinoma. University of Leiden. 2017. Available at: https://openaccess.leidenuniv.nl/handle/1887/55944

[137] Mould DR, Upton RN. Basic concepts in population modeling, simulation, and model-based drug development-part 2: introduction to pharmacokinetic modeling methods. CPT pharmacometrics Syst Pharmacol. 2013;2:e38.

[138] Karlsson MO, Sheiner LB. The importance of modeling interoccasion variability in population pharmacokinetic analyses. J Pharmacokinet Biopharm. 1993;21:735–50.

[139] Byon W, Smith MK, Chan P, Tortorici MA, Riley S, Dai H, *et al*. Establishing best practices and guidance in population modeling: an experience with an internal population pharmacokinetic analysis guidance. CPT pharmacometrics Syst Pharmacol. 20133;2:e51.

[140] Hooker AC, Staatz CE, Karlsson MO. Conditional weighted residuals (CWRES): A model diagnostic for the FOCE method. Pharm Res. 2007;24:2187–97.

[141] Savic RM, Karlsson MO. Importance of shrinkage in empirical bayes estimates for diagnostics: problems and solutions. AAPS J. 2009;11:558–69.

[142] Holford N. An Introduction to Visual Predictive Checks. Accessed: 01/2017. Available at: http://holford.fmhs.auckland.ac.nz/

[143] Pearl speaks NONMEM, PsN. VPC and NPC user guide. 2016. Available at: http://psn.sourceforge.net/

[144] Bergstrand M, Hooker AC, Wallin JE, Karlsson MO. Prediction-corrected visual predictive checks for diagnosing nonlinear mixed-effects models. AAPS J. 2011;13:143–51.

[145] Pearl speaks NONMEM, PsN. CDD user guide. 2016 Accessed: 01/2017.

Available at: http://psn.sourceforge.net/

[146] Mcintosh AI. The Jackknife : Introduction and basic properties. 2016. Accessed: 01/2016. Available at: https://arxiv.org/

[147] Bendall M, Gray D. Sensitivity analysis of pharmacokinetic systems. Kybernetes. 1978;7:285–9.

[148] Beal SL. Ways to fit a PK model with some data below the quantification limit. J Pharmacokinet Pharmacodyn. 2001;28:481–504.

[149] Bergstrand M, Karlsson MO. Handling data below the limit of quantification in mixed effect models. AAPS J. 2009;11:371–80.

[150] Ahn JE, Karlsson MO, Dunne A, Ludden TM. Likelihood based approaches to handling data below the quantification limit using NONMEM VI. J Pharmacokinet Pharmacodyn. 2008;35:401–21.

[151] Imbs DC, Négrier S, Cassier P, Hollebecque A, Varga A, Blanc E, *et al*. Pharmacokinetics of pazopanib administered in combination with bevacizumab. Cancer Chemother Pharmacol. 2014;73:1189–96.

[152] Yu H, van Erp N, Bins S, Mathijssen RHJ, Schellens JHM, Beijnen JH, *et al*. Development of a pharmacokinetic model to describe the complex pharmacokinetics of pazopanib in cancer patients. Clin Pharmacokinet. 2017;56:293–303.

[153] Faivre S, Demetri G, Sargent W, Raymond E. Molecular basis for sunitinib efficacy and future clinical development. Nat Rev Drug Discov. 2007;6:734–45.

[154] Weiß C. Medizinische Statistik. Heidelberg: Springer; 2005.

[155] Miller R. Survival Analysis. Hoboken, New Jersey: John Wiley & Sons; 1998.

[156] Fox J, Weisberg S. Cox Proportional Hazards Regression for Survival Data in R. 2011. Accessed: 01/2017. Available at: https://socserv.socsci.mcmaster.ca/

[157] Hothorn T, Hornik K, van de Wiel MA, Zeileis A. A lego system for conditional inference. Am Stat. 2006;60:257–63.

[158] Ziegler A, Lange S, Bender R. Überlebenszeitanalyse: Die Cox-Regression. Dtsch Medizinische Wochenschrift. 2004;129:1-3.

[159] Efron B. The efficiency of Cox's likelihood function for censored data. J Am Stat Assoc. 1977;72:557.

[160] McCullagh P. Proportional odds model. In: Encyclopedia of Biostatistics. Hoboken, New Jersey: John Wiley & Sons; 2005.

[161] Bender R, Ziegler A, Lange S. Logistische Regression. Dtsch Med

Wochenschr. 2007;132;33–5.

[162] Schlarmann J, Galatsch M. Regressionsmodelle für ordinale Zielgrößen. GMS Med Inf Biom Epidemiol. 2014;10:1-9

[163] Lehoczky J. Markov Chains. In: Encyclopedia of Biostatistics. Hoboken, New Jersey: John Wiley & Sons; 2005.

[164] de Vries Schultink AHM, Suleiman AA, Schellens JHM, Beijnen JH, Huitema ADR. Pharmacodynamic modeling of adverse effects of anti-cancer drug treatment. Eur J Clin Pharmacol. 2016;72:645–53.

[165] Houk BE, Bello CL, Kang D, Amantea M. A population pharmacokinetic meta-analysis of sunitinib malate (SU11248) and its primary metabolite (SU12662) in healthy volunteers and oncology patients. Clin Cancer Res. 2009;15:2497–506.

[166] Diekstra MHM, Klümpen HJ, Lolkema MPJK, Yu H, Kloth JSL, Gelderblom H, *et al*. Association analysis of genetic polymorphisms in genes related to sunitinib pharmacokinetics, specifically clearance of sunitinib and SU12662. Clin Pharmacol Ther. 2014;96:81–9.

[167] Keizer RJ, Gupta A, Mac Gillavry MR, Jansen M, Wanders J, Beijnen JH, *et al*. A model of hypertension and proteinuria in cancer patients treated with the anti-angiogenic drug E7080. J Pharmacokinet Pharmacodyn. 2010;37:347–63.

[168] Nowak AK, Millward MJ, Creaney J, Francis RJ, Dick IM, Hasani A, *et al*. A phase II study of intermittent sunitinib malate as second-line therapy in progressive malignant pleural mesothelioma. J Thorac Oncol. 2012;7:1449–56.

[169] Rini BI, Michaelson MD, Rosenberg JE, Bukowski RM, Sosman J a, Stadler WM, *et al*. Antitumor activity and biomarker analysis of sunitinib in patients with bevacizumab-refractory metastatic renal cell carcinoma. J Clin Oncol. 2008;26:3743–8.

[170] Carrato A, Swieboda-Sadlej A, Staszewska-Skurczynska M, Lim R, Roman L, Shparyk Y, *et al*. Fluorouracil, leucovorin, and irinotecan plus either sunitinib or placebo in metastatic colorectal cancer: a randomized, phase III trial. J Clin Oncol. 2013;31:1341–7.

[171] Tsuji Y, Satoh T, Tsuji A, Muro K, Yoshida M, Nishina T, *et al*. First-line sunitinib plus FOLFIRI in Japanese patients with unresectable/metastatic colorectal cancer: a phase II study. Cancer Sci. 2012;103:1502–7.

[172] Hurwitz H, Fehrenbacher L, Novotny W, Cartwright T, Hainsworth J, Heim W,

*et a*l. Bevacizumab plus irinotecan, fluorouracil, and leucovorin for metastatic colorectal cancer. N Engl J Med. 2004;350:2335–42.

[173] Grothey A, Van Cutsem E, Sobrero A, Siena S, Falcone A, Ychou M, *et al*. Regorafenib monotherapy for previously treated metastatic colorectal cancer (CORRECT): an international, multicentre, randomised, placebo-controlled, phase 3 trial. Lancet. 2013;381:303–12.

[174] Gemeinsamer Bundesausschuss, G-BA.Nutzenbewertungsverfahren zum Wirkstoff Regorafenib. Accessed: 02/2017. Available at: https://www.g-ba.de/

[175] Scartozzi M, Bianconi M, Faloppi L, Loretelli C, Bittoni A, Del Prete M, *et al*. VEGF and VEGFR polymorphisms affect clinical outcome in advanced renal cell carcinoma patients receiving first-line sunitinib. Br J Cancer. 2012;108:1126–32.

[176] Leppänen V-M, Tvorogov D, Kisko K, Prota AE, Jeltsch M, Anisimov A, *et al*. Structural and mechanistic insights into VEGF receptor 3 ligand binding and activation. Proc Natl Acad Sci U S A. 2013;110:12960–5.

[177] Beuselinck B, Lambrechts D, Van Brussel T, Wolter P, Cardinaels N, Joniau S, *et al*. Efflux pump ABCB1 single nucleotide polymorphisms and dose reductions in patients with metastatic renal cell carcinoma treated with sunitinib. Acta Oncol. 2014;53:1413–22.

[178] Szakács G, Annereau J-P, Lababidi S, Shankavaram U, Arciello A, Bussey KJ, *et al*. Predicting drug sensitivity and resistance. Cancer Cell. 2004;6:129–37.

[179] Fojo AT, Ueda K, Slamon DJ, Poplack DG, Gottesman MM, Pastan I. Expression of a multidrug-resistance gene in human tumors and tissues. Proc Natl Acad Sci USA. 1987;84:265–9.

[180] van der Veldt AAM, Eechoute K, Gelderblom H, Gietema J, Guchelaar H-J, van Erp NP, *et al*. Genetic polymorphisms associated with a prolonged progression-free survival in patients with metastatic renal cell cancer treated with sunitinib. Clin Cancer Res. 2011;17:620–9.

[181] Imbs D-C, Paludetto M-N, Négrier S, Powell H, Lafont T, White-Koning M, *et al*. Determination of unbound fraction of pazopanib in vitro and in cancer patients reveals albumin as the main binding site. Invest New Drugs. 2016;34:41–8.

[182] Nicholson JP, Wolmarans MR, Park GR. The role of albumin in critical illness. Br J Anaesth. 2000;85:599–610.

[183] Wang X, Han H, Duan Q, Khan U, Hu Y, Yao X. Changes of serum albumin

level and systemic inflammatory response in inoperable non-small cell lung cancer patients after chemotherapy. J Cancer Res Ther. 2014;10:1019–23.

[184] Motzer RJ, Michaelson MD, Redman BG, Hudes GR, Wilding G, Figlin RA, *et al*. Activity of SU11248, a multitargeted inhibitor of vascular endothelial growth factor receptor and platelet-derived growth factor receptor, in patients with metastatic renal cell carcinoma. J Clin Oncol. 2006;24:16–24.

[185] Van Cutsem E, Cervantes A, Nordlinger B, Arnold D. Metastatic colorectal cancer: ESMO clinical practice guidelines for diagnosis, treatment and follow-up. Ann Oncol. 2014 ;25:iii1-9.

[186] Briasoulis A, Androulakis E, Palla M, Papageorgiou N, Tousoulis D. White-coat hypertension and cardiovascular events: a meta-analysis. J Hypertens. 2016;34:593–9.

[187] Stergiou GS, Ntineri A, Kollias A, Ohkubo T, Imai Y, Parati G. Blood pressure variability assessed by home measurements: a systematic review. Hypertens Res. 2014;37:565–72.

[188] Stergiou GS, Parati G, Vlachopoulos C, Achimastos A, Andreadis E, Asmar R, *et al*. Methodology and technology for peripheral and central blood pressure and blood pressure variability measurement: current status and future directions - Position statement of the European Society of Hypertension Working Group on blood pressure monitoring a. J Hypertens. 2016;34:1665–77.

[189] Harmon CS, DePrimo SE, Figlin RA, Hudes GR, Hutson TE, Michaelson MD, *et al*. Circulating proteins as potential biomarkers of sunitinib and interferon-α efficacy in treatment-naïve patients with metastatic renal cell carcinoma. Cancer Chemother Pharmacol. 2014;73:151–61.

[190] Rixe O, Billemont B, Izzedine H. Hypertension as a predictive factor of Sunitinib activity. Ann Oncol. 2007;18:1117.

[191] Robinson ES, Khankin E V, Karumanchi SA, Humphreys BD. Hypertension induced by vascular endothelial growth factor signaling pathway inhibition: mechanisms and potential use as a biomarker. Semin Nephrol. 2010;30:591–601.

[192] Karlsson MO. Tutorial: Introduction to markov modeling. PAGE meeting 2012 (presentation). Available at: https://www.page-meeting.org

[193] Seyidova-Khoshknabi D, Davis MP, Walsh D. A systematic review of cancer-

related fatigue measurement questionnaires. Am J Hosp Palliat Care. 2011;28:119–29.

[194] Houk BE, Bello CL, Poland B, Rosen LS, Demetri GD, Motzer RJ. Relationship between exposure to sunitinib and efficacy and tolerability endpoints in patients with cancer: results of a pharmacokinetic/pharmacodynamic meta-analysis. Cancer Chemother Pharmacol. 2010;66:357–71.

[195] Suttle AB, Ball HA, Molimard M, Hutson TE, Carpenter C, Rajagopalan D, *et al*. Relationships between pazopanib exposure and clinical safety and efficacy in patients with renal cell carcinoma. Br J Cancer. 2014;111:1909-16.

[196] Goulooze SC, Galettis P, Boddy A V, Martin JH. Monte Carlo simulations of the clinical benefits from therapeutic drug monitoring of sunitinib in patients with gastrointestinal stromal tumors. Cancer Chemother Pharmacol. 2016;78: 209–16.

[197] Noda S, Otsuji T, Baba M, Yoshida T, Kageyama S, Okamoto K, *et al*. Assessment of sunitinib-induced toxicities and clinical outcomes based on therapeutic drug monitoring of aunitinib for üatients With renal cell carcinoma. Clin Genitourin Cancer. 2015;13:350–8.

[198] de Wit D, van Erp NP, den Hartigh J, Wolterbeek R, den Hollander-van Deursen M, Labots M, *et al*. Therapeutic drug monitoring to individualize the dosing of pazopanib: a pharmacokinetic feasibility study. Ther Drug Monit. 2015;37:331–8.

[199] Verheijen RB, Swart LE, Beijnen JH, Schellens JHM, Huitema ADR, Steeghs N. Exposure-survival analyses of pazopanib in renal cell carcinoma and soft tissue sarcoma patients: opportunities for dose optimization. Cancer Chemother Pharmacol. 2017;80:1171-78.

[200] Byfield SAD, McPheeters JT, Burton TM, Nagar SP, Hackshaw MD. Persistence and compliance among U.S. patients receiving pazopanib or sunitinib as first-line therapy for advanced renal cell carcinoma: a retrospective claims analysis. J Manag Care Spec Pharm. 2015;21:515–22.

[201] Margolis J, Princic N, Doan J, Lenhart G, Motzer RJ. Analysis of real world treatment compliance in a cohort of 2,395 patients with metastatic renal cell carcinoma (mRCC). J Clin Oncol. 2016;34:517

[202] de Bruijn P, Sleijfer S, Lam M-H, Mathijssen RHJ, Wiemer EAC, Loos WJ. Bioanalytical method for the quantification of sunitinib and its n-desethyl metabolite SU12662 in human plasma by ultra performance liquid chromatography/tandem triple-quadrupole mass spectrometry. J Pharm Biomed Anal. 2010;51:934–41.

[203] Zurita AJ, Khajavi M, Wu H-K, Tye L, Huang X, Kulke MH, *et al*. Circulating cytokines and monocyte subpopulations as biomarkers of outcome and biological activity in sunitinib-treated patients with advanced neuroendocrine tumors. Br J Cancer. 2015;112:1199–205.

[204] Bilen MA, Zurita AJ, Ilias-Khan NA, Chen H-C, Wang X, Kearney AY, *et al*. Hypertension and circulating cytokines and angiogenic factors in patients with advanced non-clear cell renal cell carcinoma treated with sunitinib: Results from a phase II trial. Oncologist. 2015;20:1140–8.

[205] Oldenhuis CNAM, Oosting SF, Gietema JA, de Vries EGE. Prognostic versus predictive value of biomarkers in oncology. Eur J Cancer. 2008;44:946–53.

[206] Ebos JML, Lee CR, Bogdanovic E, Alami J, Van Slyke P, Francia G, *et al.* Vascular endothelial growth factor-mediated decrease in plasma soluble vascular endothelial growth factor receptor-2 levels as a surrogate biomarker for tumor growth. Cancer Res. 2008;68:521–9.

[207] Hansen TF, Garm Spindler K-L, Lorentzen KA, Olsen DA, Andersen RF, Lindebjerg J, *et al*. Quantitative analysis of vascular endothelial growth factor receptors 1 and 2 in colorectal cancer. Mol Med Rep. 2009;2:787–92.

[208] Bierer S, Herrmann E, Köpke T, Neumann J, Eltze E, Hertle L, *et al*. Lymphangiogenesis in kidney cancer: expression of VEGF-C, VEGF-D and VEGFR-3 in clear cell and papillary renal cell carcinoma. Oncol Rep. 2008;20:721–5.

[209] Goldstein D, Rosenberg JE, Figlin RA, Townsend RR, McCann L, Carpenter C, *et al*. Is change in blood pressure a biomarker of pazopanib and sunitinib efficacy in advanced/metastatic renal cell carcinoma? Eur J Cancer. 2016 Jan;53:96–104.

[210] George S, Reichardt P, Lechner T, Li S, Cohen DP, Demetri GD. Hypertension as a potential biomarker of efficacy in patients with gastrointestinal stromal tumor treated with sunitinib. Ann Oncol Off J Eur Soc Med Oncol. 2012;23:3180–7.

[211] Donskov F, Michaelson MD, Puzanov I, Davis MP, Bjarnason GA, Motzer RJ, *et al*. Sunitinib-associated hypertension and neutropenia as efficacy biomarkers in metastatic renal cell carcinoma patients. Br J Cancer. 2015;113:1571–80.

[212] Robert Koch Institute. Epidemiologisches Bulletin: Hypertonie. Available at: https://www.rki.de/

[213] Ribba B, Holford NH, Magni P, Trocóniz I, Gueorguieva I, Girard P, *et al*. A review of mixed-effects models of tumor growth and effects of anticancer drug treatment used in population analysis. CPT Pharmacometrics Syst Pharmacol. 2014;3:e113.

APPENDICES

Appendix A

List of covariates

A.I Pharmacokinetic models

Covariate	Comments
Gender	Categorical
Age	Continuous
Tumor entity (mRCC or mCRC)	Categorical
ABCB1 rs1128503	Additive and general model (if applicable)
ABCB1 rs2032582	Additive and general model (if applicable)
ABCB1 rs1045642	Additive and general model (if applicable)
VEGF A rs699947	Additive and general model (if applicable)
VEGF A rs833061	Additive and general model (if applicable)
VEGF A rs2010963	Additive and general model (if applicable)
IL8 rs1126647	Additive and general model (if applicable)
VEGF A Haplotype	Additive and general model (if applicable)

A.II Pharmacodynamic models

Covariate	Comments
Gender	Categorical
Age	Continuous
Weight	Continuous
BSA	Continuous
Tumor entity (mRCC or mCRC)	Categorical
ABCB1 rs1128503	Additive and general model (if applicable)
ABCB1 rs2032582	Additive and general model (if applicable)
ABCB1 rs1045642	Additive and general model (if applicable)
VEGF A rs699947	Additive and general model (if applicable)
VEGF A rs833061	Additive and general model (if applicable)
VEGF A rs2010963	Additive and general model (if applicable)
IL8 rs1126647	Additive and general model (if applicable)
VEGF A Haplotype	Additive and general model (if applicable)
Continued	
VEGFR-3 rs6877011	Additive and general model (if applicable)
VEGFR-3 rs307826	Additive and general model (if applicable)
VEGFR-3 rs307821	Additive and general model (if applicable)

A.III Survival analysis and Markov models for toxicity

Covariate	Comments
Age	Continuous
Weight	Continuous
Gender	Categorical
sVEGFR-2 Baseline value	Continuous
sVEGFR-2 above population median	Categorical
sVEGFR-3 Baseline value	Continuous
sVEGFR-3 above population median	Categorical
Prior Surgery (any type)	Categorical
Prior Nephrectomy	Categorical
Radiotherapy before/during treatment	Categorical
Hypertension diagnosed at treatment start	Categorical
Base BP(systolic)	Continuous
Base BP(diastolic)	Continuous
Total AUC_{SS}	Continuous
Total C_{SS}	Continuous
Active AUC_{SS}	Continuous
Active C_{SS}	Continuous
Total AUC_{SS} > Median	Categorical
Total C_{SS} > Median	Categorical
Active AUC_{SS} > Median	Categorical
Active C_{SS} > Median	Categorical
Number of metastases	Categorical
Toxicity of any kind ≥ Grade 3	Categorical
CYP3A5*3 rs776746	Additive and general model (if applicable)
ABCB1 rs1128503	Additive and general model (if applicable)
ABCB1 rs2032582	Additive and general model (if applicable)

Continued

ABCB1 rs1045642	Additive and general model (if applicable)
VEGF A rs699947	Additive and general model (if applicable)
VEGF A rs833061	Additive and general model (if applicable)
VEGF A rs2010963	Additive and general model (if applicable)
VEGF A rs3025039	Additive and general model (if applicable)
VEGFR3 rs307826	Additive and general model (if applicable)
IL8 rs1126647	Additive and general model (if applicable)
ABCB1 Haplotype	Additive and general model (if applicable)
VEGF A Haplotype	Additive and general model (if applicable)

A.IV Time-dependent covariates

These covariates were only tested in the model-based time-to-event analysis and the Markov models for selected adverse events.

Covariate	Comments
Active concentration of sunitinib and SU12662	Continuous
AUC of active substance	Continuous
Total concentration of sunitinib and SU12662	Continuous
AUC of total substance	Continuous
Absolute concentration of sVEGFR-2	Continuous
Relative concentration of sVEGFR-2	Continuous
AUC of sVEGFR-2	Continuous
Absolute concentration of sVEGFR-3	Continuous
Relative concentration of sVEGFR-3	Continuous
AUC of sVEGFR-3	Continuous
Systolic blood pressure	Continuous
Diastolic blood pressure	Continuous
Relative change in systolic blood pressure	Continuous
Relative change in diastolic blood pressure	Continuous

Only genotypes which were preselected based on their percentage of occurrence in the population were tested. For the PD models sVEGFR-3 related SNPs were tested despite the percentage under the threshold due to the high relevance

Legend

$AUC_{(SS)}$ = Area under the curve (steady state), BP = Blood pressure, BSA = Body surface area, $C_{(SS)}$ = Concentration (steady state), IL8 = Interleukin 8, mCRC = metastasized colorectal carcinoma, mRCC = metastasized renal cell carcinoma, (s)VEGF(R) = (soluble) vascular endothelial growth factor (receptor),

Appendix B

Standard operating procedures

B.I Blood sampling

EuroTARGET-Substudie C-IV-001: EuT-PK/PD

Entnahme und Handhabung von Plasmaproben

Blutentnahme	– Entnahmemenge: **7,5 ml** - In **EDTA**-Monovetten
Kontrolle des Etiketts	- Studienbezeichnung/Zentrumsnummer - EuroTARGET-Patientennummer - Abnahmetag und –zeitpunkt - **„P"** für Pazopanib bzw. „**S"** für Sunitinib auf den Deckel des Tubes - Das Etikett mit Klebefolie schützen! - Proben entsprechend dem Bestimmungsort mit **„Uni Bonn"** kennzeichnen
Zentrifugation	- innerhalb von **30 min** nach der Blutabnahme - **1000 g** rel. Zentrifugalbeschleunigung (bitte Umrechnung beachten, da die **rpm-Einstellung** variiert je nach Art der Zentrifuge (s.u.)) - **Mit** Bremsfunktion - bei **4°C** - für **15 min**
Abpipettieren	- Abnahmeröhrchen bis zum Pipettieren in der Zentrifuge belassen - Kontrolle der Pipette (**µL**-Einstellung, Pipettenspitze) - **500 µL** als Pipetteneinstellung - Pipettenspitze **nach jeder Probe** wechseln - Es ist darauf zu achten, dass nur **Plasma** übertragen wird und der unten liegende Blutkuchen unangetastet bleibt - Deckel des Plasmaröhrchens nach dem Pipettieren sofort schließen - Aufteilung in **6** Aliquote á **500 µL** - **Light-protected micro-tubes** als Plasmaröhrchen (**Sunitinib ist lichtempfindlich**!) - Plasmaröhrchen **sofort** danach einfrieren (aufrecht!)
Lagerung	- Bei mind. **-80°C** - Sortierung der Proben kontrollieren o aufsteigende Reihenfolge der Patientennummern von links nach rechts o zeitliche Reihenfolge von vorn nach hinten

Zentrifuge: Umrechnung von „g" in „rpm"

Sollte an der genutzten Zentrifuge keine Einstellung der Geschwindigkeit über die Erdbeschleunigung **g** möglich sein, empfiehlt sich eine Umrechnung in die üblichen **rpm** (rounds per minute).

Dies ist mit folgender Formel möglich:

$$rpm = \sqrt{\frac{g}{0{,}0000112 * r}}$$

Bitte beachten Sie, dass der **Zentrifugenradius r** (**in cm**) dabei entscheidend ist (zu entnehmen aus der Bedienungsanleitung des jeweiligen Gerätes).

Versand:

Mit **„Uni Bonn"** gekennzeichnete Proben werden **auf Trockeneis** an folgende Adresse versandt **(die Abholung wird durch die CESAR organisiert**):

Prof. Dr. Ulrich Jaehde
Pharmazeutisches Institut
Universität Bonn
An der Immenburg 4
D-53121 Bonn

Bei Unklarheiten wenden Sie sich bitte an:
Achim Fritsch
(Tel.: 0228-73 5229, E-Mail: a.fritsch@uni-bonn.de).

Dokumentation der Blutprobenentnahme

Klinik: _____

EuroTARGET-Patientennummer: _____

Zyklus	Datum [TT.MM.JJ]	Uhrzeit [HH:MM]	Abstand zur letzten Einnahme [in Stunden]	Aktuelle Dosierung [in mg] (Bitte Datum der Dosisanpassung angeben, falls zutreffend)
			Baseline	

B.II Blood pressure assessment

EuroTARGET-Substudie C-IV-001: EuT-PK/PD

Blutdruckmessung

Die Messungen erfolgen im Rahmen der klinischen Routineuntersuchung. Sollten **während der Studienzeit Langzeit-Blutdruckmessungen** durchgeführt werden, so ist dies **ebenfalls zu dokumentieren.**

Technische Ausstattung	Die Messungen werden mit einem zertifizierten Gerät der Deutschen Hochdruckliga ausgeführt. Ein solches Gerät wird jeder teilnehmenden Klinik kostenlos zur Verfügung gestellt.
Durchführung der Messung[1]	– Messung möglichst zur selben Tageszeit – Beginn der Messung nach 5 minütiger Ruhepause in sitzender Position – Entsprechende Verlängerung der Ruhephase bei außergewöhnlicher Belastung (>5 min) – Alle Störquellen vermeiden (z.B. Gespräche) – Bis mindestens eine Stunde vor der Messung sollte der Patient auf Coffein-haltige Getränke, Alkohol und Nikotin verzichten – Der Messarm darf **nicht** durch zurückgeschobene Kleidung abgeschnürt werden (entsprechende Kleidungsstücke, Uhren sowie Schmuck vor der Messung ablegen) – Der untere Rand der Manschette sollte 1-2 cm über der Ellenbeuge liegen. Der **Messfühler** mit dem Schlauch liegt an der **Arminnenseite** – Den Messarm während der Messung ruhig und leicht angewinkelt auf einer Unterlage auflegen und nicht bewegen – Manschette muss auf Herzhöhe liegen
Dokumentation	– Folgende Daten werden auf dem **Dokumentationsbogen** erfasst. o Datum und Uhrzeit der Messung o Systolischer Blutdruck o Diastolischer Blutdruck o Puls o Kommentare/Auffälligkeiten

Bei Unklarheiten wenden Sie sich bitte an Achim Fritsch (0228-73-5229; a.fritsch@uni-bonn.de)

[1] Modifiziert nach: Bundesvereinigung Deutscher Apothekerverbände (ABDA). Standardarbeitsanweisung –Blutdruckmessung in der Apotheke. Stand:04.2009. Verfügbar auf: http://www.abda.de/leitlinien.html. Letzter Zugriff: 13.04.2012

B.III Adverse events

Studie C-IV-001: EuT-PK/PD:

Dokumentation von „Adverse Events"

Allgemeine Hinweise zur Dokumentation

Dieser Dokumentationsbogen dient der Erfassung von „Adverse Events". Sollten bei einem Ihrer Patienten „Serious Adverse Events" auftreten, so melden Sie diese zusätzlich innerhalb von 24h via Fax an den Sponsor (Weiteres entnehmen Sie bitte dem entsprechenden Dokument).

Der Abschnitt „Kommentar" dient zusätzlichen Informationen, die zum Verständnis der erfassten Daten wichtig sind (z.B. Hospitalisierung aufgrund eines AE etc.).

Die häufigsten Nebenwirkungen von Sunitinib (entsprechend der Fachinformation) finden sich bereits im ersten Teil der Dokumentationstabelle aufgelistet. Nicht gelistete unerwünschte Ereignisse sowie Rezidive tragen Sie bitte in den entsprechenden freien Feldern ein.

Bitte nutzen Sie zur Dokumentation den folgenden Bewertungsschlüssel:

1. Kausalität

Unwahrscheinlich:	**[1]**
Möglich:	**[2]**
Wahrscheinlich:	**[3]**
Gesichert:	**[4]**
Nicht zutreffend:	**[5]**

2. Intervention

Keine Intervention:	**[0]**
Studientherapie angepasst:	**[1]**
Studientherapie **kurzzeitig** unterbrochen:	**[2]**
Studientherapie **dauerhaft** unterbrochen:	**[3]**
Begleitmedikation verordnet:	**[4]**
Nichtmedikamentöse Behandlung:	**[5]**

3. Outcome

Verbesserung:	**[1]**
Keine Änderung:	**[2]**
Verschlimmerung (SAE):	**[3]**
Unbekannt:	**[4]**

B.IV Immunoassays

Titel: Proteinbestimmung mittels ELISA

Gültigkeitsbereich: Klinische Pharmazie

Autor(en): Friederike Kanefendt

Datum/Unterschrift:

Datum/Prof. Dr. Ulrich Jaehde

Datum/Friederike Kanefendt

Überprüfungsvermerk/Qualitätssicherung

Name/Datum/Unterschrift

Verteiler:

- ☐ Laborleiter
- ☐ Mitarbeiter Labor 3.110
- ☐ Mitarbeiter Labor 3.116
- ☐ Mitarbeiter Labor 3.117
- ☐ weitere Mitarbeiter: _____

Inhalt

1. Zweck / Prinzip

Diese SOP regelt die Bestimmung von proteinogenen Analyten in humanem Kalium-EDTA-Plasma mit Hilfe von Enzyme-linked Immunosorbent Assays (ELISAs)

Sie sichert ein einheitliches Vorgehen bei der Vorbereitung der Proben, der Durchführung der Assays, die Qualität der Messungen und die Vergleichbarkeit der Ergebnisse.

2. Einsatzbereich

Die hier beschriebenen Methoden werden angewendet für die Bestimmung der proteinogenen Wachstumsfaktoren VEGF-A und VEGF-C und deren löslichen Rezeptoren sVEGFR-2 und sVEGFR-3 in humanem Kalium-EDTA- Plasma.

3. Messprinzip / Grundlagen

Der ELISA ist ein immunologisches Nachweisverfahren, das auf einer Antigen-Antikörper-Reaktion beruht. Generell unterscheidet man direkte und indirekte ELISA sowie Sandwich- und kompetitive ELISA. Das Messprinzip beruht auf der Bindung eines Analyten (Antigen) an freie (kompetitiv) oder immobilisierte für diesen Analyten spezifische Antikörper. Anschließend zugegebene Substrate werden von Enzymen zu farbigen Produkten umgesetzt oder führen durch die katalysierte chemische Umsetzung zu Lumineszenz, deren Intensität entsprechend mit einem UV-Spektrometer oder einem Luminometer gemessen werden kann. Diese Enzyme befinden sich entweder auf Zweitantikörpern (Sandwich-ELISA), die in einem weiteren Schritt den auf der Platte gebundenen Analyten binden, oder sind an das kompetitive Antigen (kompetitiver ELISA), das in definierter Menge hinzugefügt wird, gebunden. Anhand parallel vermessener Standards und einer entsprechenden Kalibrierkurve kann der Analyt quantifiziert werden.

4. Verfahrenskenndaten / Validierung

Die zurzeit verwendeten Testkits für VEGF-A, VEGF-C und sVEGFR-2 wurden von der Firma R&D Systems validiert; die Validierungsparameter befinden sich im Herstellerprotokoll zum entsprechenden Test. Die Handhabung der Tests verläuft nach Protokoll (mitgeltende Unterlagen). Dieses entstammt den Anweisungen für die Verwendung der Testkits. Zur Bestimmung von sVEGFR-3 wird ein vom humanen VEGFR-3 DuoSet ELISA ausgehender, für humanes Plasma validierter, ELISA verwendet [Kanefendt et al. 201X]. Für die Validierungskriterien, wie Präzision und Richtigkeit werden nach geltenden Vorschriften für Immunoassays Akzeptanzkriterien von ≤ 20 % angenommen [DeSilva et al. 2003].

5. Geräte/Geräteeinstellungen und Material

5.1 Geräte

- Pipetten/ Mehrkanalpipetten
- UV-Spektrometer *(Thermo Electron Corporation Multiscan EX)*
- Luminometer *(Fluostar Optima)*
- Schüttler *(Heidolph Instruments Unimax 1010 (d=10mm))*

5.2 Chemikalien und Reagenzien

- QuantiGlo human VEGF-A Immunoassay (#QVE00B)
- Quantikine human sVEGFR-2 Immunoassay (#DVR200)
- Quantikine human VEGF-C Immunoassay (#DVEC00)
- Materialien zur Bestimmung von VEGF-A, VEGF-C und sVEGFR-2 sind im entsprechenden Testkit enthalten

  sVEGFR-3 (R&D Systems, Abingdon, UK)
- Human sVEGFR-3 (Flt-4) DuoSet ELISA (#DY349)
- Purelab® Wasser
- Wash Buffer 0,05 % Tween® 20 in PBS, pH 7,2 – 7,4 (#WA126)
- Reagent Diluent Concentrate 2 – 1 % (#DY995)

- Substrate Solution (#DY999)
- Stop Solution – 2N H_2SO_4 (#DY994)
- CrossDown Buffer (AppliChem, A6485)
- Fetales Kälberserum (FKS) (Sigma, F7524)

5.3 Verbrauchsmaterialien

- Clear Polystyrene MicroPlates (#DY990)
- Parafilm
- Eppendorf Caps (0,5; 1,5; 2,0 mL)
- Polypropylen (PP)-Röhrchen (15, 50 mL)
- Pipettenspitzen

5.4 Geräteeinstellungen

- Die Geräte sind nach Angaben des Herstellers (Herstellerprotokoll) einzustellen.
- Zu beachten ist bei Verwendung des Schüttlers, dass die Angaben in rpm entsprechend auf den verwendeten Schüttler umgerechnet werden müssen.

  □rcf = 1,118 · 10^{-5} r · rpm^2

  rcf: relative centrifugal force [x g]; r: Radius [cm]; rpm: rotations per minute [1/min] □1 inch = 2,54 cm

6. Chemikalien und herzustellende Lösungen

VEGF-A, VEGF-C und sVEGFR-2:

Sämtliche Chemikalien, die verwendet werden, werden vom Hersteller mit jedem Testkit mitgeliefert. Hergestellt werden müssen Waschpuffer und Substratmischungen jeweils nach Anweisung des Herstellerprotokolls.

sVEGFR-3

- PBS Puffer

137 mM NaCl	8,0 g
2,7 mM KCl	0,2 g

8,1 mM Na_2HPO_4	1,15 g
1,5 mM KH_2PO_4	0,204 g
Purelab Plus® Wasser	ad 1000,0 ml
pH 7,2 – 7,4; 0,2 µm filtriert	

- Reagent Diluent (1:10)

Reagent Diluent Concentrate 2	1 T
Purelab Plus® Wasser	9 T

- Capture Antikörper Verdünnung (1:180)

Capture Antikörper Konzentrat	1 T
PBS	179 T

- Detection Antikörper Verdünnung (1:225)

Detection Antikörper Konzentrat	1 T
Reagent Diluent	224 T

- Streptavidin-HRP (1:200)

Streptavidin-HRP Konzentrat	1 T
Reagent Diluent	199 T

- Substrat-Mischung (1:1)

Reagent A	1 T
Reagent B	1 T

- FCS: 30 min bei 50 °C inaktivieren

7. Durchführung der Analyse

7.1 Probenentnahme

Vollblut wird durch entsprechend qualifizierte Personen in Kalium-EDTA enthaltende Monovetten entnommen und innerhalb von 30 Minuten bei 4 °C, 1029 x g für 15 min zentrifugiert. Das gewonnene Plasma wird aliquotiert und bei -80 °C eingefroren und gelagert.

7.2 Probenvorbereitung

Die Proben und alle weiteren Reagenzien, die für einen Test benötigt werden, werden auf Raumtemperatur gebracht. Das Plasma wird gegebenenfalls

verdünnt (Angaben in den entsprechenden Versuchsprotokollen oder wenn Plasmakonzentrationen oberhalb des oberen Kalibrierbereiches zu erwarten sind).

Während der Inkubation kann es erforderlich sein, die Platten zu schütteln. Um Temperaturschwankungen während der Inkubationszeit durch die Erwärmung des Schüttlers zu vermeiden, wird eine Styroporplatte in entsprechender Größe zur Isolation zwischen Schütteloberfläche und Versuchsplatte gelegt.

7.3 Kalibrierung

Die Kalibrierung verläuft ebenfalls nach Herstellerprotokoll. Sie basiert auf einer Surrogatmatrix auf Basis von FCS. Humanes Plasma kann nicht als Kalibriermatrix verwendet werden, da die Analyten endogen in humanem Plasma vorkommen und keine humane Leermatrix existiert. Als Kalibriermodell dient in der Regel die 4-Parameter logistische Funktion (1) für Messungen, bei denen die UV-Absorption gemessen wird, und ein Cubic Spline bei der Messung der Lumineszenz. Entsprechende Angaben werden ebenfalls in den entsprechenden Versuchsprotokollen gemacht. Zur Verifizierung der Kalibrierung werden Qualitätskontrollproben (QCs) auf jeder Platte mit vermessen, die vom Hersteller geliefert werden. Diese müssen den Herstellerspezifikationen entsprechen. Im Falle der Messung von sVEGFR-3 werden die QCs selbst hergestellt und müssen eine Präzision (CV,%) und Richtigkeit (RE, %) von ≤ ± 20 % aufweisen.

4-Parameter logistische Funktion

$$(1)\ Y = A_2 + \frac{(A_1 - A_2)}{1 + (\frac{X}{X_0})^p}$$

X: Konzentration

Y: Absorption

A_1: untere Asymptote

A_2: obere Asymptote

X_0: Konzentration bei der halber Absorption

p: Steigungsparameter

Der Cubic Spline interpoliert Messsignale innerhalb der Kalibrierkurve und schätzt somit die Analyt-Konzentrationen entsprechend der Lumineszenz ab.

7.4 Messung

Die Proben werden auf der 96-Well-Platte entweder im UV-Spektrometer oder im Luminometer vermessen. Gemessen wird nach entsprechend vorgegebener Inkubationszeit nach Zugabe des Stopp-Reagenzes oder des zur Lumineszenz befähigtem Substratgemisches. Erhalten werden die entsprechenden Rohdaten für Absorption oder Lumineszenz für jedes Well im Excel-Format.

7.5 Auswertung

Ausgewertet wird durch entsprechende Berechnung der Konzentrationen des Analyten mit Hilfe der abgeschätzten Parameter der Kalibrierkurve. Durch die parallel vermessenen QCs, die innerhalb der Akzeptanzkriterien liegen müssen, kann überprüft werden, ob die Messungen akzeptiert werden können.

8. Mitgeltende Unterlagen

- Herstellerprotokoll QuantiGlo VEGF-A ELISA (#QVE00B)
- Herstellerprotokoll Quantikine VEGF-C ELISA (#DVEC00)
- Herstellerprotokoll Quantikine sVEGFR-2 ELISA (#DVR200)
- Herstellerprotokoll VEGFR-3 DuoSet (#DV349)
- Versuchsprotokoll zur VEGF-A-Bestimmung
- Versuchsprotokoll zur VEGF-C-Bestimmung
- Versuchsprotokoll zur sVEGFR-2-Bestimmung
- Versuchsprotokoll zur sVEGFR-3-Bestimmung

Appendix C

Documentation sheets – Immunoassays

C.I sVEGFR-2

Versuchsprotokoll zur sVEGFR-2 Bestimmung Datum

1. Herstellen der Reagenzlösungen

alle Reagenzien vor dem Gebrauch auf Raumtemperatur bringen

☐ **Waschpuffer**

Wash Buffer Concentrate	20 mL
Purelab Wasser	ad 500 mL

☐ **VEGFR-2 Standard**

Rekonstitution mit 1 mL Purelab Wasser

15 min unter leichtem Schütteln stehen lassen

☐ **Kalibratoren**

Vorgegangen wird nach folgenden Schema ausgehend von dem im Kit enthaltenen Standard

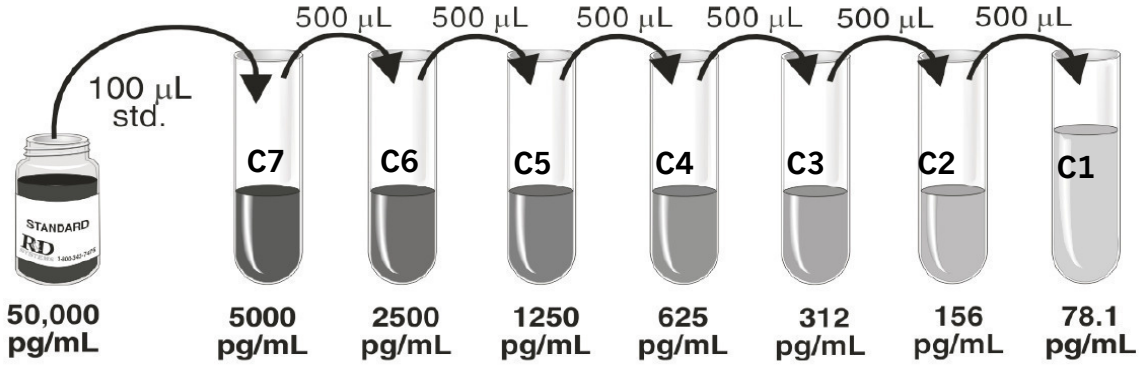

Probe	Lösung C_{x+1} [µL]	Calibrator Diluent RD6-31 [µL]	Konzentration [pg/mL]	
C7	100	900	5000.0	
C6	500	500	2500.0	
C5	500	500	1250.0	
C4	500	500	625.0	
C3	500	500	312.5	
C2	500	500	156.3	
C1	500	500	78.1	
C0		500	0.0	Leerprobe

☐ **Qualitätskontrollproben**

unverdünnt auftragen

Probe	Konz.-Bereich [pg/mL]
QC1	216-370
QC2	1171-1920
QC3	2340-3413

☐ **Probenherstellung**

Plasma muss 1:5 verdünnt werden

60 µL Plasma und 240 µL **Calibrator Diluent RD6-31**

2. ELISA Durchführung

☐ 100 µL **Assay Diluent RD1W** in jedes Well pipettieren

☐ 100 µL Standard, QC oder Probe in die entsprechenden Wells pipettieren

☐ mit der adhäsiven Folie abkleben

☐ Inkubation für 2 h bei Raumtemperatur Start: Temp.:
Ende: Temp.:

☐ Waschen mit Waschpuffer (4 x 400 µL)
Platte ausklopfen und nach dem letzten Schritt absaugen

☐ 200 µL s**VEGFR-2 Conjugate** in jedes Well pipettieren

☐ mit der adhäsiven Folie abkleben

☐ Inkubation für 2 h bei Raumtemperatur Start: Temp.:
Ende: Temp.:

☐ Waschen mit Waschpuffer (4 x 400 µL)
Platte ausklopfen und nach dem letzten Schritt absaugen

☐ 200 µL **Substrate Solution** in jedes Well pipettieren

Reagenz A	10 mL
Reagenz B	10 mL

☐ Inkubation für 30 min bei Raumtemparatur Start: Temp.:
Lichtschutz!!! Ende: Temp.:

☐ 50 µL **Stop Solution** in jedes Well pipettieren

☐ innerhalb von 30 min Messung der Absorption bei 450 nm und bei 570 nm zur Korrektur

C.II sVEGFR-3

Versuchsprotokoll zur sVEGFR-3 Bestimmung Datum

1. Herstellen der Reagenzlösungen

alle Reagenzien vor dem Gebrauch auf Raumtemperatur bringen

☐ **Waschpuffer**

Wash Buffer Concentrate	20 mL
Purelab Wasser	ad 500 mL

☐ **sVEGFR-3 Standard**

Rekonstitution mit 1 mL Purelab Wasser

15 min unter leichtem Schütteln stehen lassen

☐ **Reagent Diluent (1:10)**

Reagent Diluent Concentrate 2	5.2 mL
Purelab Wasser	46.8 mL

☐ **Kalibratoren**

Begonnen wird die Verdünnungsreihe mit C7 bestehend aus 45 µL Standard und 1530 µL FKS für alle weiteren Verdünnungen C_x wird die jeweil vorherige C_{x+1} verwendet

Probe	Lösung C_{x+1} [µL]	FKS* [µL]	Verdünnungs-faktor	Konzentration [pg/mL]
C7	45	1530	35	10571.4
C6	700	200	45	8222.2
C5	600	200	60	6166.7
C4	480	240	90	4111.1
C3	300	300	180	2055.6
C2	300	300	360	1027.8
C1	300	300	720	513.9
C0		250		0.0

* inaktiviert 30 min bei 50°C

☐ **Qualitätskontrollproben**

Gleiches Vorgehen gilt für die Herstellung der QCs, es werden 3 QCs für den Assay verwendet

Probe	Lösung C_{x+1} [µL]	FKS [µL]	Verdünnungs-faktor	Konzentration [pg/mL]
QC2	300	300	360	1027.8
	300	300	180	2055.6
QC4	480	240	90	4111.1
	600	200	60	6166.7
QC6	700	200	45	8222.2
	45	1530	35	10571.4

☐ **Probenvorbereitung**

Verdünnung 1:10 mit CrossDown Buffer

2. Plattenvorbereitung 1. Tag

☐ pH-Wert bestimmen pH: (Soll: 7,2 - 7,4)

☐ Sterilfiltration der PBS (Sterilfilter 0,2 µm)

☐ Bubble-point-Test

☐ 100 µL Capture-Antikörper Verdünnung in jedes Well pipettieren

4,0 µg/mL	Capture-AB	57 µL
	PBS	10.2 mL

☐ 100 µL in jedes Well pipettieren

☐ Inkubation über Nacht Start: Temp:
bei Raumtemperatur (RT) Ende: Temp:
in Dunkelheit

---

2. Tag Datum

☐ Waschen mit Waschpuffer
3 x mit jeweils 340 µL pro Well
ausklopfen und nach dem letzten Schritt absaugen

☐ 300 µL Reagent Diluent in jedes Well (Reagent Diluent immer frisch herstellen)

☐ Inkubation für 2 h bei RT Start: Temp.:
Ende: Temp.:

☐ Waschen mit Waschpuffer
3 x mit jeweils 340 µL pro Well
ausklopfen und nach dem letzten Schritt absaugen

---

3. ELISA-Durchführung

				Datum
☐	100 µL Proben-Lösung in jedes Well pipettieren			
☐	Abdecken mit Parafilm			
☐	Inkubation für **2 h bei 30 °C**	Start:		Temp.:
	cave: Verdunstung!!!	Ende:		Temp.:
☐	Waschen mit Waschpuffer 3 x mit jeweil (2x 170µL) ausklopfen und nach dem letzten Schritt absaugen			
☐	100 µL Detection-Antikörper Verdünnung in jedes Well pipettieren			
	0,4 µg/mL	Detection-AB	48 µL	
		Reagent Dil.	10.75 mL	
☐	Abdecken mit Parafilm			
☐	Inkubation für **2 h bei RT**	Start:		Temp.:
	Schütteln bei 272 rpm	Ende:		Temp.:
☐	Waschen mit Waschpuffer			
☐	100 µL Streptavidin-HRP	Strept-HRP	52 µL	
	innerhalb von 60 min	Reagent Dil.	10.35 mL	
☐	Abdecken mit Parafilm und Alufolie --> **Lichtausschluss**			
☐	Inkubation für **20 min bei RT**	Start:		Temp.:
	Schütteln bei 272 rpm	Ende:		Temp.:
☐	Waschen mit Waschpuffer			
☐	100 µL Substrat Verdünnung in jedes Well pipettieren			
	innerhalb von 15 min	Reagenz A	5.1 mL	
		Reagenz B	5.1 mL	
☐	Abdecken mit Parafilm und Alufolie --> **Lichtausschluss**			
☐	Inkubation für 20 min bei RT	Start:		Temp.:
		Ende:		Temp.:
☐	50 µL Stop Solution in jedes Well pipettieren			
☐	sofortige Messung 1. 2 x Schüttelschritt 2. Messung der Absorption bei 450 nm und bei 570 nm > Differenz: Abs.(450 nm) - Abs.(570 nm)			

Appendix D

Goodness-of-fit plots and visual predictive checks

D.I Pharmacokinetics (Sunitinib and SU12662)

Sunitinib

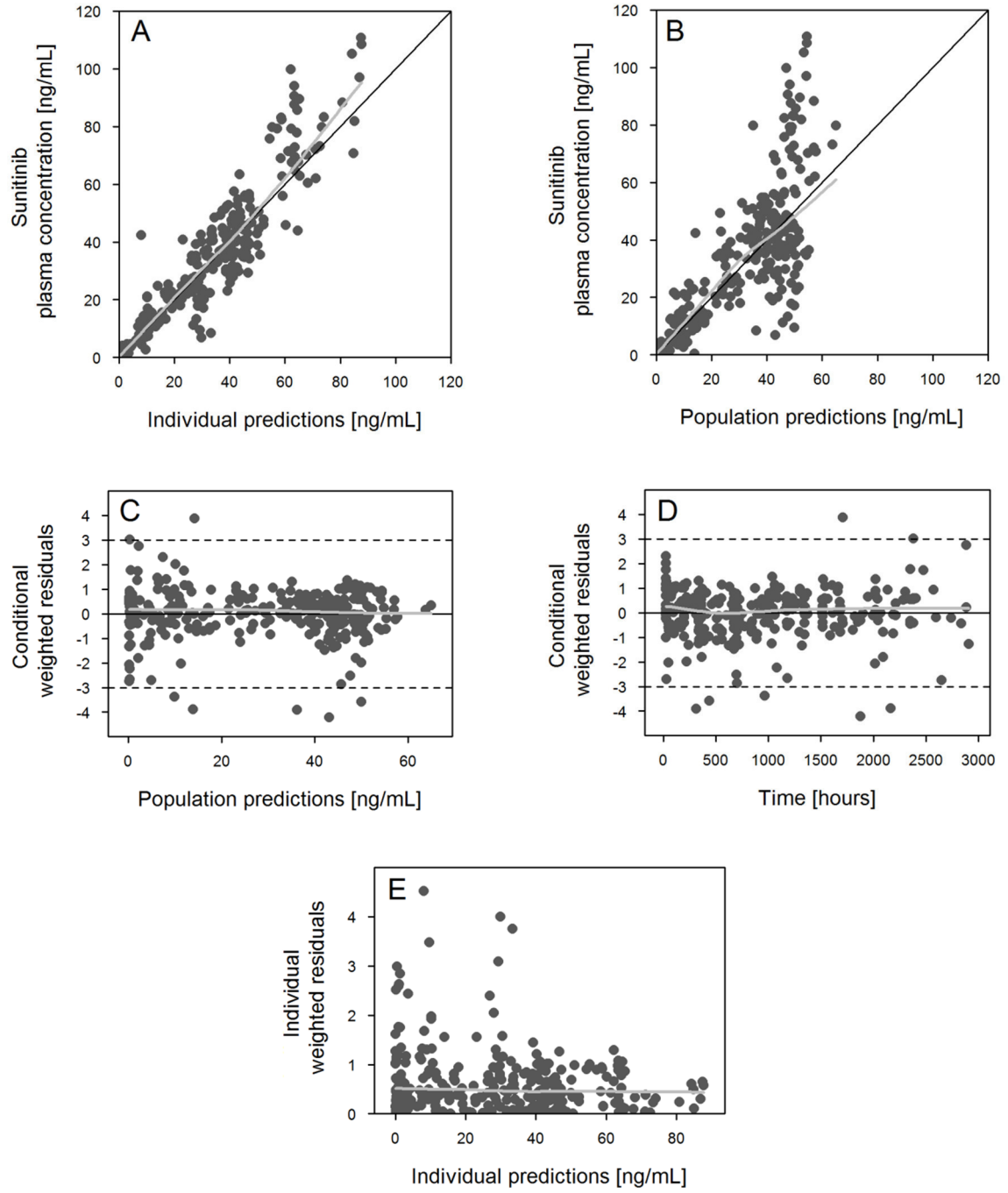

OBS vs IPRED (**A**), OBS vs PRED (**B**), CWRES vs PRED (**C**), CWRES vs Time (**D**) , |IWRES| vs IPRED (**E**)

OBS = Observed values, IPRED = Individual predictions, PRED = Population predictions, CWRES = Conditional weighted residuals, IWRES = Individual weighted residuals

SU12662

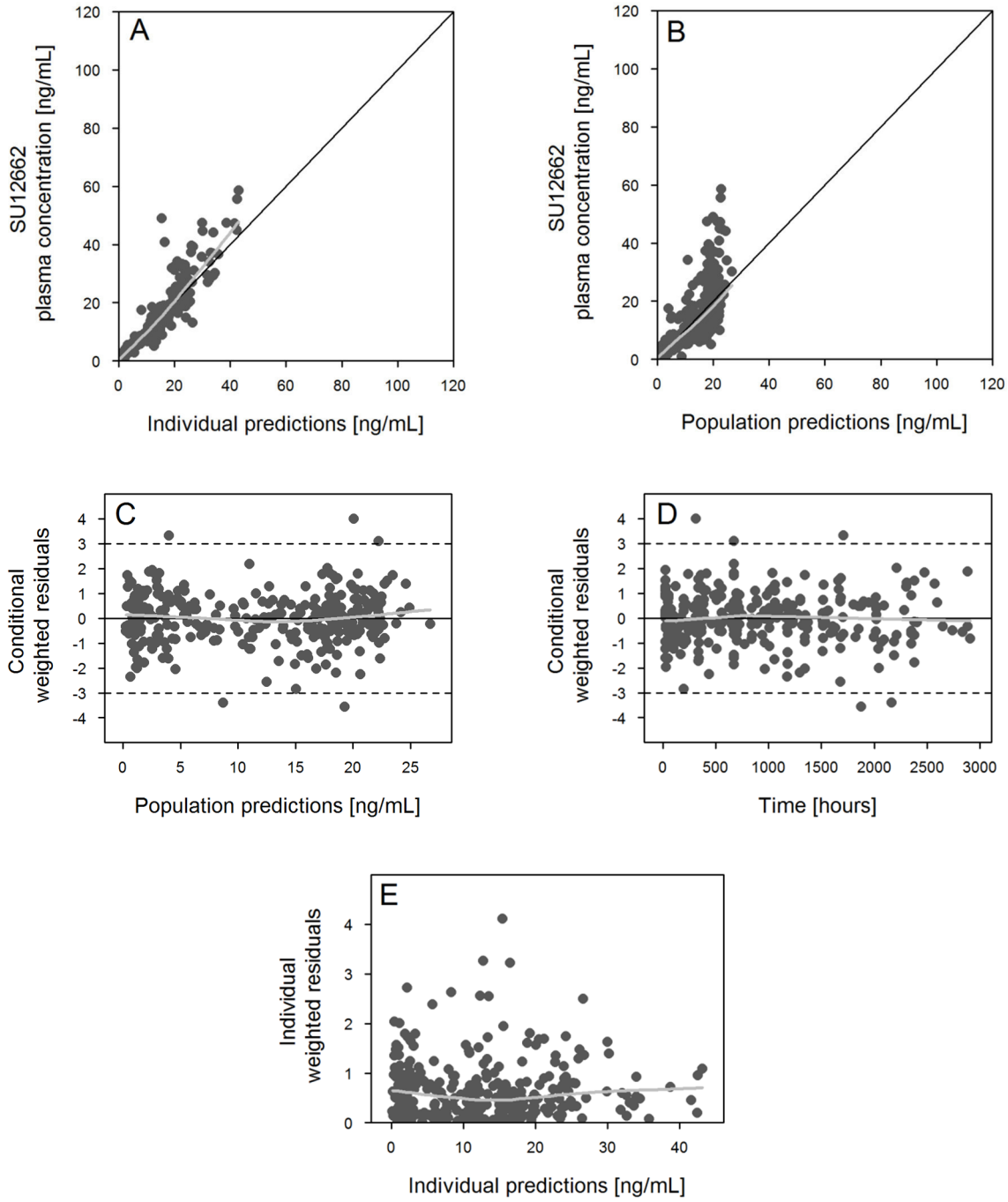

OBS vs IPRED (**A**), OBS vs PRED (**B**), CWRES vs PRED (**C**), CWRES vs Time (**D**) , |IWRES| vs IPRED (**E**)

OBS = Observed values, IPRED = Individual predictions, PRED = Population predictions, CWRES = Conditional weighted residuals, IWRES = Individual weighted residuals

Comparison between the two different pharmacokinetic models for **sunitinib** by Yu *et al*. [**110**] and Lindauer *et al*. [**109**]

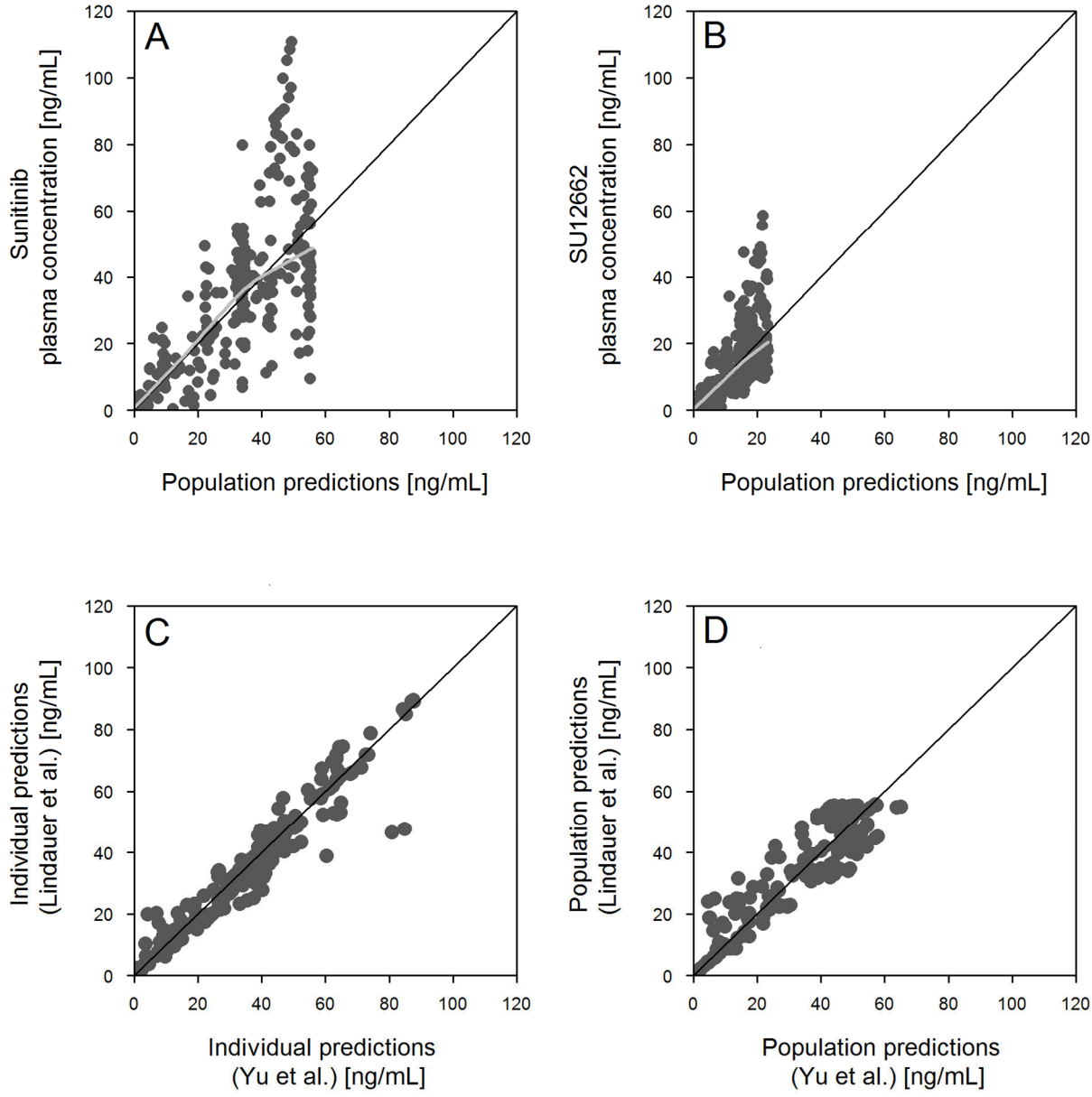

OBS vs IPRED (Lindauer *et al*) (**A**), OBS vs PRED (Lindauer *et al*) (**B**), CWRES vs Scatter plot if individual predictions (Sunitinib) (**C**), Scatter plot if population predictions (Sunitinib) (**D**)
OBS = Observed values, IPRED = Individual predictions, PRED = Population predictions, CWRES = Conditional weighted residuals, IWRES = Individual weighted residuals

D.II PK/PD – sVEGFR-2 (Sunitinib)

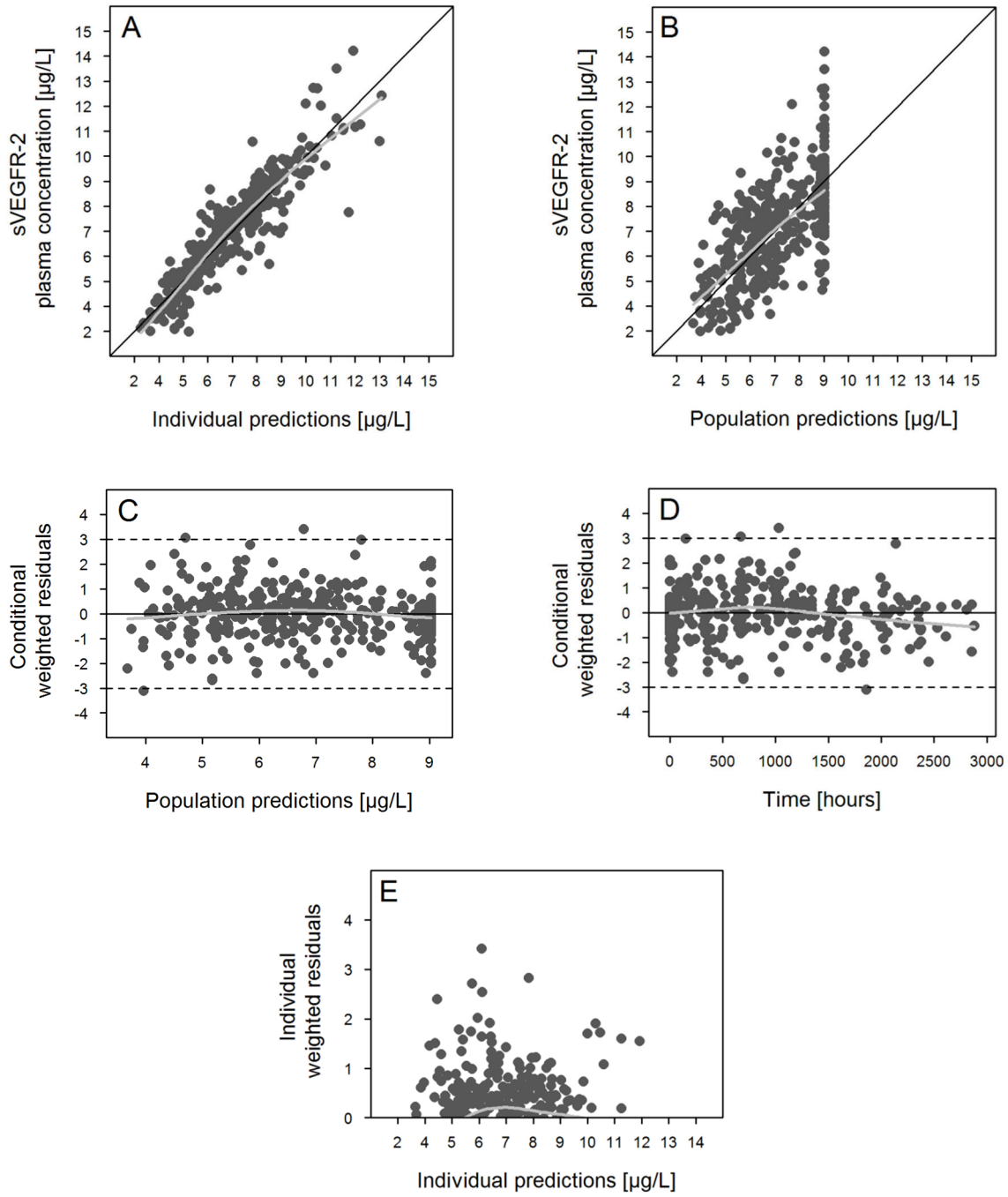

OBS vs IPRED (**A**), OBS vs PRED (**B**), CWRES vs PRED (**C**), CWRES vs Time (**D**) , |IWRES| vs IPRED (**E**)

OBS = Observed values, IPRED = Individual predictions, PRED = Population predictions, CWRES = Conditional weighted residuals, IWRES = Individual weighted residuals

D.III PK/PD – sVEGFR-3 (Sunitinib)

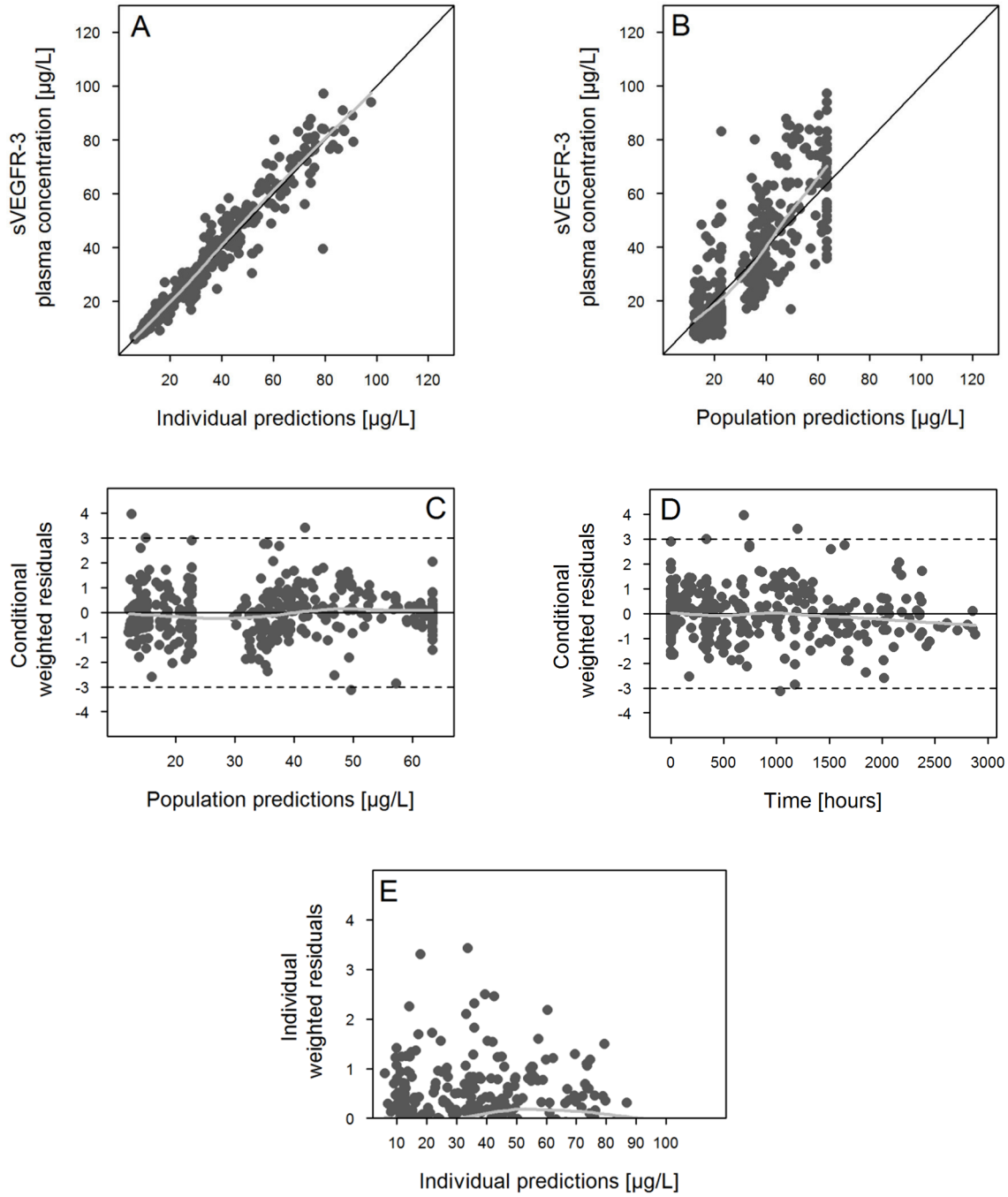

OBS vs IPRED (**A**), OBS vs PRED (**B**), CWRES vs PRED (**C**), CWRES vs Time (**D**) , |IWRES| vs IPRED (**E**)

OBS = Observed values, IPRED = Individual predictions, PRED = Population predictions, CWRES = Conditional weighted residuals, IWRES = Individual weighted residuals

D.IV PK/PD – Blood pressure (Sunitinib)

Systolic blood pressure

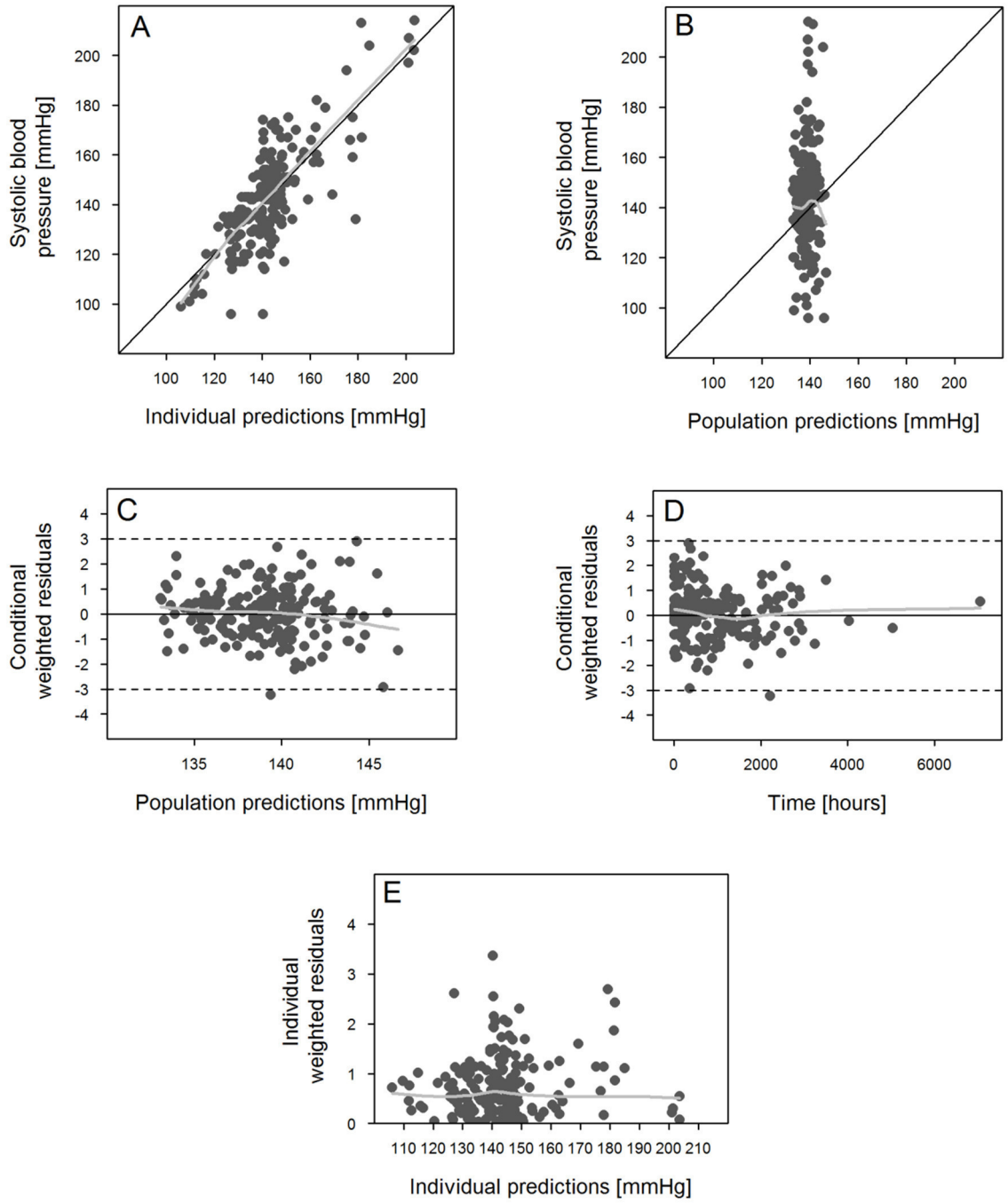

OBS vs IPRED (**A**), OBS vs PRED (**B**), CWRES vs PRED (**C**), CWRES vs Time (**D**) , |IWRES| vs IPRED (**E**)

OBS = Observed values, IPRED = Individual predictions, PRED = Population predictions, CWRES = Conditional weighted residuals, IWRES = Individual weighted residuals

Diastolic blood pressure

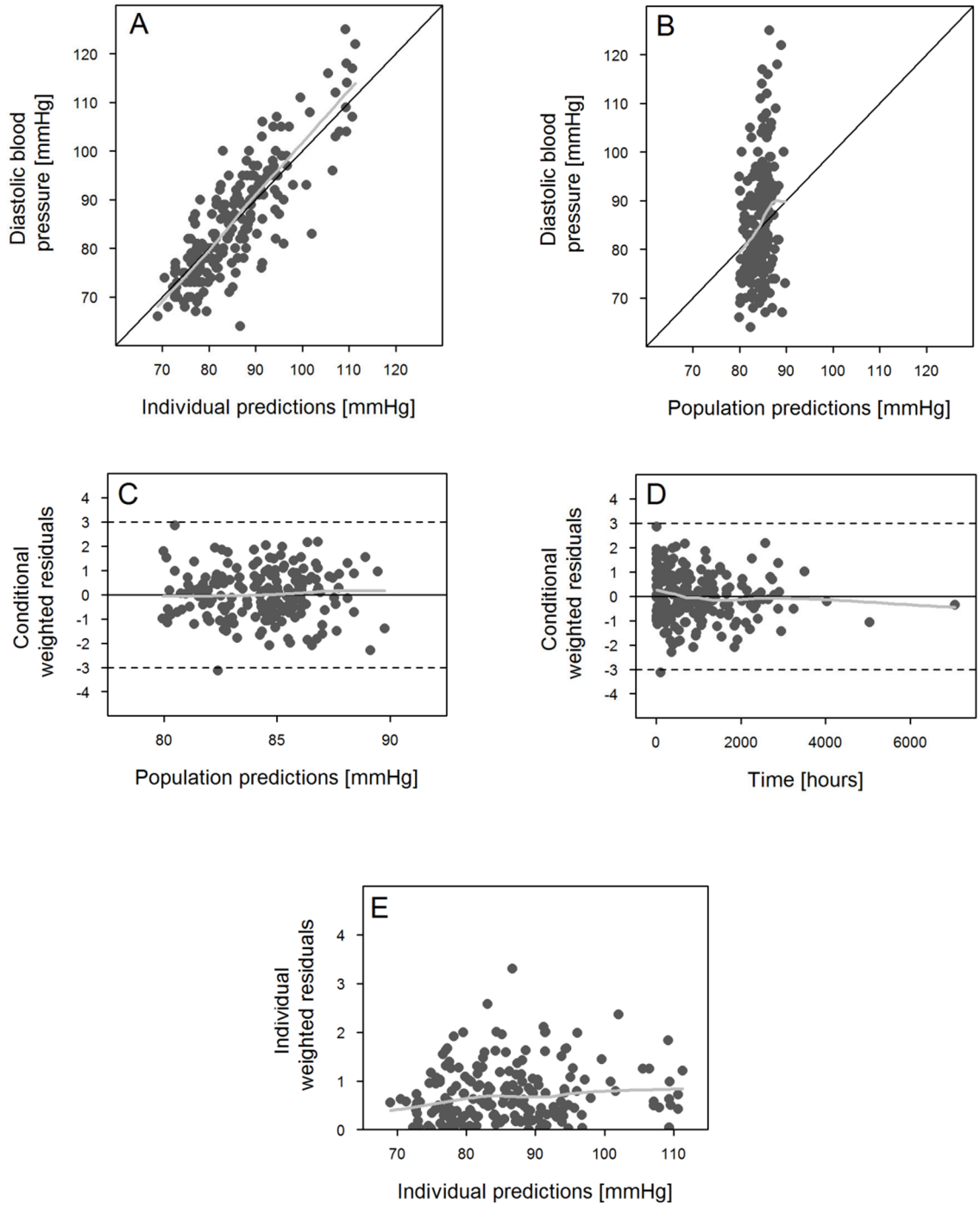

OBS vs IPRED (**A**), OBS vs PRED (**B**), CWRES vs PRED (**C**), CWRES vs Time (**D**) , |IWRES| vs IPRED (**E**)

OBS = Observed values, IPRED = Individual predictions, PRED = Population predictions, CWRES = Conditional weighted residuals, IWRES = Individual weighted residuals

D.V PK/PD – sVEGFR-2 (Pazopanib)

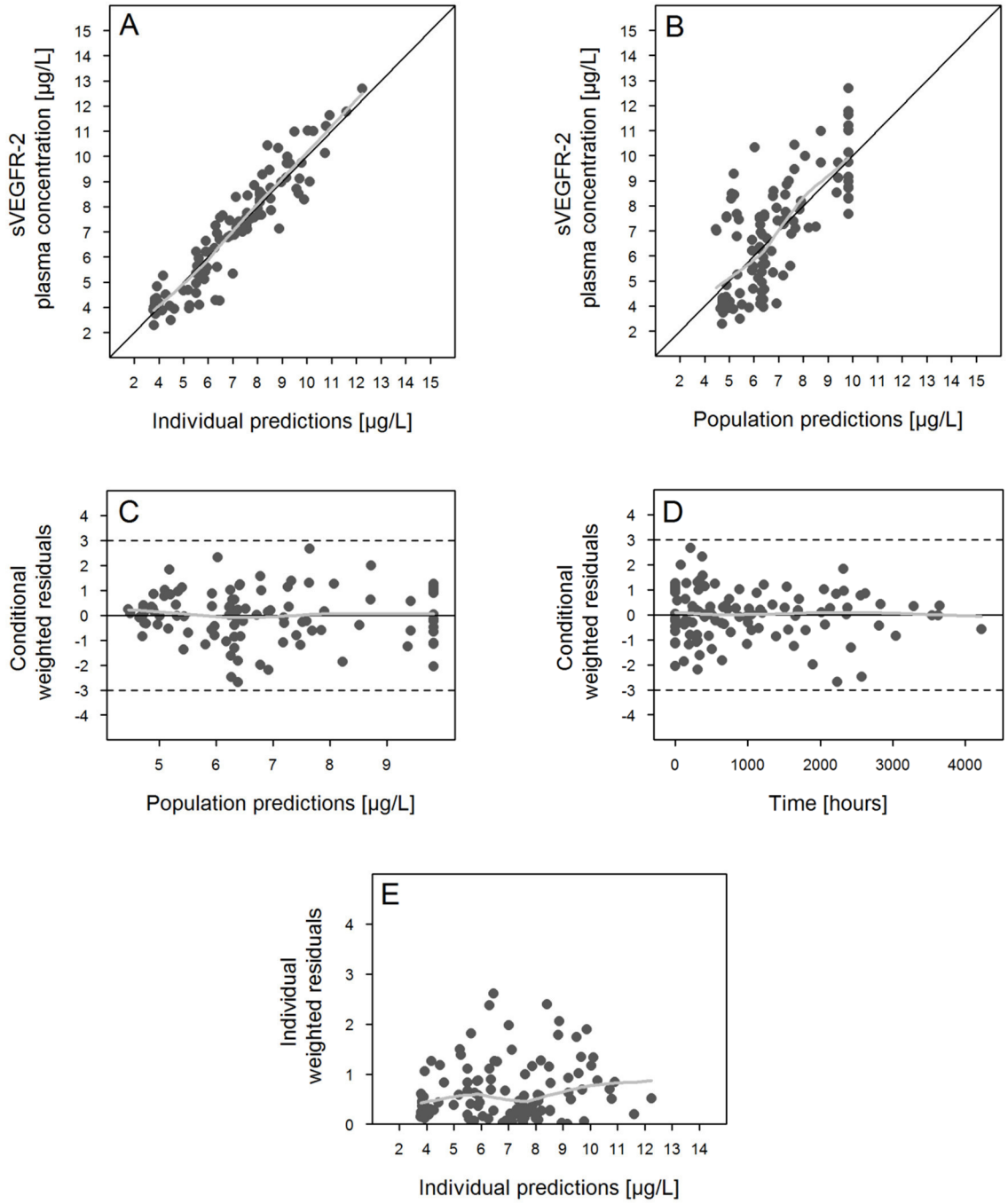

OBS vs IPRED (**A**), OBS vs PRED (**B**), CWRES vs PRED (**C**), CWRES vs Time (**D**) , |IWRES| vs IPRED (**E**)

OBS = Observed values, IPRED = Individual predictions, PRED = Population predictions, CWRES = Conditional weighted residuals, IWRES = Individual weighted residuals

D.VI PK/PD – sVEGFR-3 (Pazopanib)

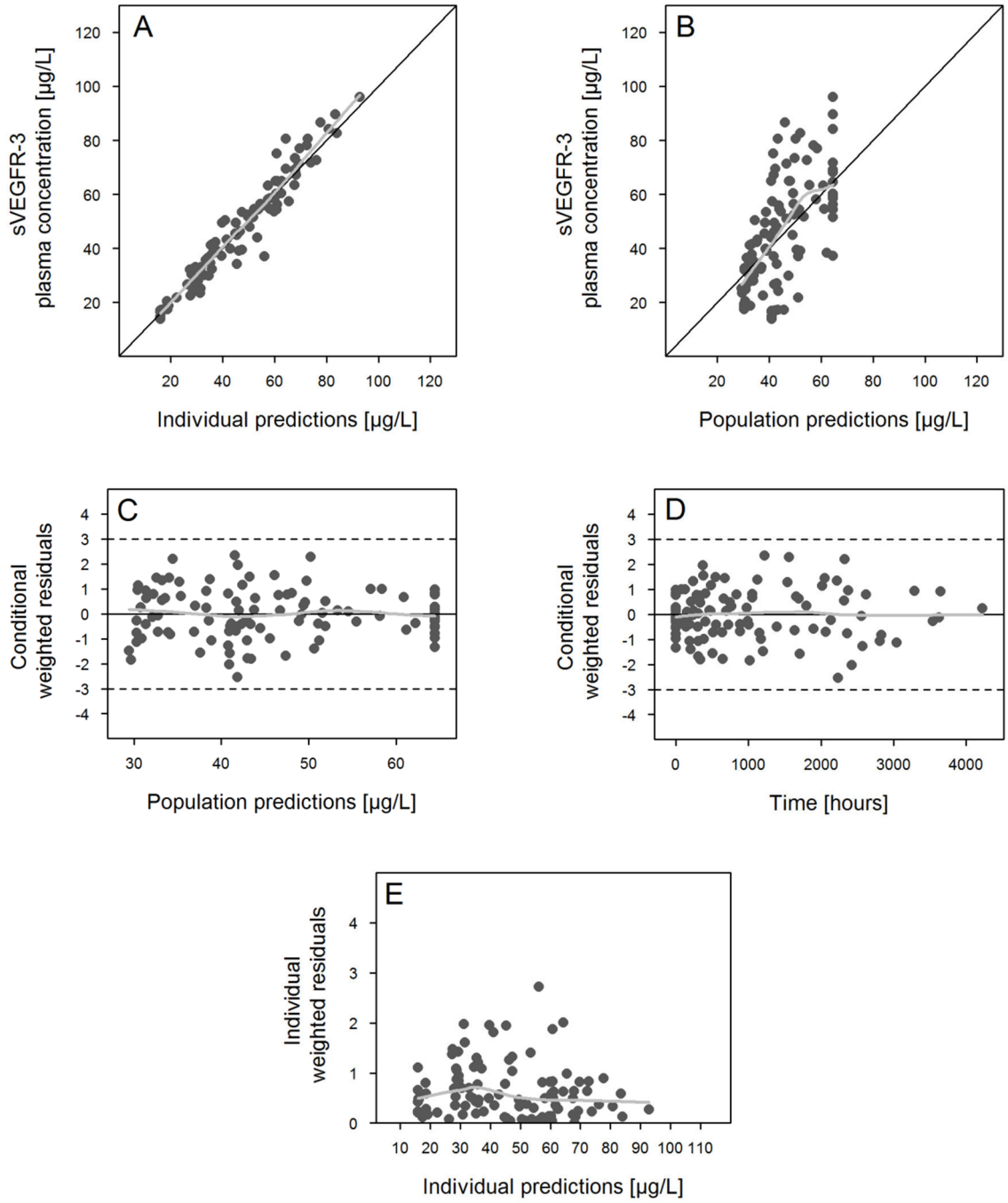

OBS vs IPRED (**A**), OBS vs PRED (**B**), CWRES vs PRED (**C**), CWRES vs Time (**D**) , |IWRES| vs IPRED (**E**)

OBS = Observed values, IPRED = Individual predictions, PRED = Population predictions, CWRES = Conditional weighted residuals, IWRES = Individual weighted residuals

D.VII PK/PD - Blood pressure (Pazopanib)

Systolic blood pressure

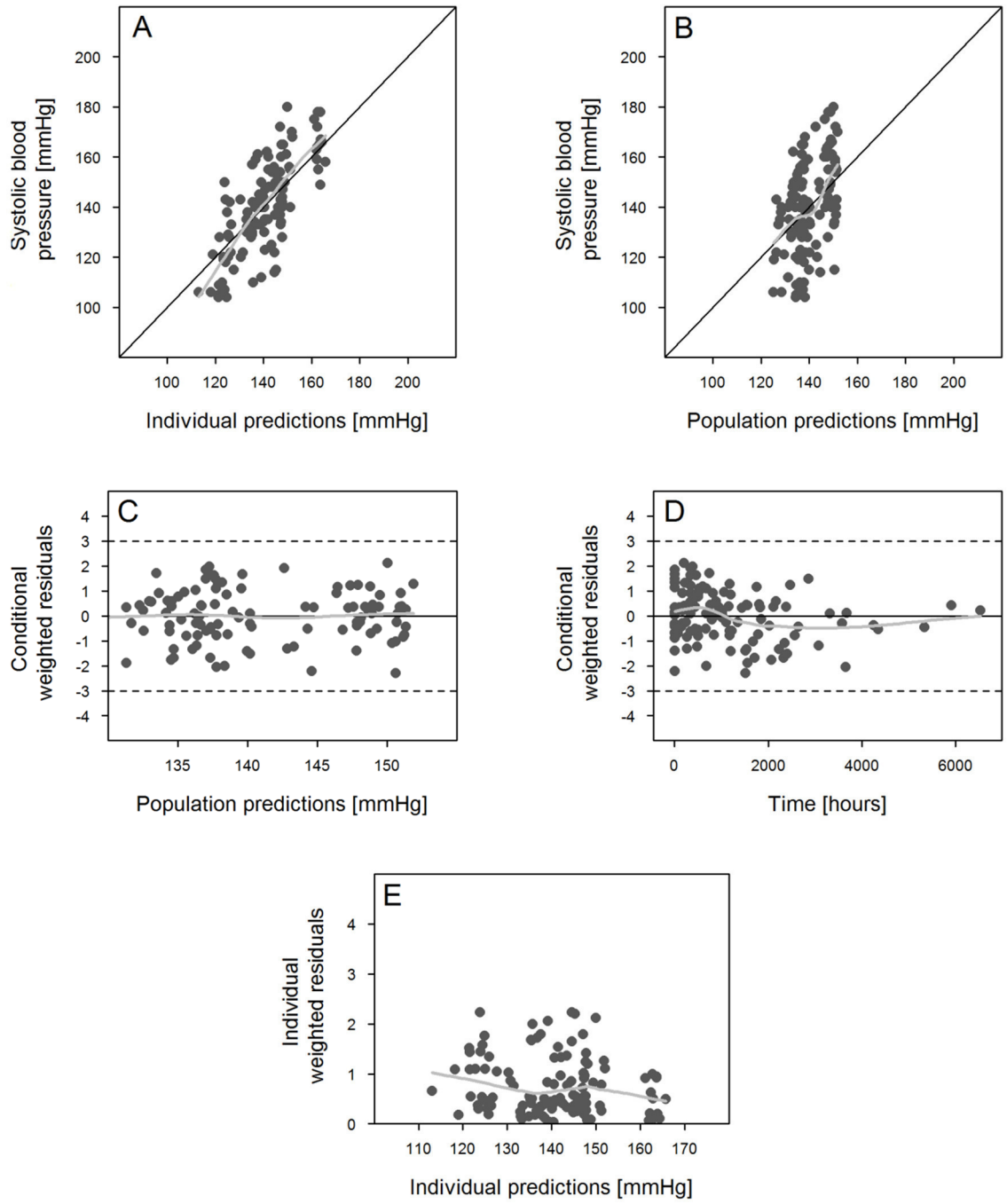

OBS vs IPRED (**A**), OBS vs PRED (**B**), CWRES vs PRED (**C**), CWRES vs Time (**D**) , |IWRES| vs IPRED (**E**)

OBS = Observed values, IPRED = Individual predictions, PRED = Population predictions, CWRES = Conditional weighted residuals, IWRES = Individual weighted residuals

Diastolic blood pressure

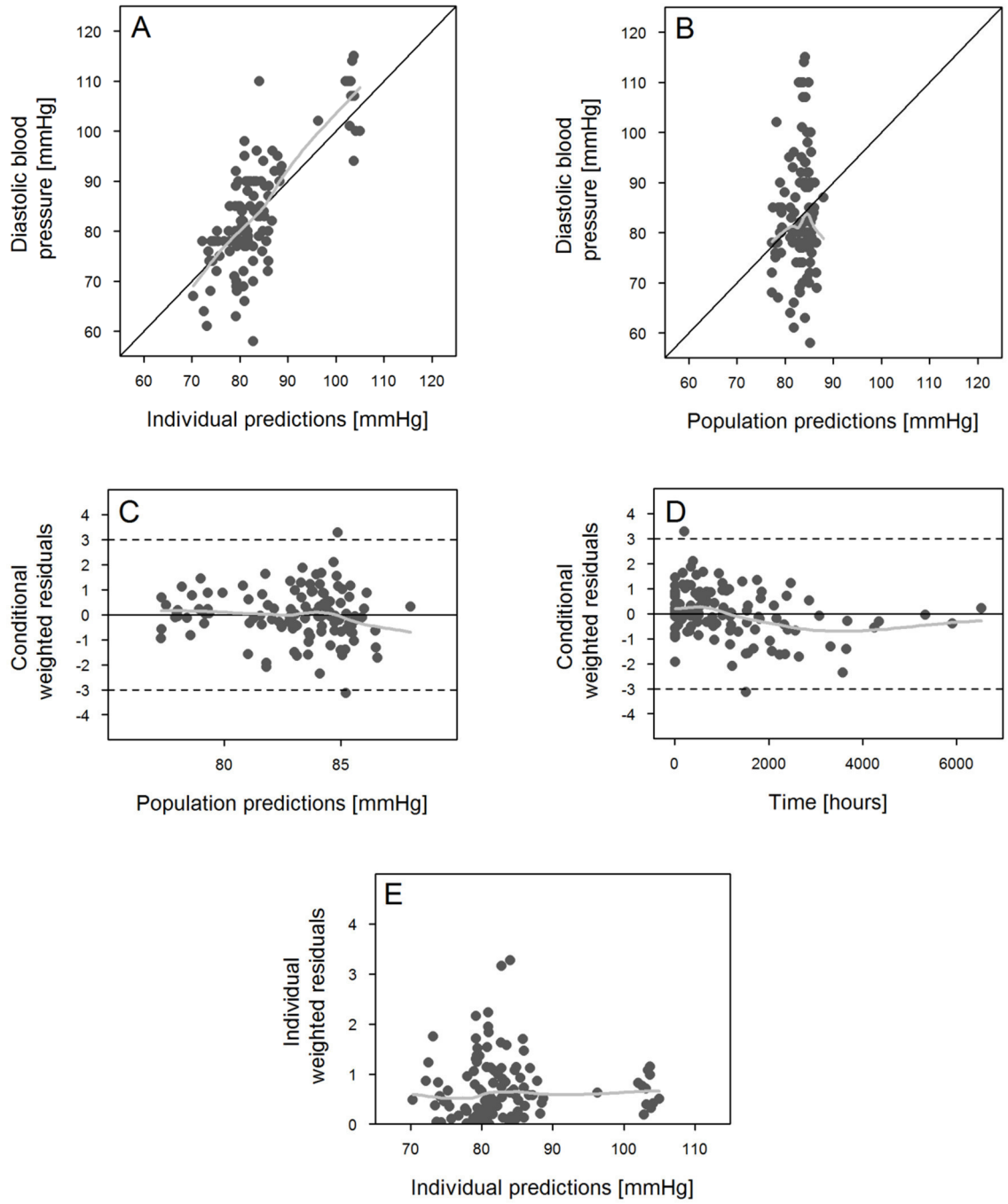

OBS vs IPRED (**A**), OBS vs PRED (**B**), CWRES vs PRED (**C**), CWRES vs Time (**D**) , |IWRES| vs IPRED (**E**)

OBS = Observed values, IPRED = Individual predictions, PRED = Population predictions, CWRES = Conditional weighted residuals, IWRES = Individual weighted residuals

D.VIII Visual predicitive check – Sunitinib/SU12662 pharmacokinetics

Sunitinib

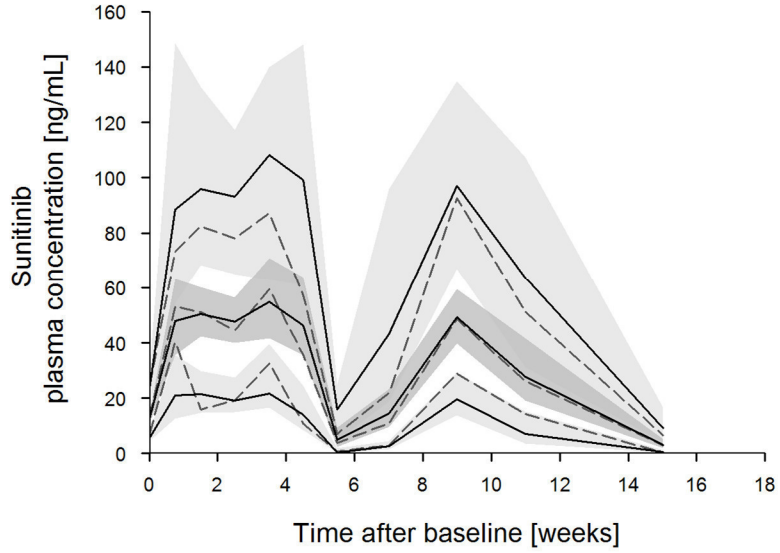

SU12662

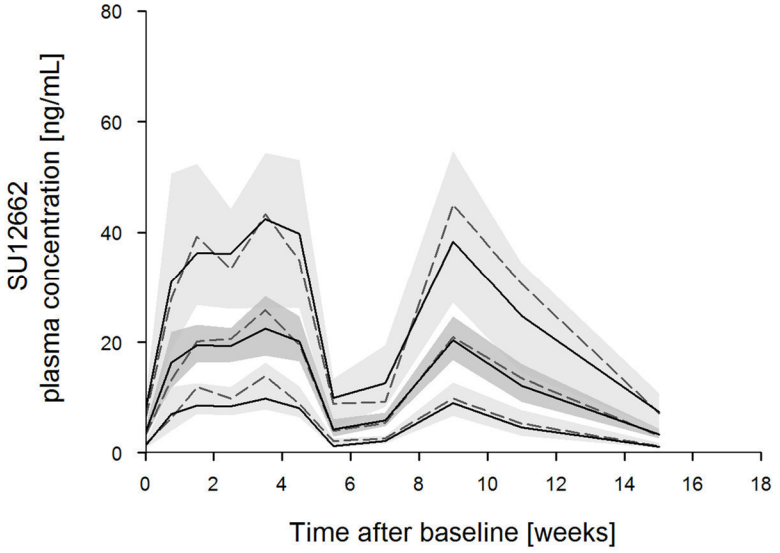

D.IX Visual predictive check - PK/PD – sVEGFR-2 and sVEGFR-3 (Sunitinib)

sVEGFR-2

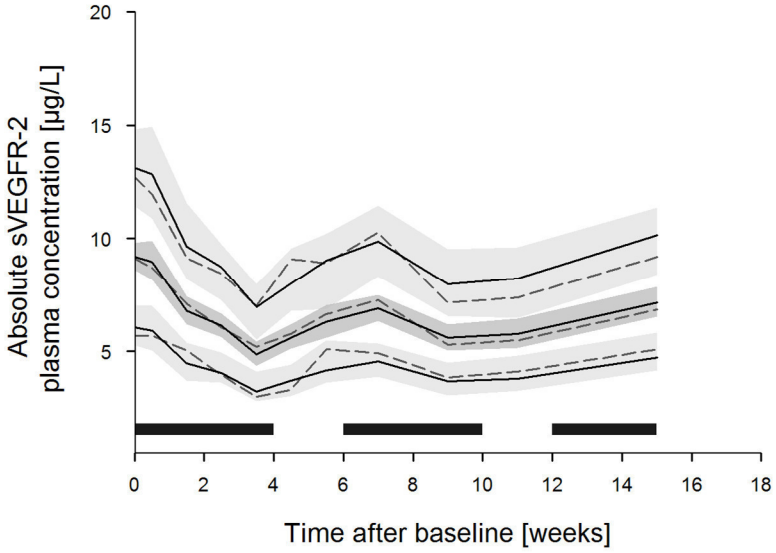

sVEGFR-3

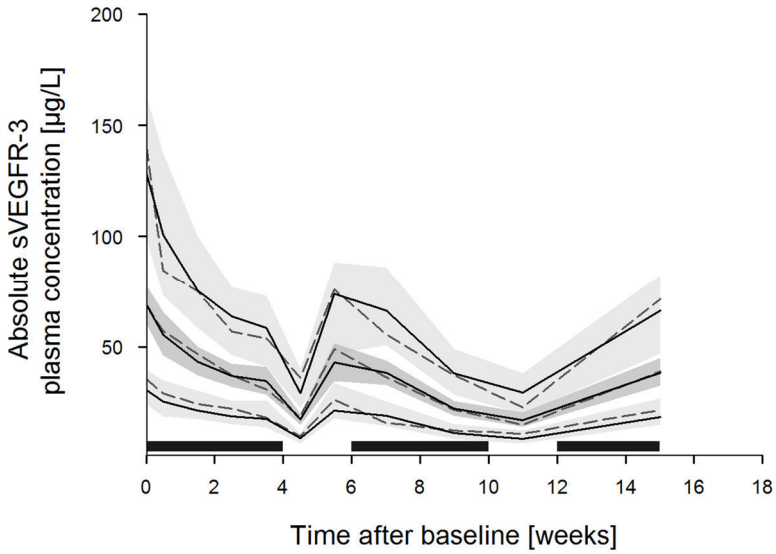

The black solid lines indicate the mean model prediction and the 90 % prediction interval. Dotted lines show the measured mean and interval, respectively. Dark and light grey areas represent the respective confidence bands. The dark-grey rectangle represents the time on treatment.

sVEGFR-3 – Stratified by tumor entity

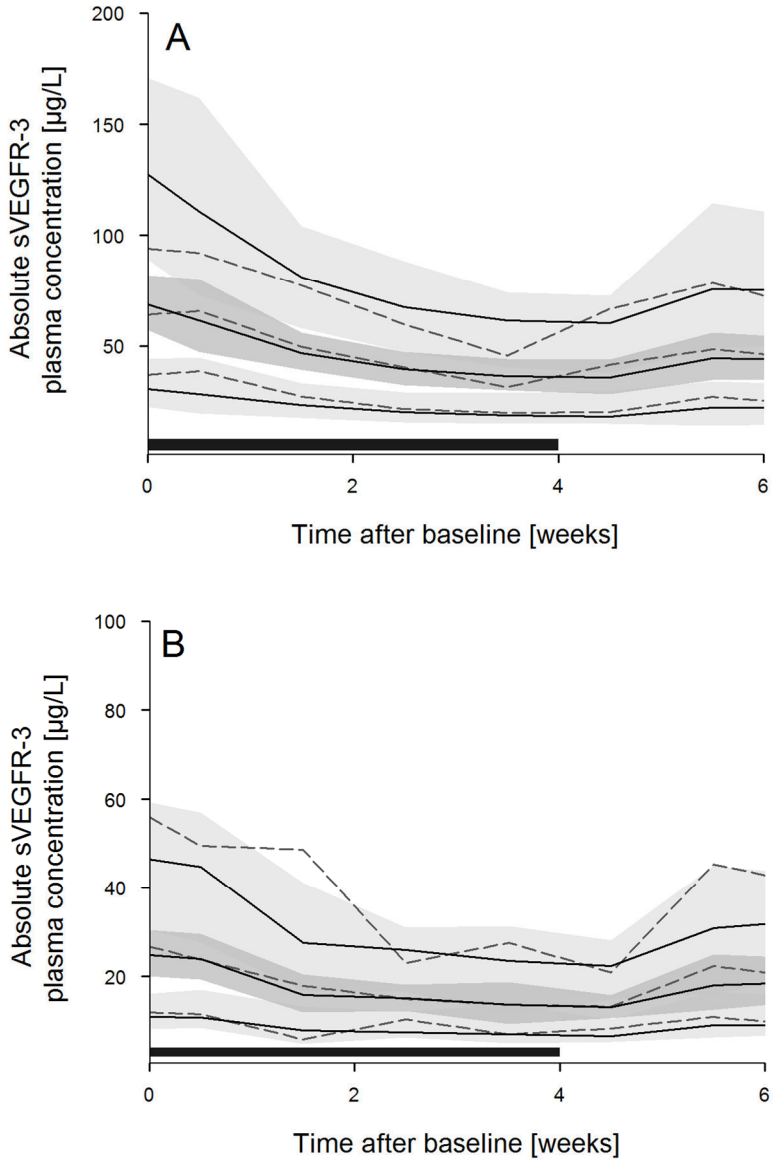

mRCC (**A**) and mCRC (**B**).

The black solid lines indicate the mean model prediction and the 90 % prediction interval. Dotted lines show the measured mean and interval, respectively. Dark and light grey areas represent the respective confidence bands. The dark-grey rectangle represents the time on treatment.

D.X Visual predictive check - PK/PD – Blood pressure (Sunitinib)

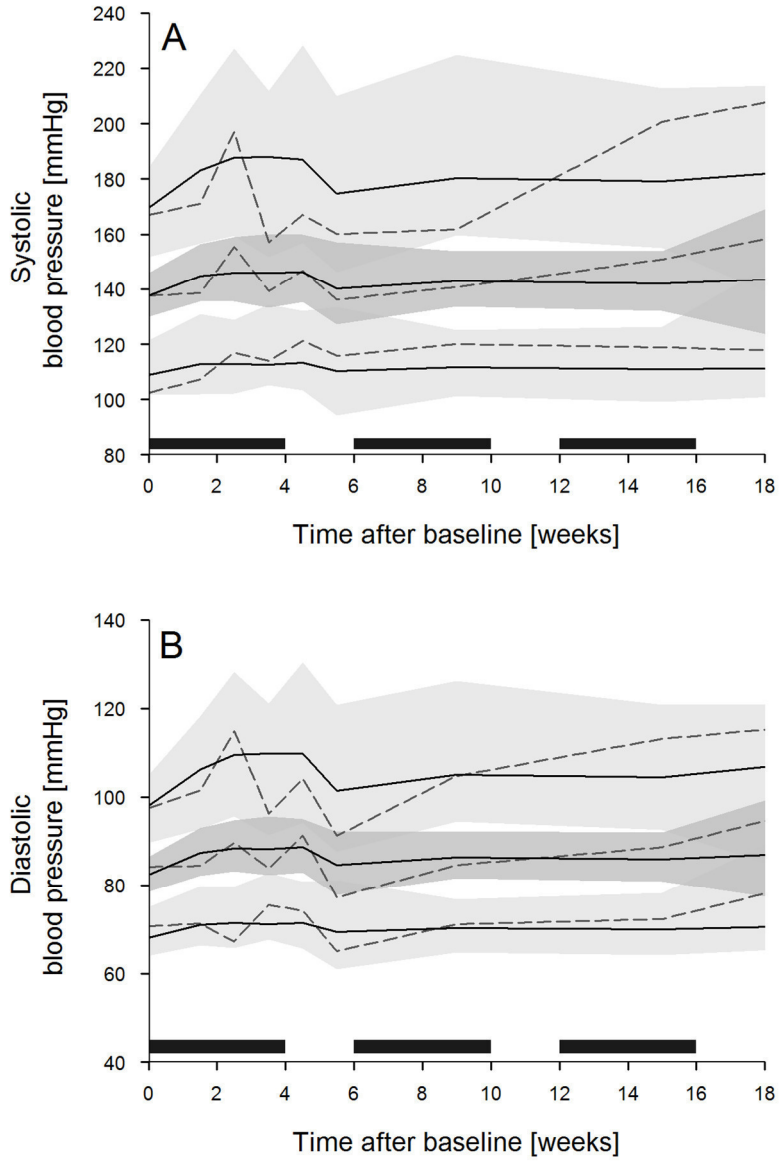

Systolic (**A**) and diastolic (**B**) blood pressure

The black solid lines indicate the mean model prediction and the 90 % prediction interval. Dotted lines show the measured mean and interval, respectively. Dark and light grey areas represent the respective confidence bands. The dark-grey rectangle represents the time on treatment.

D.XI Visual predictive check - PK/PD – sVEGFR-2 and sVEGFR-3 (Pazopanib)

sVEGFR-2

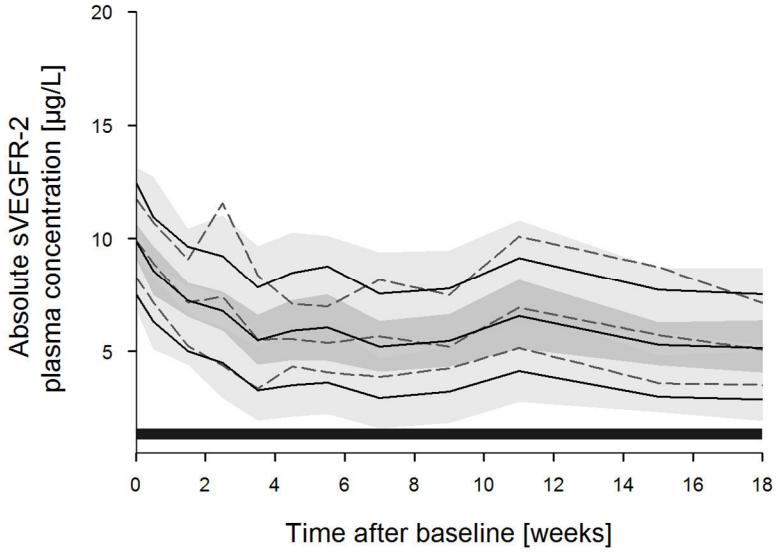

sVEGFR-3

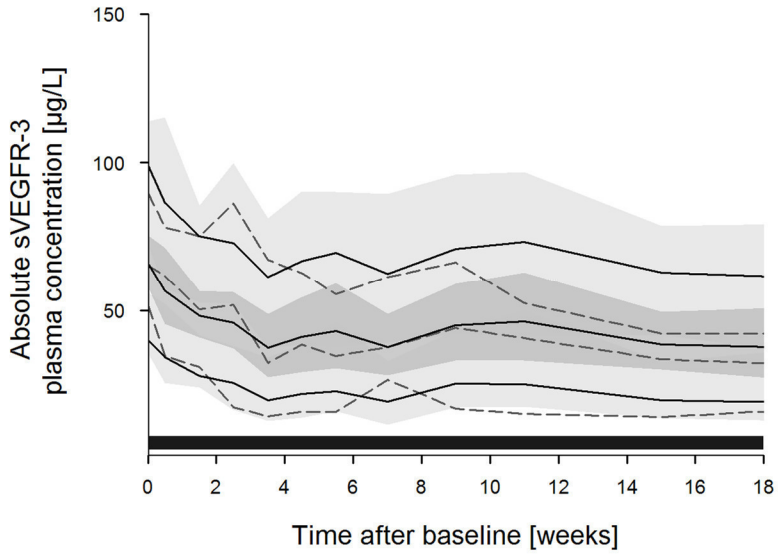

The black solid lines indicate the mean model prediction and the 90 % prediction interval. Dotted lines show the measured mean and interval, respectively. Dark and light grey areas represent the respective confidence bands. The dark-grey rectangle represents the time on treatment.

D.XII Visual predictive check - PK/PD – Blood pressure (Pazopanib)

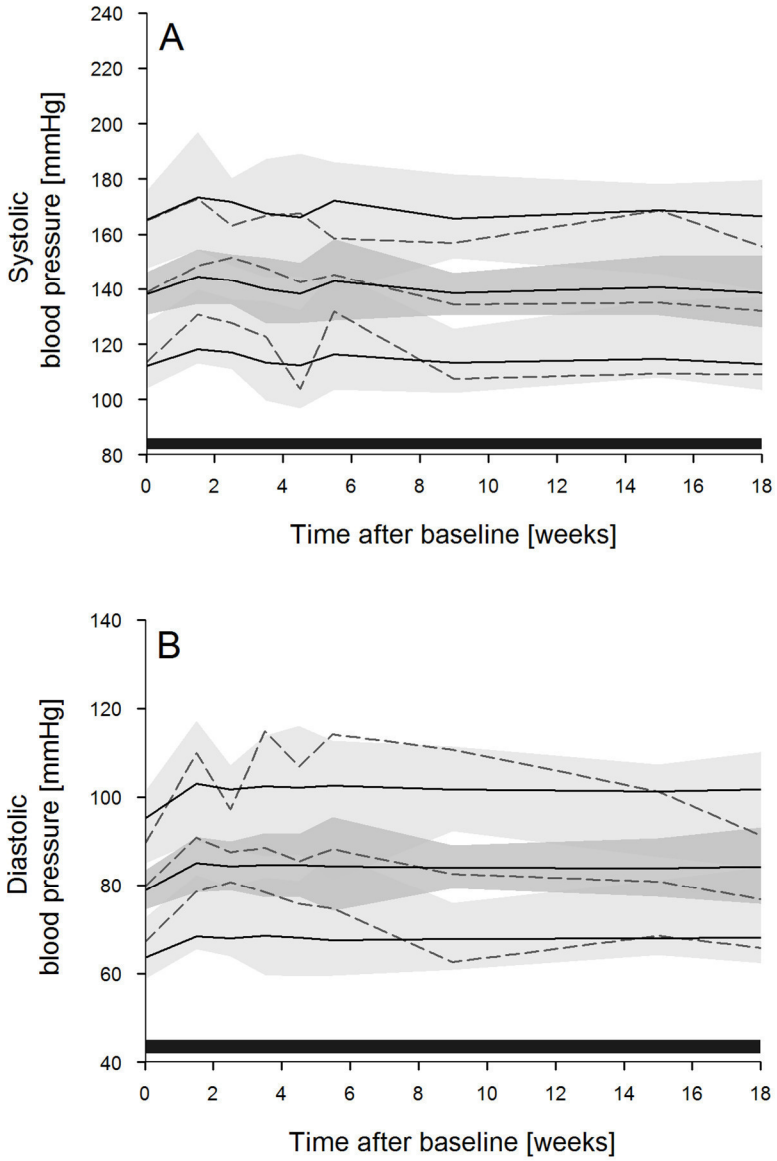

Systolic (**A**) and diastolic (**B**) blood pressure

The black solid lines indicate the mean model prediction and the 90 % prediction interval. Dotted lines show the measured mean and interval, respectively. Dark and light grey areas represent the respective confidence bands. The dark-grey rectangle represents the time on treatment.

Appendix E

Survival analysis

E.I Overview on documented events

Registered events in patients treated with sunitinib first-line (n = 24)

ID	Comment	Event	TTE [months]
NM S1	Died as result of malignancy	1	4.83
NM S2	Lost to follow-up	0	0.43
NM S3	Lost to follow-up	0	1.45
NM S4	Lost to follow-up	0	0.3
NM S5	Started new treatment, w/o reason	0	4.17
NM S6	Lost to follow-up	0	10.09
NM S13	Started new treatment, w/o reason	0	12.42
NM S15	PD documented	1	12.65
NM S17	Died as result of malignancy	1	5.35
NM S19	Died as result of malignancy	1	6.87
NM S21	Censored on 01.07.2015	0	6.6
NM S22	New lesion during first-line	1	9.07
NM S24	New lesion during first-line	1	5.88
NM S25	Died as result of malignancy	1	3.45
NM S27	Lost to follow-up	0	0.23
NM S28	Lost to follow-up	0	15.24
NM S29	PD documented	1	0.76
NM S30	Died as result of malignancy	1	7.03
NM S31	Censored (brainmetastases)	0	0.36
NM S32	Therapy stop due to progression	1	4.11
NM S33	Died as result of malignancy	1	0.46
NM S39	New lesion during first-line	1	2.96
NM S42	Lost to follow-up	0	4.2
NM S43	Died as result of malignancy	1	0.99

ID = Dataset Identifier, PD = Progressive disease, TTE = Time-to-event

Registered events in patients treated with pazopanib first-line (n = 16)

ID	Comment	Event	TTE [months]
NM P7	PD documented	1	12.1
NM P8	PD documented	1	12.5
NM P9	New lesion during first-line therapy	1	5.3
NM P10	New lesion during first-line therapy	1	2.6
NM P11	Censored on 01.07.2015	0	3.8
NM P12	Censored on 01.07.2015	0	1.5
NM P16	Started second-line treatment w/o documented PD	0	5.2
NM P18	PD documented	1	6.0
NM P20	Censored on 01.07.2015	0	13.1
NM P23	Changed treatment due to toxicity	0	8.3
NM P26	Censored on 01.07.2015	0	3.9
NM P34	Censored on 01.07.2015	0	7.7
NM P35	New lesion during first-line	1	1.1
NM P36	Censored on 01.07.2015	0	5.6
NM P38	New lesion during first-line therapy	1	0.7
NM P40	Patient died during first-line therapy	1	0.8

ID = Dataset Identifier, PD = Progressive disease, TTE = Time-to-event

Appendix F:

NONMEM Control streams

F.I PK model Sunitinib/SU12662

```
$SUBROUTINE ADVAN6 TOL=4

$MODEL
NCOMP =5
COMP = (DEPOT, DEFDOSE)
COMP = (OBSLIV)
COMP = (CENTRALM)
COMP = (PERIM)
COMP = (PERISUN)

$PK

WT = WEIGHT
IF(WEIGHT.EQ.-99.AND.SEX.EQ.1) WT = 83  ; ET Population mean - male
IF(WEIGHT.EQ.-99.AND.SEX.EQ.0) WT = 75  ; ET Population mean - female
ASCL   = (WT/70)**0.75
ASV    = WT/70

KA     = THETA(1)
V2     = THETA(2)*ASV * EXP(ETA(1))
QH     = THETA(3)*ASCL
CLP    = THETA(4)*ASCL* EXP(ETA(3))
CLM            = THETA(5)*ASCL
V3     = THETA(6)*ASV * EXP(ETA(2))
Q34            = THETA(7)*ASCL
V4     = THETA(8)*ASV
FM     = THETA(9)     * EXP(ETA(4))
Q25            = THETA(10)*ASCL
V5     = THETA(11)*ASV

K34 = Q34/V3
K43 = Q34/V4
K25 = Q25/V2
K52 = Q25/V5

S2 = V2
S3 = V3

$DES

CLIV = (KA*A(1) + QH/V2*A(2))/(QH+CLP)

DADT(1) = -KA*A(1)
DADT(2) = QH*CLIV-QH/V2*A(2) - K25*A(2) + K52*A(5)
DADT(3) = FM*CLP*CLIV-CLM/V3*A(3)-K34*A(3) + K43*A(4)
DADT(4) = K34*A(3)-K43*A(4)
DADT(5) = K25*A(2) - K52*A(5)
```

PK model Sunitinib/SU12662 – continued

```
$ERROR
TY = LOG(F)
IF(F.LT.0.001) TY = 0.001
IPRED = TY

IF (CMT.EQ.2) THEN
W = SQRT(THETA(12)**2)
Y = IPRED+W*EPS(1)
ENDIF

IF (CMT.EQ.3) THEN  ; DV log-transformed
W = SQRT(THETA(13)**2)
Y = IPRED+W*EPS(2)
ENDIF

IRES = DV-IPRED
DEL = 0
IF(W.EQ.0) DEL = 0.0001
IWRES = IRES/(W+DEL)

$THETA
(0, 0.133)              ;1 = KA
(0, 1820)               ; 2 = V2
(80) FIX                ; 3 = QH
(0, 33.9)               ;4 = CLP
(0, 16.5)               ;5 = CLM
(0, 730)                ;6 = V3
(0, 2.75)               ;7 = Q34
(0, 592)                ;8 = V4
(0.21) FIX              ;9 = FM
(0, 0.371)              ;10 = Q25
(588) FIX               ;11 = V5
(0,0.367)               ;12 = Prop. Error Suni
(0,0.281)               ;13 = Prop. Error Metab

$OMEGA BLOCK(4)
 0.0621                 ;1 IIV V2
 0.0473 0.169           ;2 IIV V3
 0 -0.0613 0.088        ;3 IIV CLP
 0 0 -0.0421 0.113      ;4 IIV FM

$SIGMA
 1 FIX
 1 FIX

$ESTIMATION SIG=2 SIGL=4 PRINT=1 METHOD=1 INTER MAXEVAL=9999
NOABORT
```

F.II PK/PD model – sVEGFR-2 (Sunitinib)

```
$SUBROUTINE ADVAN6 TOL=4

$MODEL
NCOMP=6
COMP        =(DEPOT,DEFDOSE)
COMP        =(OBSLIV)
COMP        =(CENTRALM)
COMP        =(PERIM)
COMP        =(PERISUN)
COMP        =(VEGFR2)

$PK

; Covariate relationships

;;; ALFAABCR2-DEFINITION START
IF(ABCR2.EQ.1) ALFAABCR2 = 1
IF(ABCR2.EQ.-99) ALFAABCR2 = 1
IF(ABCR2.EQ.0) ALFAABCR2 = ( 1 + THETA(8))
;;; ALFAABCR2-DEFINITION END


;;; ALFASTUDY-DEFINITION START
IF(STUDY.EQ.1) ALFASTUDY = 1
IF(STUDY.EQ.2) ALFASTUDY = ( 1 + THETA(7))
;;; ALFASTUDY-DEFINITION END


;;; ALFAFLT1-DEFINITION START
IF(FLT1.EQ.0) ALFAFLT1 = 1
IF(FLT1.EQ.-99) ALFAFLT1 = 1
IF(FLT1.EQ.1) ALFAFLT1 = ( 1 + THETA(6))
;;; ALFAFLT1-DEFINITION END

;;; ALFA-RELATION START
ALFACOV=ALFAFLT1*ALFASTUDY*ALFAABCR2
;;; ALFA-RELATION END


;PHARMACODYNAMICS

TVBLV2 = THETA(1
BLV2   = TVBLV2*EXP(ETA(1))

TVALFA = THETA(2)

ALFA   = TVALFA*ALFVACOV*EXP(ETA(2))
```

PK/PD model – sVEGFR-2 (Sunitinib) - continued

```
TVKOUT      = THETA(3)
KOUT        = TVKOUT*EXP(ETA(3))

A_0(6) = BLV2

KIN = BLV2*KOUT

TVKD = THETA(4
KD   = TVKD*EXP(ETA(4))

;PHARMACOKINETICS

KA   = 0.133
V2   = V2X
QH   = QHX
CLP  = CLPX
CLM  = CLMX
V3   = V3X
Q34  = Q34X
V4   = V4X
FM   = FMX
Q25  = Q25X
V5   = V5X

K34  = Q34/V3
K43  = Q34/V4
K25  = Q25/V2
K52  = Q25/V5

S2   = V2
S3   = V3

$DES

CLIV = (KA*A(1) + QH/V2*A(2))/(QH+CLP)

DADT(1) = -KA*A(1)
DADT(2) = QH*CLIV-QH/V2*A(2) - K25*A(2) + K52*A(5)
DADT(3) = FM*CLP*CLIV-CLM/V3*A(3)-K34*A(3) + K43*A(4)
DADT(4) = K34*A(3)-K43*A(4)
DADT(5) = K25*A(2) - K52*A(5)


CONC = A(3)/V3+A(2)/V2

FC= A(3)/V3*(1-0.90)+A(2)/V2*(1-0.95)

IF(FC.LE.0) THEN
```

PK/PD model – sVEGFR-2 (Sunitinib) - continued

```
BND=0
  ELSE
 BND=FC/(KD+FC)
  ENDIF

INH = BND

SF=1/(1+ALFA*INH)

 DADT(6)= KIN*SF-KOUT*A(6)

$ERROR

IPRE  = A(6)
RBL   = IPRE/BLV2
IRES  = DV-IPRE
W     = THETA(5)*IPRE
Y     = IPRE+EPS(1)*W
 DVRL= DV/BLV2

 DEL = 0
 IF(W.EQ.0) DEL = 1
 IWRE = IRES/(W+DEL)

$THETA
(0, 9030)            ; TVBLV2
(0, 2.31)            ; TValfa
(0, 0.00428)         ; THKOUT
(4) FIX              ; THKD
(0, 0.124)           ; CV
(-1, -0.565,5)       ; ALFAFLT11
(-1, -0.328,5)        ; ALFASTUDY1
(-1, -0.311,5)       ; ALFAABCR21

$OMEGA 0.0388    ; ETABLVR2
$OMEGA 0 FIX     ; ETAalfa
$OMEGA 0 FIX     ; ETAKOUT
$OMEGA 0 FIX     ; ETAKD

$SIGMA 1 FIX

$ESTIMATION SIG=2 PRINT=1 METHOD=1 INTER MAXEVAL=9999 NOABORT
```

F.III PK/PD model – sVEGFR-3 (Sunitinib)

```
$SUBROUTINE ADVAN6 TOL=4

$MODEL

COMP=6
COMP        =(DEPOT,DEFDOSE)
COMP        =(OBSLIV)
COMP        =(CENTRALM)
COMP        =(PERIM)
COMP        =(PERISUN)
COMP        =(VEGFR3)

$PK

; Covariate relationships

;;; BLV3STUDY-DEFINITION START
IF(STUDY.EQ.1) BLV3STUDY = 1
IF(STUDY.EQ.2) BLV3STUDY = ( 1 + THETA(6))
;;; BLV3STUDY-DEFINITION END

;;; BLV3-RELATION START
BLV3COV=BLV3STUDY
;;; BLV3-RELATION END


TVBLV3 = THETA(1)
BLV3   = TVBLV3*BLV3COV*EXP(ETA(1))

TVALFA = THETA(2)
ALFA   = TVALFA*EXP(ETA(2))

TVKOUT = THETA(3)
KOUT   = TVKOUT

A_0(6)=BLV3

KIN = BLV3*KOUT

TVKD = THETA(4)          ;
KD     = TVKD

K12    = 0.133
V2     = V2X
QH     = QHX
CLP    = CLPX
CLM    = CLMX
V3     = V3X
```

PK/PD model – sVEGFR-3 (Sunitinib) – continued

```
Q34   = Q34X
V4    = V4X
FM    = FMX
Q25   = Q25X
V5    = V5X

K34   = Q34/V3
K43   = Q34/V4
K25   = Q25/V2
K52   = Q25/V5

S2    = V2
S3    = V3

$DES

CLIV = (K12*A(1) + QH/V2*A(2))/(QH+CLP)

DADT(1) = -K12*A(1)
DADT(2) = QH*CLIV-QH/V2*A(2) - K25*A(2) + K52*A(5)
DADT(3) = FM*CLP*CLIV-CLM/V3*A(3)-K34*A(3) + K43*A(4)
DADT(4) = K34*A(3)-K43*A(4)
DADT(5) = K25*A(2) - K52*A(5)

CONC = A(3)/V3+A(2)/V2

FC= A(3)/V3*(1-0.90)+A(2)/V2*(1-0.95)

IF(FC.LE.0) THEN
 BND=0
  ELSE
 BND=FC/(KD+FC)       ;
  ENDIF

INH = BND

SF=1/(1+ALFA*INH)

DADT(6)= KIN*SF-KOUT*A(6)

$ERROR

IPRE  = A(6)
RBL   = IPRE/BLV3
IRES  = DV-IPRE
W     = THETA(5)*IPRE
Y     = IPRE+EPS(1)*W
DVRL = DV/BLV3
```

PK/PD model – sVEGFR-3 (Sunitinib) – continued

```
DEL = 0
IF(W.EQ.0) DEL = 1
IWRE = IRES/(W+DEL)

$THETA
(0, 63500)    ; TVBLV3
(0, 1.74)     ; TValfa
(0, 0.0054)   ; TVKOUT
(4) FIX       ; TVKD
(0, 0.15)     ; CV
( -0.642)     ; BLV3TUMOR

$OMEGA  BLOCK(2)
0.167         ; ETABLVR3
0.124 0.258   ; ETAalfa

$SIGMA 1 FIX

$ESTIMATION SIG=2 PRINT=1 METHOD=1 INTER MAXEVAL=9999 NOABORT
```

F.IV PK/PD model – Blood pressure (Sunitinib)

```
$SUBROUTINE ADVAN6 TOL=4

$MODEL
NCOMP=8
COMP = (DEPOT, DEFDOSE)
COMP = (OBSLIV)
COMP = (PERISUN)
COMP = (CENTRALM)
COMP = (PERIM)
COMP = (SYS)
COMP = (DIA)
COMP = (SST)

$PK

TREAT = 1
IF(BPTRT.EQ.1) TREAT = (1+THETA(14))
IF(BPTRT.EQ.2) TREAT = (1+THETA(14))
IF(BPTRT.EQ.-99) TREAT = 1

TVBLS      = THETA(1)
TVBLD      = THETA(2)
TVALDI     = THETA(3)
TVALSY     = THETA(4)
TVKD       = THETA(5)
TVTAU      = THETA(6)
TVPS1      = THETA(7)
TVPS2      = THETA(8)
TVAMP1     = THETA(9)
TVAMP2     = THETA(10) * TREAT
PROP       = THETA(13)

BLS  = TVBLS  *EXP(ETA(1))
BLD  = TVBLD  *EXP(ETA(2))
ALDI = TVALDI *EXP(ETA(3))
ALSY = TVALSY *EXP(ETA(3)*PROP)
TAU  = TVTAU

KD = TVKD

; PS1  = TVPS1
AMP1 = TVAMP1*EXP(ETA(4))

PS2  = TVPS2
AMP2 = TVAMP2*EXP(ETA(5))

K12    = 0.133
```

PK/PD model – Blood pressure (Sunitinib) - continued

```
V2     = V2X
QH     = QHX
CLP    = CLPX
CLM    = CLMX
V3     = V3X
Q34    = Q34X
V4     = V4X
FM     = FMX
Q25    = Q25X
V5     = V5X

K34    = Q34/V3
K43    = Q34/V4
K25    = Q25/V2
K52    = Q25/V5

S2     = V2
S3     = V3

A_0(8)=0

$DES
;PK MODEL
CLIV = (K12*A(1) + QH/V2*A(2))/(QH+CLP)

DADT(1) = -K12*A(1)
DADT(2) = QH*CLIV-QH/V2*A(2) - K25*A(2) + K52*A(5)
DADT(3) = FM*CLP*CLIV-CLM/V3*A(3)-K34*A(3) + K43*A(4)
DADT(4) = K34*A(3)-K43*A(4)
DADT(5) = K25*A(2) - K52*A(5)

CONC = A(3)/V3+A(2)/V2

FC= A(3)/V3*(1-0.90)+A(2)/V2*(1-0.95)

DADT(6) = BLS*(1+(AMP1*COS((TIME+6)*6.283/24-
PS1)+AMP2*COS((TIME+6)*6.283/12-PS2)))
DADT(7) = BLD*(1+(AMP1*COS((TIME+6)*6.283/24-
PS1)+AMP2*COS((TIME+6)*6.283/12-PS2)))

IF(FC.LE.0) FC=0

 INH    = FC/(KD+FC)
 DADT(8) = 1/TAU*INH-1/TAU*A(8)


$ERROR
 FCx  = A(3)/V3*(1-0.90)+A(2)/V2*(1-0.95)
```

PK/PD model – Blood pressure (Sunitinib) - continued

```
INHx = FCx/(KD+FCx)

CBLS =BLS*(1+(AMP1*COS((TIME+6)*6.283/24-
PS1)+AMP2*COS((TIME+6)*6.283/12-PS2)))
CBLD =BLD*(1+(AMP1*COS((TIME+6)*6.283/24-
PS1)+AMP2*COS((TIME+6)*6.283/12-PS2)))

IF(CMT.EQ.6) THEN
 IPRE = CBLS*(1+ALSY*(INHx+A(8)))
IRES = DV - IPRE
 W = THETA(11) * IPRE
 Y = IPRE+ERR(1)*W
 DVRL  = DV/BLS
 RESP  = 1
 ENDIF

IF(CMT.EQ.7) THEN
IPRE = CBLD*(1+ALDI*(INHx+A(8
IRES = DV - IPRE
W = THETA(12) * IPRE
Y = IPRE+ERR(1)*W
DVRL  = DV/BLD
RESP  = 2
ENDIF


 DEL = 0
 IF(W.EQ.0) DEL = 1
 IWRE = IRES/(W+DEL)

$THETA
(0, 138)            ; TVBLS
(0, 82.8)           ; TVBLD
(0.0637)            ; TVALSY
(0.0482)            ; TVALDI
(4) FIX             ; TVKD
(121) FIX           ; TVTAU
(0) FIX             ; TVPS1
(1.4) FIX           ; TVPS2
(0.025) FIX         ; TVAMP1
(-0.016) FIX        ; TVAMP2
(0.0938)            ; PROP_SYS
(0.0791)            ; PROP_DIA
(1.21)              ; THSPROP
(-2.02)             ; BPAMP2
```

PK/PD model – Blood pressure (Sunitinib) - continued

```
$OMEGA 0.00854   ; ETABLS
$OMEGA 0.00551   ; ETABLD
$OMEGA 0.751     ; ETA ALSY/ALDI
$OMEGA 0 FIX     ; ETAAMP1
$OMEGA 0 FIX     ; ETAAMP2

$SIGMA 1 FIX

$ESTIMATION SIG=3 PRINT=1 METHOD=1 INTER MAXEVAL=9999 NOABORT
```

F.V PK model Pazopanib

```
$SUBROUTINE ADVAN6 TRANS1 TOL=4
$MODEL
COMP=(PAZD1)
COMP=(CENTSN,DEFOBS)
COMP=(PAZD2)
COMP=(PERIPH)

$PK
DOSE = DOS

CL          = THETA(1)*EXP(ETA(1))
V2          = THETA(2)
KAF         = THETA(3)*EXP(ETA(3))
KAS         = THETA(4)
ALAG3       = THETA(5)
Q24         = THETA(6)
V4          = THETA(7)*EXP(ETA(2))

ED50        = THETA(8)
EMAX        = THETA(9)
LAMBDA      =THETA(10)/24
DCRP        = THETA(11)
TVFD        = (1-(DOSE-200)*EMAX/(ED50+DOSE-200))
TVFT        = 1-DCRP+DCRP*EXP(-LAMBDA*TIME)
TVF         = TVFD*TVFT *EXP(ETA(4))
FR          = THETA(12)
F1          = FR*TVF
F3          = TVF-F1

K20   = CL/V2
K24   = Q24/V2
K42   = Q24/V4
S2    = V2

$DES

DADT(1)     = -KAF*A(1)
DADT(2)     = KAF*A(1)+KAS*A(3)-K20*A(2)-K24*A(2)+K42*A(4)
DADT(3)     = -KAS*A(3)
DADT(4)     = K24*A(2)-K42*A(4)

$ERROR

TY=F

IF(F.LT.0.001) THEN
TY=0.001
ENDIF
```

PK model Pazopanib – continued

```
IPRE = TY

W = THETA(13)*IPRE + THETA(14)
Y = IPRE + W*EPS(1)

IRES        = DV-IPRE
DEL         = 0
IF(W.EQ.0) DEL = 0.0001
IWRE        = IRES/(W+DEL)

$THETA
(0.27) FIX     ; 1  CL
(2.43) FIX     ; 2  V2
(0.40)   FIX   ; 3  KAF
(0.12)   FIX   ; 4  KAS
(0.98) FIX     ; 5  ALAG3
(0.99) FIX     ; 6  Q24
(25.1) FIX     ; 7  V4
(480) FIX      ; 8  ED50
(1 FIX)        ; 9  EMAX
(0.15) FIX     ; 10 LAMBDA  (1/day in 1/h)
(0.501) FIX    ; 11 DCRP
(0.63) FIX     ; 12 FR
0.064 FIX      ;13 proportional error
3.1 FIX        ;14 addtive error

$OMEGA
0.095 FIX      ; 1 CL
0.96 FIX       ; 2 V4
1.96 FIX       ; 3 KAF
0.13 FIX       ; 4 FREL

$SIGMA
1 FIX

$ESTIMATION METHOD=1 INTER NOABORT MAXEVAL=0 SIG=3 PRINT=1
```

F.VI PK/PD model – sVEGFR-2 (Pazopanib)

```
$SUBROUTINE ADVAN6 TOL=4

$MODEL
COMP =(PAZD1)
COMP =(CENTSN,DEFOBS)
COMP =(PAZD2)
COMP =(PERIPH)
COMP = (VEGFR2
COMP = (AUCV2

$ABBREVIATED COMRES = 2

$PK

TVBLV2      = THETA(1)
BLV2        = TVBLV2*EXP(ETA(1))

TVALFA      = THETA(2)
ALFA        = TVALFA*EXP(ETA(2))

TVKOUT      = THETA(3)
 KOUT       = TVKOUT

A_0(5) = BLV2

KIN = BLV2*KOUT

CL          = YCLX
V2          = 2.43
KAF         = YKAFX
KAS         = 0.12
ALAG3               = 0.98
Q24         = 0.99
V4          = YV4X

TVF         = YF1X
FR          = 0.63
F1          = FR*TVF
F3          = TVF-F1

K20         = CL/V2
K24         = Q24/V2
K42         = Q24/V4
S2          = V2
```

PK/PD model – sVEGFR-2 (Pazopanib) – continued

```
$DES

DADT(1) =  -KAF*A(1)
DADT(2) =   KAF*A(1)+KAS*A(3)-K20*A(2)-K24*A(2)+K42*A(4)
DADT(3) =  -KAS*A(3)
DADT(4) =   K24*A(2)-K42*A(4)
CONC = A(2)/V2

FC= A(2)/V2*(1-0.999)

IF(FC.LE.0) THEN
 BND=0
  ELSE
 BND=FC
  ENDIF
INH = BND

SF=1/(1+ALFA*INH)

DADT(5)= KIN*SF-KOUT*A(5)
DADT(6)= A(3)/1000

$ERROR

AUCV2 = A(6)

IPRE  = A(5)
RB    = IPRE/BLV2
IRES  = DV-IPRE
W     = THETA(5)
Y     = IPRE+EPS(1)*W
DVRL  = DV/BLV2

DEL= 0
IF(W.EQ.0) DEL = 1
IWRE = IRES/(W+DEL)

$THETA
(0, 9820)      ; TVBLV2
(0, 22.1)      ; TVALFA
(0, 0.00377)  ; TVKOUT
(-846)         ; RES_ADD

$OMEGA 0.0159    ; ETABLVR2
$OMEGA 0.192     ; ETAalfa

$SIGMA 1 FIX
$ESTIMATION SIG=2 PRINT=1 METHOD=1 INTER MAXEVAL=9999 NOABORT
```

F.VII PK/PD model – sVEGFR-3 (Pazopanib)

```
$SUBROUTINE ADVAN6 TOL=4

$MODEL
COMP =(PAZD1)
COMP =(CENTSN,DEFOBS)
COMP =(PAZD2)
COMP =(PERIPH)
COMP = (VEGFR3)
COMP = (AUCV2)

$ABBREVIATED COMRES = 2

$PK

TVBLV3      = THETA(1)
BLV3        = TVBLV3*EXP(ETA(1))

TVALFA      = THETA(2)
ALFA        = TVALFA*EXP(ETA(2))

TVKOUT      = THETA(3)          ;
KOUT        = TVKOUT

A_0(5) = BLV3

KIN = BLV3*KOUT


CL          = YCLX
V2          = 2.43
KAF         = YKAFX
KAS         = 0.12
ALAG3       = 0.98
Q24         = 0.99
V4          = YV4X

TVF         = YF1X
FR          = 0.63
F1          = FR*TVF
F3          = TVF-F1

K20         = CL/V2
K24         = Q24/V2
K42         = Q24/V4
S2          = V2
```

PK/PD model – sVEGFR-3 (Pazopanib) -continued

```
$DES

DADT(1) =  -KAF*A(1)
DADT(2) =   KAF*A(1)+KAS*A(3)-K20*A(2)-K24*A(2)+K42*A(4)
DADT(3) =  -KAS*A(3)
DADT(4) =   K24*A(2)-K42*A(4)


CONC = A(2)/V2

FC= A(2)/V2*(1-0.999)

IF(FC.LE.0) THEN
 BND=0
  ELSE
 BND=FC
  ENDIF

INH = BND
;Signal Function
SF=1/(1+ALFA*INH)

DADT(5)= KIN*SF-KOUT*A(5)
DADT(6)= A(5)/1000

$ERROR

AUCV3        = A(6)
IPRE  = A(5)
RBL   = IPRE/BLV3
IRES  = DV-IPRE
W     = THETA(5)*IPRE
Y     = IPRE+EPS(1)*W
DVRL = DV/BLV3

DEL   = 0
IF(W.EQ.0) DEL = 1
IWRE = IRES/(W+DEL)

$THETA
(0, 64300)    ; TVBLVR3
(0, 17.5)     ; TVALFA
(0, 0.00471)  ; TVKOUT
0, 0.142)     ; RES_PROP

$OMEGA 0.0543    ; ETABLVR3
$OMEGA 0.324     ; ETAalfa
```

PK/PD model – sVEGFR-3 (Pazopanib) -continued

```
$SIGMA 1 FIX

$ESTIMATION SIG=2 PRINT=1 METHOD=1 INTER MAXEVAL=9999 NOABORT
```

F.VIII PK/PD model – Blood pressure (Pazopanib)

```
$SUBROUTINE ADVAN6 TOL=4

$MODEL
NCOMP=8
COMP = (PAZD1)
COMP = (CENTSN,DEFOBS)
COMP = (PAZD2)
COMP = (PERIPH)
COMP = (AUC)
COMP = (SYS)
COMP = (DIA)
COMP = (SST)

$PK

IF(BPDIAG.EQ.1)THEN
DIAG = (1+THETA(10))
ELSE
DIAG = 1
ENDIF

TVBLS      = THETA(1) * DIAG
TVBLD      = THETA(2)
TVALSY     = THETA(3)
TVTAU      = THETA(4)
TVPS1      = THETA(5)
TVPS2      = THETA(6)
TVAMP1     = THETA(7)
TVAMP2     = THETA(8)


BLS   = TVBLS *EXP(ETA(1))
BLD   = TVBLD *EXP(ETA(2))
ALSY  = TVALSY *EXP(ETA(4))
ALDI  = TVALSY *EXP(ETA(3))
TAU   = TVTAU

PS1   = TVPS1
AMP1 = TVAMP1*EXP(ETA(5))

PS2   = TVPS2
AMP2 = TVAMP2*EXP(ETA(6))

CL         = YCLX
V2         = 2.43
KAF        = YKAFX
KAS        = 0.12
ALAG3      = 0.98
```

PK/PD model – Blood pressure (Pazopanib) – continued

```
Q24    = 0.99
V4     = YV4X

TVF    = YF1X
FR     = 0.63
F1     = FR*TVF
F3     = TVF-F1

K20    = CL/V2
K24    = Q24/V2
K42    = Q24/V4
S2     = V2

A_0(8) = 0

$DES

DADT(1) = -KAF*A(1)
DADT(2) =  KAF*A(1)+KAS*A(3)-K20*A(2)-K24*A(2)+K42*A(4)
DADT(3) = -KAS*A(3)
DADT(4) =  K24*A(2)-K42*A(4)

CONC = A(2)/V2

FC= A(2)/V2*(1-0.999)

DADT(5) = FC

AUCF    = A(5)

DADT(6) = BLS*(1+(AMP1*COS((TIME+6)*6.283/24
PS1)+AMP2*COS((TIME+6)*6.283/12-PS2)))

DADT(7) = BLD*(1+(AMP1*COS((TIME+6)*6.283/24-
PS1)+AMP2*COS((TIME+6)*6.283/12-PS2)))

IF(FC.LE.0) FC=0

INH     = FC

DADT(8) = 1/TAU*INH-1/TAU*A(8)

$ERROR

 FCx  = A(2)/V2*(1-0.999)
 INHx = FCx
```

PK/PD model – Blood pressure (Pazopanib) – continued

```
CBLS =BLS*(1+(AMP1*COS((TIME+6)*6.283/24-
PS1)+AMP2*COS((TIME+6)*6.283/12-PS2)))
CBLD =BLD*(1+(AMP1*COS((TIME+6)*6.283/24-
PS1)+AMP2*COS((TIME+6)*6.283/12-PS2)))

IF(CMT.EQ.6) THEN
 IPRE = CBLS*(1+ALSY*(INHx+A(8)))
 IRES = DV - IPRE
 W    = THETA(9) * IPRE          ;
 Y    = IPRE+ERR(1)*W
 DVRL= DV/BLS
 RESP= 1
ENDIF

IF(CMT.EQ.7) THEN
 IPRE = CBLD*(1+ALDI*(INHx+A(8)))
 IRES = DV - IPRE
 W    = THETA(9) * IPRE
 Y    = IPRE+ERR(1)*W
 DVRL= DV/BLD
ENDIF

DEL = 0
IF(W.EQ.0) DEL = 1
IWRE = IRES/(W+DEL)

$THETA
(0, 130)      ; TVBLS
(0, 80.2)     ; TVBLD
(0.907)       ; TVALSY
(121) FIX     ; TVTAU
(0) FIX       ; TVPS1
(1.4) FIX     ; TVPS2
(0.025) FIX   ; TVAMP1
(-0.016) FIX  ; TVAMP2
(0.0948)      ; PROP_SYS
(0.0907)      ; COV effect

$OMEGA 0.00456  ; ETABLS
$OMEGA 0.00613  ; ETABLD
$OMEGA 0 FIX    ; ETA ALSY
$OMEGA 0 FIX    ; ETA ALDI
$OMEGA 0 FIX    ; ETAAMP1
$OMEGA 0 FIX    ; ETAAMP2

$SIGMA 1 FIX

;$ESTIMATION SIG=3 PRINT=1 METHOD=1 INTER MAXEVAL=9999 NOABORT
```

F.IX Time-to-event models

Sunitinib patients (mRCC)

```
$SUBROUTINE ADVAN6 TOL=4

$MODEL
NCOMP       =1
COMP        = (CUMHAZ)

$PK

TVBLHAZ     = THETA(1)
BLHAZ       = TVBLHAZ*EXP(ETA(1))

TVBETA      = THETA(2)
BETA  = TVBETA*EXP(ETA(2))

PMN = 8814.3
IF(VG2B.GT.PMN)THEN
VGB = 1
ELSE
VGB = 0
ENDIF

$DES

DADT(1) = BLHAZ*EXP(BETA*VGB)

$ERROR

CHZ   = A(1)

SUR    = EXP(-CHZ
HAZNOW = BLHAZ*EXP(BETA*VGB)

IF(DV.EQ.1) THEN
 Y = HAZNOW*SUR
ELSE
 Y = SUR
ENDIF

$THETA
(0, 0.00007)    ;  TVBLHAZ
(1.45)          ;  TVBETA

$OMEGA 0 FIX        ;  ETA_HAZ
$OMEGA 0 FIX        ;  ETA_BETA

$ESTIMATION SIG=2 SIGL=6 MAXEVAL=9999 METHOD=COND LAPLACE LIKE
```

Sunitinib and pazopanib patients (mRCC)

```
$SUBROUTINE ADVAN6 TOL=4

$MODEL
NCOMP=12
COMP = (SUND)
COMP = (OBSLIV)
COMP = (PERISUN)
COMP = (CENTRALM)
COMP = (PERIM)
COMP = (PAZD1)
COMP = (CENTSN)
COMP = (PAZD2)
COMP = (PERIPH)
COMP = (VEGFR2)
COMP = (AUCV2)
COMP = (CUMHAZ)

$PK

TVBLHAZ = THETA(1)
BLHAZ = TVBLHAZ*EXP(ETA(1))

TVBETA  = THETA(2)
BETA  = TVBETA*EXP(ETA(2))

;PHARMACOKINETICS SUNITINIB

K12_S       = 0.133
V2_S        = V2X
QH_S        = QHX
CLP_S       = CLPX
CLM_S       = CLMX
V3_S        = V3X
Q34_S       = Q34X
V4_S        = V4X
FM_S        = FMX
Q25_S       = Q25X
V5_S        = V5X

K34_S = Q34_S/V3_S
K43_S = Q34_S/V4_S
K25_S = Q25_S/V2_S
K52_S = Q25_S/V5_S

S2 = V2_S
S3 = V3_S

;PHARMACOKINETIC PAZOPANIB

CL_P        = YCLX
V2_P        = 2.43
KAF_P       = YKAFX
KAS_P       = 0.12
```

Sunitinib and pazopanib patients (mRCC) – continued

```
ALAG8       = 0.98
Q24_P       = 0.99
V4_P        = YV4X
TVF_P       = YF1X
FR_P        = 0.63
F6          = FR_P*TVF_P
F8          = TVF_P-F6

K20_P       = CL_P/V2_P
K24_P       = Q24_P/V2_P
K42_P       = Q24_P/V4_P
S7          = V2_P

;PHARMACODYNAMICS  sVEGFR2

BLV2   = BSL2X
ALFA   = AL2X

IF(TRTM.EQ.1)THEN   ; Sunitinib
KOUT    = 0.0043
ENDIF

IF(TRTM.EQ.2)THEN   ; Pazopanib
KOUT    = 0.0038
ENDIF

KD      = 4

BASE   = BLV2/1000

A_0(10) = BLV2

KIN    = BLV2*KOUT

$DES

;PHARMACOKINETICS SUNITINIB

IF(TRTM.EQ.1) THEN

CLIV = (K12_S*A(1) + QH_S/V2_S*A(2))/(QH_S+CLP_S)

DADT(1) = -K12_S*A(1)
DADT(2) = QH_S*CLIV-QH_S/V2_S*A(2) - K25_S*A(2) + K52_S*A(5)
DADT(3) = FM_S*CLP_S*CLIV-CLM_S/V3_S*A(3)-K34_S*A(3) + K43_S*A(4)
DADT(4) = K34_S*A(3)-K43_S*A(4)
DADT(5) = K25_S*A(2) - K52_S*A(5)

DADT(6) = 0
DADT(7) = 0
DADT(8) = 0
DADT(9) = 0
```

Sunitinib and pazopanib patients (mRCC)

```
ENDIF

;;;;TOTAL DRUG PLASMA CONCENTRATION
CONCS = A(3)/V3_S+A(2)/V2_S

;;;;FREE DRUG CONCENTRATION
FCS  = A(3)/V3_S*(1-0.90)+A(2)/V2_S*(1-0.95)

;PHARMACOKINETICS PAZOPANIB

IF(TRTM.EQ.2) THEN

DADT(1) = 0
DADT(2) = 0
DADT(3) = 0
DADT(4) = 0
DADT(5) = 0

DADT(6) =  -KAF_P*A(6)
DADT(7) =   KAF_P*A(6)+KAS_P*A(8)-K20_P*A(7)-K24_P*A(7)+K42_P*A(9)
DADT(8) =  -KAS_P*A(8)
DADT(9) =   K24_P*A(7)-K42_P*A(9)

ENDIF

CONCP = A(7)/V2_P

FCP= A(7)/V2_P*(1-0.999)

; PHARMACODYNAMIC MODEL

BND=0

;Sunitinib
IF(TRTM.EQ.1.AND.FCS.GT.0)THEN
BND=FCS/(KD+FCS)
ENDIF

;Pazopanib
IF(TRTM.EQ.2.AND.FCP.GT.0)THEN
BND=FCP
ENDIF

INH = BND

SF=1/(1+ALFA*INH)   ; Inverse linear model

DADT(10) = KIN*SF-KOUT*A(10)
DADT(11) = A(10)/1000

CV2     = A(10)/1000
RV2     = A(10)/BLV2
```

Sunitinib and pazopanib patients (mRCC)

```
DADT(12) = BLHAZ*EXP(BETA*CV2)

$ERROR
CV2x   = A(10)/1000
CHZ    = A(12)

SUR    = EXP(-CHZ)

IF(DV.EQ.1) THEN
 HAZNOW = BLHAZ*EXP(BETA*CV2x)
 Y = HAZNOW*SUR
ELSE
 Y = SUR
ENDIF

$THETA
(0, 0.00002)    ; TVBLHAZ
(0.292)         ; TVBETA

$OMEGA 0 FIX  ; ETA_HAZ
$OMEGA 0 FIX  ; ETA_BETA

$ESTIMATION SIG=2 SIGL=6 MAXEVAL=9999 METHOD=COND LAPLACE LIKE
```

F.X Adverse event models

Myelosuppression (Sunitinib only, mRCC)

```
$ABBREVIATED COMRES = 1

$SUBROUTINE ADVAN6 TOL=4

$MODEL
NCOMP = 9
COMP=(DEPOTD)
COMP=(CENTRAL)
COMP=(PERIPH)
COMP=(METC)
COMP=(METP)
COMP=(G0)
COMP=(G1)
COMP=(G2)
COMP=(G3)

$PK

IF(NEWIND.NE.2) THEN
PSDV   = 0
COM(1) = 0
ENDIF

IF(NEWIND.NE.2.AND.TIME.EQ.0) F6 =1

PRDV = PSDV

IF(PRDV.EQ.1) COM(1) = 0
IF(PRDV.EQ.2) COM(1) = 1
IF(PRDV.EQ.3) COM(1) = 2
IF(PRDV.EQ.4) COM(1) = 3

;;-------- PK Model ----------

KA              = 0.133 * 24
V2              = V2X
QH              = QHX   * 24
CLP             = CLPX  * 24
CLM             = CLMX  * 24
V3              = V3X
Q34             = Q34X  * 24
V4              = V4X
FM              = FMX
Q25             = Q25X  * 24
V5              = V5X

K34             = Q34/V3
K43             = Q34/V4
K25             = Q25/V2
K52             = Q25/V5
```

Myelosuppression (Sunitinib only, mRCC) – continued

```
S2              = V2
S3              = V3

;;-------- AE Model ----------

F6 = 0
F7 = 0
F8 = 0
F9 = 0

IF(COM(1).EQ.0) F6 = 1
IF(COM(1).EQ.1) F7 = 1
IF(COM(1).EQ.2) F8 = 1
IF(COM(1).EQ.3) F9 = 1


; Typical values for rate constants / probabilities

TVK01           = THETA(1)
TVK12           = THETA(2)
TVK23           = THETA(3)
TVKB            = THETA(4)

TVGAM           = THETA(5)
TVEFF           = THETA(6)

; Individual Parameters

K01             = TVK01  * EXP(ETA(1))
K12             = TVK12
K23             = TVK23

KB              = TVKB
GAM             = TVGAM
EFF             = TVEFF

$DES

;;-------- PK Model ----------

CLIV = (KA*A(1) + QH/V2*A(2))/(QH+CLP)

DADT(1) = -KA*A(1)
DADT(2) = QH*CLIV-QH/V2*A(2) - K25*A(2) + K52*A(5)
DADT(3) = FM*CLP*CLIV-CLM/V3*A(3)-K34*A(3) + K43*A(4)
DADT(4) = K34*A(3)-K43*A(4)
DADT(5) = K25*A(2) - K52*A(5)

CONC = A(3)/V3+A(2)/V2

FC= A(3)/V3*(1-0.90)+A(2)/V2*(1-0.95)
```

Myelosuppression (Sunitinib only, mRCC)

```
;;-------- AE Model ----------

K01_F = K01 * EXP(GAM*T)
K12_F = K12 * EXP(GAM*T)
K23_F = K23 * EXP(GAM*T)

KB10  = KB   * EXP(FC*EFF)
KB21  = KB   * EXP(FC*EFF)
KB32  = KB   * EXP(FC*EFF)

DADT(6) = A(7)*KB10                - A(6) * K01_F                          ; No Grade
DADT(7) = A(6)*K01_F  + A(8)*KB21     - A(7) * (KB10 + K12_F)              ; Grade 1
DADT(8) = A(7)*K12_F  + A(9)*KB32     - A(8) * (KB21 + K23_F)              ; Grade 2
DADT(9) = A(8)*K23_F               - A(9) *  KB32                          ; Grade 3/4

$ERROR

Y = 1
IF(DV.EQ.1.AND.CMT.EQ.0) Y = A(6)
IF(DV.EQ.2.AND.CMT.EQ.0) Y = A(7)
IF(DV.EQ.3.AND.CMT.EQ.0) Y = A(8)
IF(DV.EQ.4.AND.CMT.EQ.0) Y = A(9)

PB0 = A(6)
PB1 = A(7)
PB2 = A(8)
PB3 = A(9)

; Cumulative Probabilities

CUP0 = PB0
CUP1 = PB0 + PB1
CUP2 = PB0 + PB1 + PB2
CUP3 = PB0 + PB1 + PB2 + PB3

IF(ICALL.EQ.4) THEN
 IF(CMT.EQ.0)THEN
  CALL RANDOM (2,R)
    IF(R.LE.CUP0)              DV = 1              ;grade 0
    IF(R.GT.CUP0.AND.R.LE.CUP1)   DV = 2           ;grade 1
    IF(R.GT.CUP1.AND.R.LE.CUP2)   DV = 3           ;grade 2
    IF(R.GT.CUP2)              DV = 4              ;grade 3/4
 ENDIF
ENDIF

PSDV = DV
$THETA
(0, 0.0149)     ;1 TVK01
(0, 0.101)      ;2 TVK12
(0, 0.438)      ;3 TVK23
(0, 0.058)      ;4 TVKB
(-0.0207)       ;5 TVGAM
```

Myelosuppression (Sunitinib only, mRCC)

(-0.337) ;6 EFF

$OMEGA
 0 FIX ; OM_K01

$ESTIMATION SIG=2 MAXEVAL=9999 PRINT=1 METHOD=1 LAPLACIAN LIKE

Fatigue (Sunitinib only, mRCC)

```
$ABBREVIATED COMRES = 1

$SUBROUTINE ADVAN6 TOL=4

$MODEL
NCOMP = 9
COMP=(DEPOTD)
COMP=(CENTRAL)
COMP=(PERIPH)
COMP=(METC)
COMP=(METP)
COMP=(G0)
COMP=(G1)
COMP=(G2)
COMP=(G3)

$PK

IF(NEWIND.NE.2) THEN
PSDV   = 0
COM(1) = 0
ENDIF

IF(NEWIND.NE.2.AND.TIME.EQ.0) F6 =1


PRDV = PSDV

IF(PRDV.EQ.1) COM(1) = 0
IF(PRDV.EQ.2) COM(1) = 1
IF(PRDV.EQ.3) COM(1) = 2
IF(PRDV.EQ.4) COM(1) = 3

;;-------- PK Model ----------

KA              = 0.133
V2              = V2X
QH              = QHX
CLP             = CLPX
CLM             = CLMX
V3              = V3X
Q34             = Q34X
V4              = V4X
FM              = FMX
Q25             = Q25X
V5              = V5X

K34             = Q34/V3
K43             = Q34/V4
K25             = Q25/V2
K52             = Q25/V5

S2              = V2
```

Fatigue (Sunitinib only, mRCC) – continued

```
S3              = V3

;;-------- AE Model ----------

F6 = 0
F7 = 0
F8 = 0
F9 = 0

IF(COM(1).EQ.0) F6 = 1
IF(COM(1).EQ.1) F7 = 1
IF(COM(1).EQ.2) F8 = 1
IF(COM(1).EQ.3) F9 = 1


; Typical values for rate constants / probabilities

TVK01           = THETA(1)
TVK12           = THETA(2)
TVKB            = THETA(3)

TVGAM           = THETA(4)

; Individual Parameters

K01     = TVK01  * EXP(ETA(1))
K12     = TVK12
K23     = TVK12

KB      = TVKB
GAM     = TVGAM

$DES
;;-------- PK Model ----------

  CLIV = (KA*A(1) + QH/V2*A(2))/(QH+CLP)

DADT(1) = -KA*A(1)
DADT(2) = QH*CLIV-QH/V2*A(2) - K25*A(2) + K52*A(5)
DADT(3) = FM*CLP*CLIV-CLM/V3*A(3)-K34*A(3) + K43*A(4)
DADT(4) = K34*A(3)-K43*A(4)
DADT(5) = K25*A(2) - K52*A(5)

CONC = A(3)/V3+A(2)/V2

FC= A(3)/V3*(1-0.90)+A(2)/V2*(1-0.95)

;;-------- AE Model ----------

K01_F = K01 * EXP(GAM*T)
K12_F = K12 * EXP(GAM*T)
K23_F = K23 * EXP(GAM*T)
```

Fatigue (Sunitinib only, mRCC) – continued

```
KB10  = KB
KB21  = KB
KB32  = KB

DADT(6) = A(7)*KB10                - A(6) * K01_F                          ; No Grade
DADT(7) = A(6)*K01_F  + A(8)*KB21  - A(7) * (KB10 + K12_F)                 ; Grade 1
DADT(8) = A(7)*K12_F  + A(9)*KB32  - A(8) * (KB21 + K23_F)                 ; Grade 2
DADT(9) = A(8)*K23_F               - A(9) *  KB32                          ; Grade 3/4

$ERROR

Y = 1
IF(DV.EQ.1.AND.CMT.EQ.0) Y = A(6)
IF(DV.EQ.2.AND.CMT.EQ.0) Y = A(7)
IF(DV.EQ.3.AND.CMT.EQ.0) Y = A(8)
IF(DV.EQ.4.AND.CMT.EQ.0) Y = A(9)

PB0 = A(6)
PB1 = A(7)
PB2 = A(8)
PB3 = A(9)

; Cumulative Probabilities

CUP0 = PB0
CUP1 = PB0 + PB1
CUP2 = PB0 + PB1 + PB2
CUP3 = PB0 + PB1 + PB2 + PB3

PSDV = DV
$THETA
(0, 0.00938) ;1 TVK01
(0, 0.0937) ;2 TVK12
(0, 0.0704) ;4 TVKB
(-0.0134) ;5 TVGAM

$OMEGA
 0 FIX  ; OM_K01

$ESTIMATION SIG=2 MAXEVAL=9999 PRINT=1 METHOD=1 LAPLACIAN LIKE
```